The effect of depletion of histone demethylase Jarid1A on cell proliferation, histone modifications, radiation response and gene expression

Dissertation der Fakultät für Biologie der

Ludwig-Maximilians-Universität München

durchgeführt an der Klinik und Poliklinik für Strahlentherapie und Radioonkologie in der Arbeitsgruppe Molekulare Strahlenbiologie

vorgelegt von

Corina Penterling

15. Mai 2018

Erstgutachterin: PD Dr. Anna A. Friedl

Zweitgutachter: Prof. Dr. Heinrich Leonhardt

Tag der Abgabe: 15.05.2018

Tag der mündlichen Prüfung: 12.03.2019

Eidesstattliche Erklärung

Ich versichere hiermit an Eides statt, dass die vorgelegte Dissertation von mir selbständig und ohne unerlaubte Hilfe angefertigt ist.

München, den 15.05.2018

Corina Penterling

Erklärung

Hiermit erkläre ich,

dass die Dissertation nicht ganz oder in wesentlichen Teilen einer anderen Prüfungskommission vorgelegt worden ist.

dass ich mich anderweitig einer Doktorprüfung ohne Erfolg nicht unterzogen habe.

München, den 15.05.2018

Corina Penterling

Table of contents

Publication

Parts of this work are published in:

Penterling, Corina; Drexler, Guido A.; Böhland, Claudia; Stamp, Ramona; Wilke, Christina; Braselmann, Herbert; Caldwell, Randolph, B.; Reindl, Judith; Girst, Stefanie; Greubel, Christoph; Siebenwirth, Christian; Mansour, Wael Y.; Borgmann, Kerstin; Dollinger, Günther; Unger, Kristian; Friedl, Anna A. (2016): Depletion of Histone Demethylase Jarid1A Resulting in Histone Hyperacetylation and Radiation Sensitivity Does Not Affect DNA Double-Strand Break Repair. In: *PLoS ONE* 11 (6), S. e0156599. DOI: 10.1371/journal.pone.0156599.

Summary

In the last years histone demethylases were excessively studied regarding their role in cancer development and their involvement in DNA damage response. Especially the members of the Jarid1 demethylase family that are associated with numerous oncogenic diseases came into focus of researchers. Many studies that screened for specific inhibitors were initiated to reveal the exact roles in cell cycle regulation and oncogenic signaling and to target the Jarid1 demethylase family for cancer treatment. In several cancer cell lines I investigated the effects of siRNA-mediated depletion of histone demethylase Jarid1A (KDM5A, RBP2), which demethylates transcription activating tri- and dimethylated lysine 4 at histone H3 (H3K4me3/me2), on cellular proliferation, H3K4 methylation and certain histone acetylation levels as well as on cellular response to radiation. In unirradiated cells Jarid1A depletion leads besides the expected increase in H3K4me3 methylation levels to histone hyperacetylation without affecting cellular growth and proliferation properties. In irradiated cells, depletion of Jarid1A significantly increased cellular radiosensitivity without altering cell cycle regulation. Unexpectedly, the hyperacetylation phenotype did not affect accumulation of the DNA damage response and repair factors γH2AX, 53BP1, BRCA1, or Rad51 at damage sites. It did furthermore not influence the resolution of radiation-induced foci DSB repair pathways as indicated in a DSB reporter assay. Gene expression microarray analysis after Jarid1A depletion and irradiation did not hint at major disturbance of pathways related to DNA damage or general cellular stress response. Single DDR genes that showed a slightly altered expression in the microarray displayed no changes on protein level. I therefore conclude, that the radiation sensitivity observed following depletion of Jarid1A is neither caused by deregulation of typical damage response pathways nor by deficiencies in the repair of DNA double-strand breaks.

1 Introduction

1.1 Organization of chromatin

Chromatin is a complex of DNA and histone proteins in the eukaryotic cell. During the interphase of the cell cycle chromatin is widespread in the nucleus, while it is condensed and builds microscopically visible chromosomes during cell division. The repeating unit of the chromatin is the nucleosome that consists of approximately 146 bp DNA wrapped around a histone octamer (Luger et al. 1997). The octamer is composed of two histone H2A-H2B heterodimers and a tetramer of the histones H3 and H4 (Kornberg 1977). The linker histone protein H1 binds to the DNA that is located between the nucleosomes. It is, amongst others, responsible for the formation of higher-order structures and plays a role in chromatin dynamics (Izzo and Schneider 2016).

In 2012 a higher-order chromatin organization in three-dimensional megabase-sized structures called topologically associating domains (TADs) was observed by Dixon and colleagues. TADs are sequences that preferentially contact with each other and form domains distinct from other chromatin domains (Dixon et al. 2012). It is assumed that these highly conserved structures enable the distinct formation of euchromatin and heterochromatin (Solovei et al. 2016) - the two structurally and functionally distinct chromatin regions. They differ in gene-density and time of replication and also interact with different structures in the nucleus (Solovei et al. 2016). Heterochromatin is associated with late replication and is assumed to have a condensed structure with either non-coding and repetitive DNA-sequences (constitutive heterochromatin) or locally silenced genes (facultative heterochromatin). Facultative heterochromatin is either restricted to distinct chromosomal regions or affects entire chromosomes (e.g. the inactive x chromosome). It has the potential to convert into euchromatin via epigenetic alterations under certain conditions, such as during cell differentiation. Constitutive heterochromatin has to be kept stably silenced to preserve genome integrity, like e.g. centromeric and telomeric DNA (Trojer and Reinberg 2007). Euchromatin by contrast is gene-rich, preferentially localized in the interior of the nucleus and replicates early in S-phase (Dileep et al. 2015). Recent research begins to unravel the classical view of the densely packed, transcriptionally inactive heterochromatin. It was shown that some pericentric regions are only around 1.5-fold denser than surrounding euchromatin. Consequently, binding of transcription factors is enabled in this regions and low-level transcription is performed as shown for several non-coding RNAs transcribed from heterochromatin (Saksouk et al. 2015; Imai et al. 2017).

Chromatin structure plays a critical role in all cellular processes involving DNA, such as transcription, replication, recombination and repair. The DNA-histone interaction and the accessibility of DNA for DNA-regulating protein complexes is accomplished by ATP-driven chromatin remodeling and post-translational modifications of the core histones (Swygert and Peterson 2014).

1.1.1 Post-translational modifications of histones

The different histones underlie a high variability of covalent modifications, especially within their amino-terminal tails protruding from the nucleosomes, but also in the nucleosome core region (Mersfelder and Parthun 2006). The modifications occur at specific amino acids of the histones and include phosphorylation, methylation, acetylation, ADP-ribosylation, glycosylation, ubiquitination and SUMOylation (reviewed in Zhang et al. 2016). Depending on the type of modification and on the affected amino acid, the post-translational modifications (PTMs) can form a binding site for the recruitment of proteins/complexes with specific enzymatic activities or can change the interplay between DNA and histones directly. Strahl and Allis (2000) proposed that distinct histone modifications at amino acids act sequentially or in combination to generate a ´histone code`. It is now widely accepted that this code can be read by relevant proteins that initiate the appropriate downstream events, influencing transcription, repair and other processes concerning the DNA. The different PTMs and the cross-talk between them results in a vast number of possible combinations and effects on chromatin structure (Zhang et al. 2015). PTMs are added or removed by different histone-modifying enzymes. The regulation of acetylations e.g., is performed by histone acetyltransferases (HATs) and histone deacetylases (HDACs). Acetylations are thought in general to lead to an opening of the chromatin structure and enable transcription, as they neutralize the positive charge of the lysine at the histone tails, thus decreasing the interaction with the negative charged DNA backbone (Tse et al 1998).

The impact of histone methylations, which are accomplished by the action of methyltransferases and demethlyases, is more complex and depends on the altered amino acid residue. Since they occur as mono-, di- or tri-methylations and can be found at lysine and arginine residues, they offer a high diversity of functional consequences (Alam et al. 2015). Figure 1 gives an overview of exemplary histone modifications and their impact on chromatin structure and transcriptional regulation. Tri-methylation of histone H3 on lysine 27 (H3K27me3) is a typical mark of facultative heterochromatin (Probst et al. 2009), while di- or tri-methylations of histone H3 on lysine 9 (H3K9me3/2) are associated with maintaining and establishing constitutive heterochromatin. H3K9me2/3 is accompanied by binding of HP1 to chromatin, providing a platform for the recruitment of several factors that are involved in preserving the

condensed structure (Muramatsu et al. 2016). H3K4me3/2 in contrast is usually enriched at transcriptionally active genes and often found in the promoter regions (Soares et al. 2017).

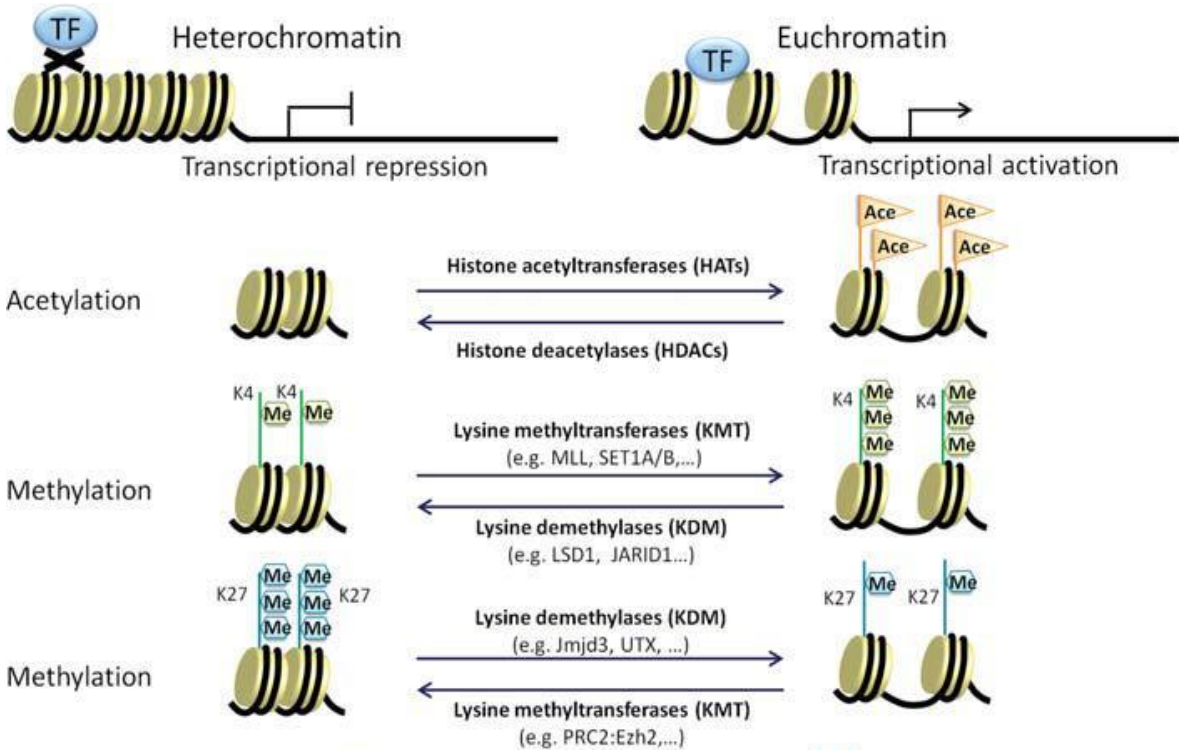

Figure 1: Regulation of transcription based on chromatin structure

Schematic representation of typical exemplary posttranslational histone modifications for transcriptional repression and silencing. The corresponding enzymes modify i.a. acetylation and methylation levels at designated amino acids of the histones. Thereby higher chromatin organization is regulated enabling or preventing binding of transcription factors (TF) (Ohtani and Dimmeler 2011, modified).

1.2 DNA damage response and double-strand break repair

DNA lesions induced by endogenous reactions or by exogenous sources like chemical substances, UV light and ionizing radiation can have severe consequences to cells. DNA double-strand breaks (DSBs) are the most deleterious lesions as both strands of the DNA are affected. Due to missing or defective repair, cells lose their genomic stability resulting in cell death or leading to chromosomal aberrations and in the end to carcinogenesis (van Gent et al. 2001). To prevent this, cells have to repair those breaks rapidly and efficiently with a highly specialized repair mechanism called the DNA DSB repair.

One of the first factors sensing a DSB is the MRN complex – a complex of the proteins Mre11, Rad50 and Nbs1 (Mirzoeva and Petrini 2003). Binding of MRN to the break leads to the monomerization and auto-phosphorylation of the kinase ATM (Paull 2015). ATM belongs to the phosphoinositide 3-kinase (PI3K) related protein kinase family, which also includes the ATR kinase. ATM triggers complex signal transduction pathways, particularly following damage to DNA, by phosphorylation of various downstream proteins that are involved in cell cycle control, apoptosis and DNA repair (Bensimon et al. 2011).

An important step in the DDR is the phosphorylation of the histone variant H2AX at serine 139 (γH2AX) in a 1-2 Mb large region surrounding the DSB by the kinase ATM (Rogakou et al. 1998). γH2AX is one of the earliest detectable protein in the region around the break and is widely accepted as a marker for DSBs. The accumulation of proteins of the DDR in the region of the damage after irradiation leads to the formation of so called ionizing radiation-induced foci (IRIF) that can be detected by immunofluorescence microscopy (Misteli and Soutoglou 2009). Other proteins associated with chromatin in the regions of a DSB are e.g. the mediator proteins 53BP1 or MDC1 that can also be detected as foci by immunofluorescence techniques (Pandita and Richardson 2009).

1.2.1 Non-homologous end joining

In mammals most DSBs are repaired via the non-homologous end joining (NHEJ) pathway. It is relatively error-prone as the NHEJ promotes direct ligation of the DSB ends, which often results in deletions or insertions at the repair junction sites. Nevertheless it is the major pathway in the G0/G1 phase, as it can be accomplished rapidly and independently of the cell cycle phase (Mao et al. 2008).

The process of NHEJ is illustrated in Figure 2 on the left. The heterodimer Ku70-Ku80 is the first factor that binds to the break, which results in stabilization and protection from unspecific processing. The DNA-dependent protein kinase catalytic subunit (DNA-PKcs) is recruited to Ku70-Ku80 and leads to the formation of the DNA-PK holoenzyme, which helps to promote the end stability, and builds - together with XRCC4 and maybe other elements - a scaffold for additional factors involved in NHEJ. For the formation of ligatable ends several factors perform DNA end processing, including the nucleases Artemis and APLF, the kinase PNKP and DNA polymerases. Ligation of the broken ends by DNA ligase IV and its binding partner XRCC4 completes the NHEJ repair and leads to the dissociation of the repair factors (reviewed in Davis and Chen 2013).

1.2.2 Homologous recombination

Homologous recombination (HR) is classified as relatively error-free pathway, since it uses homologous sequences as template for the repair. Accordingly, this repair pathway can only proceed in the late S and G2 phases of the cell cycle, when a sister chromatid is available.

The pathway begins with the resection of the DSB ends by 5′ to 3′ exonucleases resulting in the production of 3′-OH ending single-stranded DNA tails. The ssDNA is bound by the human replication protein A (RPA) and subsequently replaced by Rad51. In an ATP-consuming reaction, Rad54 stabilizes the filament and enables the homology search and DNA strand invasion by Rad51, generating a Holliday junction and a heteroduplex molecule (Simandlova et al. 2013). Then either the invading strand reanneals with the second end of the DSB or both ends of the DSB anneal to the template DNA, whereby a double Holliday junction is formed. The pathway proceeds, using the undamaged strand as a template, followed by the repair of ssDNA gaps by DNA polymerase and ligases. Finally the junction is resolved, resulting in either crossover or non-crossover products (Srivastava and Raman 2007; Li and Heyer 2008).

1.2.3 Pathway choice

As accurate repair of DSBs is crucial for cell survival and the maintenance of genomic stability, the choice of the appropriate repair pathway is of fundamental importance.

Besides the cell cycle phase, the chromatin structure and the structure of the DSB ends play a major role in directing repair towards HR or NHEJ (Aymard et al. 2014; Shibata et al. 2017). 53BP1-RIF1 competes with BRCA1-CtIP for the broken DNA ends of the DSB. While the role of 53BP1-RIF1 is to protect the end of DNA from processing, BRCA1-CtIP triggers the processing of the DNA ends (Bakr et al. 2016). Independently of the cell cycle phase or the DSB end structure 53BP1 is always recruited to the ends of DSBs to protect the end from misrepair or induction of resection by BRCA1. Then, either the DSB is subsequently repaired via NHEJ or - if the structure of the DSB ends does not enable NHEJ – BRCA1 is recruited and weakens the binding of 53BP1 to the break ends by triggering its dephosphorylation (reviewed in Shibata et al. 2017). BRCA1 binding to the break enables the initiation of 5′-end resection and recruitment of factors that trigger the homology search and strand invasion by the Rad51 nucleofilament (Grabarz et al. 2012).

As mentioned above, pathway choice is also strongly regulated by the chromatin environment. Some claim the existence of a “DSB repair choice histone code”, where posttranslational modifications, like the methylation and acetylation states of specific histone positions near or/and at the break sites are assumed to directly influence the pathway choice (Clouaire and Legube, 2015). It was observed that histone acetylation antagonizes 53BP1 binding and

53BP1 foci formation at the break site, thereby enabling BRCA1 accumulation, triggering end resection and repair via homologous recombination (Hsiao et al. 2013; Tang et al, 2013).

In summary, studying spatial and temporal recruitment of the different foci forming DDR and repair proteins like 53BP1, BRCA1 or Rad51 to DSBs after ionizing irradiation allows to draw conclusions about the interplay between HR and NHEJ and to identify and characterize modified, inefficient or defective repair in different treated cells.

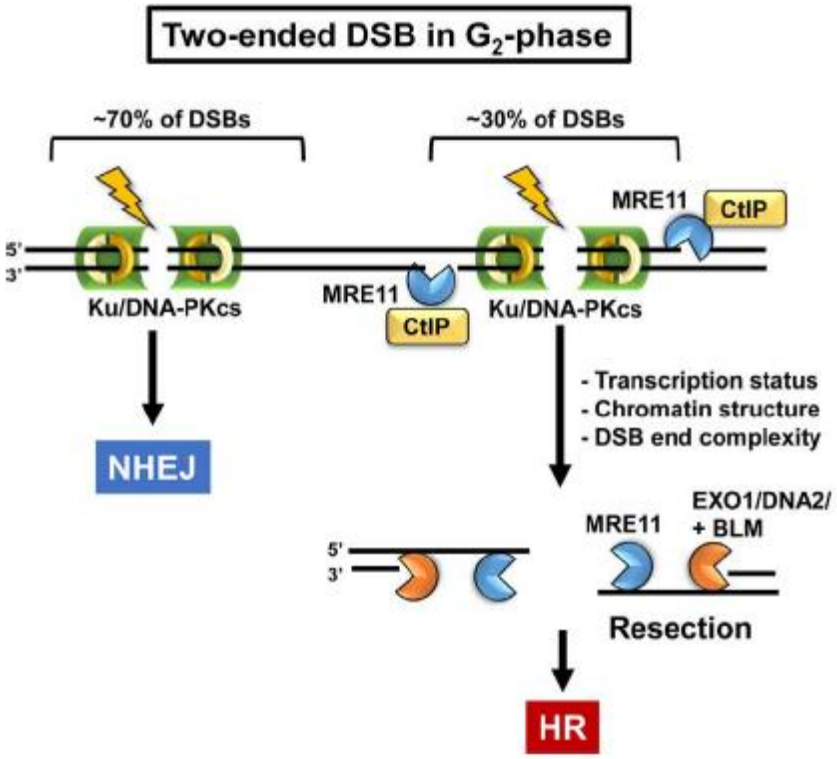

Figure 2: Repair of typical IR-induced DSBs in G2-phase

70% of the typically IR induced two-ended DSBs are repaired via NHEJ in G2-phases. The remaining 30% that cannot be repaired via NHEJ due to transcription status, chromatin structure or DSB end complexity, are repaired via HR. In case of HR the Ku70/Ku80 complex at the DNA ends is removed, followed by recruitment of exonucleases that promote resection (Shibata at el. 2017).

1.3 DSB-induced chromatin dynamics

In case of the occurrence of a DSB, modification of the chromatin structure is a highly important prearrangement to enable the access to the break site, the repair of the damage and the restoration of the chromatin to the original state according to the `access-repair-restore`-model (Soria et al. 2012). Hence the DNA damage response (DDR) must be accompanied by reorganization of chromatin, including local chromatin decondensation, alterations of histone modifications and exchange of histones. In recent years a large number of chromatin-based events after DSB-induction have been discovered. Some variations lead to a relaxation of the chromatin to simplify the access of repair factors, others direct the chromatin to a more repressive state to prevent transcription at the DSBs (reviewed in Friedl et al. 2012).

The most investigated alteration of the chromatin after induction of a DSB is the earlier mentioned phosphorylation of the histone variant H2AX rapidly after induction of a DSB. The emerging γH2AX recruits downstream DDR factors like MDC1 arranging the site of the DSB for further signaling and repair. Binding of MDC1 to γH2AX leads to recruitment of the E3 ubiquitin ligase RNF8. Its ubiquitination of H2A and H2AX primes the chromatin at the break site and recruits the E3 ubiquitin ligase RNF168, which catalyzes the formation of lysine 63-linked ubiquitin chains. This amplification leads to the accumulation of the repair factors BRCA1 and 53BP1 at the DSB (Doil et al. 2009; Campbell et al. 2012).

The kinase ATM facilitates the repair of heterochromatic DSBs by phosphorylation of the transcriptional repressor Kap1 at Ser 824. p-Kap1 directly interacts with the SUMO1-proteins, what disrupts the interaction between SUMO1 and the catalytic subunit CHD3 of the NuRD complex, mediating transient chromatin relaxation (Goodarzi et al. 2011). Kap1 is further phosphorylated at Ser 473 by the checkpoint kinase 2 (Chk2), which leads to disruption of the Kap1-HP1-β interaction and release of HP1-β from chromatin, promoting DNA repair (Bolderson et al. 2012).

As acetylation is associated with a relaxed chromatin structure, it is not surprising that, following DSB induction, histones show an increased level of acetylation. The acetyltransferase Tip60 has been identified as candidate involved in DNA-damage induced chromatin acetylation. It is recruited to DSBs, where its chromodomain interacts with H3K9me3 at the break site. This activates the acetlytransferase activity, whereupon Tip60 directly acetylates and activates the ATM kinase (Sun et al. 2009). Furthermore, Tip60 is responsible for the acetylation of the histones H2A and H4 at DSBs. The emerging open chromatin structure leads to the recruitment of BRCA1 and 53BP1 triggering the repair of the DSBs (Murr et al. 2005). As mentioned in chapter 1.2.3 a shift in the acetylation level can influence pathway choice by directing repair towards HR or NHEJ.

Besides the PTMs mentioned before, all histones can be poly-ADP-ribosylated (PARylated). The Poly-(ADP-ribose) polymerase PARP1 is rapidly activated by DSBs and causes sequential addition of ADP-ribose at histones and other nuclear proteins (Schreiber et al. 2006; Haince et al. 2008). For years it has been accepted that PARylation of nucleosomes in the presence of NAD+ leads to chromatin relaxation (Poirier et al. 1982). However, several groups claim a contrary function of PARP1 concerning the influence to the chromatin structure in the case of DNA damage. Chou and colleagues revealed that PARP1 is associated with transient repression of transcription by recruiting components of the chromatin remodeling complexes NuRD and the polycomb group to damage sites, which are involved in epigenetic silencing (Chou et al. 2010). They also observed a loss of the actively transcribing form of RNA Polymerase II (RNA Polymerase II phosphorylated at Ser 2) at laser- and UV-induced γH2AX-domains.

How the chromatin relaxation contributing to DNA repair on the one hand and the condensation of chromatin to prevent transcription at the break site on the other hand are coordinated, is still under investigation. It is conceivable that the extremely dynamic chromatin at the damage sites enables the existence of both conditions almost simultaneously, with a tiny temporarily/ spatially separation. Figure 3 depicts some well-known chromatin dynamics in eu- and heterochromatin regions after DSB induction. This overview of Shi and Oberdoerffer shows factors and chromatin modifications accomplishing initial chromatin relaxation followed by chromatin compaction (Shi and Oberdoerffer 2012).

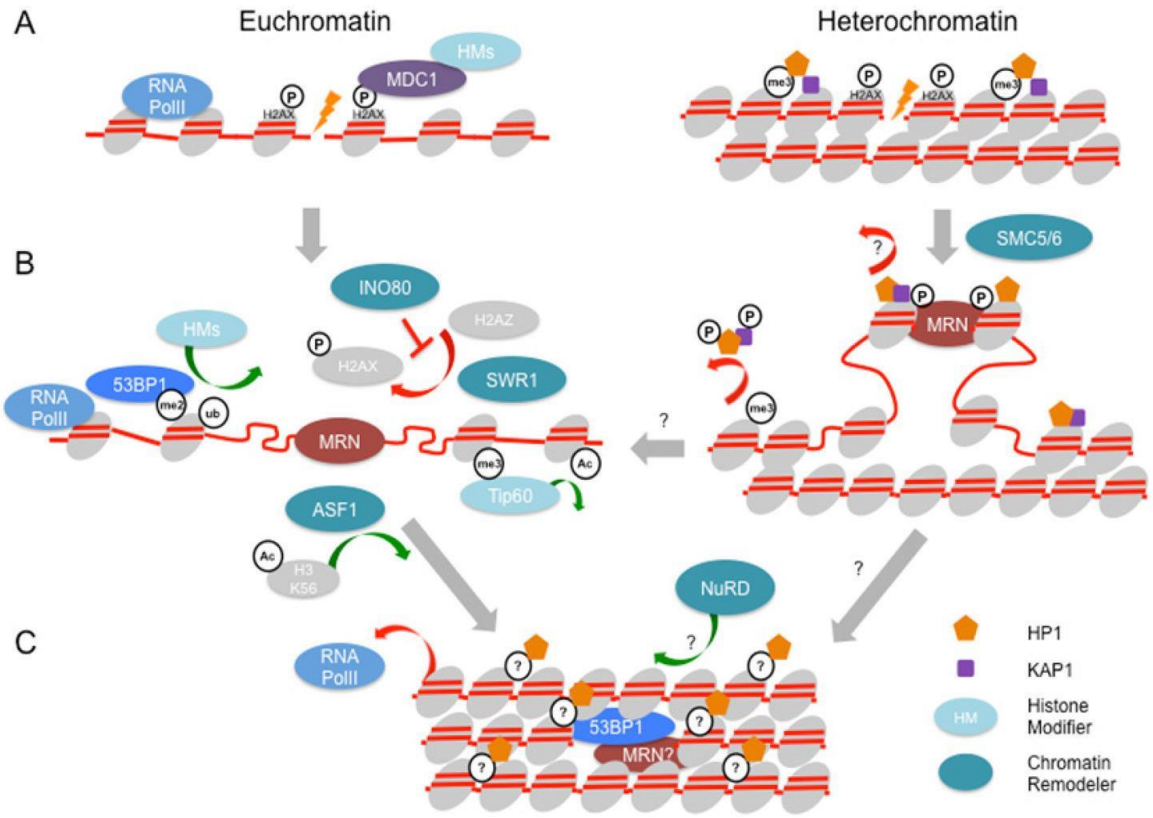

Figure 3: DSB-induced dynamics of chromatin structure

After induction of DSBs, both in eu- and heterochromatin, H2AX is phosphorylated and repair factors are recruited (A). In heterochromatin (B, right side), phosphorylated HP1 and Kap1 dissociate from the damaged chromatin and chromatin remodeler move the damage to the periphery to ensure accessibility to the break like in euchromatin. Several histone modifiers and chromatin remodelers, like e.g. Tip60 and INO80, reorganize the chromatin environment at the break site (B, left side), leading to repression of transcription and repair of the damage. During the initial steps of repair chromatin is believed to be in a more open condition followed by chromatin compaction later on (C). Compaction is mediated by the NuRD complex and the recruitment of HP1. RNA Polymerase II is temporarily excluded from the damage site (Shi and Oberdoerffer 2012).

In recent work in our laboratory a loss of di- and trimethylation of histone H3 at lysine 4 (H3K4) in the gamma-H2AX domain after ionizing irradiation was demonstrated. This was accompanied by the loss of active RNA polymerase II in γH2AX-decorated chromatin regions, suggesting that inhibition of transcription in the vicinity of break sites is associated with a loss of active histone marks. The loss of methylation increased with time after irradiation, suggesting an active removal process by a histone demethylase (Seiler at al. 2011). As members of the Jarid1 family are the only demethylases that are able to remove tri- and di-methylations at H3K4, they are strong candidates for involvement in this process. Furthermore, an accumulation of Jarid1A/KDM5A at laser-induced DNA damage sites was observed (Seiler

et al. 2011), outlining this protein as strong candidate to be responsible for the loss of the active histone modification.

1.4 Structure and function of the Jumonji C domain-containing histone demethylases

Since the discovery of histone demethylases, it is widely accepted that histone methylations are dynamic and can be regulated by an interplay of methyltransferases and demethylases. The lysine-specific demethylase 1 (LSD-1) was the first identified histone demethylase. Its structure enables the demethylation of di- or monomethylated lysines of H3K4 and H3K9 (Shi et al. 2004). In recent years a wide range of histone demethylases has been discovered. The enzymes of the Jumonji C (JmjC) domain-containing family represent the major class of histone demethylases. They are able to remove tri-, di- and monomethylations from different lysine residues in a Fe(II) and α-ketoglutarate dependent oxygenase reaction by a highly conserved mechanism (Tsukada et al. 2006). Figure 4 represents all known human JmjC demethylases with corresponding substrates. All of them contain the catalytic active JmjC domain, but differ in additional DNA and protein binding domains demonstrating their high functional diversity in distinct biological processes (Shmakova et al. 2014). Aberrant expression and deregulation of histone demethylases is often linked to diseases like neurological defects or cancer (Cloos et al. 2008), what will be taken up again in chapters 1.4.2 and 1.4.3.

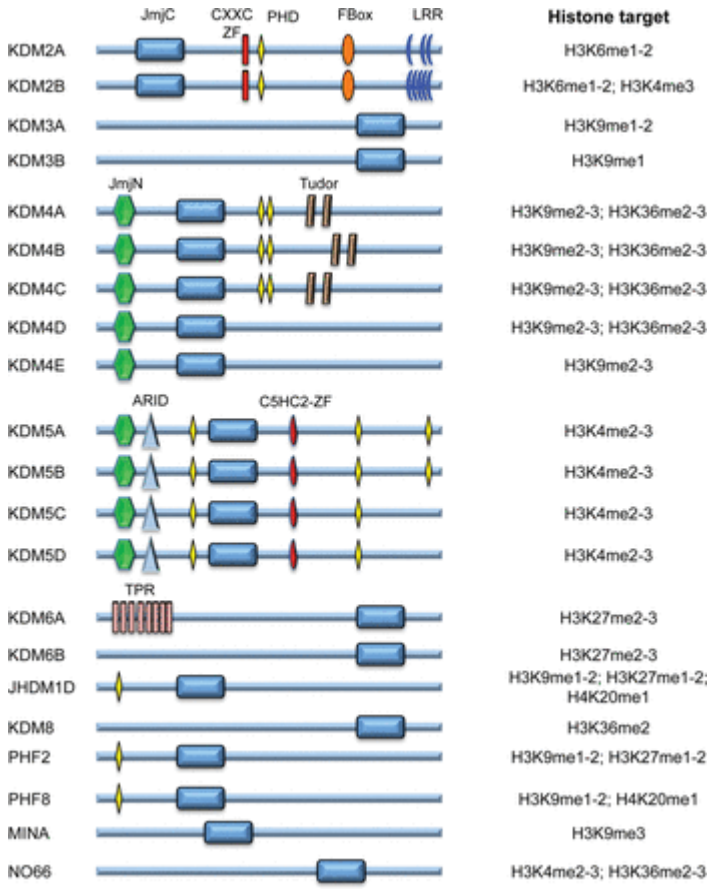

Figure 4: JmjC family domain structure and histone targets

Indicated are names, protein domains and substrate specificity of the JmjC family of demethylases. They all possess the catalytic active JmjC domain. Other potential domains: ARID - AT-rich interactive domain; C5HC2-ZF - C5HC2 zinc finger domain; CXXC-ZF - CXXC zinc finger domain; FBox - F-box domain; JmjC - Jumonji C domain; JmjN - Jumonji N domain; LRR - leucine-rich repeat domain; TPR - tetratricopeptide domain; Tudor - Tudor domain (Shmakova et al. 2014).

1.4.1 Role of JmjC histone demethylases in the DNA damage response

As there is a lot of reorganization of chromatin in the case of a DNA damage (see chapter 1.3), it is not surprising that the action of histone demethylases is of high importance in the DNA repair. At the beginning of my thesis the role of histone demethylases in the DNA damage response was scarcely investigated. In the last years during my research several histone demethylases have been implicated in contributing to the DDR in numerous modes of action. For instance overexpression of KDM4B leads to enhanced repair and higher radioresistance after γ-irradiation, associated with decreased levels of H3K9me3/me2 (Young et al. 2013). Khoury-Haddad and colleagues reported that KDM4D is linked to the first steps of the DNA damage signaling in a PARP1-dependent manner. After depletion of the histone demethylase, cells failed to activate the kinase ATM resulting in impaired DSB repair (Khoury-Haddad et al. 2014). Recently it was shown in *C. elegans* that loss of the H3K36me2 demethylase KDM8

affects repair by HR after ionizing radiation. KDM8 prevents the resolution of recombination intermediates and the release of Rad51 claiming a central role for the demethylase to maintain genome stability (Amendola et al. 2017). Further, LSD-1/KDM1A and KDM2A have been implicated in the DDR, as well as KDM5B (Mosammaparast et al. 2013; Li et al. 2014: Cao et al. 2015).

1.4.2 Jarid1 demethylases

The JmjC domain-containing Jarid1 family of demethylases in humans consists of four members: Jarid1A (RBP2/ KDM5A), Jarid1B (PLU1/ KDM5B), Jarid1C (SMCX/ KDM5C) and JARID1D (SMCY/ KDM5D). Their structure is highly conserved and includes, besides the catalytic active JmjC domain, JmjN, A-T rich interactive, C5HC2-zinc-finger and PHD-finger domains (see Figure 4) (Blair et al. 2011). All members are able to remove tri- and di-methylations at H3K4 with Fe(II) and α-ketoglutarate as co-factors (Christensen et al. 2007; Iwase et al. 2007).

Mutations in the SMCX gene on the X chromosome, coding for the demethylase Jarid1C, often lead to neuronal diseases like X-linked intellectual disability. Known are nonsense or missense mutations in the catalytic domain suggesting that loss of demethylase activity impairs neuronal functions (Iwase et al. 2007; Rujirabanjerd et al. 2010). Recent studies reveal overexpression of Jarid1C in breast cancer and hepatocellular carcinoma leading to increased cell invasion and migration (Ji et al. 2015; Wang et al. 2015).

The functions of Jarid1D are poorly described. The gene KDM5D is encoded on the Y chromosome in a region linked to spermatogenesis. Akimoto and colleagues demonstrated an interaction of the demethylase with the factor MSH5 that performs crossing-over events during meiosis. Hence, Jarid1D is presumed to play a role in regulating spermatogenesis by its chromatin modifying function (Akimoto et al. 2008).

Jarid1B is overexpressed in several kinds of cancer, including lung, epithelial ovarian and breast cancer. The overexpression implies an increased rate of proliferation and invasiveness, respectively a higher resistance to chemotherapy (Yamamoto et al. 2014; Shen et al. 2015; Wang et al. 2015). In hepatocellular tumors, Tang and colleagues revealed Jarid1B-mediated transcriptional repression of the tumor suppressor PTEN in the PI3K/ Akt pathway by decreasing H3K4me3 at the PTEN promoter (Tang et al. 2015). A similar mode of action was demonstrated in breast tumorigenesis, where Jarid1B promotes cell cycle progression by repressing the expression of the tumor suppressors BRCA1 (Scibetta et al. 2007) and microRNA let-7e (Mitra et al. 2011).

Jarid1A was initially discovered as binding partner of the tumor-suppressor retinoblastoma (Rb) protein (Benevolenskaya et al. 2005). Rb binding to the transcription factor E2F4 leads to transcriptional silencing of E2F4-regulated genes, suggesting a function of Jarid1A in transcriptional repression by demethylation of H3K4 during differentiation (Beshiri et al. 2012). Besides, the demethylase was shown to transiently interact with the PRC2 complex that mediates polycomb-mediated silencing during cell differentiation and most likely at sites of DSBs (Pasini et al. 2008; Campbell et al. 2013). Further interaction partners of Jarid1A are the chromatin remodeling complexes MRG15 and NuRD (Hayakawa et al. 2007; Nishibuchi et al. 2014). This implicates a role for Jarid1A in the regulation of transcription by binding to specific chromatin regions leading to a loss of methylation at H3K4 at these sites. Both, the identified interaction partners of Jarid1A and the observed loss of H3K4me3/me2 at radiation-induced damage sites (see chapter 1.4.13) strongly suggest a role for the demethylase in the DDR.

1.4.3 Role of JmjC-family in cancer treatment

Aberrant methylation as well as deregulated expression of histone demethylases can contribute to tumorigenesis in numerous ways. Several studies highlight the important role of histone demethylases in cancer development and resistance to therapeutic applications. In different types of cancer overexpression of Jarid1 histone demethylases was observed resulting in increased proliferation and invasiveness of affected tumor cells (see chapter 1.4.2). Recently Jarid1A was found to be overexpressed in glioblastoma cells with high resistance to temozolomide, an alkylating agent used for chemotherapy (Banelli et al. 2015). Breast cancer cells overexpressing Jarid1A also display enhanced proliferation and drug resistance (Hou et al. 2012). Besides, deregulated expression of histone demethylases that are involved in DNA repair, like KDM4D and KDM5B, might interfere with the DNA damage response and thereby provoke genomic instability.

The fact that methylations are dynamic and reversible can be exploited and genes controlling histone lysine methylation, including histone demethylases, came into focus as potential targets in cancer treatment (Itoh et al. 2015; McGrath and Trojer 2015). In contrast to HDAC inhibitors, which affect various processes causing cytotoxicities in clinical trials (Mottamal et al. 2015), inhibitors of histone demethylases seem to be very promising as demethylase activity is specific for particular histone residues. Additionally, the JmjC-family of histone demethylases is strongly reliant upon the co-factor α-ketoglutarate and can therefore be inhibited by the oncometabolite 2-hydroxyglutarate, which is a product of mutated isocitrate dehydrogenase IDH1 and IDH2 (Dang et al. 2009; Chowdhury et al. 2011).

1.5 IDH mutations

An emerging hallmark of cancer is reprogramming of energy metabolism (Hannahan and Weinberg 2011). Among the best known examples are mutations in the NADP+-dependent enzymes isocitrate dehydrogenase 1 and 2 (IDH1/2). These mutations were identified in a variety of tumors including gliomas, chondrosarcomas and acute myeloid leukemia (Yan et al. 2009; Amary et al. 2011; Mardis et al. 2009). The regular enzymatic reaction of the enzymes IDH1/2 is the conversion of isocitrate to α-ketoglutarate (α-KG). This reaction is either catalysed in the cytosol by IDH1 or in the mitochondrion by IDH2 during the tricarboxylic acid (TCA) cycle (see Figure 5). The heterozygous mutation that has a dominant effect over the remaining wild-type allele in the IDH1/2 genes enables the catalysation of this reaction, but is accompanied by a novel enzymatic gain-of-function reaction that further converts α-KG to 2-hydroxyglutarate, more precisely to the enantiomer R-2-hydroxyglutarate (R-2-HG) (Yang et al. 2012).

Under normal physiological conditions only minimal traces of 2-HG can be detected in mammalian cells, while in human glioma samples with IDH mutations cells accumulate the metabolite up to ~100-fold compared to tumors featuring wild-type IDH1 (Dang et al. 2009). The oncogenic potential of the metabolite is probably based on several effects. Accumulation of R-2-HG may cause some issues concerning the neutralization of reactive oxygen species (ROS) conducted by NADPH, since NADPH consumption is elevated, when isocitrate is converted to R-2-HG instead of α-KG (Reitman and Yan 2010). Additionally, competitive inhibition of α-KG-dependent enzymes by R-2-HG can provoke tumorigenesis due to epigenetic dysregulation, as R-2-HG was shown to inhibit several α-KG-dependent dioxygenases like histone lysine demethylases and the 5-methyl cytosine hydroxylase TET2. Consequently, the strictly regulated DNA and histone methylation status is impaired resulting in altered epigenetic patterns and disturbed gene regulation and tissue homeostasis (Xu et al. 2011). The outcome of this depends on the affected cell type. For example in hematopoietic progenitor cells IDH1/2 mutations lead to a histone hypermethylation phenotype resulting in dysregulation or blocking of hematopoietic differentiation and thereby triggering hematologic neoplasms like acute myeloid leukemia (Lu et al. 2012). Interestingly, patients with IDH1/2 mutations in lower-grade glioblastomas have a significantly longer overall survival, longer progression-free survival and better response to chemotherapy than patients without these mutations (Yan et al. 2009; Chen et al. 2016). Furthermore it was shown that glioblastoma cells expressing mutated IDH1 or IDH2 are more sensitive to radiation (Li et al. 2013). Increased radiation sensitivity may at least in part be caused by inactivation of the activity of JmjC family histone demethylases, several of which have recently been implicated in genome stability and DNA repair pathways (see chapter 1.4.1).

To mimic the IDH1 mutation cells can be treated with the cell permeable ester of R-2-HG, called (2R)-2-Hydroxyglutaric Acid Octyl Ester Sodium Salt. This ester has been reported to competitively inhibit α-KG and hence can be used to study the effects of the mutation in glioblastoma cells (Xu et al. 2011).

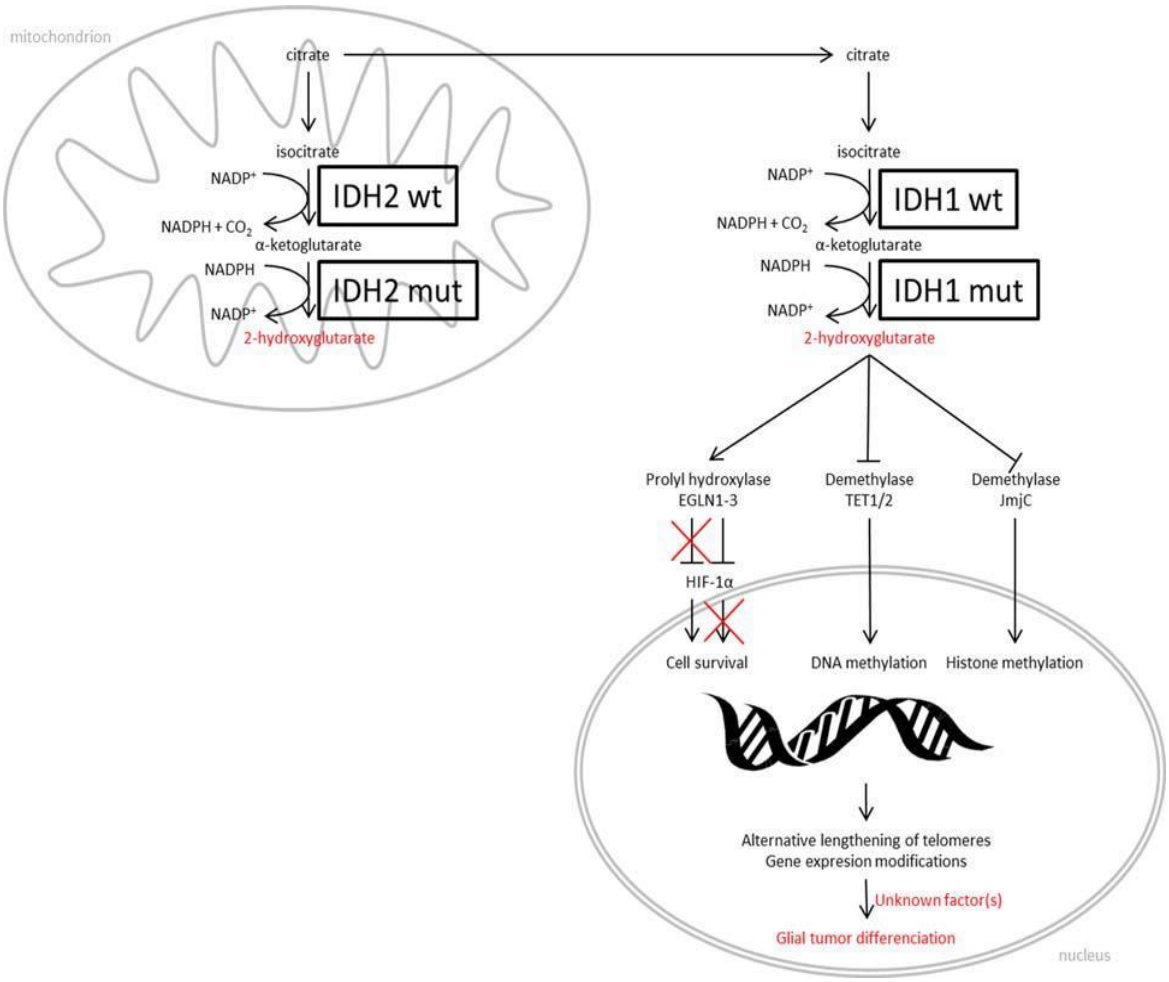

***Figure 5: Reactions of wild-type and mutant IDH enzymes in mitochondria and cytoplasm and consequences on* α-KG-dependent enzymes**

Wild-type (wt) IDH1 and IDH2 convert isocitrate to α-KG, in the cytoplasm or in mitochondria during the TCA cycle, respectively. Mutated IDH1/2 catalyzes the conversion of isocitrate to the oncometabolite 2-HG, leading to NADPH consumption and suppression of prolyl hydroxylase, and of DNA and histone demethylases. Consequences are i. a. gene expression modifications possibly provoking glial tumor differentiation (Megova et al. 2014).

1.6 Aims of the present thesis

Deregulation of the JmjC domain-containing family of histone demethylases leads to changes in pathways regulating the epigenome and the chromatin structure. In the last years some histone demethylases have also gained some interest due to their direct involvement in the DNA damage response and DNA repair as shown for the H3K9me3/me2 demethylase KDM4D or for the H3K36me2/me demethylase KDM2A. In addition, the JmjC domain-containing family of histone demethylases has attracted attention because its members rely on α-ketoglutarate as a co-factor in demethylation and can thus be inhibited by the oncometabolite 2-hydoxyglutarate, a product of mutated isocitrate dehydrogenases IDH1 or IDH2 (Chowdhury et al. 2011, Xu et al. 2011, Lu et al. 2012, Turcan et al. 2012, Kernytsky et al. 2015). To put it plainly, every aberration of histone demethylation either caused by direct inhibition of demethylases or by deregulation of their expression leads to disturbed regulation of transcription, replication or repair provoking genetic instability and carcinogenesis.

In recent work we observed a loss of di- and trimethylation of histone H3 at lysine 4 (H3K4) and a concomitant loss of active RNA polymerase II in γH2AX-decorated chromatin regions surrounding DNA double-strand breaks (DSB) after treatment with ionizing radiation (Seiler at al. 2011). As histone demethylases are quite specific and only the Jarid1 family of demethylases is able to remove di- and trimethylation at H3K4, we had four demethylases being possibly responsible for this effect. Since the histone demethylase Jarid1A (KDM5A/RBP2) is highly expressed in the cell lines used in that work and since it accumulates at laser-induced DNA damage sites (the others were not tested), it constitutes a strong candidate (Seiler et al. 2011).

The aim of the present thesis was to investigate the impact of siRNA-mediated depletion of histone demethylase Jarid1A (KDM5A, RBP2) on growth characteristics, cell survival, potential alterations in histone modifications and the chromatin structure. Preliminary data suggesting higher radiosensitivity of Jarid1A knockdown cells (Penterling 2013) should be verified and the causes of this observation should be revealed. To test for a potential role of the demethylase in the DNA damage response, cell cycle analysis experiments and recruitment kinetics of damage response proteins after Jarid1A depletion and irradiation was performed. I additionally checked for enhanced recruitment of Jarid1A to the damage site and for efficiency of DSB repair in Jarid1A-depleted cells via DSB repair reporter assays.

Another issue was the potential involvement of Jarid1A in the loss of di- and trimethylation at H3K4 at γH2AX regions surrounding ionizing radiation induced DSBs. To study this I performed intensity correlation analysis, with and without Jarid1A depletion, and also analysed the effects of inhibition of Jarid1B, ATM, ATR and PARP1. To elucidate the effects of the

Jarid1A depletion on transcriptional regulation, potential changes in gene expression after Jarid1A knockdown with and without irradiation were investigated via microarray experiments.

In the final part of this thesis glioblastoma cell lines were treated with the cell permeable ester of R-2-HG to mimic the IDH1 mutation. The impact of the unspecific inhibition of α-KG-dependent JmjC demethylases on the level of histone modifications as well as on cell proliferation and migratory behaviour was analysed.

2 Material

2.1 Cell lines

Cell line	Origin	Source	Medium
HeLa*	Human cervix carcinoma	DSMZ	RPMI-1640 + 10% FBS + 1% Penicillin/Streptomycin
HeLa pEJ	Human cervix carcinoma	Friedl group	RPMI-1640 + 10% FBS + 1% Penicillin/Streptomycin + 400 µg/ml G418
HeLa pGC	Human cervix carcinoma	Friedl group	RPMI-1640 + 10% FBS + 1% Penicillin/Streptomycin + 0.4 µg/ml Puromycin
HTC116	Human colorectal carcinoma	Kind gift of K. Lauber	McCoy's 5a Medium + 10% FBS + 1% Penicillin/Streptomycin
MCF-7*	Human breast adenocarcinoma	DSMZ	RPMI-1640 + 10% FBS + 1% Penicillin/Streptomycin
U2OS*	Human osteosarcoma	Kind gift of P. Grigaravicius	RPMI-1640 + 10% FBS + 1% Penicillin/Streptomycin
A172*	Human glioblastoma	Kind gift of K. Lauber	DMEM + 10% FBS+ 1% Penicillin/Streptomycin
U-87 MG*	Human glioblastoma	Kind gift of K. Lauber	DMEM + 10% FBS + 1% Penicillin/Streptomycin

* STR (short tandem repeat) typed cell lines

2.2 Solutions and reagents for cell culture and siRNA transfection

Product	Manufacturer
R-2-Hydroxyglutaric Acid Octyl Ester Sodium Salt	Toronto Research Chemicals
Cell-TAK Tissue Adhesive	BD Biosciences
Dimethylsulfoxid (DMSO)	Sigma-Aldrich
DMEM	Gibco
Fetal Bovine Serum (FBS)	Sigma-Aldrich
Geneticin disulfate (G418) Solution	Roth
Lipofectamine 2000	Invitrogen
McCoy's 5a	Sigma-Aldrich
Opti-MEM I Reduced Serum Medium	Gibco
Penicillin/Streptomycin	Sigma-Aldrich
Phosphate Buffered Saline (PBS)	Sigma-Aldrich
Puromycin Solution	Sigma-Aldrich
RPMI-1640	Sigma-Aldrich
Trypsin-EDTA	Sigma-Aldrich

2.2.1 Inhibitors

Inhibitor	Targets	Manufacturer
KU-60019	ATM	Selleckchem
Olaparib	PARP1	Selleckchem
PBIT	Jarid1B/KDM5B	Cayman Chemical
VE-821	ATR	Selleckchem

2.2.2 Stealth siRNAs

siRNA	Sequence	Manufacturer	Cat. Number
Stealth RNAi Jarid1A A1	CCA AAC UCC AGA UGU UGA UAG AUA U	Invitrogen	HSS109096
Stealth RNAi Jarid1A A3	GAG CCU GAG GUU CUC AGC ACU GAU A	Invitrogen	HSS109098
Stealth RNAi Negative Control Medium GC Duplex	unspecified	Invitrogen	12935-300

2.2.3 Plasmids

Plasmid	Resistance E.coli	Resistance human	Source
pEJ	Kanamycin	G418	Kind gift of W. Y. Mansour (Mansour et al. 2008)
pGC	Ampicillin	Puromycin	Kind gift of W. Y. Mansour (Mansour et al. 2008)
pMCC-GFP-P	Ampicillin	Puromycin	Designed in our lab.
pMCV-I-SceI	Ampicillin	-	Kind gift of W. Y. Mansour (Rouet et al. 1994; Mansour et al. 2008)

The sequences of the plasmids are listed in appendix A.

2.3 Reagents and buffers for protein extraction and Westernblotting

Reagent/buffer	Composition
4x Laemmli	9.6 ml Tris (1M, pH 8.6), 3.2 g SDS, 16 ml 21lycerine, 4 ml β-mercaptoethanol, 0.14 g bromphenol blue, 11.2 ml aqua dest.
Blocking solution (BSA)	5% BSA in PBS-T
Blocking solution (milk)	5% milk powder in PBS-T
ECL reagent	ECL Ultra solution A and B 1:1 (Lumigen Inc.)
SDS-PAGE running buffer I	20x NuPAGE MES SDS Running Buffer (Invitrogen) 1:20 in aqua dest.
SDS-PAGE running buffer II	20x NuPAGE Tris-Acetate Running Buffer (Invitrogen) 1:20 in aqua dest.
RIPA buffer	1% Triton X-100, 150 mM NaCl, 10 mM Tris, 1 mM EDTA, 1% deoxycholic acid
Rotiblock	10 Roti-Block (Roth) 1:10 in aqua dest.
Transfer buffer	20x NuPAGE Transfer Buffer (Invitrogen) 1:20 in aqua dest. + 10% methanol
Wash buffer for Westernblotting	0.1% Tween 20 in PBS (PBS-T)

2.4 Reagents and buffers for immunofluorescence

Reagent/buffer	Composition
Blocking buffer	1% BSA, 0.15% glycine in PBS
Fixation buffer	2% paraformaldehyde dissolved in PBS at 72°C
Permeabilization buffer	0.15% Triton X-100 in PBS
Pre extraction buffer	25 mM Hepes pH 7.5, 50 mM NaCl, 1 mM EDTA, 3 mM $MgCl_2$, 300 mM sucrose, 0.5% Triton X-100

2.5 Chemicals

Chemical	Manufacturer
100 bp DNA ladder gene ruler	Fermentas
Agarose peq GOLD	Peqlab
β-mercaptoethanol	Sigma-Aldrich
Boric acid	Merck
Bovine serum albumin (BSA)	Sigma-Aldrich
Calcium chloride	Alfa Aesar
Citric acid	Applichem
Complete Mini Protease Inhibitor	Roche
DAPI	Sigma-Aldrich
Deoxycholic acid	Sigma-Aldrich
Ditihiothreitol	Applichem
EDTA	Sigma-Aldrich

Ethanol absolut	VWR
Ethidium bromide	Roth
Glucose	Sigma-Aldrich
Glycine	Sigma-Aldrich
Glyzerin	Sigma-Aldrich
Hepes	Sigma-Aldrich
Magnesium chloride	Sigma
Methanol	Sigma-Aldrich
Methylen blue	Applichem
Micrococcal nuclease	Thermo Scientific
Milk powder	Roth
Nonidet P40 Substitute	Fluka
Paraformaldehyde (PFA)	Sigma-Aldrich
Phenol:Chloroform:Isoamyl Alcohol 25:24:1 Saturated with 10 mM Tris, pH 8.0, 1 mM EDTA	Sigma-Aldrich
PhosSTOP Phosphatase Inhibitor Cocktail	Roche
Potassium chloride	Sigma-Aldrich
Precision Plus Dual Color Protein Standard	BioRad
ProLong Gold antifade reagent	Molecular Probes
Propidium iodide solution	Sigma-Aldrich
Proteinase K	Merck
Rnase A	Sigma-Aldrich
Rnase Zap Wipes	Ambion
Sodium acetate	Merck
Sodium butyrate	Sigma-Aldrich
Sodium chloride	Merck
Sodium citrate	Roth
Sodium dodecyl sulfate (SDS)	Sigma-Aldrich
Sucrose	Roth
Tris	Merck
Tween 20	Sigma-Aldrich
Triton X-100	Sigma-Aldrich
Vectashield	Vector Laboratories

2.6 Antibodies

2.6.1 Antibodies for Westernblotting

Antibody	**Source**	**Dilution**	**Blocking solution**
goat-anti-mouse-HRP	Santa Cruz sc-2005	0.35 µl/ 20 ml	Same as primary antibody
goat-anti-rabbit-HRP	Santa Cruz sc-2004	0.25 µl/ 20 ml	Same as primary antibody
mouse-anti-Jarid1A	Abcam ab78322	1:1000	5% BSA
mouse-anti-Jarid1B	Sigma-Aldrich SAB1404865	1:4000	5% milk
mouse-anti-H3	Millipore 05-1341	1:5000	5% milk

mouse-anti-H3K4me3	Abcam ab12209	1:1000	Roti block
mouse-anti-H4	Abcam ab31830	1:1000	5% milk
mouse-anti-HDAC3	Upstate 06-890	1:750	5% milk
mouse-anti-PARP1	Trevigen 4338-MC-50	1:2000	5% milk
mouse-anti-Tubulin α	Abcam ab7291	1:6000	Roti block
mouse-anti-γH2AX	Millipore 05-636	1:2000	5% milk
rabbit-anti-CENPF	Novus Biologicals NB500-101	1:1000	5% milk
rabbit-anti-H3K4me3	Abcam ab8580	1:1000	Roti block
rabbit-anti-H3K4me2	Abcam ab32356	1:1000	Roti block
rabbit-anti-H3K9me3	Millipore 07-442	1:1000	Roti block
rabbit-anti-H3K9me2	Millipore 04-768	1:1000	Roti block
rabbit-anti-H3K9ac	Millipore 06-942	1:1000	Roti block
rabbit-anti-H3K56ac	Millipore 07-677	1:1000	Roti block
rabbit-anti-H4K16ac	Millipore 07-329	1:1000	5% milk
rabbit-anti-HSP90	Cell Signaling 4877	1:1000	5% milk
rabbit-anti-NFKBIE	Sigma-Aldrich SAB4300544	1:1000	5% milk
rabbit-anti-p21	Cell Signaling 2947P	1:1000	5% BSA

2.6.2 Antibodies for immunofluorescence

Antibody	**Source**	**Dilution**
mouse-anti-Jarid1A/RBP2	Abcam 78322	1:400
mouse-anti-BRCA1	Abcam 16780	1:100
mouse-anti-H3K4me3	Abcam ab12209	1:500
mouse-anti-RNAPol II	Kindly provided by D. Eick	1:10
mouse-anti-Ubiquitin-conjug.	Biomol PW8810	1:1000
mouse-anti-XRCC1	Abcam ab1838	1:500
mouse-anti-γH2AX	Millipore 05-636	1:500
rabbit-anti-53BP1	Novus Biologicals NB100-305	1:500
rabbit-anti-H3K4me3	Abcam ab8580	1:400
rabbit-anti-pChk1	Cell Signaling 2348	1:100
rabbit-anti-pChk2	Cell Signaling 2661	1:100
rabbit-anti-Rad51	Calbiochem PC130	1:250

2.7 Primer for qRT-PCR

TaqMan Gene Expression Assay FAM-MGB 20x (Thermo Scientific)	**Assay ID**
KDM5A	Hs00231908_m1
β-Actin	Hs01060665_g1
GAPDH	Hs99999905_m1

2.8 Kits

Kit	Manufacturer
TaqMan® Gene Expression Master Mix	Thermo Scientific
RNeasy Mini Kit	Qiagen
SuperScript First-Strand Synthesis System for RT-PCR	Thermo Scientific
Mycoplasma Detection Kit for conventional PCR Venor GeM Classic	Minerva Biolabs
SurePrint G3 Human Gene Expression v2 8x60K Microarray Kit	Agilent Technologies
Low Input Quick Amp Labeling Kit, One-Color	Agilent Technologies
Subcellular Protein Fractionation Kit	Thermo Scientific
RNA 6000 Nano Kit	Agilent Technologies
Qubit RNA BR Assay Kit	Thermo Scientific

2.9 Equipment

Instrument	Manufacturer
SLI 18 linear accelerator	Elekta
Flow Cytometer BD LSR II	Becton Dickinson
Bioanalyzer 2100	Agilent Technologies
AxioCam Mr3 camera	Zeiss
Chemismart documentation system	PeqLab
Nitrocellulose Blotting Membrane 0.2 µm	GE Healthcare
NanoDrop 2000 spectrophotometer	Thermo Scientific
Microarray Hybridization Oven	Agilent Technologies
AxioObserver Z1 Microscope	Zeiss
ViiA 7 Real Time PCR System Cycler	Thermo Scientific
SureScan Microarray Scanner	Agilent Technologies
Qubit 2.0 Fluorometer	Thermo Scientific

3 Methods

3.1 Cell biology methods

3.1.1 Cultivation of cells

Detailed information about the origin and the cultivation conditions of the cell lines are listed in chapter 2.1. All used cell lines have a human origin and adherent growth properties. Periodically monitoring for mycoplasma infection was performed by PCR (Kit Minerva Biolabs) and only cell lines negative for mycoplasma were used for experiments. HeLa, MCF-7 and U2OS cells were cultivated in RPMI 1640 medium, HCT116 cells were cultivated in Mc Coy`s 5 A medium and the glioblastoma cell lines A172 and U-87 MG were grown in DMEM medium. All media were supplemented with 10% FBS, 100 U/ml penicillin and 50 µg streptomycin. Cell lines were kept in a humidified incubator at 37°C with 5% CO_2. For optimal growth conditions, cells were split 1:10 every three to four days. For this the old medium was removed and the cells were washed with PBS. For detachment of the cells Trypsin/EDTA was added to the cell layer and the sample was incubated for 5 min at 37°C. To stop the enzymatic reaction of the Trypsin cells were resuspended in supplemented medium. One-tenth of the cell suspension was transferred to a new culture vessel with medium and further cultivated in the incubator. To seed a designated amount of cells cell number was determined with a Buerker counter chamber after trypsinization and resuspension.

For long-term storage cells were collected by centrifugation and the pellet was resuspended in freezing solution containing 10% DMSO as frost protection agent and 90% FBS. The suspension was transferred to a 2 ml cryo tube. The tube was placed in a freezing box with isopropanol enabling the gentle freezing of cells by cooling of 1°C per minute. The box was transferred to a -80°C freezer overnight. The following day, the cryo tubes were relocated from –80°C into liquid nitrogen for long-term storage. Thawing of cells has to be performed quickly as the DMSO is toxic for cells at RT. After incubation of the cryo tube at 37°C for 1 min, the cell suspension was transferred to a tube with 10 ml prewarmed supplemented medium. Cells were collected by centrifugation, resuspended in fresh supplemented medium and seeded in new vessels. To remove residual DMSO, the medium has to be replaced the following day.

3.1.2 Seeding of cells for irradiation

For irradiation with x-rays cells can be seeded in usual plastic culture vessels as this sort of radiation can entirely pass the material. Thus, for colony formation assays or Western Blot analysis after x-rays, cells were seeded in 6 well plates. If immunofluorescence detection was performed, cells were seeded on glass coverslips in 6 well plates.

For irradiation with accelerated 55 MeV carbon ions at the ion microirradiation facility SNAKE (see chapter 3.1.3.2), cells were seeded 24 h prior to irradiation on 6 µm Mylar foil fixed in stainless steel containers (Figure 6) or steel rings (Figure 7). While glass or plastic culture vessels would hinder the ions from transition, the Mylar foil enables the passage of the ions to the cell layer. Proper attachment of the cells is ensured by pre-coating the foil with Cell-TAK (BD Bioscience). The steel containers can be equipped with a foil, where a grid of coordinates is indicated. This facilitates the location of the irradiated area after applying single ions in a distinct pattern (e.g. lines or matrix pattern) to the cells. For irradiation in a small angle, cells were seeded on Mylar foil in steel rings.

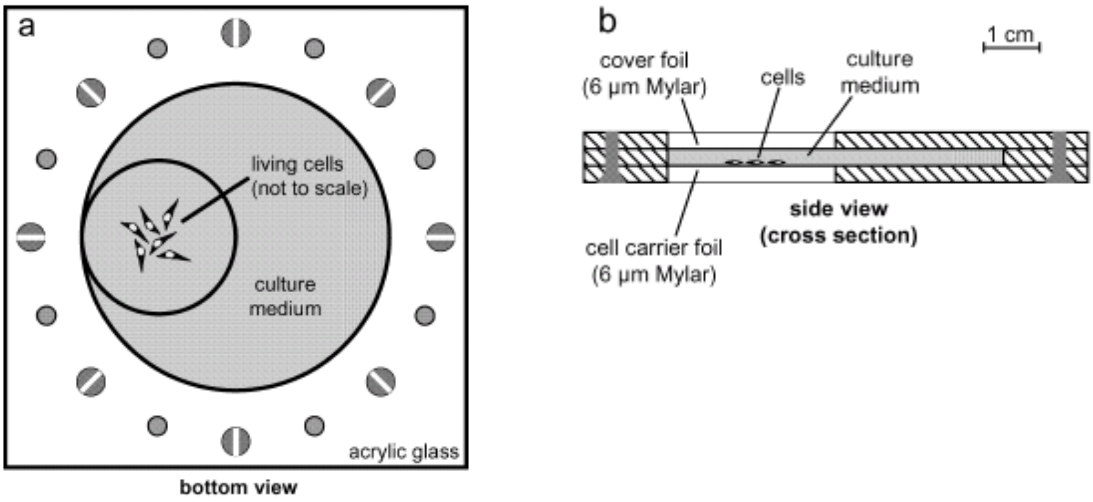

Figure 6: Steel container for irradiation of cells in a distinct pattern at the ion microbeam SNAKE
(a) Bottom view of the cell chamber. Cells are attached to the inserted Mylar foil in the midddle. (b) Side view of the container. For irradiation the chamber is closed with a lid (Hauptner et al. 2004).

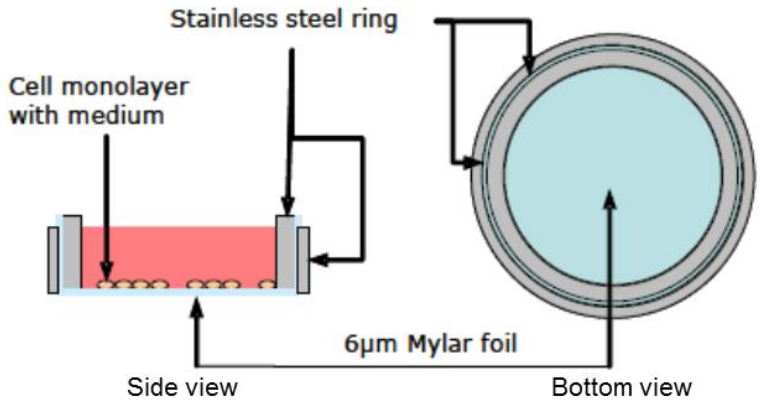

Figure 7: Steel ring for small angle irradiation of cells at the ion microbeam SNAKE
Outlined are the side and the bottom view of the ring chamber with the inserted Mylar foil in the middle (Auer et al. 2011).

3.1.3 Irradiation of cells

3.1.3.1 Irradiation with x-rays

Irradiation with different doses of X-rays was performed with an Elekta SLI 18 linear accelerator (dose rate 2 Gy/min).

3.1.3.2 Ion microirradiation with SNAKE

The ion microbeam SNAKE (Superconducting Nanoscope for Applied Nuclear Experiments) at the 14 MV tandem accelerator in Garching enables targeted irradiation of structures in cells or cell nuclei with single ions of a broad energy range. The possibility to applicate single ions to nuclei in a distinct pattern makes SNAKE a perfect tool to analyse DSB repair. In this way it is possible to distinguish between ion-induced and spontaneous foci. Subsequent detection of specific DNA damage factors and potential changes in histone modifications by indirect immunofluorescence helps to elucidate the procedure of DNA damage response directly at the DSBs.

For analysis of correlation between γH2AX and H3K4me3 or RNA Pol II after ion irradiation, cells were irradiated with single ions applied in a linear pattern with 1 µm lateral distance and 5 µm distance between the “lines” thus formed (Hable et al. 2012), or in a matrix pattern of 5 µm x 5 µm distance (Girst et al. 2013; Drexler et al. 2015). In this set-up, single ions arrive at a perpendicular angle to the cell layer (Figure 8), which results in a dose of approximately 0.46 Gy per ion hit.

After closing the cell container with a lid it can be clamped in a perpendicular angle between the exit nozzle of the ion beam and a detector (Figure 8). During irradiation the cell layer is not

covered with medium as this would arrest the ions during the transition. With the help of the integrated microscope, a suitable position of the cell layer is defined for irradiation and noted with the help of the coordinates indicated on the Mylar foil. Thereby the irradiated area can be localized easily later on during microscopy. After the irradiation of the cells, the lid of the container was removed and the medium was replaced. Before fixation the cells were incubated for 1 h in a humidified incubator at 37°C to start the DNA damage response signaling.

For analysis of foci formation after Jarid1A knockdown I performed small angle irradiation in steel rings, where the ion beam hits the cell layer at an angle of 10° (Figure 8), allowing to visualize protein accumulations along the track of ion-induced damage (Du et al. 2011). After irradiation cells were incubated in fresh medium for different periods of time, dependent on the purposes of the experiments. Subsequently, cells were fixed and immunofluorescence was performed.

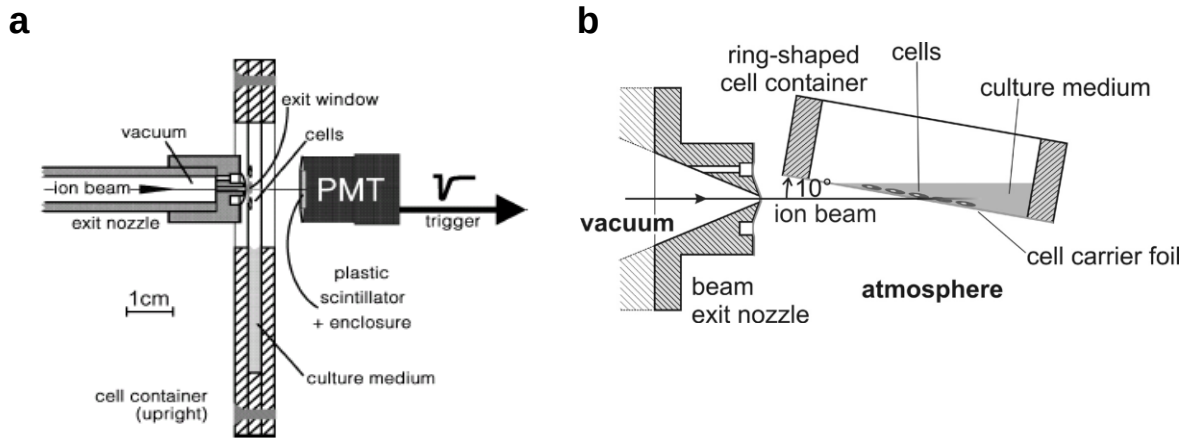

Figure 8: Position of cell container and steel ring during irradiation at SNAKE

(a) In the container cells are located between the exit nozzle of the ion beam and a scintillator and are irradiated in a perpendicular angle (Hauptner et al. 2004). (b) Cells in steel rings are irradiated at an angle of 10° (Hauptner et al. 2006).

3.1.4 Transfection of cells with siRNA

Double-stranded short interfering RNAs (siRNAs), consisting of 21-23 RNA nucleotides, can be used to rapidly silence the expression of specific genes.

To study the effects of the demethylase Jarid1A I depleted the protein via transfection with siRNA. All siRNA transfections were performed with stealth siRNAs using Lipofectamine 2000 as transfection reagent (both purchased from Life Technologies). The stealth scrambled (scr) RNAi was used as control to exclude transfection effects. If not indicated otherwise, a 1:1

combination of the two siRNAs A1 and A3 was used as this resulted in the highest knockdown efficiencies (Penterling 2013).

For transfection 180000 cells were seeded in 6 well plates in medium without penicillin/ streptomycin. SiRNA transfection was performed the following day (12-16 h after seeding recommended). In the first step, separate mixtures of the siRNA and serum-reduced OPTI-MEM I medium and of Lipofectamine 2000 and OPTI-MEM I were prepared and incubated for 15 min at RT. Per sample, 2.5 µl Lipofectamine and 6.25 µl of the respective siRNA was used and diluted with OPTI-MEM I to 250 µl, resulting in a siRNA concentration of 50 pmol. In a second step, the Lipofectamine 2000 mixture was combined 1:1 with the single siRNAs mixtures and again incubated for 15 min at RT. After this second incubation, 500 µl of the siRNA/ Lipofectamine 2000 mixtures were added to the cells.

Depending on the purposes of the experiment, cells were irradiated or harvested 72 h later. For DSB-repair assay cells were transfected with I-SceI 24 h later. Efficiency of depletion was verified for every single experiment by Western Blotting and Jarid1A was normalized to the sample transfected with scr siRNA.

3.1.5 Cell Cycle Analysis

For cell cycle analysis after Jarid1A depletion 20000 HeLa cells per well were seeded 48 h after siRNA transfection into 24 well plates and allowed to adhere overnight. After irradiation of the cells with 0 Gy or 5 Gy at the next day, cells were incubated and harvested at different time points (before irradiation and 4 h, 8 h, 12 h, 24 h, 48 h after irradiation). Cell suspension was centrifuged, pellet was washed with PBS and resuspended in DNA staining solution I for fixation and staining (see Table 1). After incubation for 30 min at RT in the dark, DNA staining solution II was added (see Table 1). Samples were stored at 4°C until cell cycle data were collected with FACS BD LSR II (Becton Dickinson). Forward scatter (FSC), sideward scatter (SSC), and PI fluorescence of the nuclei were analyzed flow cytometrically and all nuclei with less than diploid DNA content were considered apoptotic. Evaluation was performed with the free flow cytometry software FlowPy.

Table 1: Composition of DNA staining solution I and II for cell cycle analysis

Solution	Composition
DNA staining solution I	10 µg/ml RNase, 0.6 mg/ml NaCl, 1 mg/ml Sodium citrate, 0.07% NP-40, 10 µg/ml propidium iodide (PI) in PBS
DNA staining solution II	15 µg/ml citric acid, 85 µg/ml sucrose, 10 µg/ml PI in PBS

3.1.6 Colony formation assay

To determine the sensitivity to radiation after Jarid1A depletion in a colony formation assay 72 h after siRNA transfection cells were plated in triplicates in a range of 150 – 50000 cells per well depending on the dose of radiation. After attachment of the cells, 6 well plates were irradiated with 0 Gy, 2 Gy, 5 Gy or 10 Gy x-rays and incubated for 10 days in a humidified incubator.

Fixation and staining was done by incubating the cells in a solution consisting of 0.3% methylene blue and 80% ethanol for 30 min at RT. After removing the solution, cells were washed with aqua dest. and air-dried. Colonies comprising more than 50 cells were counted. Cell survival curves were calculated with the following linear-quadratic model:

S0e - ad - bd^2

S0 represents the plating efficiency, d the radiation dose, a [Gy-1] the linear coefficient and b [Gy-2] the coefficient of the quadratic component. Curve coefficients were calculated with the R-package CFAssay (Braselmann 2014; Braselmann et al. 2015) using the maximum likelihood method. Curves were compared with the F-test (Faraway 2006).

3.1.7 Incubation of glioblastoma cells with 2-hydroxyglutaric acid

IDH1 mutations can be simulated by addition of 2-hydroxyglutaric acid octyl ester sodium salt (2-HG) to glioblastoma cells (Dang et al. 2009; Reitmann et al. 2014). U-87 MG and A172 cells were seeded in 6 well plates and incubated with different concentrations of 2-HG for 7 d. As no manufacturer`s instructions were available, 2-HG was solved in DMSO and concentrations

from 0.01 mM to 1.0 mM of 2-HG were used and added to the cells. It was reported that a concentration of 0.1 mM R-2-HG in the medium for 7 d results in the same level of intracellular R-2HG as produced in knock-in IDH1 mutant HTC116 cells (Reitmann et al. 2014). DMSO was added to the cells as control. After 7 d either wound healing assays to study migration or extraction of proteins for Western blotting was performed.

3.1.8 Wound healing assay

To investigate the migration of glioblastoma cells after incubation with 2-HG, wound healing assays were performed. Cells were seeded into silicone culture inserts consisting of two chambers for cell seeding separated with a defined gap (µ-dishes, Ibidi) placed in conventional culture dishes. 35000 U-87 MG cells were seeded in each of the two areas with 0.22 cm² and allowed to attach overnight. To compare the migratory capacity of different treated cells, one culture insert was provided with control cells, while a second insert was provided with cells treated with 2-HG for 6 d. On the next day when cells reached confluency, the cell-free gap of 500 µm was generated for both samples by removing the insert. Cell migration into the “wound” was monitored using an inverse microscope with a 5x objective and an AxioCam Mr3 camera (Zeiss). Images were acquired every 30 min over a period of 8 h using the AxioVision 4.6 software (Zeiss). Every 30 min the cell free area was measured with the function “Analyze” and “Measure” in WCIF ImageJ 1.37c. The colonized area was calculated according to the following formula:

Colonized area at t_1 [μm^2] = Cell free area [μm^2] at t_1 - cell free area in [μm^2] at t_0

Potential existing differences in the rate of migration of control cells and 2-HG treated cells can finally be revealed by comparing the colonized area over time.

3.2 Biochemical methods

3.2.1 Protein extraction and Westernblotting

3.2.1.1 Whole cell protein extraction

To prepare whole cell protein lysates cells were trypsinized, counted and collected by centrifugation (5 min, 500 x g, 4°C). The proteins were extracted by adding RIPA-buffer supplemented with PhosSTOP Phosphatase Inhibitor, Complete Mini Protease Inhibitor (Roche) and 5 mM sodium butyrate as HDAC inhibitor. To ensure similar protein amount in the samples, 20 µl buffer per 100 000 cells was used for lysis. After vigorous vortexing, lysates

were incubated for 10 min on ice, heated for 10 min to 104°C and subsequently stored at -80°C until usage.

3.2.1.2 SDS-PAGE and Western immunoblotting

For separation of the proteins, lysates were thawed on ice and cleared by centrifugation for 5 min at 11000 x g at 4°C. 4x Laemmli loading dye was added to the lysates and heated to 95°C for 10 min. Depending on the size of the protein of interest, lysates were loaded on 3-8% Tris-Acetate or 12% Bis-Tris NuPAGE gels (Invitrogen) and separated by electrophoresis for 1.5 h at 120 V.

After separation of the proteins via SDS-PAGE, they were transferred to a nitrocellulose membrane. For this, 6 Whatman papers, 2 sponges, the nitrocellulose membrane and the gel were equilibrated in 1x transfer buffer (Invitrogen) + 10% methanol and stacked together that the negative charged proteins from the gel were transferred to the membrane via electricity. The transfer was performed over night at 40 V and 4°C in a blotting chamber filled with transfer buffer. After immunoblotting membranes were cut and blocked for 1 h at RT with Roti-Block (Roth), 5% milk or 5% BSA, each in PBS + 0.1% Tween, depending on the primary antibody used (see chapter 2.6.1). Primary antibodies were diluted in the respective blocking solutions and membranes were incubated in 2 ml of the antibody solution for 1 h at RT or overnight at 4°C in rotating 50 ml tubes. After three washing steps with PBS + 0.1% Tween for 5 min at RT, membranes were incubated with the appropriate goat polyclonal secondary antibodies, coupled with horse reddish peroxidase (HRP). 0.35 µl of goat-α-mouse-HRP and 0.35 µl of goat-α-rabbit-HRP (Santa Cruz) per 20 ml blocking solution were used and membranes were incubated for 45 min at RT. Following three more washing steps with PBS + 0.1% Tween for 5 min and a short wash in PBS, membranes were developed with Lumigen ECL Ultra (TMA-6). Therefore, solution A and solution B of the ECL kit were mixed 1:1 and membranes were incubated for 5 min at RT in the dark. Chemiluminescence was detected and images were acquired with a CHEMISMART documentation system (Peqlab, Vilber Lourmat) and the Chemi-Capt 5000 software. Quantitative analysis was performed with the Bio-1D software (Vilber Lourmat). The signals were normalized with respect to the scr siRNA transfected, unirradiated or - in the case of 2-HG incubation – to the control samples (DMSO).

3.2.2 Subcellular Protein Fractionation

To analyse the localization of Jarid1A in the cell after irradiation a stepwise extraction of proteins from different cell compartments was performed with the Subcellular Protein Fractionation Kit (Thermo Scientific). All buffers were supplemented 1:100 with a Protease Inhibitor Cocktail directly before use. Ice-cold CEB buffer was added to the cell pellet and the

extraction was started by using the volumes indicated in Table 2 depending on the number of cells:

Table 2: Buffer volumes for different packed cell volumes. 1x10^6 HeLa cells are equivalent to 10 µl packed cell volume

Packed Cell Volume (µl)	CEB (µl)	MEB (µl)	NEB (µl)	NEB (µl) + $CaCl_2$, MNase	PEB (µl)
10	100	100	50	50	50
20	200	200	100	100	100
50	500	500	250	250	250

If not indicated otherwise, all incubation and centrifugation steps were performed at 4°C with ice-cold buffers. Cell pellets with CEB buffer were mixed gently for 10 min before centrifugation at 500 x g for 5 min. The supernatant was transferred to a pre-chilled tube (cytoplasmic extract). MEB buffer was added to the remaining cell pellet and the tube was vortexed vigorously for 5 s. After incubating the tube for 10 min with gentle mixing, it was centrifuged at 3000 x g for 5 min. The supernatant containing the membrane proteins was transferred to a pre-chilled tube. The pellet was mixed with NEB buffer, vortexed for 15 s and then incubated for 30 min with gentle mixing. After the following centrifugation step at 5000 x g for 5 min, the supernatant was again transferred to a new tube (soluble nuclear extract). The buffer for the extraction of chromatin-bound proteins was prepared by adding 5 µl of 100 mM $CaCl_2$ and 3 µl MNase to 100 µl NEB buffer at RT. This supplemented buffer was added to the cell pellet at RT. The tube was vortexed vigorously for 15 s and incubated for 5 min at 37°C. After vortexing the tube again for 15 s and centrifugation at 16000 x g for 5 min, the supernatant (chromatin-bound nuclear extract) was transferred to a pre-chilled tube. For my purposes the extraction of the final fraction - the cytoskeletal proteins - was not necessary.

The different fractions were either directly used for Western Blotting or stored at -80°C until usage.

3.2.3 Immunofluorescence

For the immunofluorescence staining experiments cells were grown on glass coverslips or Mylar foils. If not indicated otherwise, a volume of 2 ml for 6 well plates and steel rings and a volume of 3 ml for steel containers were used for all steps of the immunofluorescence protocol (except for the incubation with antibodies). After treatment and different incubation periods, medium was removed and cells were washed with PBS. Fixation of the cells was performed

for 15 min with 2% paraformaldehyde. After that cells were washed 1x with PBS and permeabilized by three incubation steps with PBS + 0.15% Triton X-100 for 5 min. Before incubation with primary antibodies, nonspecific binding sites were blocked three times for 10 min with PBS containing 1% BSA and 0.15% Glycine. Cells were then stained with 75 µl of the appropriate primary antibody solution (antibody diluted in blocking solution) for 1 h at RT or overnight at 4°C in a humidified chamber. Subsequently, the samples were washed for 5 min with PBS, for 10 min with PBS + 0.15% Triton X-100 and again for 5 min with PBS. Following another blocking step for 7 min, the cells were incubated with 75 µl of the secondary antibody solution for 45 min at RT in a humidified chamber. From this on, all steps need to be performed in the dark as secondary antibodies are coupled with a fluorochrome. After additional washing steps with PBS 1x for 10 min and 2x for 5 min, DNA was counterstained with DAPI. Therefor a stock solution of 1 mg/ ml was diluted 1:10000 in PBS and added to the cells. After 90 s incubation of cells with the DAPI solution, remaining DAPI was removed by two washing steps with PBS for 2 min. For mounting 10 µl Vectashield or a drop of Prolong Gold was added to a Ø 22 mm cover glass and applied to the cell layer without producing bubbles. In the case of a steel ring or container the foil with the attached cells mounted with a cover glass was cut out with a soldering bolt, sticked to an objective slide and sealed with nail polish. Samples mounted with Vectashield should immediately be transferred to 4°C and have to be visualized soon, while longer-lasting samples mounted with Prolong Gold need to harden for at least 24 h at RT before transferring them to 4°C.

3.3 Epifluorescence microscopy

Image acquisition was performed with an inverse epifluorescence microscope (Zeiss AxioObserver Z1) using a Zeiss LCI Plan Neofluor 63×/1.3 glycerine objective, the software AxioVision 4.8 and a AxioCam Mrm camera (Zeiss). Z-stacks were collected sequentially for all channels with 250 nm distance between optical sections. Filters used were 01 (BP 365/12) for DAPI, 38HE (BP 470/40 (HE) for GFP or A488 and filter 20 (BP 546/12) for Cy3 (all obtained from Zeiss).

All z-stack images were deconvolved with Huygens deconvolution software (Scientific Volume Imaging) (Greubel et al. 2008). Images were further processed using the free software WCIF (Wright Cell Imaging Facility) ImageJ 1.37c (www.uhnresearch.ca/wcif).

3.3.1 Image processing for intensity correlation analysis

Images used for intensity correlation analysis (Li et al. 2004) had to be processed according to the instructions for the ImageJ-based ICA (intensity correlation analysis) module. The nucleus was cut out from the image in all channels by “Polygon Selection”. The sharpest three to four sections of the z-stack were selected and remaining sections removed with the plug in “Slice Remover”. Gray values were normalized to 8 bit via the plug in “Eightbit Converter”. Subsequently a background subtraction was performed. Therefore, the background was measured in areas without any signals, e.g. nucleoli. By choosing the plug-in “Background Substraction” mean intensity of the background signal plus standard deviation was subtracted from the image. It is necessary to normalize the gray values again to 8 bit before accomplishing the analysis via the plug-in “Intensity Correlation Analysis”. This plug-in enables the qualitative and quantitative measuring of the correlation between pixel pairs in the red (Cy3) and the green (Alexa488) channels. More precisely the “product of the differences from the mean” (PDM) is calculated by $(A_i\text{-}a)*(B_i\text{-}b)$, where A_i and B_i represent the intensities of the single pixel pairs, while a and b represent the mean intensities of the pixels in both channels. In the case of colocalization, the intensities of the pixel pairs are similar and as a result the PDM will have a positive value. If the pixel pairs are randomly distributed, the PDM is around zero. PDM value will be negative, when the pixel pairs show anti-correlation. The plug in compiles a PDM plot of every channel that shows the distribution of the pixel intensities and the PDM values. Additionally a scatter plot is compiled, which shows the pixel intensities of the channels 1 and 2. This enables to differentiate between high and low intensities and its correlations (Figure 9). Furthermore, a LUT (Look Up Table) is produced to give an overview of the PDM values. Negative correlation is indicated in pink, positive correlation in green and random distribution in black (see PDM maps in chapter 4.1.7). The plots and the LUT only permit qualitative evaluation of the pixel correlation.

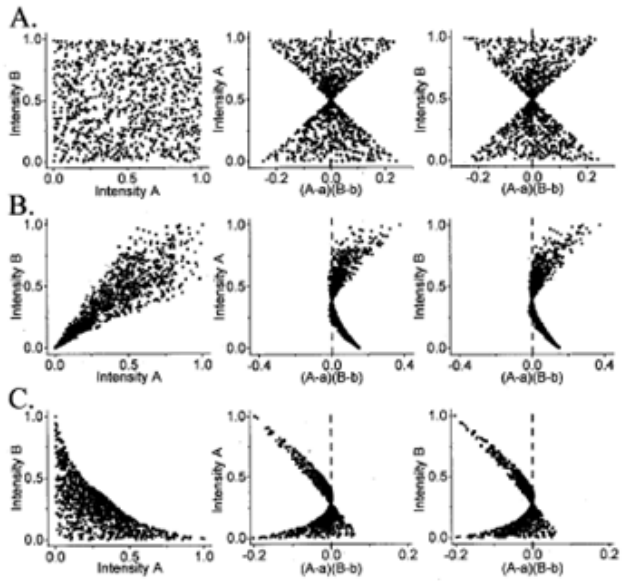

Figure 9: Intensity correlation analysis for three simulated cases

(A) Random distribution of pixels, **(B)** positive correlation and **(C)** negative correlation between pixel pairs. The analysis calculates the product of the differences from the mean (PDM) for pixel pairs of two channels (channel A and B) with the following formula: PDM = (Ai-a)*(Bi-b). The scatter plots on the left show the distribution of pixels in both channels with their corresponding intensities. PDM plots in the middle and on the right show the PDM values with corresponding intensities for every pixel (Li et al. 2004).

3.3.2 Quantitative analysis of γH2AX, BRCA1, 53BP1 and Rad51 foci

For foci analysis with ImageJ, deconvolved z-stacks were converted to an 8-bit format. The settings of the PlugIn FociPicker 3D (Du et al. 2011) had to be optimized for the different antibody stainings by changing the parameters “Tolerance Setting” and “Minimal pixels number in the focus”. The output is a 3D FociMask that displays all counted foci in different colours, a result table, where the number of foci per cell and the size of each focus is listed and a log file as summary of each processed image with file name, parameter setting and number of foci detected. For determination of residual foci, the foci number and size of at least 20 cells per sample were evaluated.

For determination of foci forming capability of BRCA1, 53BP1 and Rad51 at least 50 cells with clearly identifiable γH2AX tracks were evaluated. Cells were categorized into (1) full overlap of protein in question with γH2AX track, (2) some foci of protein in question coinciding with γH2AX track, or (3) no foci of protein in question coinciding with γH2AX track.

3.4 Molecular biological methods

3.4.1 Isolation of RNA

For microarray analysis or quantitative real-time PCR total RNA was isolated using the RNeasy Mini Kit (Qiagen). After harvesting the cells, lysis was performed by adding 350 µl (<5*10^6 cells) RLT buffer to the cell pellet. Homogenization was accomplished by vortexing the lysates. After addition of 350 µl 70% ethanol, lysates were mixed well by pipetting and transferred to an RNeasy spin column. The columns were centrifuged for 15 s at 8000 x g and the flow-through was discarded. The columns were washed with 700 µl buffer RW1 and two times with 500 µl buffer RPE. Before placing the columns in new collection tubes, an additional centrifugation step at full speed for 1 min was performed to remove residual RPE buffer. For elution of the RNA 30 µl RNase-free water were directly added to the column and centrifuged for 1 min at 8000 x g.

RNA was quantified using the NanoDrop 2000 spectrophotometer (Thermo Scientific). To determine the RNA concentration in ng/µl the absorption at 260 nm was measured. The 260/280 ratio should be around 2.0, while the 260/230 ratio should be in the range of 2.0-2.2. Lower ratios indicate the presence of contaminants.

As RNA is highly instable, the samples were immediately frozen at -80°C or transcribed into cDNA.

3.4.2 Reverse transcription

Isolated RNA was transcribed into cDNA with the SuperScript First-Strand Synthesis System for RT-PCR (Thermo Scientific). In the first step, 1 µg RNA was mixed with the dNTP mix, random hexamer primers and diethylpyrocarbonate (DEPC)-treated water to get a total volume of 10 µl per sample as follows:

Table 3: Preparation of RNA-primer mix

Component	Amount
RNA	1 µg
10 mM dNTP mix	1 µl
Random hexamers (50 ng/µl)	1 µl
DEPC-treated water	add to a total volume of 10 µl

This RNA-primer mix was incubated for 5 min at 65°C and then transferred to ice for at least 1 min. In the second step, a 2 x reaction mix of RT buffer, $MgCl_2$, DTT and RNase OUT was prepared and added to the RNA-primer mix (see Table 4).

Table 4: Preparation of 2x reaction mix for reverse transcription

Component	Amount
10 x RT buffer	2.0 µl
25 mM $MgCl_2$	4.0 µl
0.1 M DTT	2.0 µl
RNase OUT (40 U/µl)	1.0 µl

After incubation for 2 min at RT, 1 µl of Super Script II reverse transcriptase was added and incubated for 10 min at RT and afterwards for 50 min at 42°C. The reverse transcription reaction was terminated by incubation for 15 min at 70°C. Finally, RNase H was added and samples were incubated for 20 min at 37°C. Synthesized cDNA was directly used for PCR or stored at -80°C.

3.4.3 Quantitative real-time PCR

To verify the Jarid1A *knockdown* on mRNA level in the samples used for microarray analysis, quantitative real-time PCR (qRT-PCR) was used. QRT-PCR enables to study the relative expression levels of a gene of interest in comparison to a stably expressed housekeeping gene. qRT-PCR was performed in a 384 well plate format on a ViiA 7 Real Time PCR System Cycler (Thermo Scientific). The TaqMan probe is coupled with a FAM dye label on the 5' end and a quencher on the 3' end. During synthesis the Taq polymerase cleaves the probe via its 5´–3´ exonuclease activity, which results in a fluorescence signal that is directly proportional to the amount of DNA template in the PCR.

The PCR was performed in triplicates. Used housekeeping genes were beta-actin and GAPDH. The qRT-PCR reaction mix was prepared as follows:

Table 5: Reaction mix for qRT-PCR

Component	Amount
20 x TaqMan gene expression assay (probe)	0.5 µl
2 x TaqMan gene expression mastermix	5.0 µl
RNase-free H_2O	3.5 µl

9 µl of the reaction mix were pipetted into the wells on ice. 1 µl cDNA or - in the case of a negative control – H_2O were added to each well. The plate was sealed with a foil, centrifuged briefly and loaded into the cycler. qRT-PCR was performed under the following conditions:

Table 6: Thermal cycling conditions for qRT-PCR

Stage	Temp (°C)	Time (mm:ss)
Hold	95	10:00
Cycle (40 cycles)	95 60	00:15 01:00

The relative amounts of mRNA can be calculated by establishing the cycle threshold (Ct) values of the reference genes and the genes of interest. The Ct value is the number of PCR cycles that is necessary to reach a fluorescence intensity signal that is higher than the background signal. In the first step of the evaluation the Ct value of the reference gene is subtracted from the gene of interest:

$$\Delta Ct = Ct\ (gene\ of\ interest) - Ct\ (reference\ gene)$$

In the next step the Δ Ct value of the control sample is subtracted from the Δ Ct value of the treated sample:

$$\Delta\Delta Ct = \Delta Ct\ (treated\ sample) - \Delta Ct\ (control\ sample)$$

The relative expression of the treated sample compared to the control sample is called ratio and can be calculated as follows:

$$Ratio = 2^{-\Delta\Delta Ct}$$ (Pfaffl 2001).

3.5 MNase digestion

Digestion of chromatin by the enzyme micrococcal nuclease (MNase) represents a simple method to obtain information about the compaction of chromatin. MNase cuts the DNA between the nucleosomes leading to polynucleosomal or mononucleosomal DNA dependent on incubation time and concentration of the enzyme. These fragments with different size can be separated via gel electrophoresis and give a hint on chromatin accessibility and compaction.

72 h after siRNA transfection cells were harvested and $1x10^6$ cells per sample and treatment were transferred to a tube. After washing the cell pellet with PBS, 400 µl buffer A was added that was prepared as indicated in Table 7. Shortly before use buffer A was supplemented with Complete Mini Protease Inhibitor - EDTA free (Roche).

Table 7: Composition of hypotonic buffer A

Component	Amount for 100 ml
10 mM HEPES	10 ml
1.5 mM $MgCl_2$	0.01428 g
10 mM KCl	0.074 g
0.5 mM DTT	500 µl of 0.1 M stock solution

Cells were incubated in the hypotonic buffer A for 10 min on ice allowing them to swell. To release the nuclei, 4 µl 10% NP-40 was added per sample and incubated for 5 min at RT. After vortexing the tubes for 10 s, they were centrifuged at 3800 x g for 10 min at 4°C. Supernatant was rejected and isolated nuclei were digested at 37°C for different periods of time with 0.5 U MNase in 650 µl of MNase reaction buffer, prepared as follows:

Table 8: MNase reaction buffer

Component	Amount for 100 ml
50 mM Tris (pH 8.0)	5 ml Tris (1M, pH 8.0)
5 mM $CaCl_2$	73.51 mg

Aliquots of 100 µl were taken every 8 min and MNase activity was inactivated by adding 4 µl 0.5 M EDTA pH 8.0 to the samples. DNA isolation was performed by adding SDS to a final concentration of 1% and incubating with RNase A (200 µg/ml) at 37°C for 30 min. Next, Proteinase K (400 µg/ml) was added and the sample was incubated at 55°C for 2 h. Genomic DNA was purified by phenol-chloroform extraction by addition of phenol:chloroform:isoamyl alcohol 1:1 to the digested DNA. After vortexing and centrifugation at 10000 x g for 10 min at 4°C, aqueous phase was transferred to a new tube followed by DNA precipitation with ethanol and sodium acetate. For this, 1/10 volume of 3 M sodium acetate pH 5.0 and 2.5 times volume of 100% ethanol was added and precipitated at -20°C overnight. After centrifugation for 20 min at 10000 x g at 4°C, pellet was washed twice with 70% ethanol, dried and finally dissolved in 21.5 µl H_2O. DNA concentration was measured with the NanoDrop 2000 spectrophotometer and similar amounts of the partially digested DNA were loaded on a 2.0% agarose gel and separated by electrophoresis.

3.6 DSB repair reporter assay

To study the usage of the different DNA DSB repair pathways after depletion of Jarid1A, I used two GFP-based repair plasmids. They were a kind gift of Dr. Wael Mansour from the

Uniklinikum Hamburg-Eppendorf (Mansour et al. 2008). The principle of the repair substrates pEJ and pGC are based on activation of GFP by repair of endonuclease I-SceI-induced DSBs via NHEJ or HR, respectively. Repair via NHEJ can be detected with the pEJ plasmid, which has two sites for I-SceI cutting (Figure 10A). An artificial start codon that is not in frame with the original start codon is located between these cutting-sites. Hence, expression of GFP is prevented. After I-SceI transfection, a DSB is produced leading to loss of the artificial start codon. If repair via NHEJ takes place, DNA ends are ligated and GFP can be expressed. Repair via HR can be monitored with the GC substrate (Figure 10B). GFP cannot be expressed as the I-SceI site is directly located in the GFP sequence. A truncated, also non-functional GFP sequence with 520 bp sequence homology is in vicinity. GFP expression can only take place, after cutting of I-SceI in the GFP sequence followed by repair via gene conversion, one mechanism of HR.

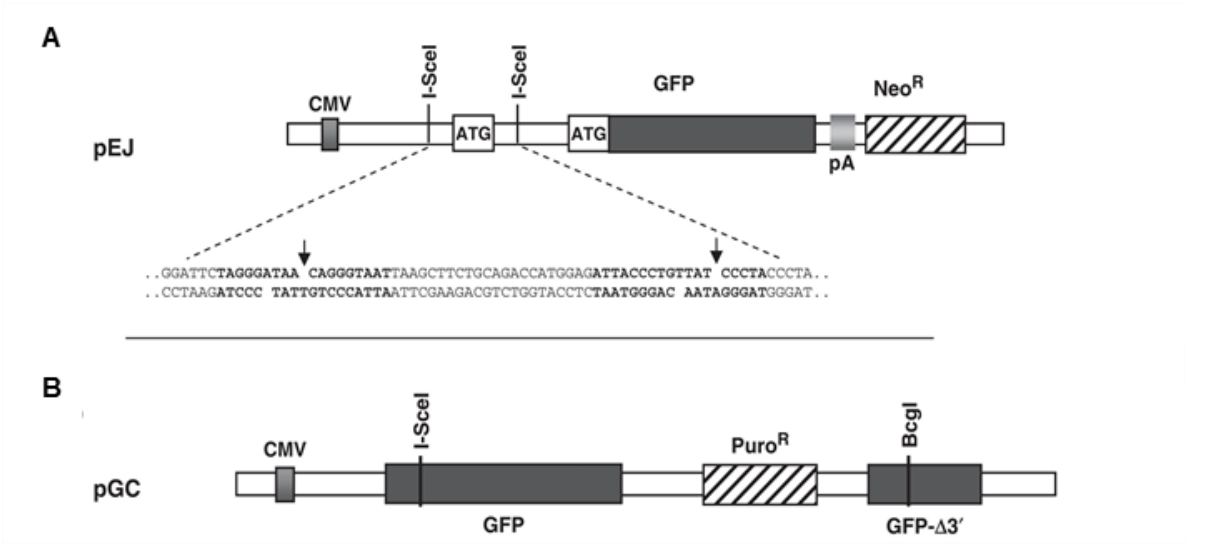

Figure 10: GFP-based reporter constructs to monitor repair via NHEJ and HR

(A) Schematic illustration of the reporter construct for NHEJ repair. The GFP gene is only expressed after cutting out the artificial start codon by I-SceI and repair of the I-SceI-induced DSB. **(B)** GFP-based substrate to monitor HR repair. After I-SceI transfection, the two non-functional GFP genes with 520 bp homology can be fused together by HR leading to functional GFP and green fluorescence (Mansour et al. 2008).

The same HeLa isolate as used in the other experiments was stably transfected with pEJ and HeLa pGC (Claudia Böhland, personal communication). Then cells were transfected with scr or Jarid1A A1+A3 as described in chapter 3.1.4. 24 h later cells were transfected with 1 µg of the I-SceI expression vector pMCV-I-SceI to induce DSBs. A vector expressing GFP (pMCC-gfp-P) was used as positive control. Transfections were performed using Lipofectamine 2000 as transfection reagent.

Separate mixtures of DNA and supplemented DMEM and of Lipofectamine 2000 and DMEM were prepared and incubated for 5 min at RT. Per sample, 1 µg of DNA and 2 µl of Lipofectamine 2000 were mixed with DMEM, respectively, to a final volume of 250 µl. After 5 min, mixtures were combined 1:1 and incubated for additional 15 min at RT. After this second incubation step 500 µl of the DNA/ Lipofectamine 2000 mixtures were added to the cells. To reduce the toxicity of the transfection reagent, medium was replaced 24 h after transfection of pMCV-I-SceI or pMCC-gfp-P. After 48 h cells were harvested and prepared for FACS analysis. All steps were performed on ice and only ice cold buffers were used. Cell pellet was washed with 10 ml PBS, centrifuged for 5 min at 500 x g at 4°C and washed again with 5 ml PBS. After an additional centrifugation step cells were fixed with 1 ml of a solution consisting of 3% PFA and 2% glucose in PBS for 10 min on ice. 14 ml PBS was added after fixation, centrifuged for 5 min at 500 x g at 4°C and pellet was washed one more time with 5 ml of PBS. Samples were stored at 4°C in PBS with 10% FBS until measuring fluorescence of GFP with FACS BD LSR II.

3.7 Gene expression microarray analysis

3.7.1 Sample preparation

To study possible changes in gene expression after the depletion of Jarid1A in HeLa cells I performed One-Color Microarray-Based Gene Expression Analysis (Agilent Technologies). This was carried out in cooperation with the group Integrative Biology of Dr. Kristian Unger from the Helmholtz Zentrum in Munich.

Four biological replicates of every sample - control, scr siRNA and Jarid1A A1+A3 siRNA, 0 Gy and 5 Gy respectively - were prepared. 72 h after siRNA transfection cells were irradiated with x-rays and harvested 2 h later to isolate the total RNA. Integrity and purity of the isolated RNA were checked via the Bioanalyzer (Agilent Technologies) using a Bioanalyzer RNA Nanochip. For all total RNA samples that achieved the required RIN (RNA integrity number) of 7, 25 ng of the RNA were Cy3-labeled with the One-Color Low Input Quick Amp Labelling Kit (Agilent Technologies). 1.5 µl diluted RNA were mixed with 2 µl of diluted spike mix and 1.8 µl of the T7 promoter primer mix. Primer and template were denatured for 10 min at 65°C and subsequently incubated for 5 min on ice. In the next step the cDNA master mix was prepared as follows:

Table 9: cDNA master mix

Component	Amount
5x first strand buffer	2.0 µl
0.1 M DTT	1.0 µl
10 mM dNTP mix	0.5 µl
AffinityScript RNAse block mix	1.2 µl

4.7 µl of cDNA master mix was transferred to each sample tube (total volume: 10 µl) and incubated for 2 h at 40°C and subsequently for 15 min at 70°C. Samples were transferred to ice before the reverse transcription reaction and the labelling is started. Table 10 shows the components of the transcription master mix.

Table 10: Transcription master mix

Component	Amount
Nuclease-free water	0.75 µl
5x transcription buffer	3.2 µl
0.1 M DTT	0.6 µl
NTP mix	1.0 µl
T7 RNA polymerase blend	0.21 µl
Cyanine 3-CTP	0.24 µl

6 µl of transcription master mix was added to each sample (total volume: 16 µl) and incubated for 2 h at 40°C. The labelled cRNA was purified using the RNeasy Mini Kit (Qiagen) as described before (chapter 3.4.1). The quantity of labelled RNA (cRNA) and the fluorochrome incorporation rate was determined using a Nanodrop sprectrophotometer and a specific activity score (concentration Cy3 / concentration of labelled cRNA x 1000 pmol Cy3 per µg cRNA) was calculated. At least 0.825 µg of cRNA with a specific activity of 6 pmol Cy 3 per µg cRNA is needed to fulfil the recommendations on quality assessment. All cRNA samples that accomplished these recommendations were used for hybridization to the microarray.

3.7.2 Hybridization

For the preparation of the sample hybridization, the fragmentation mix was pipetted as shown in Table 11:

Table 11: Fragmentation mix for 8-pack microarray formats

Component	Amount
Cyanine 3-labeled, linearly amplified cRNA	600 ng
10x blocking agent	5.0 µl
Nuclease-free water	ad 24.0 µl
25x fragmentation buffer	1.0 µl

To fragment the RNA, the fragmentation mix was incubated for 30 min at 60°C and placed on ice for 1 min. 25 µl 2x hybridization buffer was added to the samples to stop the fragmentation reaction. Samples were mixed well by pipetting up and down without introducing bubbles and then placed on ice until they were loaded onto the arrays. 40 µl per hybridization were loaded onto the slides in an Agilent SureHyb chamber base. After the complete assembly of the slide chambers they were placed to a hybridization oven heated to 65°C and hybridized four 17 h. The gene expression wash buffer 2 + 0.005% Triton-X100 had to be prewarmed to 37°C overnight. All dishes, racks and stir bars were washed thoroughly with Milli-Q water.

The next day the microarray slides were washed. The hybridization chambers were disassembled and immediately transferred to a slide-staining dish with wash buffer 1 at RT. The slides were then removed to a second dish with wash buffer 1 and the buffer was stirred for 1 min at RT. The prewarmed wash buffer 2 was now filled in a fresh slide-staining dish, slides were transferred to it and the buffer was stirred for 1 min. After the washing steps the slides were put in a slide holder with an ozone-barrier slide cover on top and scanned immediately with the SureScan Microarray Scanner (Agilent Technologies).

3.7.3 Differential gene expression analysis and pathway enrichment analysis

Text files containing the fluorescence intensities of the array probes were extracted using the Agilent Feature Extraction software. Differential gene expression and pathway enrichment analysis were performed by Dr. Kristian Unger (Helmholtz Zentrum, Munich) and will here only be described shortly.

In order to analyse the data for differential gene expression between groups the text files were imported into the R statistical platform using the Bioconductor library Agi4x44PreProcess. After quantile normalisation the data points were quality filtered and only data from microarray probes of HGNC annotated genes were kept. Differential gene expression analysis was conducted with functions from the Bioconductor limma package (https://bioconductor.org/packages/release/bioc/html/limma.html). The resulting p-values were

corrected for multiple-testing error by applying Benjamini-Hochberg false-discovery approach (Benjamini and Hochberg, 1995).

For the purpose of interpretation of the results the list with differentially expressed genes were subjected to pathway enrichment analysis. An in-house written function was used that applied Fisher's exact test assessing enrichment of genes from the gene lists in gene sets defining pathways. The Reactome pathway database (https://reactome.org) was used as source for the pathway enrichment analysis to investigate the function and interaction of the diffentially expressed genes (Matthews et al. 2009).

3.8 Statistical analysis

To examine the differences between the cells transfected with scrambled siRNA and Jarid1A A1+A3 siRNA regarding histone acetylations, an unpaired, 2-tailed t-test was performed using Microsoft Excel 2010. P-values < 0.05 were defined as statistically significant differences.

Statistical evaluation of colony formation assay is described in chapter 3.1.6.

4 Results

4.1 Impact of Jarid1A depletion on cellular growth characteristics and radiation response

4.1.1 Knockdown of Jarid1A is associated with global increase of H3K4me3

By Western Blotting both known isoforms of Jarid1A are detected in HeLa cells (Figure 11A), as well as in MCF-7 and U2OS cells and total expression of the Jarid1A protein is comparable in these three cell lines (see Appendix B, Figure B.1). Knockdown of Jarid1A was established previously using stealth siRNAs (Penterling 2013). 72 h after transfection of Jarid1A A1+A3 siRNA, protein levels in HeLa whole cell extracts are reduced to 20-30% compared to scr siRNA transfected HeLa cells. Preliminary results showed an increase of cellular H3K4me3 levels in immunofluorescence and Western Blotting as a consequence of the Jarid1A depletion. This has been reported before by others (Pasini et al. 2008; Beshiri et al. 2012). The efficiency of the Jarid1A knockdown with subsequent increase of H3K4me3 could be verified within this thesis in all three tested cell lines (HeLa, U2OS and MCF-7 cells) and is shown in Figure 11. Figure 11A shows a representative Western blot image of knockdown of Jarid1A with associated increase of H3K4me3 in HeLa cells. The normalized relative expression of Jarid1A (mean of 10 independent experiments) and of H3K4me3 (mean of 3 independent experiments) in whole cell extracts 72 h after siRNA transfection is displayed in the graph next to it. After transfection with Jarid1A A1+A3 siRNA, the demethylase is reduced to about 25%. This drastic reduction of nuclear Jarid1A after transfection with Jarid1A A1+A3 siRNA can also be observed in immunofluorescence analysis (see Figure 11B). The decrease of the Jarid1A protein is associated with a strong increase of H3K4me3 of about 1.8-fold in HeLa cells that is evident from Western Blotting (Figure 11A) and immunofluorescence (Figure 11B). Figure 11C shows the Western Blotting results of Jarid1A and H3K4me3 expression in U2OS and MCF-7 cells. Cellular H3K4me3 levels increase about 1.5- to 1.7-fold in MCF-7 and U2OS cells.

The antibody recognizing the histone modification H3K4me3 is very specific in immunofluorescence, whereas it also binds to H3K4me2 in Western Blotting experiments (see Appendix B, Figure B.2 and B.3).

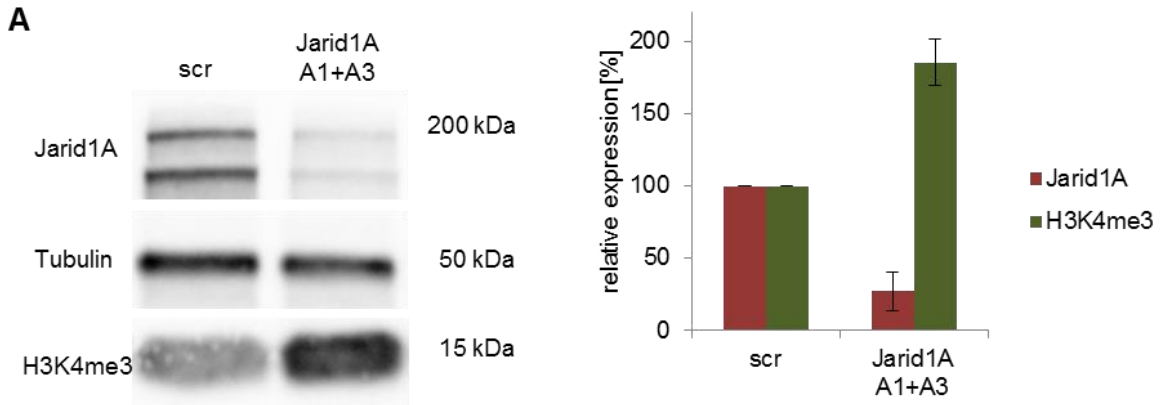
A
scr
Jarid1A A1+A3
Jarid1A
Tubulin
H3K4me3
200 kDa
50 kDa
15 kDa
relative expression [%]
200
150
100
50
0
scr
Jarid1A A1+A3
Jarid1A
H3K4me3

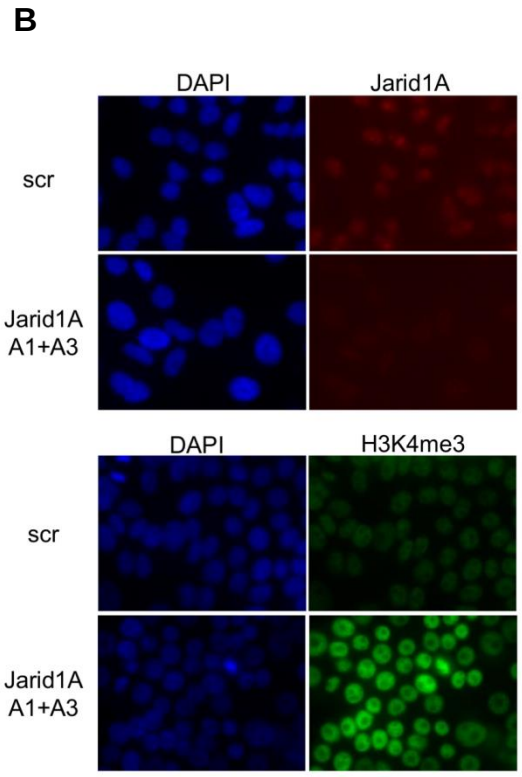
B
DAPI
Jarid1A
scr
Jarid1A A1+A3
DAPI
H3K4me3
scr
Jarid1A A1+A3

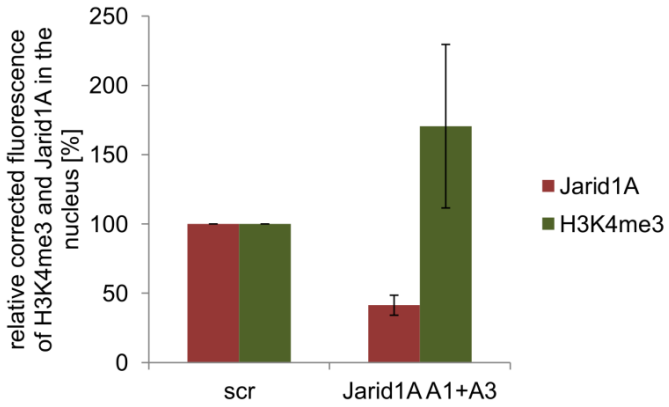
relative corrected fluorescence of H3K4me3 and Jarid1A in the nucleus [%]
250
200
150
100
50
0
scr
Jarid1A A1+A3
Jarid1A
H3K4me3

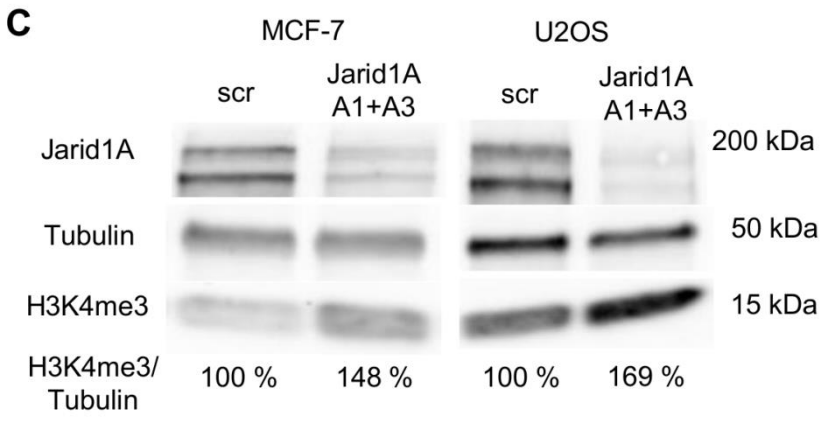

Figure 11: Efficient down-regulation of Jarid1A is associated with global increase of H3K4me3
(A) Decreased levels of Jarid1A are associated with increased levels of H3K4me3 in whole cell protein extracts of HeLa cells after siRNA transfection. Western blot images show levels of Jarid1A and H3K4me3 72h after transfection with scrambled siRNA (scr) or Jarid1A A1+A3 siRNA. Graph displays the normalized average amount (+/- SD) of Jarid1A and H3K4me3 protein after siRNA transfection of HeLa cells determined by quantitative analysis of Western blots of protein extracts obtained in 10 (Jarid1A) and 3 (H3K4me3) independent experiments.
(B) Decreased Jarid1A and increased H3K4me3 signal intensity after indirect immunofluorescence in HeLa cells transfected with Jarid1A A1+A3 siRNA. Microscopic images were obtained at comparable exposure times and display the cell nuclei stained with DAPI in blue (left), the protein Jarid1A in red (right) and the histone modification H3K4me3 in green. The graph indicates normalized average fluorescence of Jarid1A and H3K4me3 in nuclei of 20 randomly chosen cells.
(C) Increase of H3K4me3 in whole cell protein extracts of MCF-7 cells and U2OS cells after knockdown of Jarid1A. Western blot images show levels of Jarid1A and H3K4me3 in cells transfected with scr siRNA and Jarid1A A1+A3 siRNA 72 h after transfection. Numbers give levels of H3K4me3 normalized to scr sample after quantitative analysis.

4.1.2 Knockdown of Jarid1A does not affect cell growth

Contradicting reports about the influence of Jarid1A on growth characteristics of cells exist in the literature. It has been reported that depletion of Jarid1A in SAOS-2 cells leads to increase of the cyclin-dependent kinase inhibitors p21 and p27 associated with stop of cell proliferation in G1 and S-phase (Benevolenskaya et al. 2005). Increase of p21 and p16, both mediating cellular senescence, was also seen in Jarid1A-depleted cells in gastric and cervical cancer (Zeng et al. 2010). On the contrary, Chicas et al. observed, that Jarid1A and Jarid1B induce senescence in cooperation with the Rb protein by silencing of Rb target genes (Chicas et al. 2012).

In a preliminary approach, knockdown of Jarid1A did not seem to affect cell growth in HeLa cells (Penterling 2013). To study the effect of siRNA-mediated Jarid1A depletion on cell growth

of HeLa, U2OS and MCF-7 cells, cell yield was determined 72 h after transfection with scr or Jarid1A siRNA and was normalized to untransfected cells (= contr). Figure 12A shows a minor reduction in the cell numbers after siRNA transfection compared to the control, probably due to cytotoxic effects of the transfection reagent Lipofectamine 2000. The Jarid1A knockdown *per se* seems not to have an influence on short-term viability and proliferation of HeLa, MCF-7 or U20S cells. Additionally, cell cycle analysis of HeLa cells was performed after transfection with siRNA. Therefore, cells were harvested 72 h and 96 h after siRNA transfection and nuclei were stained with PI before flow cytometry analysis. No differences in the cell cycle distribution of cells transfected with scr siRNA or Jarid1A A1+A3 siRNA (see Figure 12B) were observed. Jarid1A knockdown cells show neither cessation of the cell cycle nor G1/S-phase arrest.

It was also reassessed, if the cell lines exhibit up-regulation of p21 after Jarid1A knockdown. HeLa and U2OS cells in general feature a relatively low level of p21 compared to MCF-7 cells (Figure 12C). In fact, in HeLa cells p21 expression even seem to slightly decrease after Jarid1A depletion, while MCF-7 cells show a slight increase. Anyway, the minor changes in p21 expression after knockdown of Jarid1A are negligible. Corresponding to our data concerning proliferation and cell cycle analysis, there is no evidence for substantial up-regulation of p21 in HeLa, MCF-7 and U2OS cells after Jarid1A depletion and thereby no indication of induction of cellular senescence.

Additionally, long-term viability and growth properties after Jarid1A knockdown were investigated in HeLa cells by determining the plating efficiency and the colony size in colony formation experiments. Both plating efficiency (Figure 12D) as well as average size of the colonies (Figure 12E) were unaffected in Jarid1A-depleted cells. In summary, these data demonstrate that siRNA-mediated knockdown associated with strong reduction of Jarid1A level and increase in cellular H3K4me3 levels does neither affect cellular viability nor growth behaviour in the cell lines tested here.

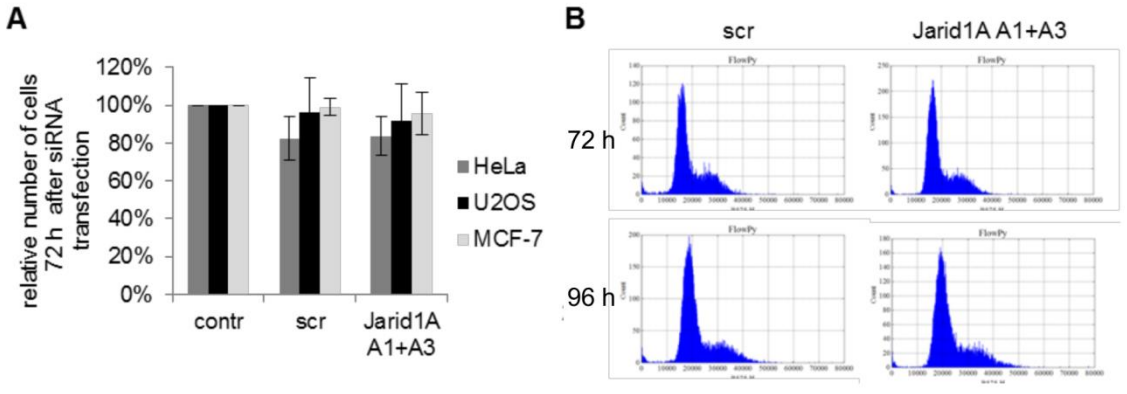

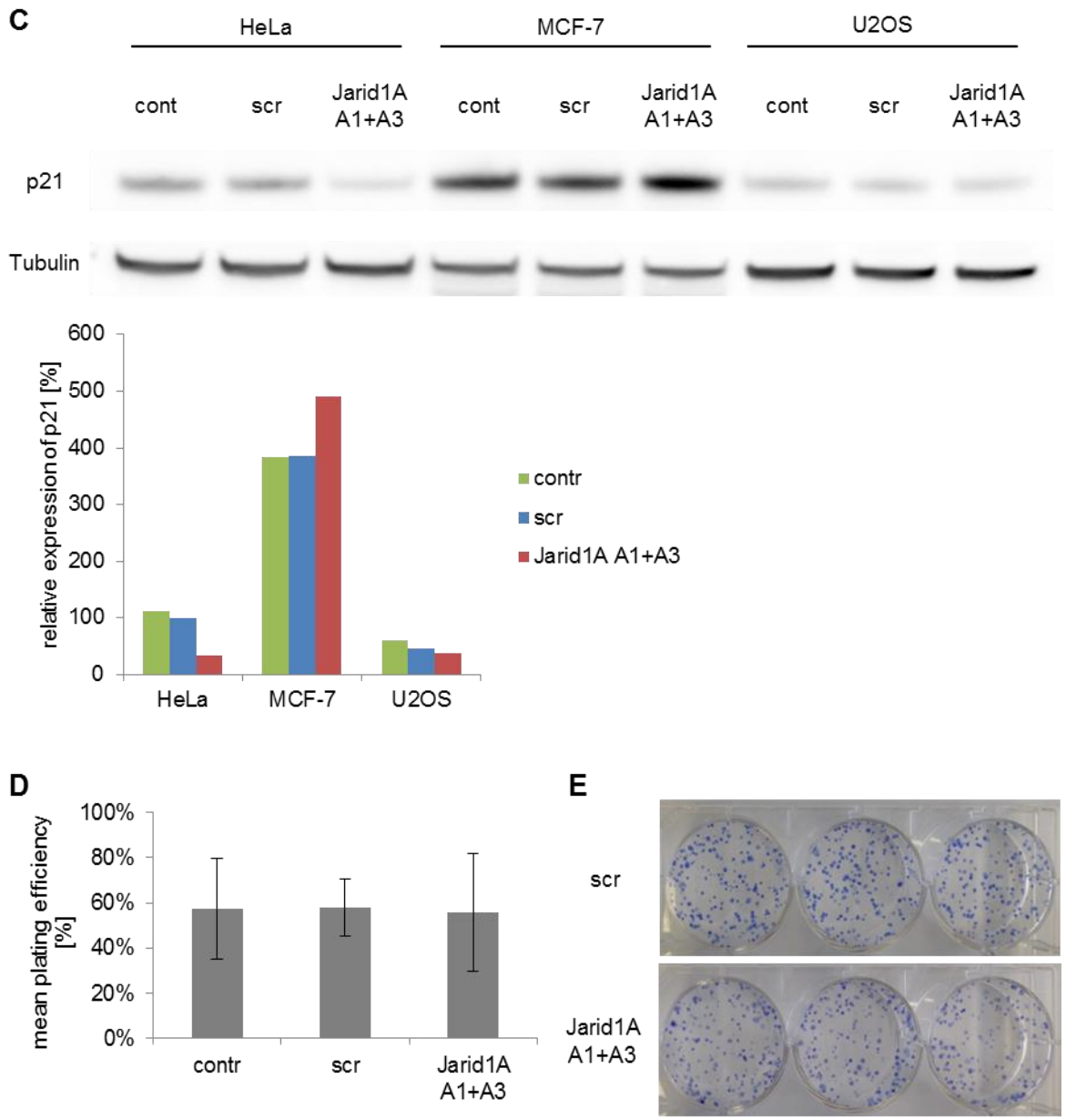

Figure 12: Jarid1A depletion does not affect cell viability or proliferation

(A) No difference in the cell number 72 h after transfection with scr or Jarid1A siRNA. In all experiments involving protein extracts, the cell number of the different transfection samples was determined prior to protein extraction. Indicated are mean cell numbers (+/- SD) of HeLa cells (12 experiments), U2OS cells (3 experiments) and MCF-7 cells (2 experiments), each normalized with respect to the untransfected control samples.

(B) Consistent cell cycle distribution after down-regulation of Jarid1A. 72 h and 96 h after siRNA transfection HeLa cells were harvested, stained with PI and analyzed by flow cytometry. Experiment was performed in triplicates for every treatment and time point. Exemplary cell cycle distributions are displayed. The x-axis shows fluorescence of propidium iodide, the y-axis the cell count.

(C) Depletion of Jarid1A does not lead to strong induction of p21. Expression of p21 after depletion of Jarid1A in HeLa, MCF-7 and U2OS cells, 72 h after transfection with scr or Jarid1A siRNA.

(D) Constant plating efficiency of the transfected cells. After incubating transfected and control HeLa cells for 10 days, colonies were stained with methylene blue and the number of colonies was determined. Graph indicates the mean plating efficiency (+/- SD) of 3 independent colony forming assays.
(E) Exemplary methylene blue stained colonies 10 days after seeding of 300 cells per well.

4.1.3 Downregulation of Jarid1A leads to histone hyperacetylation

As mentioned before in chapter 1.4.2, Jarid1A interacts with several histone deacetylase complexes (Hayakawa et al. 2007; Nishibuchi et al. 2014). This suggests a possible contribution of the demethylase in chromatin remodeling or rather in repression of specific target genes cooperatively with HDACs. Coexistence of histone acetylations and H3K4me3 is often observed at transcriptional start sites and promoters of active genes and it was reported that there may be a direct association between H3K4me3 and histone acetylations (Liang et al. 2004; Zhang et al. 2015). This implied the question if depletion of Jarid1A and associated changes in the H3K4me3 level provoked altered levels of histone acetylations.

To elucidate this, I analysed the levels of acetylation at H3K9, H3K56 and H4K16 by Western blotting experiments 72 h after Jarid1A knockdown. The respective antibodies were tested for specificity by peptide competition assays in our lab (Maroschik et al. 2014). All investigated acetylation levels increased after Jarid1A knockdown as displayed by representative Western blot images (Figure 13A). The graphs on the right depict the average expression of the investigated acetylation levels of five or three independent experiments. While the increase of H3K9ac and H3K56ac was statistically not significant ($p = 0.0530$ and $p = 0.1891$), increase of acetylations at H4K16 showed a statistically significant increase of about 100% ($p = 0.0035$). To exclude general effects on the expression of the histones H3 and H4 after Jarid1A-depletion, I also checked for potential alterations in the expression of the core histone proteins by Western blotting (Figure 13B). The amounts of H3 and H4 remain unaffected after the Jarid1A knockdown.

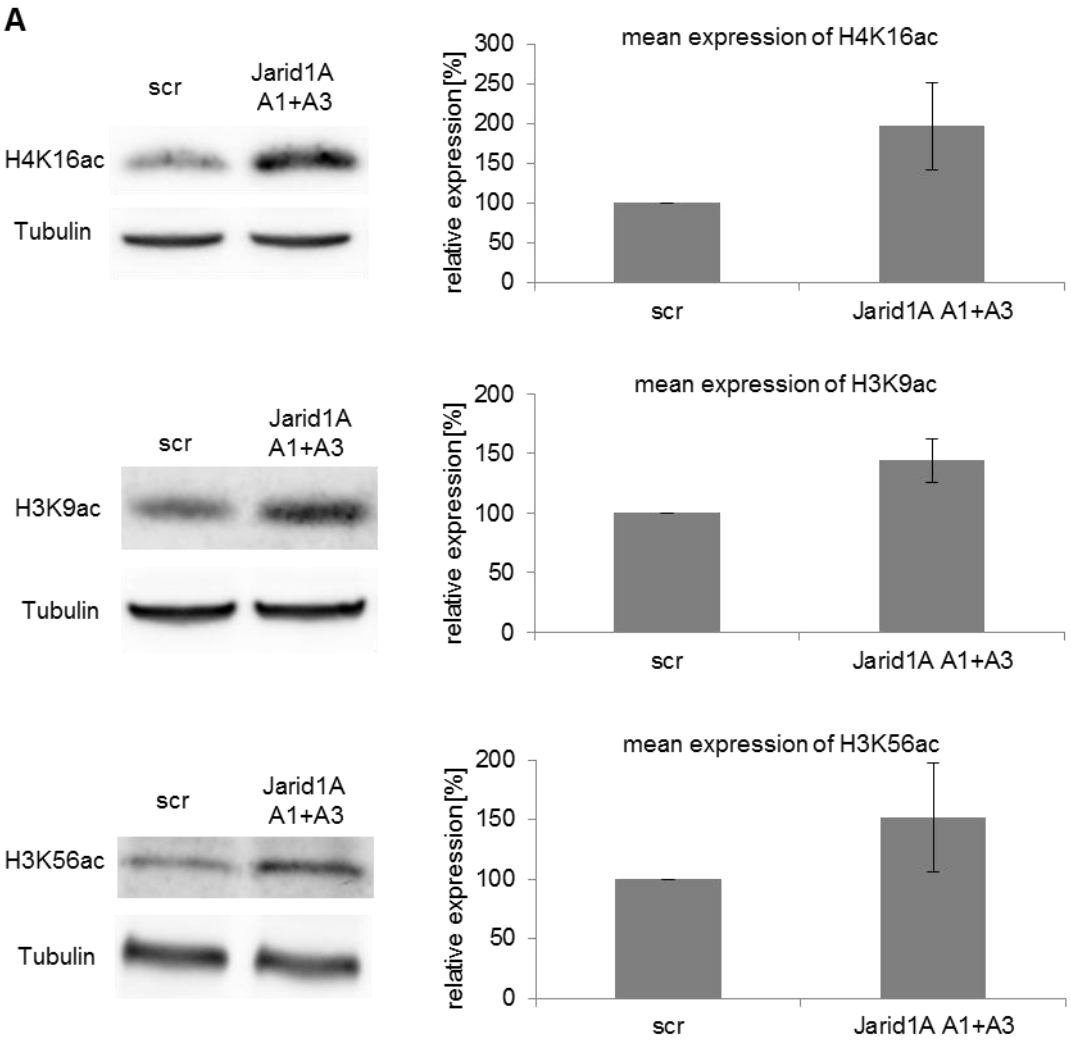
A
scr
Jarid1A A1+A3
H4K16ac
Tubulin
mean expression of H4K16ac
relative expression [%]
300
250
200
150
100
50
0
scr
Jarid1A A1+A3
scr
Jarid1A A1+A3
H3K9ac
Tubulin
mean expression of H3K9ac
relative expression [%]
200
150
100
50
0
scr
Jarid1A A1+A3
scr
Jarid1A A1+A3
H3K56ac
Tubulin
mean expression of H3K56ac
relative expression [%]
200
150
100
50
0
scr
Jarid1A A1+A3

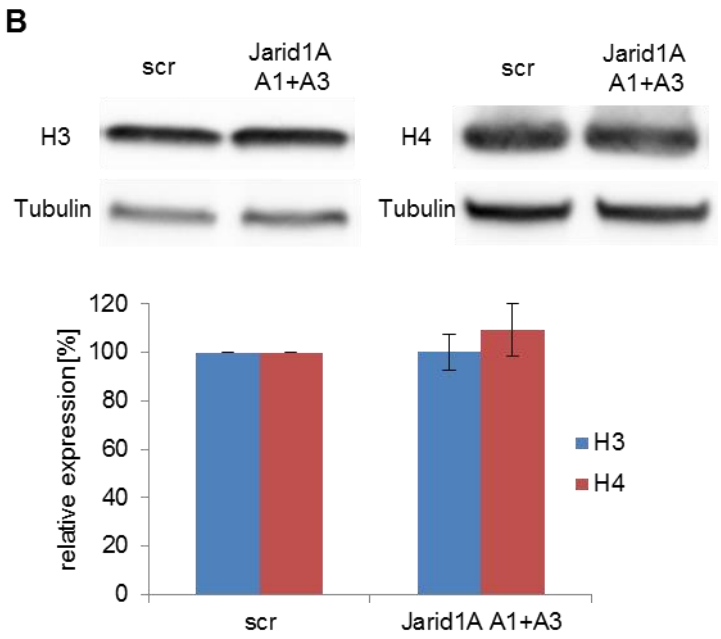

Figure 13: Depletion of Jarid1A results in histone hyperacetylation

(A) Increase of H4K16ac, H3K9ac, and H3K56ac in whole cell protein extracts of HeLa cells after siRNA transfection. Western blot images show levels of the histone modifications in cells transfected with scrambled siRNA (scr) and Jarid1A A1+A3 siRNA. Graphs indicate the means (+/- SD) from 5 independent experiments for H4K16ac and 3 independent experiments for H3K9ac and H3K56ac after quantitative analysis of Western blots. The effect of H4K16ac is statistically significant ($p = 0.0035$).

(B) The amounts of the histones H3 and H4 in whole-cell extract are not affected by down-regulation of Jarid1A. Indicated are means (+/- SD) from 3 experiments.

4.1.4 Chromatin accessibility is not affected after Jarid1A-depletion

Next, the impact of histone hyperacetylation on the global structure of chromatin had to be investigated. Histone hyperacetylation may lead to a more open chromatin structure that can have several consequences in cellular processes possibly influencing transcriptional regulation and disturbing interaction of chromatin with chromatin-binding proteins (Perry and Chalkley 1981; Shogren-Knaak et al. 2006).

To study the influence of the hyperacetylation after Jarid1A depletion on the global structure of chromatin, nuclei can be partially digested with micrococcal nuclease (MNase). MNase is an enzyme derived from Staphylococcus aureus that is able to digest nucleic acids by cutting the DNA between nucleosomes in the region of the linker histone H1 (Telford et al. 1989). Dependent on the sensitivity of the chromatin to the MNase, it allows drawing conclusions about the chromatin compaction. 72 h after siRNA transfection nuclei of Jarid1A depleted cells and control transfected cells were isolated, digested with MNase and purified DNA was loaded

onto an agarose gel. A ladder of DNA fragments according to mono-, di-, trinucleosomes, and so on, is visible on the gel (Figure 14). The longer the nuclei were digested with MNase, the smaller are the resulting oligonucleosomes. Both samples show similar sensitivity to MNase digestion suggesting no or minor global effect of the observed hyperacetylation on chromatin accessibility.

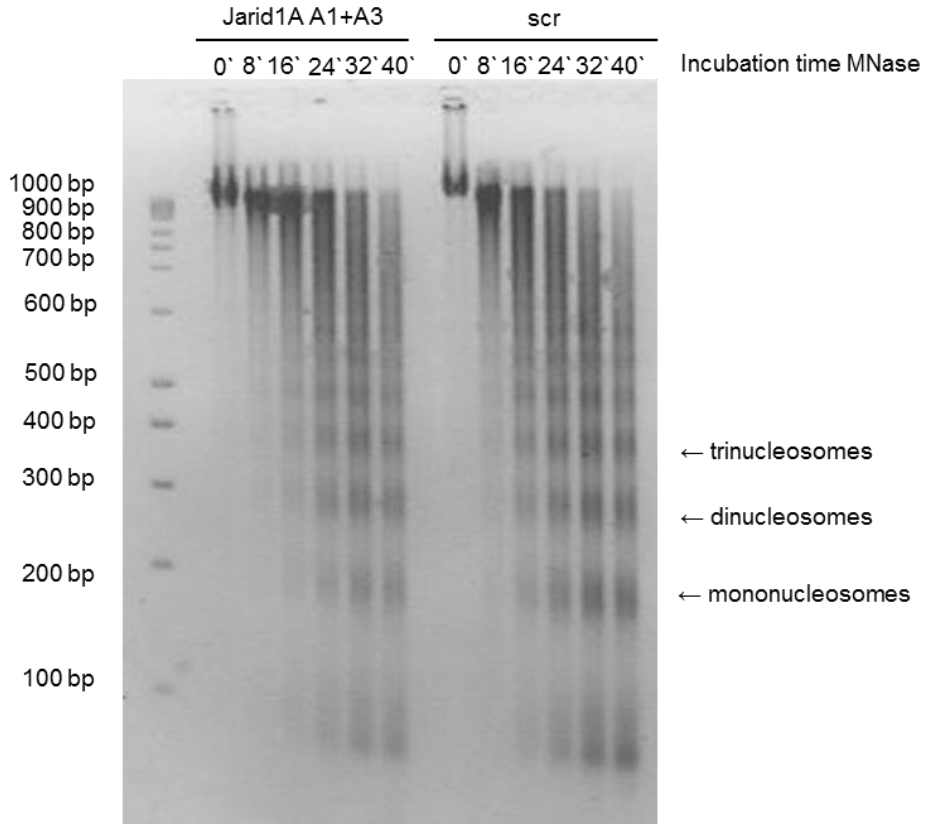

Figure 14: MNase accessibility is not affected by Jarid1A depletion

Analysis of chromatin accessibility by MNase digestion of isolated nuclei. After different incubation periods with 0.5 U MNase, comparable amounts of partially digested DNA were loaded onto an agarose gel. The emerging ladder of mono- and oligonucleosomes is comparable in Jarid1A A1+A3 and scr transfected cells indicating regular nucleosome distribution in bulk chromatin after Jarid1A depletion.

4.1.5 Depletion of Jarid1A enhances radiosensitivity

It was observed by our group that Jarid1A accumulates at laser-induced damage sites and preliminary results further suggested higher radiosensitivity in Jarid1A knockdown cells (Seiler et al. 2011; Penterling 2013). The additional observation that Jarid1A-depletion influences histone acetylation levels intensifies this assumption, even without indications for notable global changes in chromatin structure. Treatment of cells with HDAC inhibitors (HDACi)

leading to histone hyperacetylation is often linked to radiosensitization (Kim et al. 2010). Especially the use of low concentrations of HDACi, where the only evident effect is chromatin hyperacetylation, suggests a direct influence of hyperacetylation on radiation sensitivity (Karagiannis et al. 2007).

To investigate the influence of Jarid1A-downregulation on cell survival after x-irradiation, colony forming experiments were performed. Differently transfected HeLa cells were irradiated with 0 Gy, 2 Gy, 5 Gy and 10 Gy 72 h after siRNA transfection and incubated for 10 days. Figure 15 shows the average cell survival of the untransfected control, and of cells transfected with scr siRNA and with Jarid1A A1+A3 siRNA depending on the dose of irradiation. In Figure 15 a clear and statistically significant radiosensitization can be observed after Jarid1A depletion compared to untransfected cells ($p < 0.0001$) and to control-transfected cells ($p = 0.0025$) (Braselmann et al. 2015) within 3 independent colony forming experiments. The data confirm recent observations and demonstrate clearly that the demethylase Jarid1A is important for the cellular resistance to radiation damage. Sensitization was also observed after transfection with each of the Jarid1A siRNAs alone (A1 and A3), thus ruling out off-target effects (see Appendix C, Figure C).

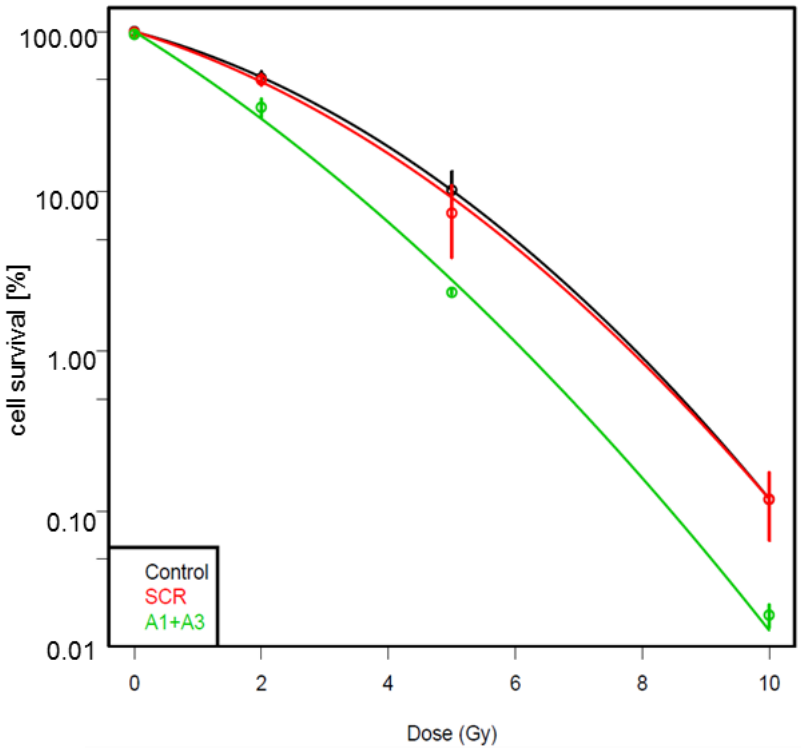

Figure 15: Depletion of Jarid1A enhances radiosensitivity

Survival fraction of the differently treated HeLa cells irradiated at 72 h after siRNA transfection. Cells were irradiated with 0 Gy, 2 Gy 5 Gy or 10 Gy x-rays and incubated for 10 days before fixation and methylene blue staining of colonies. For every dose the mean value of the cell survival (+/- SD) of 3

independent colony forming assays is shown. Data were fitted with a linear-quadratic model and statistical significance was determined by F test. After Jarid1A depletion, survival is significantly reduced as compared to scr siRNA transfected cells ($p = 0.0025$) and untransfected controls ($p < 0.0001$).

4.1.6 Investigation of factors possibly responsible for the observed enhanced radiosensitvity after Jarid1A knockdown

Having shown that Jarid1A depletion sensitizes cells to radiation, the impact of Jarid1A knockdown on damage response and DSB repair needs to be investigated. For this, cell cycle distribution and recruitment of Jarid1A to chromatin after irradiation with x-rays was studied. I additionally analysed the recruitment and dissociation of repair foci after irradiation of Jarid1A-depleted cells via induction of DSBs with the ion microbeam and investigated I-SceI-induced DSB repair reporter assay to exclude disturbance of the DNA DSB repair pathway choice.

4.1.6.1 Cell cycle checkpoint and apoptosis

First, cell cycle distribution of Jarid1A depleted cells compared to control transfected cells after irradiation with x-rays was analysed. Radiation generally induces cell cycle arrest to guarantee repair of damage prior to mitosis (Jeggo and Löbrich 2006). The phase the cell cycle arrest occurs depends on the p53 status of the cell line. Cell lines with a stably expressed p53 generally arrest in G1/S phase, while cells with mutant p53 tend to arrest in G2/M phase of the cell cycle (Halacli et al. 2013). Due to infection with HPV18, p53 status is compromised in HeLa cells (Scheffner et al. 1990). Figure 16 shows cell cycle distribution directly, 24 h and 48 h after irradiation with 5 Gy x-rays. Scr and Jarid1A A1+A3 transfected cells both feature a clear G2 phase arrest 24 h after irradiation. Regular cell cycle distribution is achieved 48 h after irradiation in both samples. No accumulation of sub-G1 DNA is evident, indicating poor apoptosis induction in both samples.

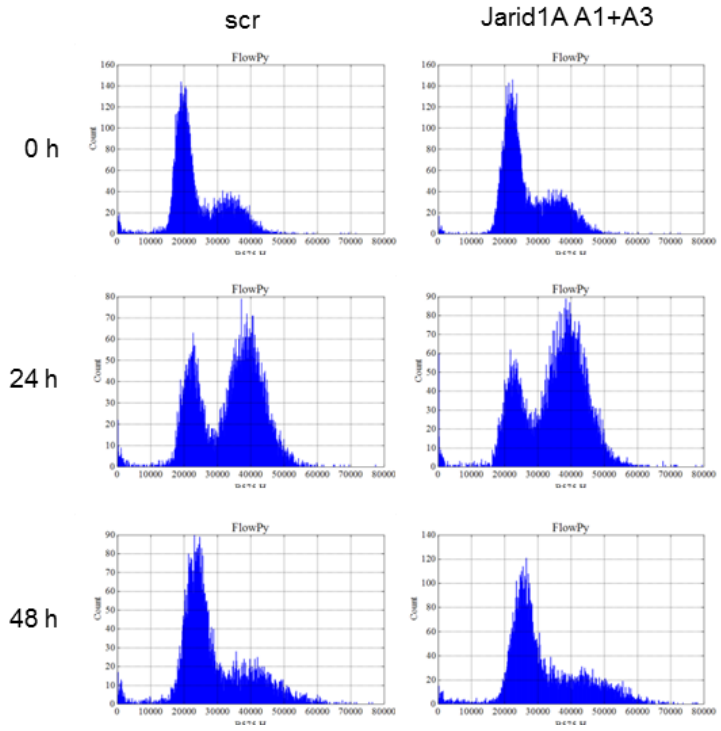

Figure 16: Depletion of Jarid1A does not affect cell cycle checkpoints

Consistent cell cycle distribution after down-regulation of Jarid1A and irradiation with 5 Gy x-rays. 72 h after siRNA transfection, cells were irradiated. Directly, 24 h and 48 h after irradiation HeLa cells were harvested, stained with PI and analysed by flow cytometry. Experiment was performed in triplicates for every treatment and time point. Exemplary cell cycle distributions are displayed. The x-axis shows fluorescence of propidium iodide, the y-axis the cell count.

4.1.6.2 No accumulation of Jarid1A at chromatin after irradiation

It has been reported previously that Jarid1A visibly accumulates at laser-induced γH2AX sites, but not at ion-induced γH2AX foci (Seiler et al. 2011). Laser irradiation results in extremely high local damage load, hence often enabling visualization of factors at damage sites that cannot be detected after irradiation with other, more physiological sources. An additional disadvantage is that the laser-induced damage is poorly characterized and often leads to misrepresentation of the recruitment analysis to the damage (Reynolds et al. 2013). To verify the accumulation of Jarid1A at irradiation-induced damage sites, subcellular protein fractionation was performed after irradiation with 5 Gy x-rays. Different protein fractions were used for Western blotting. Figure 17 displays the detection of Jarid1A and respective characteristic proteins for the subcellular fractions. As expected, γH2AX is detected only in the chromatin-bound fraction and the amount is much stronger after irradiation. Tubulin and HDAC3 served as controls for the soluble nuclear fraction and the cytoplasmic fraction. The large isoform of Jarid1A is almost exclusively found in the nucleus, while the small isoform can also be found in the cytoplasmic fraction. There is no enhanced recruitment of Jarid1A to the

chromatin after irradiation with 5 Gy. Under comparable conditions, enhanced chromatin binding was reported for Jarid1B (Li et al. 2014).

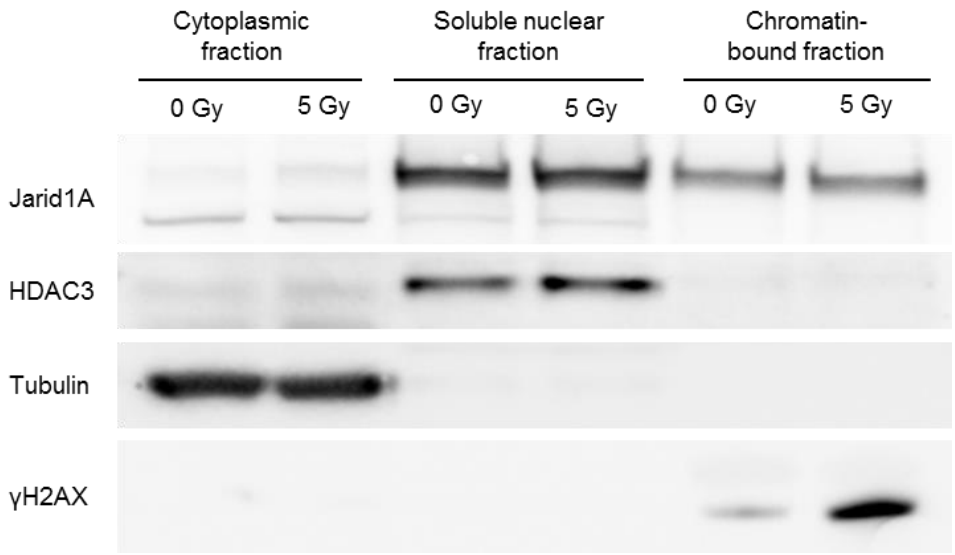

Figure 17: No enhanced accumulation of Jarid1A at chromatin after irradiation

1 h after irradiation of HeLa cells with 5 Gy of x-rays cytoplasmic, soluble nuclear and chromatin-bound protein fractions were extracted and used for Western blotting analysis with the indicated antibodies. HDAC3 and Tubulin are characteristic for the respective protein fractions serving as control for proper fractionation, while γH2AX functions as control for the irradiation and for the chromatin-bound fraction simultaneously. After irradiation amount of Jarid1A in the respective fractions remains constant. Displayed is an exemplary Western Blotting image (experiment was performed two times).

4.1.6.3 Recruitment and dissociation of repair foci is not affected

Chromatin modification and remodeling play a crucial role in DNA damage repair and have to be tightly coordinated with DNA damage factors. Among histone modifications, acetylations gained more and more attention regarding their importance in DNA damage response (Li et al. 2010; Hsiao and Mizzen 2013; Ikura et al. 2015). Both, acetylation and deacetylation at H4K16 was observed after damage induction (Murr et al. 2005; Li et al. 2010; Neumayer and Nguyen 2014;). The prevalent model is a loss of acetylation at H4K16 directly after damage induction, followed by increased acetylation at later time points. Deacetylation of H4K16 promotes 53BP1 binding, thus leading to NHEJ and suppressing repair by HR. Hence, one would expect that increased acetylation of H4K16 may interfere with 53BP1 recruitment to radiation-induced damage sites, as shown after HDACi treatment (Tang et al. 2013). Thus, recruitment and dissociation of repair factors was investigated after Jarid1A knockdown and associated increase in H4K16ac. Previous results revealed regular formation and resolution of γH2AX foci

at ion-induced DSBs after knockdown of Jarid1A. Kinetics of the damage response proteins 53BP1 and Rad51 also seemed ordinary (Penterling 2013). To verify these observations, repair kinetics of 53BP1, Rad51 and BRCA1, including foci formation and dissociation, were monitored via immunofluorescence in Jarid1A-depleted cells after induction of DSBs by ion microirradiation. Irradiation was performed in a small angle (10°) with 55 MeV carbon ions 72 h after siRNA transfection. Cells were fixed at the indicated time points after irradiation and immunofluorescence was performed. Foci formation of all factors was tested at 1 h after irradiation. To account for possibly slower recruitment of Rad51, this protein was also assessed after 3 h. Figure 19 shows epifluorescence images of randomly chosen cells after immunofluorescence with BRCA1 (A), Rad51 (B), and 53BP1 (C). γH2AX was used as marker for DSBs in all samples. Images show regular accumulation of 53BP1, Rad51 and BRCA1 at γH2AX sites at all tested time points. Quantification was done by dividing cells with γH2AX tracks into 3 groups. The protein of interest showed either a total, a partial or no colocalization with γH2AX. Control transfected and Jarid1A depleted cells showed no differences in the distribution of these 3 groups with the indicated antibodies and fixation time points after irradiation. Besides the time points 1 h and 3 h that showed no differences between src siRNA and Jarid1A siRNA transfected samples, we also investigated early time points (5 min, see Figure 18C), where a full colocalization of 53BP1 and γH2AX is not yet given due to ongoing recruitment of 53BP1. These early time points did also not point towards different repair kinetics of scr siRNA compared to Jarid1A siRNA transfected samples. Recruitment analysis reveals that depletion of Jarid1A and concomitant hyperacetylation of H4K16 does not affect recruitment of 53BP1 and BRCA1 at ion irradiation-induced damage sites. Furthermore, downstream recombinational repair steps seem not to be affected as shown by Rad51 recruitment.

There were also no visible differences in the early steps of DSB detection and signaling, since γH2AX foci formation after carbon ion or x-irradiation happens similarly fast in Jarid1A depleted and control cells. The formation of foci after irradiation with carbon ions was evaluated 5 min (see Appendix D, Figure D panel A) and 2 min (Figure D panel B) after irradiation. Because of the experimental set-up, the shortest time that can be studied post-irradiation is 2 min. Also after this short time, no evident difference in γH2AX formation could be found. 15 minutes after x-irradiation, γH2AX foci have comparable brightness in both samples as well (Appendix D, Figure D panel C). Because of these observations, I conclude that Jarid1A is not involved in the pathways regulating the accumulation of DSB repair factors at damage sites, even if it has an influence on the cellular H4K16 acetylation level.

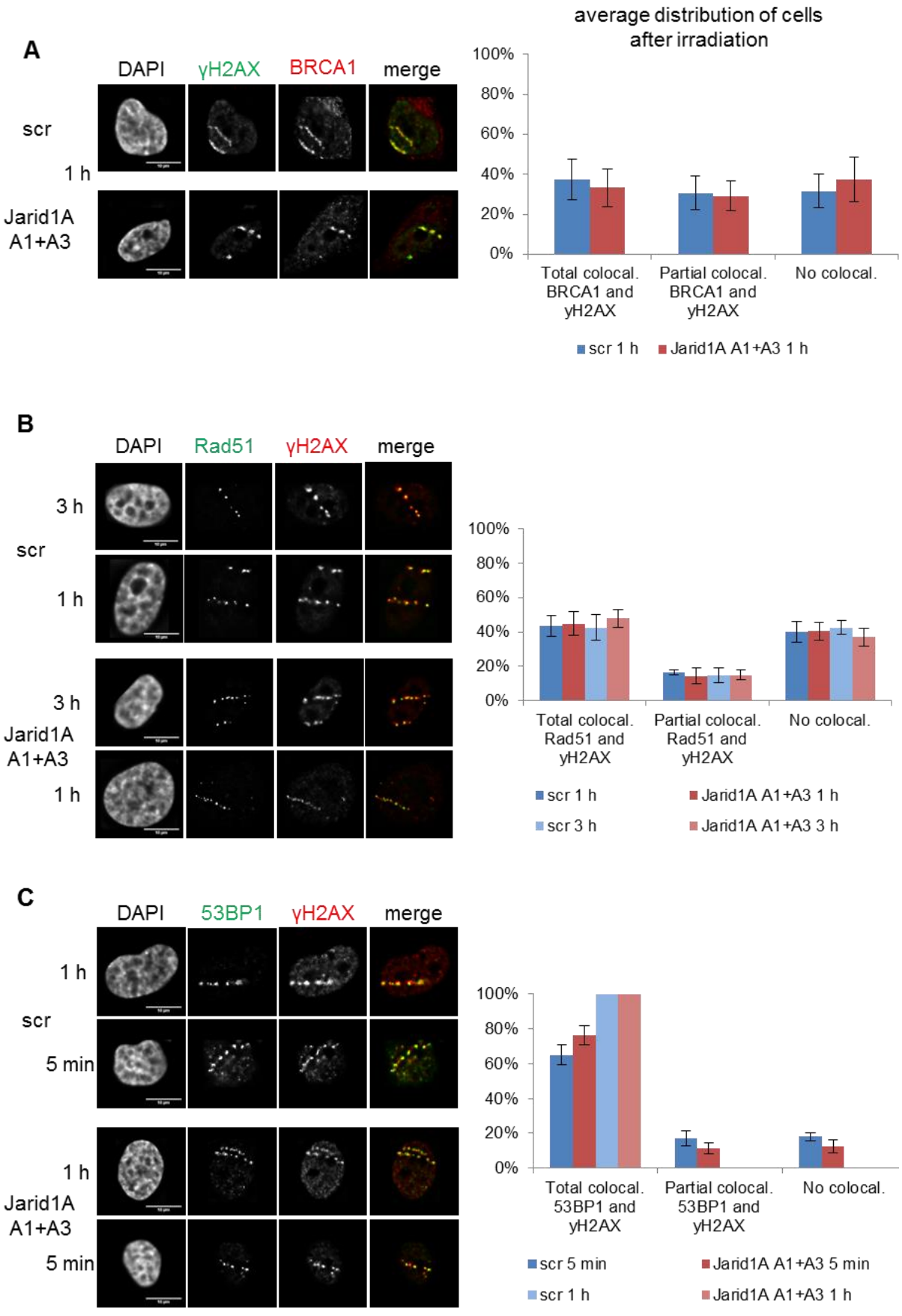

Figure 18: Formation of radiation-induced protein foci is not affected by depletion of Jarid1A

Detection of repair foci in scr or Jarid1A A1+A3 siRNA transfected HeLa cells after ion microirradiation. 72 h after transfection cells were irradiated in a small angle (10°) with 55 MeV carbon ions. After incubation, cells were fixed and indirect immunofluorescence was performed to detect the foci formation of BRCA1 and γH2AX **(A)**, Rad51 and γH2AX **(B)** or 53BP1 and γH2AX **(C)**. For quantitative evaluation, cells with γH2AX tracks were divided in 3 groups, depending on whether the protein of question formed foci that overlapped with γH2AX foci in the whole track, or occasional foci that overlapped with some of the γH2AX foci in the track, or no overlapping foci. Indicated are means (+/- SEM) from at least 50 evaluated cells. Displayed are exemplary epifluorescence images. Scale bars in the images represent 10 µm. Experiment was performed two times during different beam times.

Disturbed dissociation of damage response factors from the damage sites after knockdown of Jarid1A was also conceivable. I therefore monitored γH2AX, 53BP1 and Rad51 by immunofluorescence for longer periods of time after irradiation with x-rays (up to 48 h) and determined the number of residual foci (Figure 19), which represents a frequently used method for estimation of DSB repair efficiency (Löbrich et al. 2010). Spontaneous foci formation is not increased in Jarid1A depleted cells as seen by the number of foci in unirradiated cells (0 Gy). The number of γH2AX and Rad51 foci is similar in Jarid1A knockdown cells and control transfected cells at all analysed time points implicating ordinary recruitment and dissociation kinetics. For 53BP1 slight differences are seen, which seem, however, not to affect Rad51 recruitment and overall repair as judged by resolution of γH2AX foci. From the fact that the number of γH2AX foci 48 h after x-irradiation with 5 Gy in Jarid1A-depleted and control cells returned almost to the level of unirradiated cells, it may be concluded that the repair of the DSBs was regularly accomplished.

Despite H4K16 hyperacetylation, the results show no evidence for disturbed DSB repair in Jarid1A depleted cells as shown by monitoring the most common DSB repair factors at different time points after irradiation, both with low-LET x-rays and high-LET ions and spontaneous damage foci before damage induction.

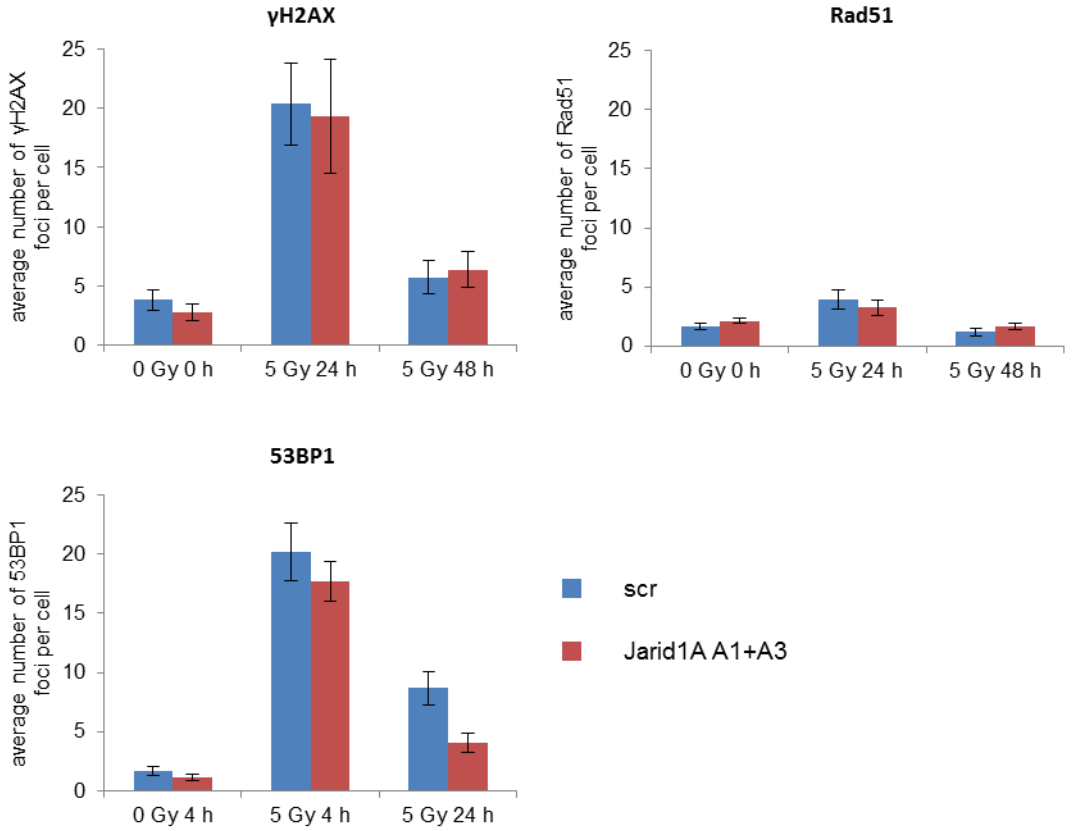

Figure 19: Dissociation of radiation-induced protein foci is not affected by depletion of Jarid1A

Detection of repair foci in scr or Jarid1A A1+A3 siRNA transfected HeLa cells after x-irradiation. Mean background and residual foci number (+/- SEM) of γH2AX, 53BP1 and Rad51 in at least 20 cells after 5 Gy X-rays. Cells were fixed before and 4 h, 24 h or 48 h after irradiation and indirect immunofluorescence was performed. Semi-automatic detection and characterization of spontaneous and residual γH2AX foci in the cells was performed by using the PlugIn FociPicker3D.

4.1.6.4 DNA DSB reporter assay

To verify that DSB repair is not reduced in Jarid1A-depleted cells, repair efficiency of NHEJ and HR was analysed directly after Jarid1A depletion by using plasmid-based DSB repair assay. Efficient repair of I-SceI-induced DSB leads to expression of GFP that can be detected by flow cytometry (Mansour et al. 2008 and 2010). The reporter plasmids pEJ and pGC were used to monitor NHEJ and HR events, respectively, by stable integration in the same HeLa cell isolate as used for the other experiments described here.

After transfection of the I-SceI expression plasmid, the number of GFP-expressing cells increased 16.2-fold in HeLa pEJ and 11.8-fold in HeLa pGC cells (Figure 20) indicating recent DSB repair. Comparable frequencies of productive DSB repair events were observed after transfection with scr siRNA, Jarid1A A1+A3 siRNA and no siRNA transfection (Figure 20).

These results substantiate that depletion of Jarid1A under the conditions used in this work does not reduce DSB repair efficiency, nor does it change pathway use.

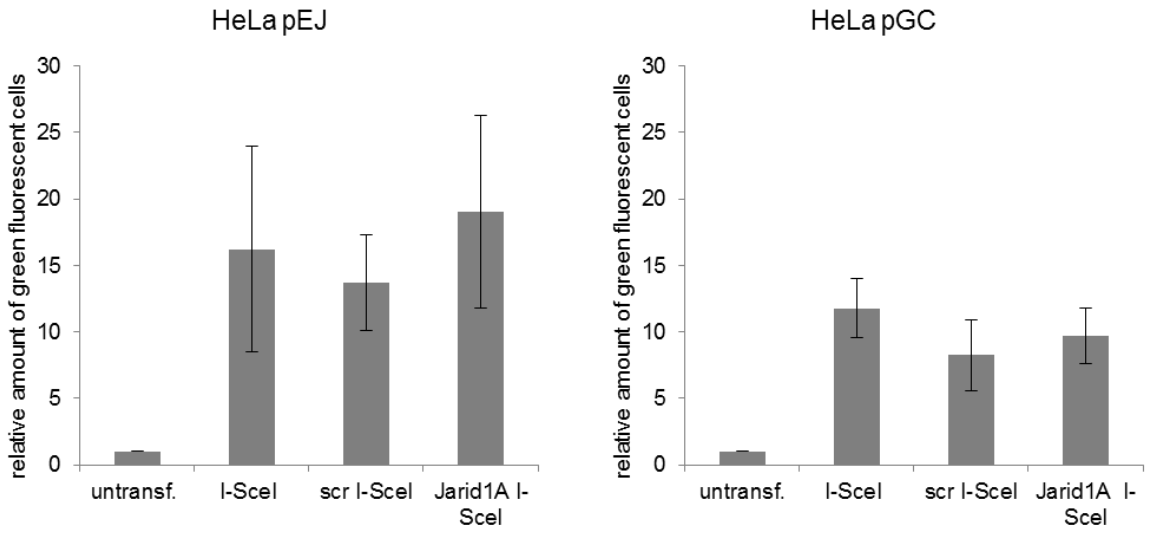

Figure 20: Repair of endonuclease-induced DSB via NHEJ or HR after are not affected by depletion of Jarid1A

Relative number of GFP expressing cells, normalized to the frequency in untransfected HeLa pEJ (left panel) and pGC (right panel) control cells, after transfection of I-SceI expression plasmid into untreated cells and cells treated with scr siRNA or Jarid1A A1+A3 siRNA. Graph displays the mean results +/- SEM of 5 independent experiments each with 20000 analysed cells.

4.1.7 Intensity correlation analysis

The initial interest in the histone demethylase Jarid1A was motivated by the observation that H3K4me3/me2 and elongation-active RNA polymerase II (RNA Pol II Ser2) is removed at chromatin regions decorated by γH2AX after ion microirradiation (Seiler et al. 2011). Due to its capacity to remove tri- and dimethylations from H3K4 and its interaction with chromatin remodeling factors, Jarid1A seemed to be a suitable candidate to be responsible for the loss of methylations at the damage sites. Previous results suggested that knockdown of Jarid1A has no influence on the loss of H3K4me3 and RNA Pol II Ser2 at damage sites (Penterling 2013). Here, these observations should be verified and the influence of alternative factors on the loss of H3K4me3 at γH2AX decorated chromatin regions should be investigated, including the closely related demethylase Jarid1B and important damage signalling factors like ATM, ATR and PARP1.

4.1.7.1 Jarid1A is not responsible for radiation-induced loss of H3K4me3 at γH2AX-decorated chromatin domains

To verify our preliminary results, HeLa cells were irradiated with carbon ions in a line pattern at the ion microirradiation facility SNAKE 72 h after transfection with scr or Jarid1A siRNA. At 1 h after irradiation, underrepresentation of H3K4me3 and RNA Pol II Ser2 at damage sites is comparable in both samples (Figure 21A and 21B), indicated by predominantly pink signals in the map, where the product of the differences from the mean is displayed (PDM map). In the PDM maps areas highlighted in pink show negative correlation of the pixels from both channels, green signals indicate positive correlation and black signals display random distribution of pixels. At high pixel intensities PDM plots skew to negative values demonstrating negative correlation, as well as the scatter plots display anti-correlation between H3K4me3 and γH2AX (Figure 21A) and between RNA Pol II Ser2 and 53BP1 (Figure 21B), respectively. The plot profiles gained by measuring signal intensities in the respective channels along the indicated lines also demonstrate underrepresentation of H3K4me3 and active RNA Pol II Ser2 at damage sites. Unfortunately, with the method that was used here, a quantitive analysis of the intensity correlation was not possible. I conclude, however, that depletion of Jarid1A does not lead to major disturbance of H3K4me3 demethylation at damage sites and radiation-induced transcriptional silencing at chromatin regions decorated by γH2AX/53BP1.

During the course of this thesis it was reported that the demethylase Jarid1B accumulates at damage sites in a PARP1-dependent manner and that its depletion leads to deficiencies in the DSB repair after ionizing radiation and to reduced loss of H3K4me3 at DSB regions (Li et al. 2014). Unfortunately, I could not study the effects of siRNA-mediated knockdown of Jarid1B in our system. Under a variety of experimental conditions, there was either no visible reduction of Jarid1B on the protein level after siRNA transfection or cells detached rapidly once Jarid1B levels were strongly reduced (data not shown). Incubation of cells with PBIT, a recently identified inhibitor of Jarid1B (Sayegh et al. 2013), had no effect on the methylation levels of H3K4 in our lab. Although the substance was tested at different concentrations and in different cell lines, there was no evidence for inhibition of Jarid1B, as indicated by consistent H3K4me3 level in immunofluorescence and Western Blotting experiments (see Western Blot images in Appendix E, Figure E.1). Nevertheless, we performed intensity correlation analysis of H3K4me3 and γH2AX in cells treated with 15 µM PBIT 72 h prior to irradiation with single ions in a line pattern. Loss of H3K4me3 at γH2AX-decorated domains was still visible (see Appendix E, Figure E.2).

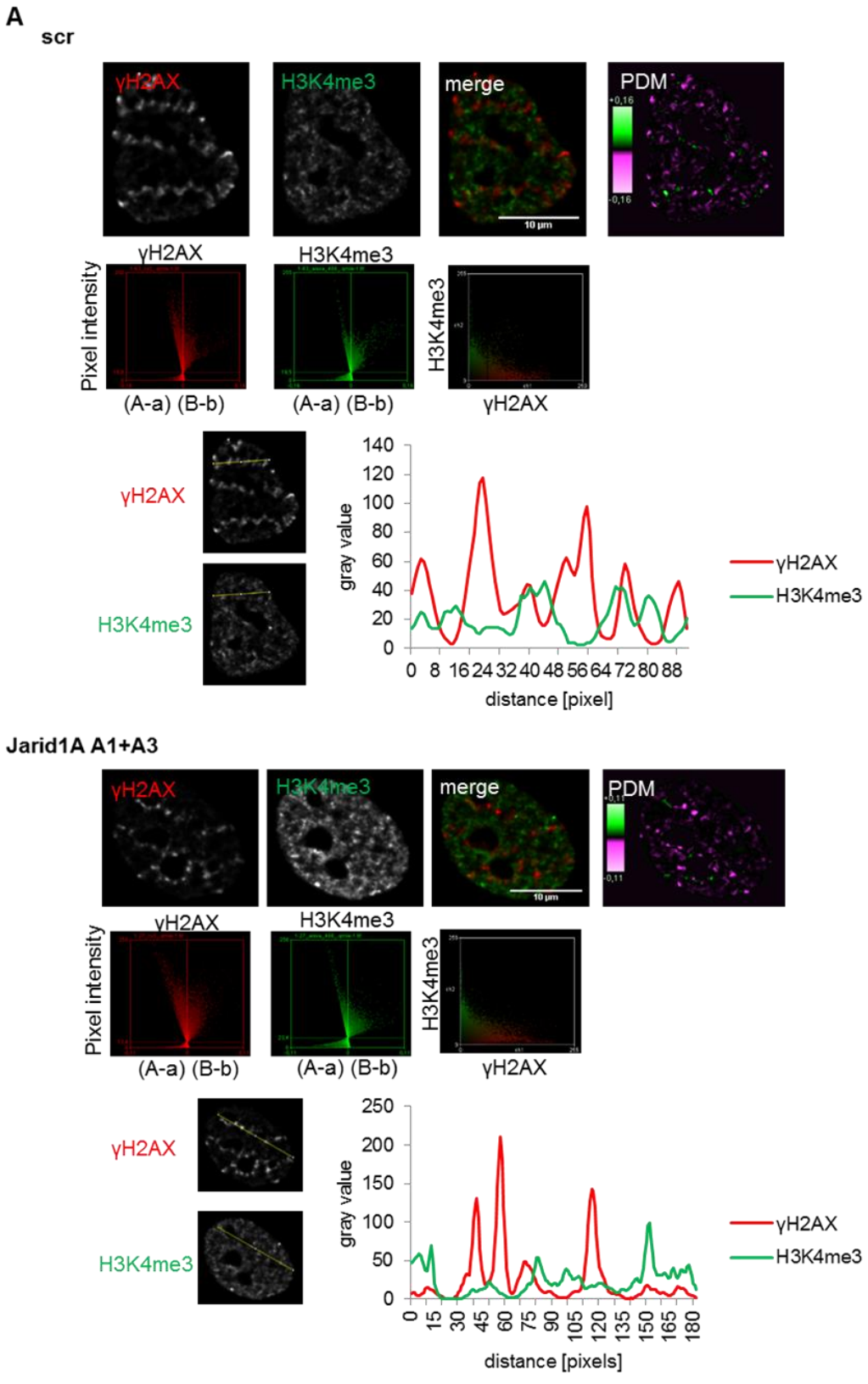
A
scr
γH2AX
H3K4me3
merge
PDM
10 µm
Pixel intensity
(A-a) (B-b)
H3K4me3
gray value
distance [pixel]
Jarid1A A1+A3
distance [pixels]

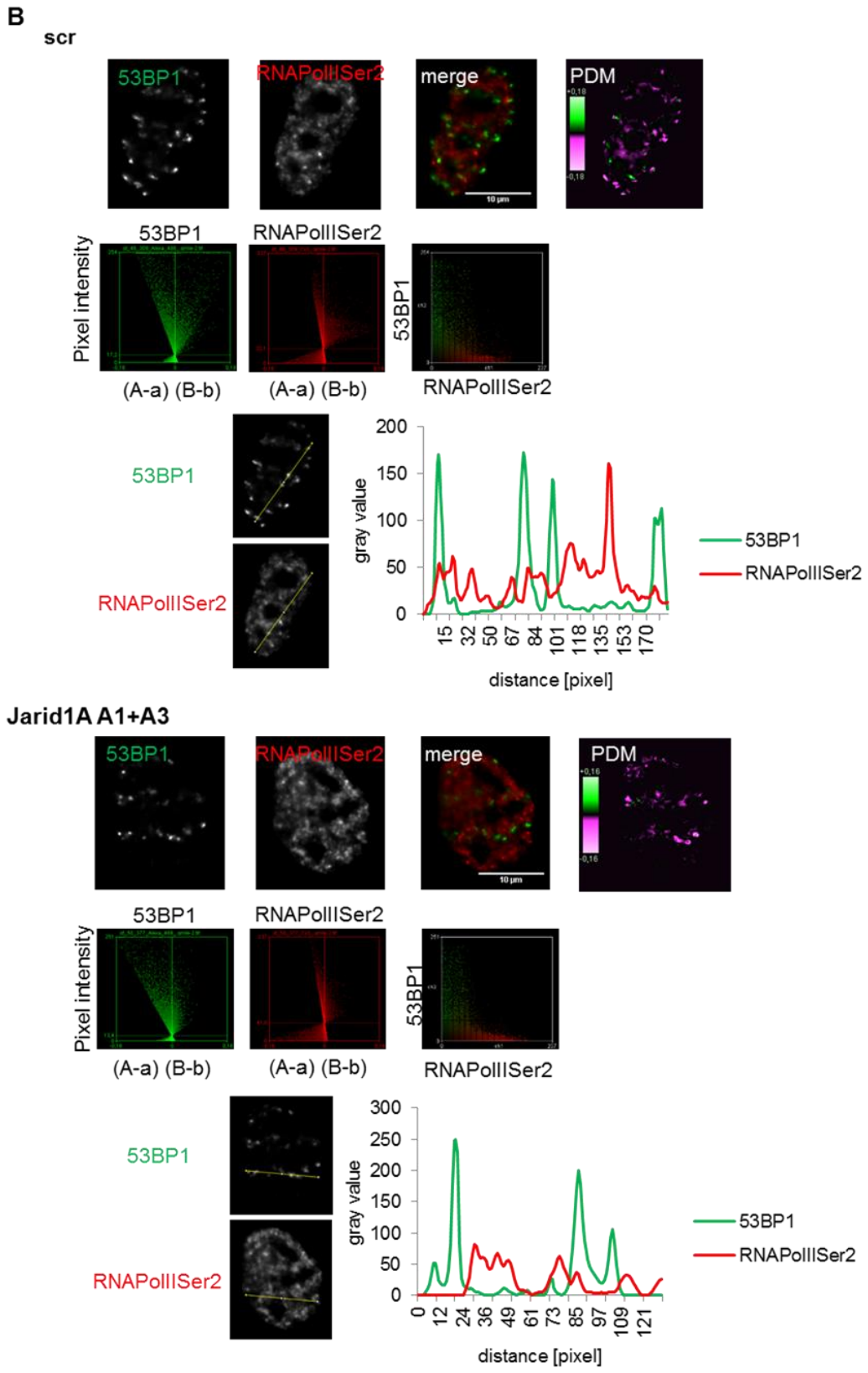

Figure 21: Depletion of Jarid1A does not disturb H3K4me3 demethylation and loss of RNA Pol II Ser2 at damage sites

HeLa cell transfected with scr or Jarid1A A1+A3 siRNAs were subject to ion microirradiation with single carbon ions applied in line patterns (lateral distance between single ion hits 1 µm, distance between "lines" 5 µm). Cells were incubated for 1 h before fixation and indirect immunofluorescence detection of γH2AX and H3K4me3 **(A)** or elongation-proficient RNA Pol II Ser2 **(B)**. Correlation analysis was done as described in chapter 3.3.1. In all panels the top rows show single slices of 3D microscopic images (red channel, green channel and merge). In addition, to determine positive or negative correlation between signal intensities in both channels for each pixel, the product of the mean (PDM) map is shown. In the PDM maps, negative correlation at positions of γH2AX foci is visualized by pink signals; positive correlation is shown by green signals, whereas black indicates random distribution of both signals. In the second row of each panel, plots of signal intensity vs. PDM in the respective channels and the corresponding intensity scatter plots are shown. PDM plots skewed to negative values demonstrate anti-correlation. In the third row, profiles of the signal intensities along the indicated lines also demonstrate underrepresentation of H3K4me3 and active RNA Pol II at damage sites. Displayed are exemplary epifluorescence images. Experiment was performed three times during different beam times.

4.1.7.2 ATM, ATR and PARP1 are not responsible for radiation-induced loss of H3K4me3 at γH2AX-decorated chromatin domains

To identify the factors responsible for the observed loss of H3K4me3 at ion-induced γH2AX foci, I used small molecule inhibitors to inhibit the important damage signalling factors ATM, ATR and PARP1. Each of them is involved in the early steps of damage signalling and may be responsible for the rapidly emerging loss of H3K4me3 at damage sites. Especially PARP1 represents a suitable candidate to be involved in transcriptional silencing of the damaged region, because of the before mentioned involvement of Jarid1B in the damage response in a PARP1-dependent manner (Li et al. 2014).

HeLa cells were irradiated with carbon ions in a 5 x 5 µm matrix pattern at the ion microirradiation facility SNAKE 72 h after inhibition of ATR, ATM and PARP1 with the respective inhibitor. I chose irradiation in matrix pattern, as this allows an even clearer visible pattern than irradiation in line patterns. At 1 h after irradiation, underrepresentation of H3K4me3 at γH2AX regions is visible in the controls treated with DMSO and in the cells treated with the particular inhibitors (Figure 22 and Appendix, Figure E.2 and E.3). This is shown by predominantly pink signals in the PDM map that highlight areas of negative correlation. After inhibition of ATM by KU-60019 (Figure 22A), inhibition of PARP1 by Olaparib (Figure 22B) and inhibition of ATR by VE-821 (see Appendix E, Figure E.3), PDM plots skew to negative values at high γH2AX pixel intensities, demonstrating negative correlation, and the scatter plots also display anti-correlation between H3K4me3 and γH2AX. The plot profiles gained by measuring signal intensities in the respective channels along the indicated lines also demonstrate

underrepresentation of H3K4me3 and γH2AX. Figure 22C demonstrates the proper inhibition of ATM and PARP1 as shown by reduction at the damage site of phosphorylated Chk2 1 h and XRCC1 3 min after irradiation with single ions, respectively. Similar exposure times were used for the comparison of the single signals after treatment with DMSO or inhibitors. The disturbed accumulation of pChk2 is a direct consequence of the inhibition of the kinase ATM, while absent accumulation of XRCC1 can be traced to the inhibition of the catalytic activity of PARP1. Potent inhibition of ATM with KU-60019 is also reflected by a reduction in size and intensity of γH2AX foci (see Figure 22A and 22C), as ATM, together with ATR, is responsible for phosphorylation of γH2AX. I failed to prove the inhibition of the kinase ATR, as the anti-pChk1antibody showed neither signals in the control cells nor in the cells treated with VE-821 (data not shown). I conclude that inhibition of ATM or PARP1 has no major effect on demethylation of H3K4me3 at damage sites and radiation-induced transcriptional silencing at chromatin regions decorated by γH2AX. Concerning the potential involvement of ATR, a final statement is not possible at the moment.

A

DMSO

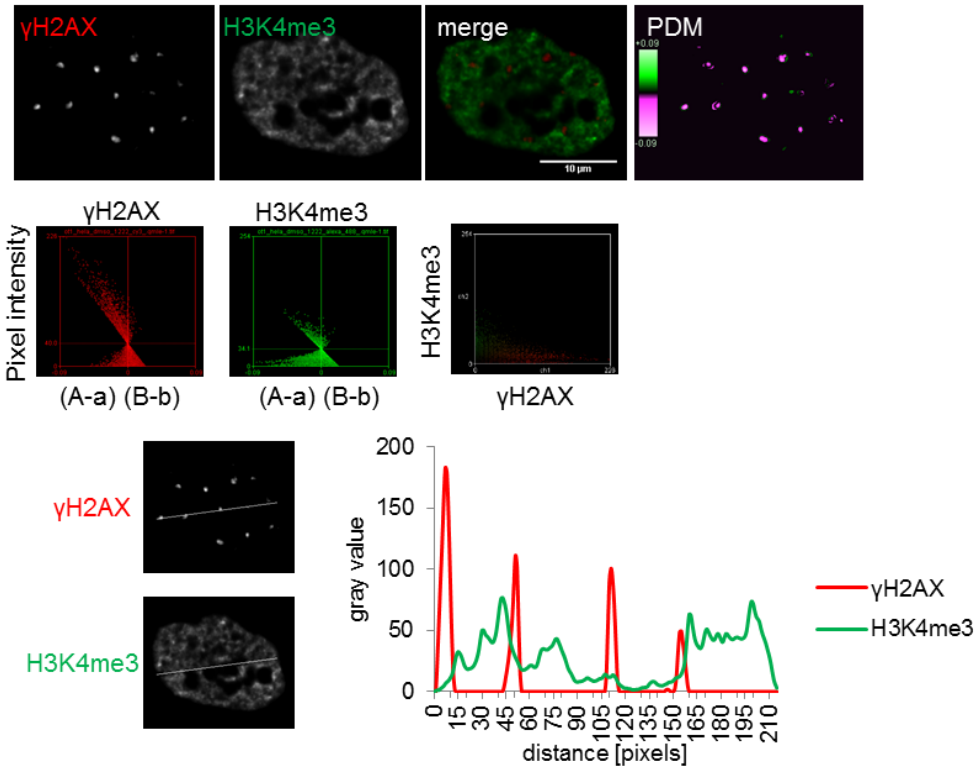

KU-60019

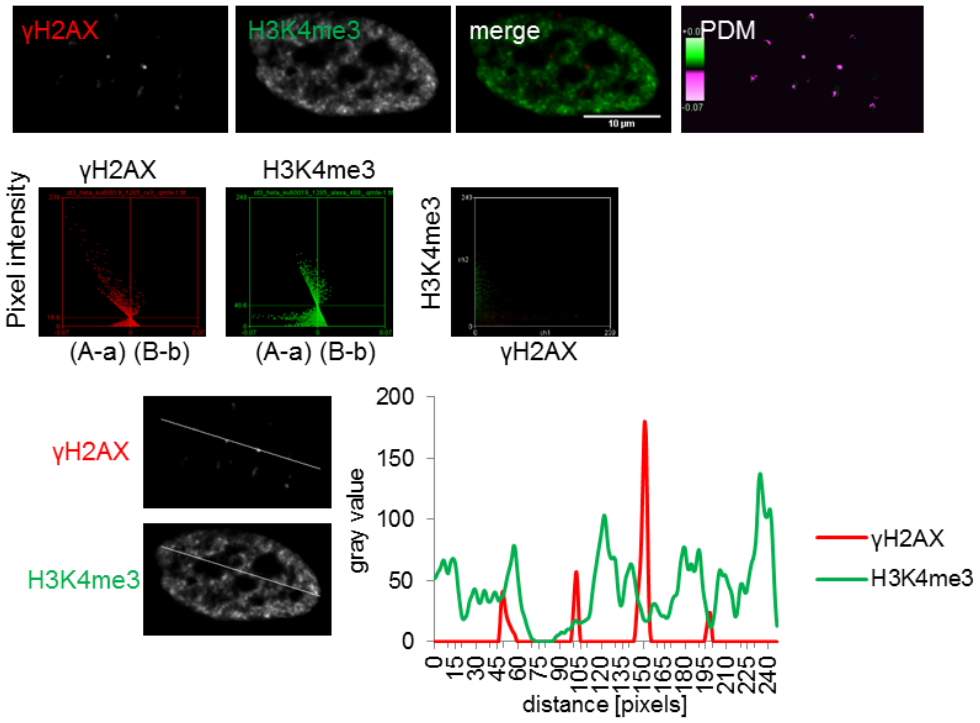

B

DMSO

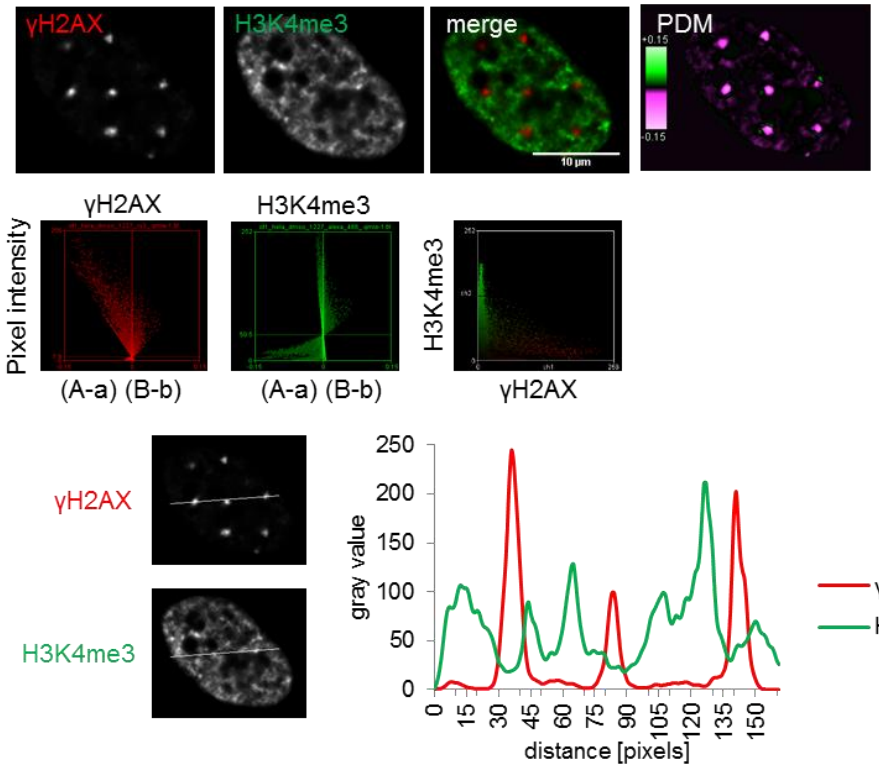

Olaparib

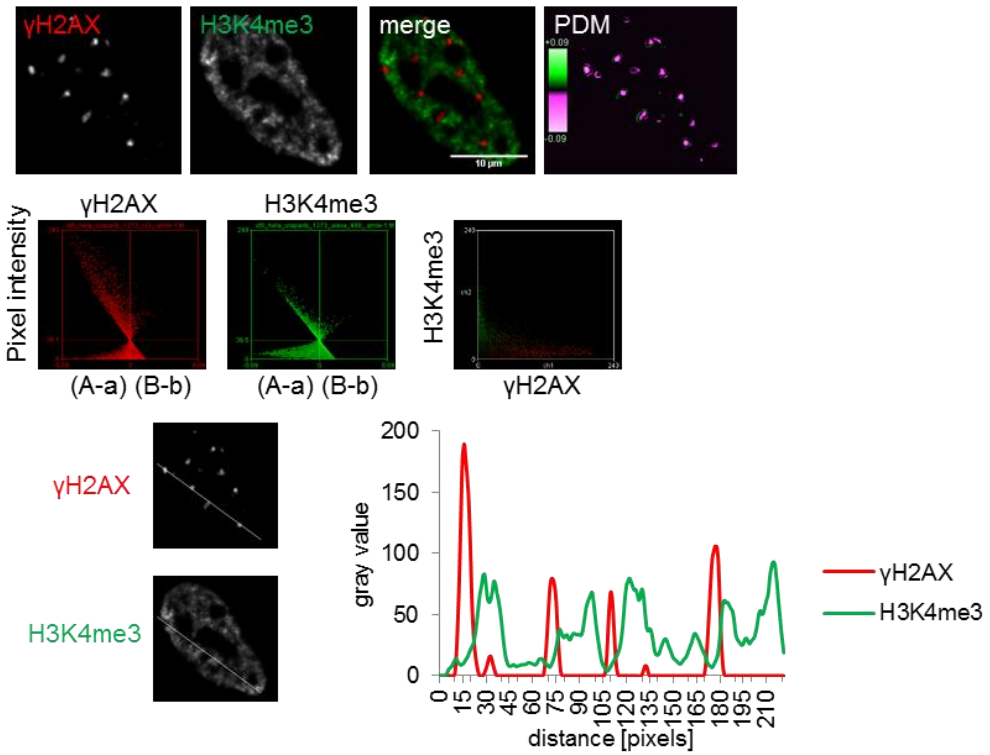

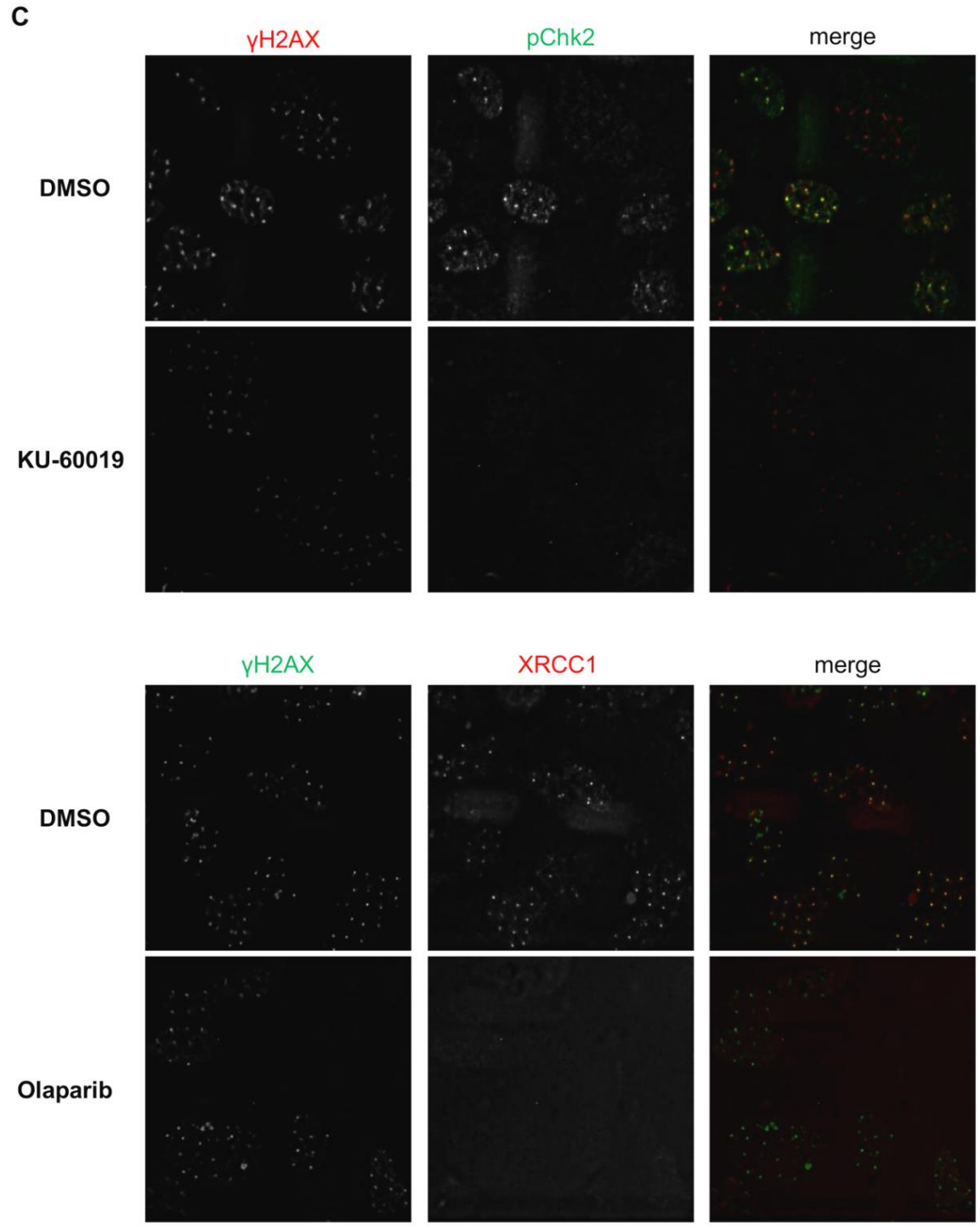

Figure 22: Inhibition of ATM or PARP1 does not disturb H3K4me3 demethylation at damage sites

HeLa cells were treated with **(A)** 10 µM KU-60019 for ATM inhibition and with **(B)** 10 µM Olaparib for PARP1 inhibtion 1 h prior to irradiation. DMSO was used as control. Cells were exposed to ion microirradiation with single carbon ions applied in a 5 µm x 5 µm matrix pattern. Cells were incubated for 1 h before fixation and indirect immunofluorescence detection of γH2AX and H3K4me3. Correlation analysis was done as described in chapter 3.3.1. In all panels the top rows show single slices of 3D microscopic images (red channel, green channel and merge). In addition,

to determine positive or negative correlation between signal intensities in both channels for each pixel, the product of the mean (PDM) map is shown. In the PDM maps, negative correlation at positions of γH2AX foci is visualized by pink signals; positive correlation is shown by green signals, whereas black indicates random distribution of both signals. In the second row of each panel, plots of signal intensity vs. PDM in the respective channels and the corresponding intensity scatter plots are shown. PDM plots skewed to negative values demonstrate anti-correlation. In the third row, profiles of the signal intensities along the indicated lines also demonstrate underrepresentation of H3K4me3 at damage sites.

(C) Decreased signal of pChk2 and XRCC1 after indirect immunofluorescence in HeLa cells treated with KU-60019 or Olaparib. Microscopic images were obtained at comparable exposure times and display γH2AX as damage marker in the left row, pChk2 or XRCC1 in the middle row and merged signals on the right.

4.1.8 Gene expression changes after Jarid1A depletion

As an H3K4me3 demethylase Jarid1A is expected to have a major influence on regulation of transcription. Depletion of Jarid1A has been connected to deregulation of developmentally regulated or cell cycle specific genes (Benevolenskaya et al. 2005; Chicas et al. 2012; Nishibuchi et al. 2014). Since there was neither a hint at disturbed cell viability and cell growth nor impaired recruitment of damage response and DSB repair proteins initiated by depletion of Jarid1A in our experiments, differences in radiosensitivity may result from different transcriptional responses to radiation insults. Therefore the transcription response in Jarid1A knockdown cells was compared to untransfected and control transfected Hela cells with and without irradiation by gene expression microarray analysis. To increase the validity four biological replicates were analysed for every condition - control, scr siRNA and Jarid1A A1+A3 siRNA, 0 Gy and 5 Gy respectively.

Table 12 shows the number of genes with significantly altered expression when comparing the different transfected cells without radiation. After knockdown of Jarid1A mRNA levels of 1731 genes were significantly altered, when comparing to scr transfected cells. Only genes with a fold-change of at least 1.5 and a p-value < 0.05 are included. Of these, 959 genes (55.4%) were down-regulated and 772 genes (44.6%) were up-regulated after Jarid1A depletion. When comparing unirradiated knockdown cells to untransfected cells, 400 genes (58.5%) were down-regulated and 284 genes (41.5%) were up-regulated. A similar proportion of up- and down-regulated genes after Jarid1A depletion in HeLa cells was observed in gene expression microarray analysis by Nishibuchi and colleagues (Nishibuchi et al. 2014). Comparison of mRNA levels of scr transfected cells with untransfected cells reveals 381 significantly altered genes. Efficient depletion of Jarid1A on mRNA level was verified via qRT-PCR (data not shown).

Table 12: Numbers of genes with significantly altered gene expression in microarray analysis in the different transfected cells without radiation

	Comparison Jarid1A A1+A3 to scr	Comparison Jarid1A A1+A3 to contr	Comparison scr to contr
Altered genes	1731	648	381
Up-regulated genes	772 (44.6%)	248 (38.3%)	186 (48.8%)
Down-regulated genes	959 (55.4%)	400 (61.7%)	195 (51.2%)

Pathway enrichment analysis by Reactome (http://www.reactome.org) revealed 6 significantly (FDR ≤ 0.05) deregulated pathways of various hierarchical levels when comparing cells treated with Jarid1A A1+A3 siRNA and scr siRNA. The affected deregulated pathways play a role in level 1 pathways “Extracellular matrix organization” or “Metabolism” and are listed in Table 13. Responsible for the affected extracellular matrix (ECM) organization are mostly deregulated genes that express integrines, collagens and lamins. Modified expression of genes expressing kinases, like PRKAA2, PRKCA or MVK and of genes expressing (parts of) transferases or transporters, like e.g. SPTLC3, ABCC1, ABCC3, ABCG1, provoke deregulated metabolism pathways. Similar pathways are also affected when comparing Jarid1A-depleted cells to untransfected cells. Additionally, some signal transduction pathways and two pathways related to the immune system are involved (see Appendix F, table F.1). The impact on signal transduction pathways is also referable to the deregulation of kinases mentioned above.

Table 13: Significantly deregulated pathways revealed by Reactome pathway enrichment analysis after Jarid1A depletion in unirradiated cells (p < 0.05; FDR < 0.05). *Bold face: level 1, normal font: level 2; blue: Metabolism, pink: Extracellular matrix organization*

Gene Set	Deregulated genes in Gene Set [%]	Genes
Metabolism	11.54	ABCB7, ABCC1, ABCC3, ABCG1, ABHD5, ACACA, ACAT1, ACSL3, ACSL4, ADA, ADSS, AGL, AGPAT2, AGPS, AGT, AK5, ALDH4A1, ALDH6A1, AMPD2, AOX1, APIP, AQP1, ARF1, ASS1, AZIN1, B4GALT4, BCAT2, BCKDHA, BCKDHB, BDH1, CA12, CA2, CACNA1A, CAT, CBR1, CDK19, CERS2, CGA, CHST11, CHSY3, CIAO1, CKMT1A, COL4A3BP, CSGALNACT1, CSPG5, CTGF, CYCS, CYP24A1, CYP2R1, CYP2U1, DCK, DCN, DECR1, ETNK1, FAH, G6PC3, GATM, GBA, GCGR, GCLC, GCLM, GDA, GLA, GLCE, GLIPR1, GLS, GM2A, GNB5, GNG11, GPAT2, GPC5, GPD1L, GPD2, GPX1, GYG1, HACL1, HADHB,

		HAS2, HEXA, HPD, HS6ST1, HS6ST2, HSD17B12, HSD17B7, IDH3B, INPP5A, ISYNA1, ITPR1, LBR, LDLRAP1, LIPE, LPCAT2, LRPPRC, LTA4H, MAPKAPK2, MBOAT2, MCCC1, MED13, MED26, MGLL, MLXIPL, MMACHC, MTHFR, MTMR2, MTR, MVD, MVK, NADK, NCOA3, NCOR1, NDUFA10, NDUFA7, NDUFB1, NDUFB5, NDUFC2, NNMT, NOSTRIN, NPAS2, NT5C3A, NT5E, NUDT4, NUP43, OCRL, PCBD1, PCCB, PDK2, PDK4, PDP2, PGAM1, PGLS, PHKA2, PHYH, PIP4K2A, PLA2G4A, PLD1, POM121, PPIP5K2, PRKAA2, PRKAR1A, PRKAR2A, PRKCA, PSAP, PSAT1, PSMB2, PSMB9, PSMC5, PTGES, PTGS1, PYGB, QPRT, RAP1A, SAT1, SDC4, SDHD, SEC23A, SEC24A, SEC24D, SGMS1, SGMS2, SLC25A32, SLC25A6, SLC27A2, SLC35B2, SLC35D2, SLC44A1, SMOX, SMPD1, SMPD4, SPHK1, SPTLC3, SREBF2, ST3GAL4, STS, SULT4A1, TBL1X, TEAD4, TMLHE, UGDH, UQCR10, UQCRH, WASL
Metabolism of lipids and lipoproteins	13.68	ABCC1, ABCC3, ABCG1, ABHD5, ACACA, ACAT1, ACSL3, ACSL4, AGPAT2, AGPS, AGT, ARF1, BDH1, CBR1, CDK19, CERS2, CGA, COL4A3BP, CTGF, CYP24A1, CYP2R1, CYP2U1, DECR1, ETNK1, GBA, GLA, GLIPR1, GM2A, GPAT2, GPD1L, GPD2, GPX1, HACL1, HADHB, HEXA, HSD17B12, HSD17B7, LBR, LDLRAP1, LIPE, LPCAT2, LTA4H, MAPKAPK2, MBOAT2, MED13, MED26, MGLL, MTMR2, MVD, MVK, NCOA3, NCOR1, NPAS2, OCRL, PCCB, PHYH, PIP4K2A, PLA2G4A, PLD1, PRKAA2, PSAP, PTGES, PTGS1, SEC23A, SEC24A, SEC24D, SGMS1, SGMS2, SLC27A2, SLC44A1, SMPD1, SMPD4, SPHK1, SPTLC3, SREBF2, STS, TBL1X, TEAD4
Extracellular matrix organization	16.35	ADAM17, ADAMTS8, BMP2, COL15A1, COL16A1, COL18A1, COL25A1, COL27A1, COL4A3, COL4A4, COL5A1, COL7A1, COL8A1, COL9A3, COLGALT1, CTSL, DCN, F11R, FGF2, FURIN, ITGA1, ITGA11, ITGA5, ITGAE, ITGAV, ITGB4, LAMA1, LAMA4, LAMB1, LAMB3, LAMC1, LOXL1, LOXL4, LTBP3, MFAP3, MFAP5, MMP24, PCOLCE, PLOD2, PRKCA, SDC4, TGFB3, TRAPPC4
Laminin interactions	39.13	COL18A1, ITGA1, ITGAV, ITGB4, LAMA1, LAMA4, LAMB1, LAMB3, LAMC1
Collagen formation	22.09	COL15A1, COL16A1, COL18A1, COL25A1, COL27A1, COL4A3, COL4A4, COL5A1, COL7A1, COL8A1, COL9A3, COLGALT1, CTSL, ITGB4, LAMB3, LOXL1, LOXL4, PCOLCE, PLOD2
Assembly of collagen fibrils and other multimeric structures	25.93	COL15A1, COL18A1, COL27A1, COL4A3, COL4A4, COL5A1, COL7A1, COL8A1, CTSL, ITGB4, LAMB3, LOXL1, LOXL4, PCOLCE

The significant modifications in gene expression after irradiation with 5 Gy and 2 h post-irradiation incubation are shown in Table 14. In untransfected cells, irradiation led to significantly altered mRNA levels in 245 genes, of which 117 genes (47.8%) were up-regulated and 128 (52.2%) were down-regulated. SiRNA transfected cells (scr and Jarid1A A1+A3) show down-regulation of more than 75% of genes. In all samples, the number of deregulated genes after irradiation is rather low. Generally p53 is the key regulator of the transcriptional response to irradiation (Rashi-Elkeles et al. 2014). Due to inactivated p53 in HeLa cells it is not surprising that the number of significantly deregulated genes is comparably low.

Table 14: Numbers of significantly altered genes in gene expression microarray analysis in the different transfected cells 2 h after irradiation with 5 Gy

	Comparison untransfected cells 0 Gy to 5 Gy	Comparison scr transfected cells 0 Gy to 5 Gy	Comparison Jarid1A transfected cells 0 Gy to 5 Gy
Altered genes	245	93	208
Up-regulated genes	117 (47.8%)	20 (21.5%)	51 (24.5%)
Down-regulated genes	128 (52.2%)	73 (78.5%)	157 (75.5%)

In untransfected cells Reactome analysis indicates 9 pathways that are significantly deregulated after irradiation, all of them belonging to the level 1 pathways “Cell Cycle” and “Cellular responses to stress” (see Table 15). According to the overlap of deregulated genes, similar pathways are affected when analyzing the effects of irradiation in control transfected HeLa cells after irradiation with 5 Gy. The two level 2 pathways of “Programmed cell death” and “Signal Transduction” are additionally affected after irradiation with 5 Gy in scr transfected cells (see Appendix F, table F.2). Besides the pathways “Cell Cycle” and “Cellular responses to stress” Jarid1A depleted cells show also deregulation of the level 1 pathway “Immune system” mostly due to deregulation of toll-like receptor cascades (see table 16). A deregulation of apoptosis related pathways could only be observed in the control transfected cells. Table F.2 shows that the impact on this pathway is referable to the deregulation of three genes encoding proteins of the histone H1 family - HIST1H1A, HIST1H1D and HIST1H1E. The same three genes are also deregulated in untransfected cells and Jarid1A depleted cells, but the pathway is not significantly affected there.

Rashi-Elkeles et al. (2014) showed that inactivation of p53 compromises almost the whole transcriptional response to irradiation, both on the levels of induction and repression. Several pathways generally found responsive to irradiation, such as apoptosis, show only modest

deregulation in our study presumably because of the lack of p53 activity. Most affected pathways rely on the before mentioned deregulated expression of histone and M-phase genes that are predominantely associated with cell cycle control and general response to stress like senescence. These pathways are deregulated in all samples after irradiation independent of siRNA transfection. Deregulation of genes encoding cell cycle factors, in particular down-regulation of factors involved in M-phase, is a typical and well-described response to irradiation (Crawford and Piwnica-Worms 2001, Landsverk et al. 2011). Comprisingly, the gene expression patterns after irradiation of the different transfected cells are very similar.

Table 15: Significantly deregulated pathways revealed by Reactome pathway enrichment analysis in untransfected cells after irradiation (p < 0.05; FDR < 0.05). *Bold face: level 1, normal font: level 2, slanted font: level 3 and higher; green: Cell Cycle, red: Cellular responses to stress*

Gene Set	Deregulated genes in Gene Set [%]	Genes
DNA Damage/Telomere Stress Induced Senescence	15.52	CCNA2, HIST1H1A, HIST1H1D, HIST1H1E, HIST1H2AD, HIST1H2BO, HMGA2, POT1, RAD50
Cell Cycle	4.47	AJUBA, AURKA, BORA, CCNA2, CCNB1, CDCA8, CDKN2C, CENPA, CENPE, CENPL, CNTRL, DBF4, HIST1H2AD, HIST1H2BO, HJURP, LMNA, MCM3, NCAPD2, NEK2, OPTN, POT1, RAD50, SMC1A
Cell Cycle, Mitotic	4.5	AJUBA, AURKA, BORA, CCNA2, CCNB1, CDCA8, CDKN2C, CENPA, CENPE, CENPL, CNTRL, DBF4, HIST1H2AD, HIST1H2BO, LMNA, MCM3, NCAPD2, NEK2, OPTN, SMC1A
Cellular Senescence	7.59	CCNA2, CDKN2C, HIST1H1A, HIST1H1D, HIST1H1E, HIST1H2AD, HIST1H2BO, HMGA2, IL6, NFKB1, POT1, RAD50
Cellular responses to stress	6.05	CCNA2, CDKN2C, HIST1H1A, HIST1H1D, HIST1H1E, HIST1H2AD, HIST1H2BO, HMGA2, IL6, NFKB1, POT1, RAD50, SERPINH1, SOD1, SOD2
Formation of Senescence-Associated Heterochromatin Foci (SAHF)	23.53	HIST1H1A, HIST1H1D, HIST1H1E, HMGA2
Regulation of PLK1 Activity at G2/M Transition	8.75	AJUBA, AURKA, BORA, CCNB1, CNTRL, NEK2, OPTN
G2/M Transition	7.02	AJUBA, AURKA, BORA, CCNA2, CCNB1, CNTRL, NEK2, OPTN
Mitotic G2-G2/M phases	6.9	AJUBA, AURKA, BORA, CCNA2, CCNB1, CNTRL, NEK2, OPTN

Table 16: Significantly deregulated pathways revealed by Reactome pathway enrichment analysis in Jarid1A depleted cells after irradiation (p < 0.05; FDR < 0.05). *Bold face: level 1, normal font: level 2, slanted font: level 3 and higher; green: Cell Cycle, red: Cellular responses to stress, orange: Immune system*

Gene Set	Deregulated genes in Gene Set [%]	Genes
Cell Cycle, Mitotic	8.56	AURKA, BORA, CASC5, CCNA2, CCNB1, CCNE2, CDC20, CDC25A, CDCA8, CDK11A, CDK11B, CDKN1A, CDKN2D, CENPA, CENPE, CENPF, CENPL, CNTRL, HIST1H2AB, HIST1H2AC, HIST2H3A, HSP90AA1, INCENP, KIF18A, KIF23, NDC80, NDE1, NEK2, NEK9, ORC2, SET, SGOL1, SMC1A, SMC4, SPDL1, STAG2, TAOK1, UBE2C
Cell Cycle	7.57	AURKA, BORA, CASC5, CCNA2, CCNB1, CCNE2, CDC20, CDC25A, CDCA8, CDK11A, CDK11B, CDKN1A, CDKN2D, CENPA, CENPE, CENPF, CENPL, CNTRL, HIST1H2AB, HIST1H2AC, HIST2H3A, HSP90AA1, INCENP, KIF18A, KIF23, NDC80, NDE1, NEK2, NEK9, ORC2, SET, SGOL1, SMC1A, SMC4, SPDL1, STAG2, TAOK1, TERF1, UBE2C
M Phase	9.4	CASC5, CCNB1, CDC20, CDCA8, CENPA, CENPE, CENPF, CENPL, HIST1H2AB, HIST1H2AC, HIST2H3A, INCENP, KIF18A, KIF23, NDC80, NDE1, NEK9, SET, SGOL1, SMC1A, SMC4, SPDL1, STAG2, TAOK1, UBE2C
Mitotic Prometaphase	16.67	CASC5, CCNB1, CDC20, CDCA8, CENPA, CENPE, CENPF, CENPL, INCENP, KIF18A, NDC80, NDE1, SGOL1, SMC1A, SMC4, SPDL1, STAG2, TAOK1
Mitotic M-M/G1 phases	8.67	CASC5, CCNB1, CDC20, CDCA8, CENPA, CENPE, CENPF, CENPL, HIST1H2AB, HIST1H2AC, HIST2H3A, INCENP, KIF18A, KIF23,NDC80,NDE1,NEK9,ORC2,SET,SGOL1,SMC1A,SMC4,SPDL1,STAG2,TAOK1,UBE2C
Resolution of Sister Chromatid Cohesion	17	CASC5, CCNB1, CDC20, CDCA8, CENPA, CENPE, CENPF, CENPL, INCENP, KIF18A, NDC80, NDE1, SGOL1, SMC1A, SPDL1, STAG2, TAOK1
Separation of Sister Chromatids	10.56	CASC5, CDC20, CDCA8, CENPA, CENPE, CENPF, CENPL, INCENP, KIF18A, NDC80, NDE1, SGOL1, SMC1A, SPDL1, STAG2, TAOK1, UBE2C
Mitotic Anaphase	9.88	CASC5, CDC20, CDCA8, CENPA, CENPE, CENPF, CENPL, INCENP, KIF18A, NDC80, NDE1, SGOL1, SMC1A, SPDL1, STAG2, TAOK1, UBE2C
Mitotic Metaphase and Anaphase	9.83	CASC5, CDC20, CDCA8, CENPA, CENPE, CENPF, CENPL, INCENP, KIF18A, NDC80, NDE1, SGOL1, SMC1A, SPDL1, STAG2, TAOK1, UBE2C

G2/M Transition	10.53	AURKA, BORA, CCNA2, CCNB1, CDC25A, CDK11A, CDK11B, CENPF, CNTRL, HSP90AA1, NDE1, NEK2
Mitotic G2-G2/M phases	10.34	AURKA, BORA, CCNA2, CCNB1, CDC25A, CDK11A, CDK11B, CENPF, CNTRL, HSP90AA1, NDE1, NEK2
Cellular Senescence	7.59	CCNA2, CCNE2, CDKN1A, CDKN2D, HIST1H1A, HIST1H1D, HIST1H2AB, HIST1H2AC, HIST2H3A, IL6, TERF1, UBE2C
DNA Damage/Telomere Stress Induced Senescence	13.79	CCNA2, CCNE2, CDKN1A, HIST1H1A, HIST1H1D, HIST1H2AB, HIST1H2AC, TERF1
Senescence-Associated Secretory Phenotype (SASP)	10.67	CCNA2, CDKN1A, CDKN2D, HIST1H2AB, HIST1H2AC, HIST2H3A, IL6, UBE2C
Cellular responses to stress	5.24	CCNA2, CCNE2, CDKN1A, CDKN2D, HIST1H1A, HIST1H1D, HIST1H2AB, HIST1H2AC, HIST2H3A, HSP90AA1, IL6, TERF1, UBE2C
Condensation of Prophase Chromosomes	14.63	CCNB1, HIST1H2AB, HIST1H2AC, HIST2H3A, SET, SMC4
MyD88-independent cascade	8.6	BIRC3, DUSP6, HMGB1, IRAK2, NFKB2, NFKBIA, TICAM1, UBE2V1
TRIF-mediated TLR3/TLR4 signaling	8.6	BIRC3, DUSP6, HMGB1, IRAK2, NFKB2, NFKBIA, TICAM1, UBE2V1
Toll Like Receptor 3 (TLR3) Cascade	8.6	BIRC3, DUSP6, HMGB1, IRAK2, NFKB2, NFKBIA, TICAM1, UBE2V1
Centrosome maturation	9.72	CCNB1, CDK11A, CDK11B, CNTRL, HSP90AA1, NDE1, NEK2

Since pathway analysis did not hint at great differences in transcriptional radiation response between Jarid1A depleted cells and controls, I next investigated the most deregulated genes. The Venn diagram displays the remarkably great overlap of the 50 most deregulated genes in control, scr and Jarid1A A1+A3 cells, each with the same direction of alteration (see Figure 23). Down-regulation of the M-phase genes CDCA8, BORA, AURKA, CCNB1, CENPA, FAM83D and GAS2L3 was seen in all samples after irradiation. Simultaneously, genes involved in inflammatory response, like CXCL1, CXCL2, CXCL3, IL6, NFKBIA, CCL2 and NFKB2 were up-regulated after irradiation. This list contains several genes that belong to a small cluster of genes previously shown to be up-regulated after irradiation in a p53-independent manner like BIRC3, NFKB2, NFKBIA or TNFAIP3 (Rashi-Elkeles et al. 2014).

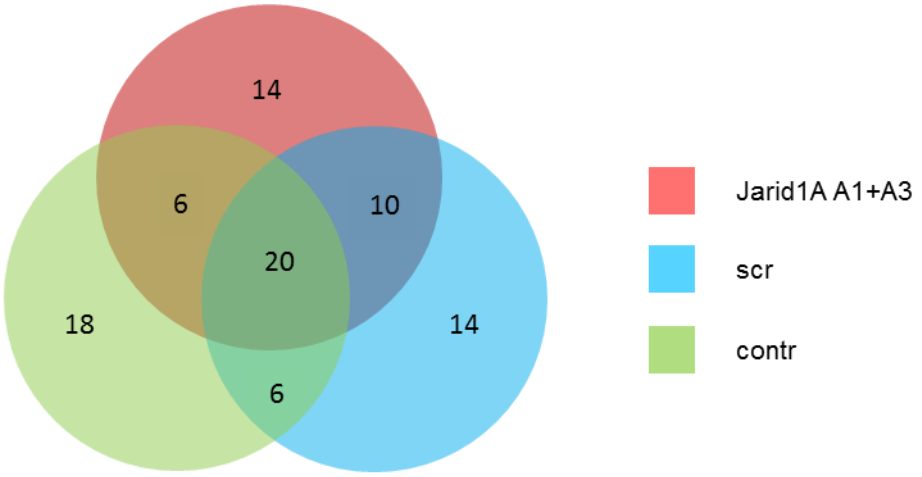

Figure 23: Overlap of deregulated genes in different transfected HeLa cells 2 h after irradiation with 5 Gy

Venn diagram displaying commonly and exclusively differentially expressed genes of the 50 most deregulated genes in control cells, scr siRNA and Jarid1A A1+A3 siRNA transfected cells 2h after irradiation with 5 Gy.

The heat map in FigureFigure 24 shows a two-dimensional hierarchical clustering based on the list of the 50 most significantly deregulated genes between control cells, cells transfected with scr siRNA and Jarid1A A1+A3 siRNA with and without irradiation. The heat map represents expression intensities by red and green signals, for high and low intensities, respectively. Black signals indicate medium intensities. This hierarchical clustering is used to realise how the microarray samples and the deregulated genes group together based on similarity of features. On top and on the left of the heat map a dendrogram illustrates the arrangement of the clusters produced by hierarchical clustering. The further the distance of the fusion of two clusters is on the top dendrogram the greater are the differences between the clusters. The dendrogram on the left clusters genes with similar behaviors in the experiment, while the dendrogram on top clusters the different treated samples due to their expression of the affected genes. Control samples and scr samples, while in general forming separate clusters, are clearly separated form the Jarid1A-depleted cells. Clustering of unirradiated samples (ctrl_0, scrmbld_0 and kd_0) versus irradiated samples (ctrl_5, scrmbld_5 and kd_5) is only partially seen, again hinting at the small effect irradiation had on the gene expression pattern.

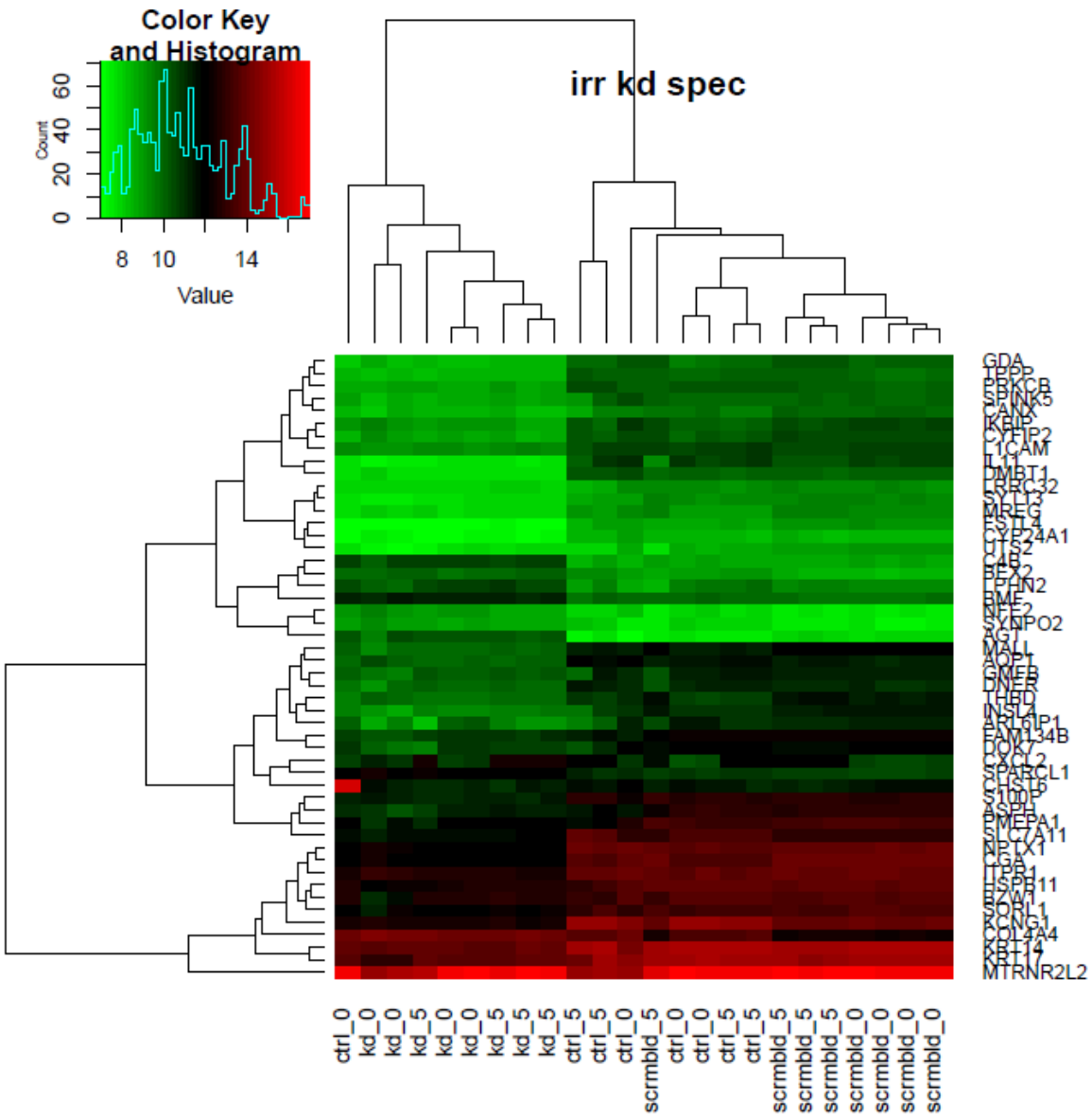

Figure 24: Heat map and hierarchical clustering of the 50 most significantly deregulated genes in the different treated samples in microarray analysis

Clustering of control samples (ctrl), scr transfected samples (scrmbld) and Jarid1A A1+A3 transfected samples (kd) after irradiation with 0 Gy and 5 Gy (_0, _5) based on expression of the most significantly deregulated genes in microarray analysis. For each condition, 4 replicates were investigated. Deregulated genes are listed on the right side of the heat map, while they are clustered beneath the map via a dendrogram. Unchanged gene expression is displayed in black, up-regulated gene expression in red and down-regulated gene expression in green. On top of the heat map a dendrogram visualizes the formed clusters of the different treated samples and their similarities. The further the distance of the fusion of two clusters is, the more different is the expression of the 50 genes in the clusters.

To reveal genes that are specifically deregulated in the Jarid1A knockdown cells after irradiation, mutual deregulated genes after knockdown in comparison to control and scr siRNA transfected cells after irradiation were defined. Thereby the direction of alteration was

considered and genes also deregulated in unirradiated cells were excluded. This results in 566 genes that were only found significantly deregulated after Jarid1A knockdown plus irradiation. Of these, 187 were up-regulated and 379 were down-regulated. Pathway enrichment analysis with solely these deregulated genes yields 3 affected pathways: The level 1 pathway “Extracellular matrix organization” and the associated level 2 pathway “Beta1 integrin cell surface interactions”. The deregulation of these pathways is mainly based on deregulation of genes that express collagens, lamins and integrins. Additionally, a third affected level 3 pathway “Complement and coagulation cascades” is involved in Jarid1A knockdown cells after irradiation (see Table 17), but with only a few affected genes. Generally, the proportion of deregulated genes in the Gene Set of the three respective pathways is relatively low with 2.65% of differentially expressed genes in the pathway “Extracellular matrix organization” and < 1% in the pathways “Beta1 integrin cell surface interactions” and “Complement and coagulation cascades”. It has, nevertheless, to be mentioned that especially the deregulation of genes of the ECM organization and beta integrin signalling can have an immense influence on DNA damage response. Dickreuter et al. (2016) postulate a regulatory function for β1 integrines in the repair of radiation-induced DSB. In our microarray analysis some genes encoding alpha integrines are markedly down-regulated. Integrins are heterodimers formed through association of an alpha integrine with a beta integrine (Hynes 2002). Consequently, down-regulation of one type of integrine might have an influence on the other type. Genes encoding collagens are either up- or down-regulated in the gene expression microarray analysis after Jarid1A-knockdown and irradiation, making it hard to correctly estimate the consequences on ECM organization.

Table 17: Unique deregulated pathways revealed by Reactome pathway enrichment analysis in Jarid1A depleted cells after irradiation (p < 0.05; FDR < 0.05). *Bold face: level 1, normal font: level 2, slanted font: level 3 and higher; pink: Extracellular matrix organization, orange: Immune system*

Gene Set	Deregulated genes in Gene Set [%]	Genes
Extracellular matrix organization	2.65	COL16A1, MMP24, FGF2, COL7A1, COL15A1, TGFB3, TGFB1, MFAP3, MFAP5, LOXL4, DCN, COL9A3, COL8A1, COL4A4, COL5A2, CD44, ITGA11, COL18A1, LAMA3, ADAM17, ITGAV, ITGA5, CTSL
Beta1 integrin cell surface interactions	0.67	COL7A1, COL4A4, COL5A2, ITGA11, COL18A1, LAMA3, PLAU, CD14, ITGAV, ITGA5
Complement and coagulation cascades	0.70	C4B, C3, THBD, C4BPB, CFH, BDKRB2, PLAT, CD55, PLAU, PROC

A selection of genes related to pathways involved in stress/ damage response or DNA repair with at least a 1.5-fold increased or decreased expression exclusively in Jarid1A depleted cells after irradiation are listed in Table 18 with their known functions. Within the scope of a research course (Babushku 2016) and additional experiments performed by the technical lab assistant Claudia Böhland the expression of these genes was analysed in control and Jarid1A-depleted cells on protein level to check for potential variances in the expression after irradiation. The selected genes are either involved in stress and damage response (PARP1, HSP90) or/and in cell cycle and transcriptional regulation (CENPF, INCENP, NFKBIE, SMC1A, YBX1). None of the just mentioned genes showed a distinct up- or downregulation on protein level as indicated by Western Blotting. The results for CENPF, PARP1 and NFKBIE can be viewed in Appendix F, Figure F.1 (the rest of the data is not shown here as no changes on the protein level are visible at all). Additionally, the observed down-regulation of KDM5B in Jarid1A knockdown cells in the microarray analysis was reassessed on protein level and could not be verified.

Table 18: Selection of significantly deregulated genes in Jarid1A depleted cells after irradiation ($p < 0.05$) that are assumed to play a role in stress/ damage response or DNA repair with at least 1.5-fold increased or decreased expression in the gene expression microarray analysis.

Significantly deregulated genes after Jarid1A depletion	Fold change	Function (https://www.ncbi.nlm.nih.gov/gene)
CENPF ↓	1.6	encodes a protein that associates with the centromere-kinetochore complex; may play a role in chromosome segregation during mitotis
SMC1A ↓	2.0	encodes a protein important for functional kinetochores; protein interacts with BRCA1, indicating a potential role in DNA repair
PARP1 ↓	1.8	encodes a chromatin-associated enzyme, which modifies various nuclear proteins by poly(ADP-ribosyl)ation; involved in regulation of various important cellular processes, including damage repsonse
HSP90AA1 ↓	1.7	encodes an inducible molecular chaperone that functions as a homodimer
NFKBIE ↑	2.3	encodes a protein that binds to components of NF-kappa-B, trapping the complex in the cytoplasm and preventing it from activating genes in the nucleus
KDM5B ↓	1.8	encodes a histone demethylase that belongs to the Jarid1 family of histone demethylases; protein is capable of demethylating lysine 4 of histone H3 and plays a role in transcriptional repression

INCENP ↓	1.7	encodes a chromosomal passenger protein crucial for multiple events that mediate chromosome separation during mitosis (Carmena and Earnshaw 2006)
YBX1 ↓	1.8	encodes a highly conserved cold shock domain protein; protein has been implicated in numerous cellular processes including regulation of transcription and DNA repair

In conclusion, the results of the microarray analysis reveal a relative small effect of x-irradiation on the gene expression in HeLa cells (independent from siRNA transfection). With regard to the different treatment of cells with siRNA, some differences in the gene expression pattern can be observed both with and without irradiation. In unirradiated cells Reactome pathway enrichment analysis reveals several pathways affected after Jarid1A depletion compared to the controls. This is not surprising as the demethylase directly influences the chromatin structure by removing tri- or di-methylations from H3K4 and is thereby involved in regulation of transcritption. Analyzing exclusively the gene expression changes in Jarid1A-knockdown cells after irradiation revealed some differentally expressed genes of the ECM organization and the complement/coagulation cascades. As only very few genes of this pathway are affected, the consequences of this observation should be negligible. Further, distinct DNA damage response genes found in the microarray analysis to be differentially expressed after knockdown and irradiation showed no differential expression on protein level. In line with the previous results of my work, gene expression microarray analysis indicates no obvious influence of the Jarid1A-depletion on genes or pathways directly involved in DSB repair or cellular responses to stress. Unfortunately, it gives also no further hints at the mechanistic basis of the increased radiosensitivity observed after Jarid1A depletion.

4.2 Influence of 2-HG incubation on histone modifications and cell behaviour

As the inhibition of the demethylase Jarid1B with the established inhibitor PBIT failed in my experiments and other Jarid1B inhibitors were not known during the experimental phase of this thesis, I decided to use an unspecific inhibitor of α-ketoglutarate (α-KG)-dependent demethylases. To analyse the effects of the unspecific inhibition of α-KG-dependent JmjC demethylases on the level of histone methylation, glioblastoma cell lines were treated with the cell permeable ester of R-2-HG. Glioblastoma cells were used to reveal the most effective incubation condition, as many reports about successful inhibition of α-KG-dependent demethylases by R-2-HG in glioblastoma cells exist (Xu et al. 2011; Dang et al. 2009). R-2-HG mimics the mutation in the enzyme IDH1 by directly inhibiting α-KG-dependent

dioxygenases. As the prognosis for glioblastomas with IDH mutations is quite favourable, a therapeutic benefit by the use of R-2-HG is conceivable. I incubated the glioblastoma cell lines A172 and U-87 MG with different concentrations of R-2-HG and investigated the effects on the histone modifications H3K4me3 and H3K9me3, as well as on proliferation and migratory behaviour, as glioma cells with IDH mutations exhibit decreased growth and migratory behaviour (Li et al. 2013)

Different concentrations of the cell permeable ester of R-2-HG and the respective concentrations of DMSO as control were added to A172 and U-87 MG cells. In the literature the concentrations of R-2-HG to obtain an effect in histone demethylase inhibition varied from 0.1 mM to 10 mM (Xu et al. 2011; Reitman et al. 2014). Since Reitman et al. 2014 showed in HTC116 cells that treatment with 0.1 mM R-2HG results in the same level of intracellular R-2HG as produced in knock-in IDH1 mutant cells, I decided to investigate concentrations from 0.01 mM to 1.0 mM. After adding R-2-HG, cells were incubated for 7 days as described in the literature (Reitmann et al. 2014). I analysed the levels of H3K4me3 and H3K9me3 by Western Blotting experiments with whole cell protein extracts after the incubation period with R-2-HG. Western Blot images in Figure 25 show the expression of the H3K4me3 levels (Figure 25A and B) and H3K9me3 levels (Figure 25C and D) in the differently treated cells. Influence of higher concentrations of R-2-HG from 0.05 mM to 1.0 mM was tested in three to five independent experiments. The average level of the respective histone modification is depicted in the diagrams below each Western Blotting image. Tri-methylation at H3K4 was neither markedly increased in A172 cells (Figure 25A) nor in U-87 MG cells (Figure 25B) at any tested concentration of R-2-HG. Apparently, Jarid1 histone demethylases are not affected by incubation with the R-2-HG cell permeable ester at concentrations from 0.01 mM to 1.0 mM in A172 and U-87 MG cells. It has to be mentioned that α-ketoglutarate-dependent histone demethylases exhibit distinct sensitivity to R-2-HG. While the H3K9me3 and H3K36me3 lysine demethylase KDM4C (JMJD2C) shows half-maximal inhibitory concentration (IC_{50}) values of 80 µM, IC_{50} values for the H3K9me3/me2 and H3K36me3 lysine demethylase KDM4A (JMJD2A) is 25 µM in HCT116 cells (Chowdhury et al. 2011). Possibly, the family of H3K9me3 histone demethylases KDM4 (JMJD2) is generally more sensitive to treatment with 2-R-HG than the KDM5 family. I therefore also analysed the levels of H3K9me3 in A172 and U-87 MG cells after 7 days incubation with cell permeable R-2-HG ester, using the same concentrations as before. Tri-methylation at H3K9me3 was also neither markedly increased in A172 cells (Figure 25C) nor in U-87 MG cells (Figure 25D) at any tested concentration of R-2-HG. H3K9me3 histone demethylases in A172 and U-87 MG cells are not affected by incubation with the R-2-HG cell permeable ester at concentrations from 0.01 mM to 1.0 mM.

Since the sensitivity to R-2-HG might be cell-line specific, I also treated HTC116 cells with 0.1 mM R-2-HG. As reported by Reitman et al. (2014) this results in a similar level of intracellular R-2HG produced in knock-in IDH1 mutant HTC116 cells. However, our Western Blotting experiments in HTC116 cells also did not show increased H3K9me3 or H3K4me3 levels in the cells (see Appendix G, Figure G). As investigated by levels of histone modifications, I failed to achieve an inhibition of α-KG-dependent JmjC demethylases in U-87 MG, A172 and HTC116 cells with our tested concentrations of cell permeable R-2-HG.

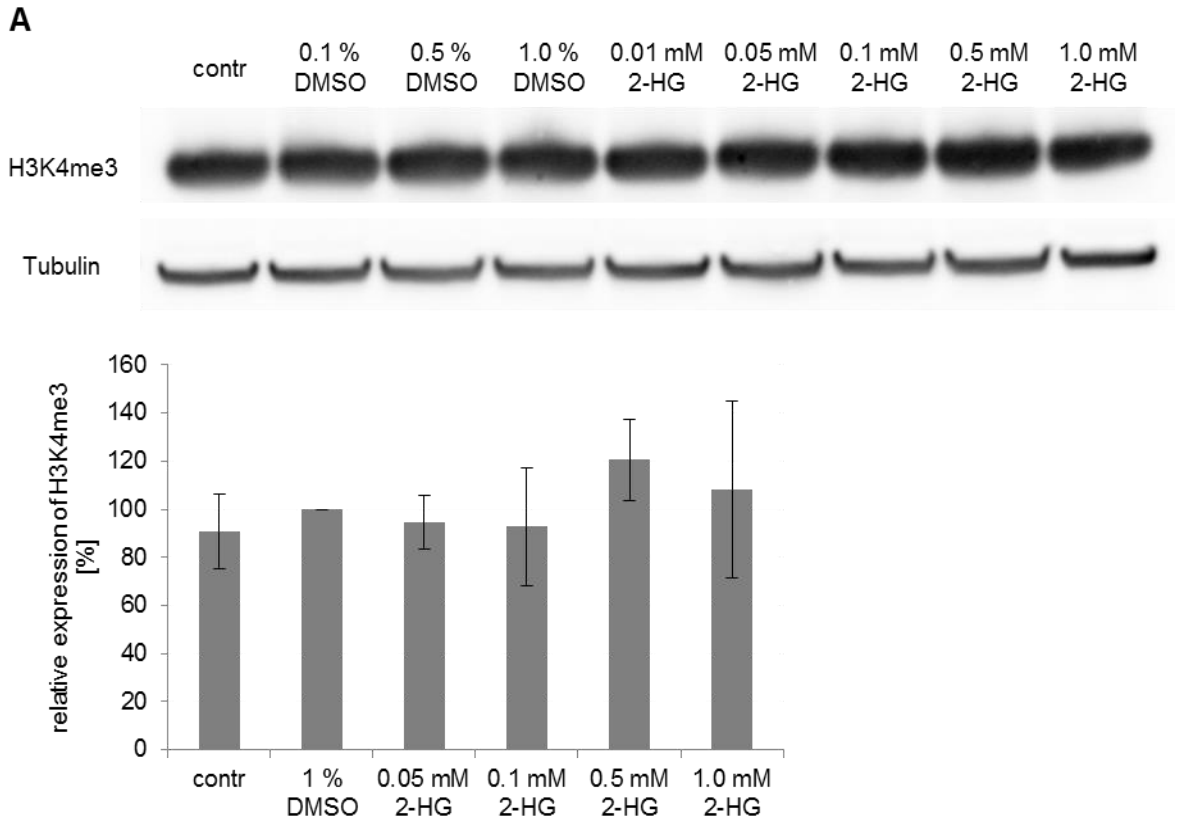

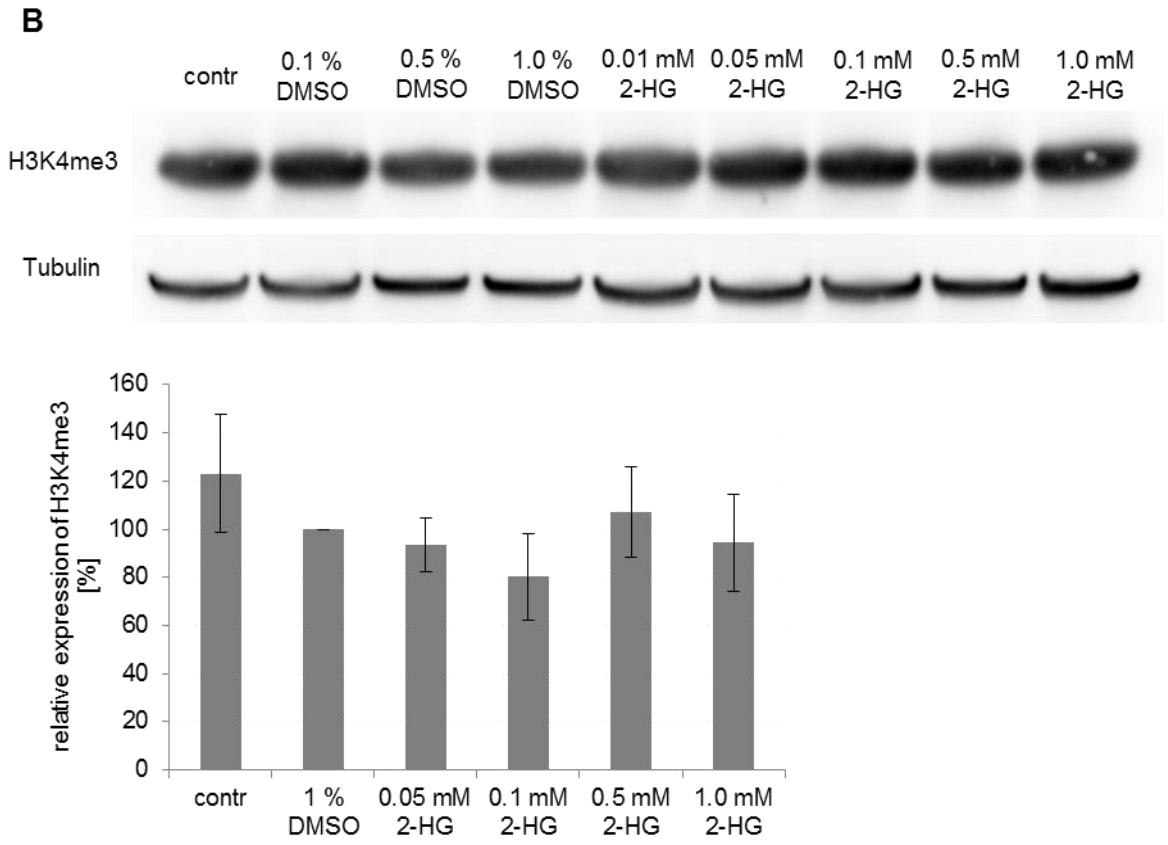
B
contr
0.1 % DMSO
0.5 % DMSO
1.0 % DMSO
0.01 mM 2-HG
0.05 mM 2-HG
0.1 mM 2-HG
0.5 mM 2-HG
1.0 mM 2-HG
H3K4me3
Tubulin
relative expression of H3K4me3 [%]
0
20
40
60
80
100
120
140
160
contr
1 % DMSO
0.05 mM 2-HG
0.1 mM 2-HG
0.5 mM 2-HG
1.0 mM 2-HG

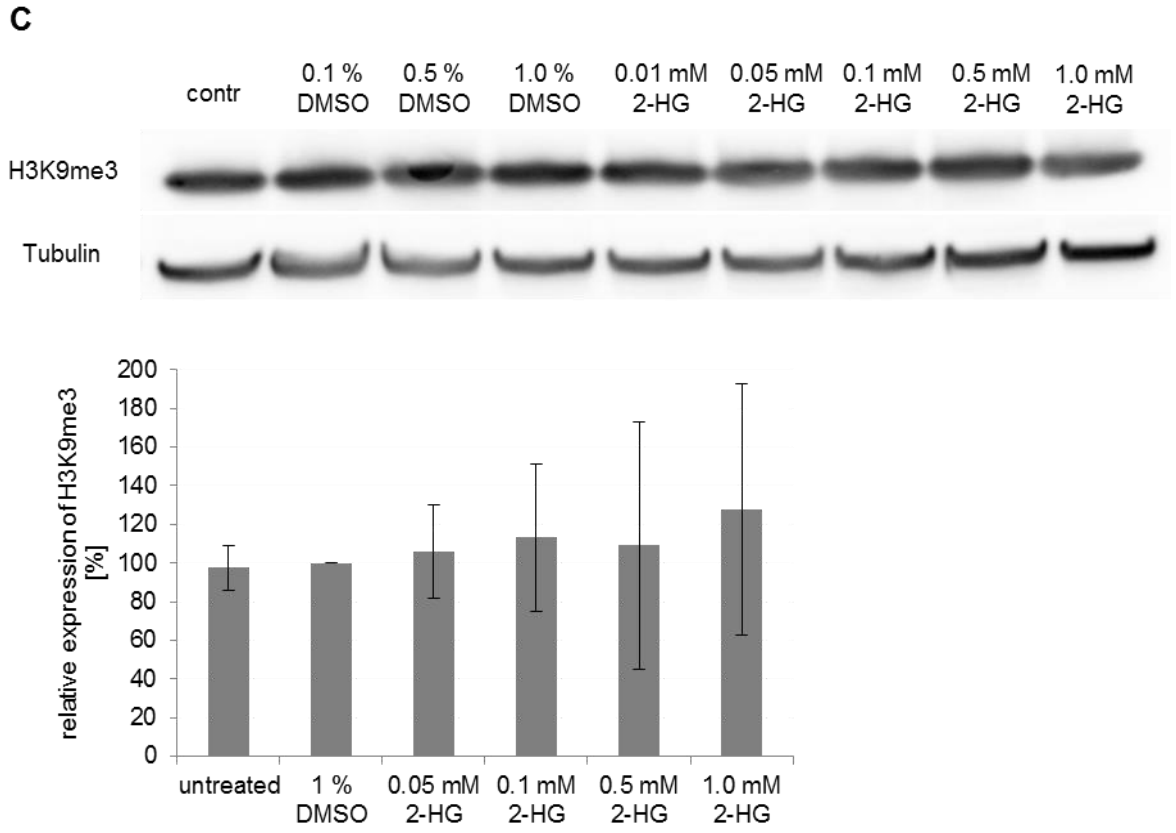
C
contr
0.1 % DMSO
0.5 % DMSO
1.0 % DMSO
0.01 mM 2-HG
0.05 mM 2-HG
0.1 mM 2-HG
0.5 mM 2-HG
1.0 mM 2-HG
H3K9me3
Tubulin
relative expression of H3K9me3 [%]
0
20
40
60
80
100
120
140
160
180
200
untreated
1 % DMSO
0.05 mM 2-HG
0.1 mM 2-HG
0.5 mM 2-HG
1.0 mM 2-HG

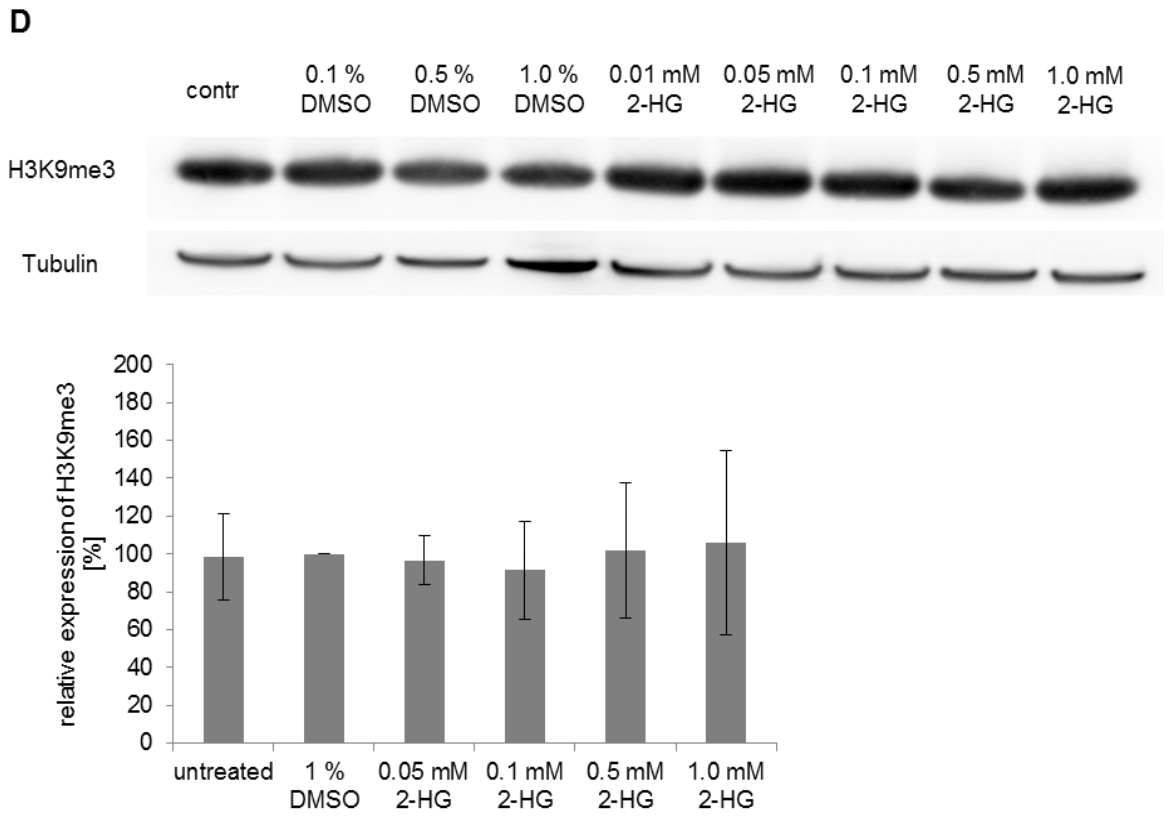

Figure 25: H3K4me3 and H3K9me3 levels in glioblastoma cell-lines after incubation with different concentrations of R-2-HG remains unchanged

Steady levels of H3K4me3 in A172 cells **(A)** and U-87 MG cells **(B)** as well as H3K9me3 in A172 cells **(C)** and U-87 MG cells **(D)** after incubation with different concentrations of R-2-HG. Western blot images show levels of H3K4me3 and H3K9me3, respectively, in glioblastoma cells treated with R-2-HG from 0.01 mM to 1.0 mM. 1% of DMSO was used as control corresponding to the DMSO concentration in the sample treated with 1.0 mM R-2-HG (for lower R-2-HG concentrations DMSO concentration was reduced accordingly). Graphs display the normalized average amount (+/- SD) of H3K4me3 and H3K9me3 protein after R-2-HG treatment for 7 days, as determined by quantitative analysis of Western blots of protein extracts obtained in three to five independent experiments with concentrations of R-2-HG from 0.05 mM to 1.0 mM.

In addition, I investigated the effect of R-2-HG on cell proliferation and migration. Glioblastoma are one of the most aggressive forms of cancer due to their highly invasive behaviour (Naumann et al. 2013; Rolon-Reyes et al. 2015). However, for glioma cells with IDH mutations decreased growth and migratory behaviour is characteristic (Li et al. 2013). For investigation of the cell growth of A172 cells, I accomplished growth curves with untreated cells, cells treated with 0.05 mM R-2-HG and cells treated with 0.05% DMSO. R-2-HG or DMSO was added 6 days before seeding and again after seeding of the cells for the growth curves. Afterwards, cells were harvested and counted every 24 h for 7 days. Figure 26A displays the cell growth

over time of the different treated glioblastoma cells. Incubation of cells with the used R-2-HG concentration seems to have no influence on the cell proliferation.

The impact of the substance on the migratory behaviour was examined by wound healing assays. As cells with IDH mutations show better therapeutic efficacy of tumor therapies such as radio- and chemotherapy (Yan et al. 2009; Cairncross et al. 2014), a possible explanation would be a reduced migration potential. To investigate this, U-87 MG cells were used as they are known to migrate really fast (Li et al. 2016). Additionally, the concentration of R-2-HG was increased tenfold compared to the cellular growth experiment. U-87 MG cells treated with 0.5 mM R-2-HG or 0.5% DMSO for 7 d were seeded into culture inserts. Furthermore, 0.5 mM fresh R-2-HG was added to the cells. To compare the migratory capacity, the insert was removed on the next day and migration into the “wound” was microscopically monitored every 30 min for 8 h. Figure 27B illustrates the migration into the gap of control and 2-HG treated cells. There is no visible difference between the movement of the DMSO-treated control cells and the R-2-HG treated cells, as shown by the photographies. Even the evaluation of the colonized area over time represented in the graph of the Figure 26B indicates similar velocity of cell migration. Taken together, both the data of the cellular growth curves and the wound healing assays, R-2-HG seems not to interfere with cell proliferation or migration of the glioblastoma cell lines under the conditions I used. It remains to be elucidated why others see an effect on α-KG dependent histone demethylases and on cellular growth properties of glioblastome cell lines with similar concentrations of 2-HG.

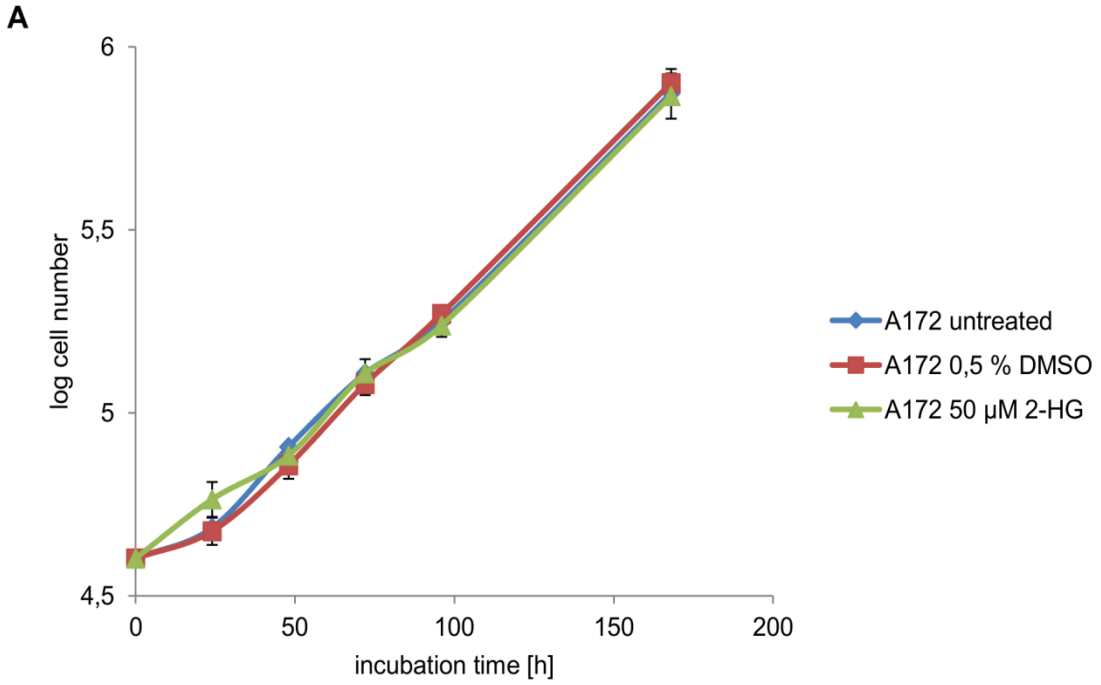
A
6
5,5
5
4,5
log cell number
0
50
100
150
200
incubation time [h]
A172 untreated
A172 0,5 % DMSO
A172 50 µM 2-HG

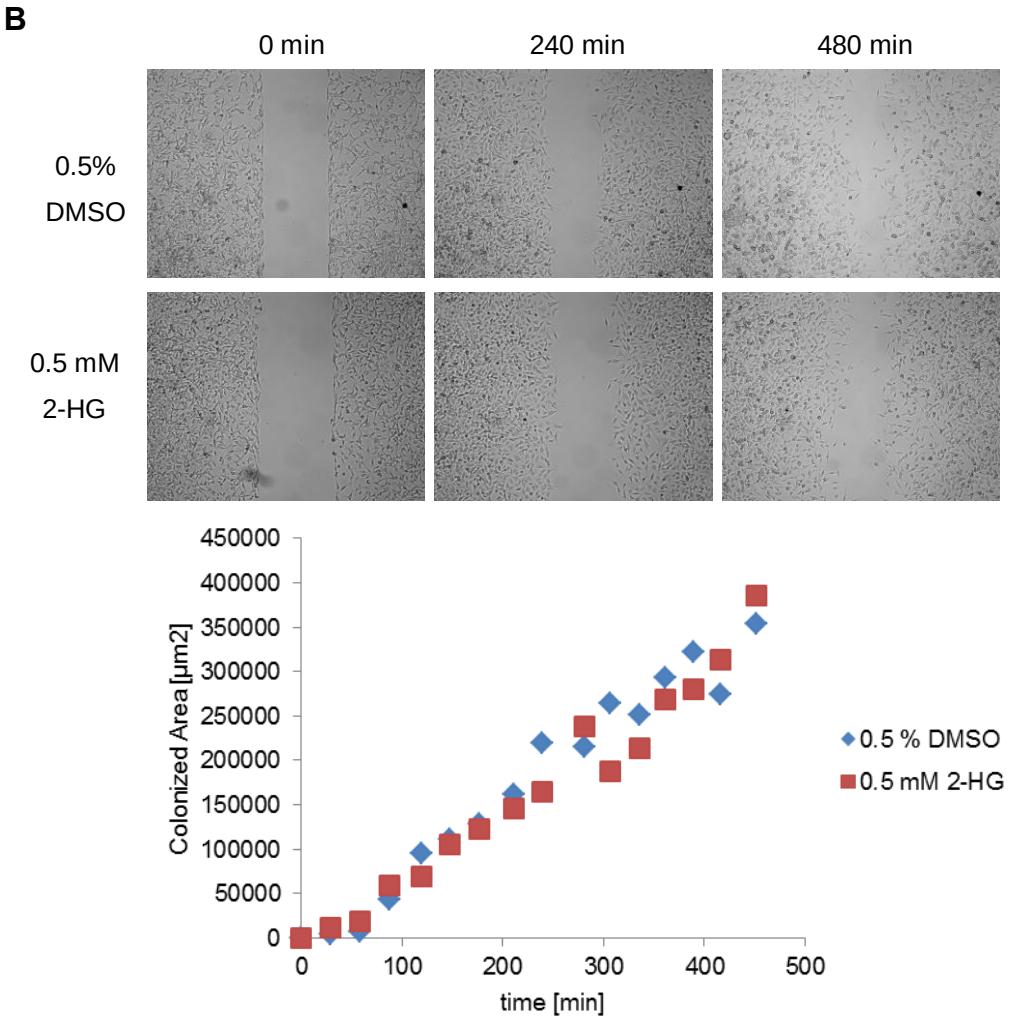

Figure 27: Cellular growth and migration behaviour is not influenced in A172 and U-87MG cells after incubation with R-2-HG

(A) Cell numbers of A172 cells untreated (in blue), treated with 0.5% DMSO (red) and treated with 0.5 mM R-2-HG plotted logarithmically against the time (in h). 0.5% of DMSO was used as control corresponding to the DMSO concentration in the sample treated with 0.5 mM R-2-HG. Data represent means ± SD of three independent experiments.

(B) Representative photographs of cell migration into the wounds (cell-free gaps) 0 min, 240 min and 480 min after removing the silicon-strip culture dish inserts. The upper row shows U-87 MG cells treated with 0.5% DMSO and the lower row U-87 MG cells treated with 0.5 mM R-2-HG for 7 days. 0.5% of DMSO was used as control corresponding to the DMSO concentration in the sample treated with 0.5 mM R-2-HG. The graph displays the colonized area within 480 min in the presence or absence of 0.5 mM R-2-HG by analyzing the photographies of every 30 min.

5 Discussion

5.1 Impact of Jarid1A depletion on cellular viability and proliferation

In the present work I investigated the role of histone demethylase Jarid1A in cell proliferation and radiation response by siRNA-mediated depletion of Jarid1A. All experiments were performed 72 h after transfection with Jarid1A siRNA under comparable levels of averagely 25% residual amount of protein. The lysine specific histone demethylase Jarid1A removes tri- and di-methylations at histone H3K4 frequently found at promoter regions of actively transcribed genes (Soares et al. 2017) and plays a crucial role in controlling transcription and chromatin organization (Dimitrova et al. 2015). Jarid1A is overexpressed in several human cancers and its overexpression is implicated in drug resistance (Itoh et al. 2015; Gale et al. 2016), making the enzyme an interesting potential target for cancer therapy. The precise biological function is, however, largely uncharacterized. Research findings regarding its role in cell proliferation are quite contradictory. Jarid1A was described to be involved in senescence pathways, both positively and negatively. In hepatocellular carcinoma cells, Liang and colleagues observed significant upregulation of the cyclin-dependent kinase inhibitors p21 and p27, suppression of cell proliferation and induction of senescence after siRNA-mediated knockdown of Jarid1A (Liang et al. 2013). Collected data of other groups describe a reduction of cell growth or/and increased senescence-associated β-galactosidase activity after knockdown of Jarid1A in different cell lines and also support the assumption of an anti-senescent role of the demethylase (Benevolenskaya et al. 2005; Zeng et al. 2010; Teng et al. 2013). I note, however, that several reports on growth inhibition after knock-down of Jarid1A apparently used wrong siRNAs that would affect RBP2 retinol-binding protein 2 rather than Jarid1A, which is occasionally also called RBP2 retinoblastoma binding protein 2 (Wang et al. 2013; Qi et al. 2014; Qiao et al. 2015). Others, however, observed in lung cancer cells a regular cell proliferation after shRNA-mediated knockdown of Jarid1A (Sharma et al. 2010). Development of Jarid1A knock-out mice proceeds quite normally with only minor defects in the hematopoietic system, arguing against a general strong reduction of cell proliferation upon Jarid1A depletion (Klose et al. 2007). Some researchers even claim a pro-senescent role for Jarid1A in senescence regulation: Chicas and colleagues report that H3K4me3 demethylation by Jarid1A and Jarid1B at target genes of the tumor suppressor protein retinoblastoma triggers gene silencing in senescent fibroblast cells. After depletion of Jarid1A senescence could be partially inhibited (Chicas et al. 2012).

No influence on cell growth or proliferation was visible in any of our tested cell lines after depletion of Jarid1A. This was shown by short-term viability experiments in HeLa, U2OS and MCF-7 cells and additionally in a long-term viability experiment for HeLa cells. Cell cycle

analysis also showed a regular distribution of phases within the cell cycle after Jarid1A knockdown. Normal cell cycle progression after depletion of Jarid1A was also described by Gong and colleagues (Gong et al. 2017). I additionally studied the expression of p21 after depletion of Jarid1A - a characteristic mediator of cellular senescence that was found increased in some publications mentioned before. Expression of p21 in HeLa and U2OS cells was slightly decreased after Jarid1A depletion, but the protein levels in both of these cell lines may be too low to make a final statement. The level of p21 is generally low in HeLa cells as this cell line shows enhanced degradation of the tumor suppressor protein p53 which leads to an instabilized p21 that is also rapidly degraded (Scheffner et al, 1990). Protein levels of p21 in U2OS cells are low due to a reduced translation of p21 mRNA (Chang and Eastman, 2012). MCF-7 cells, which exhibit regular p21 expression, show a slight increase in p21 expression after Jarid 1A knockdown, which, however, did not impact on cell viability or proliferation. Therefore, the inability to observe senescence in the cells used here cannot solely be attributed to deficiencies in the p53-p21 pathway. Another potential explanation for the lack of senescence could be insufficient down-regulation of Jarid1A. Depletion was quite efficient in our experiments and lead to a reduction by about 75%. Comparable levels of depletion were described in the publications mentioned above. In addition, considerable increase of cellular H3K4me3 levels was observed (see next chapter) indicating restricted functional activities of the demethylase. It has been suggested that depletion of the demethylase leads to reduced cell proliferation only in cell lines overexpressing Jarid1A: Data of Hou and colleagues demonstrate reduced proliferation in cells with Jarid1A amplification, while they see no effect on proliferation in cells with regular expression after Jarid1A knockdown (Hou et al. 2012). I could not observe differences in the protein level of Jarid1A among the cell lines I used - HeLa, MCF-7 and U2OS. They all exhibit a comparable expression of the demethylase and respond similarly to the knockdown via siRNA transfection.

5.2 Alterations in the level of histone modifications after Jarid1A-knockdown

The siRNA-mediated knockdown leads to an increase of global trimethylation of H3K4 by about 70%. Similar increases of global H3K4me3 after Jarid1A depletion were reported by others (Christensen et al. 2007; Pasini et al. 2008; Beshiri et al. 2012; Hou et al. 2012). This verifies efficient functional depletion of the enzymatic activity of Jarid1A, even if it cannot be excluded that residual Jarid1A partly retains some of its important cellular functions. It is conceivable that other members of the Jarid1 family can compensate the depletion of Jarid1A. Especially Jarid1B is assumed to have redundant functions to Jarid1A (Chicas et al. 2012; Islam et al. 2014). Some publications show similar increases of global H3K4 trimethylation after depletion

of Jarid1B like I observed for depletion of Jarid1A (Xie et al. 2011; Klein et al. 2014). However, Outchkourov and colleagues report that knockdown of Jarid1C does not affect global H3K4me3 levels (Outchkourov et al. 2013). There is no information about the impact of Jarid1D depletion on H3K4me3 levels, as this member is generally scarcely investigated. In any case, the drastic increase of H3K4me3 after Jarid1A depletion shows that other Jarid1 demethylases cannot fully compensate for Jarid1A. So far, a systematic comparison of the role of the different members of the Jarid1 protein family for global H3K4me3 levels is lacking.

It is widely accepted that a cross-talk between histone modifications exists (Latham and Dent 2007; Huang et al. 2010). Often histone demethylases and histone deacetylases, as well as histone acetyl transferases, are part of the same protein complex and coordinately regulate expression of specific genes by removing active histone marks and adding repressive histone marks and vice versa. Especially the interplay between the histone H3K4me1/2 demethylase LSD1 and histone deacetylation is well established. After treatment of cells with the HDAC inhibitor Trichostatin A, in addition to levels of acetylated histone H3 levels of H3K4me2 increased, suggesting that HDAC activity is linked to LSD1 activity (Lee et al. 2006). On the other hand, depletion of LSD1 results in synergistic down-regulation of HDACs, thus leading to increased H3K4me2 levels and hyperacetylation at H4K16, H3K56 and H3K14 (Vasilatos et al. 2013; Yin et al. 2014). Potential crosstalk involving demethylases of the Jarid1 family is less well investigated, although physical interaction of Jarid1A with HDACs was shown (Hayakawa et al. 2007). Huang and colleagues reported that incubation of prostate cancer cells with HDAC inhibitors leads to reduced expression of LSD1 and all members of the Jarid1 demethylase family. Dose dependent reduction of mRNA expression, as shown via qRT-PCR analysis, was accompanied by an increase of global H3K4me3 levels (Huang et al. 2010). Inhibition of Jarid1A after treatment with histone deacetylase inhibitors has also been observed by others and generates a phenotype similar to Jarid1A knockdown cells (Sharma et al. 2010; Ganai et al. 2015). To our knowledge the effect of Jarid1A depletion on histone acetylation has not yet been investigated in detail. With its chromatin-binding PHD finger and ARID domains Jarid1A interacts with the SIN3 histone deacetylase co-repressor complex (Hayakawa et al. 2007) and with the nucleosome remodeling and deacetylase (NuRD) complex (Nishibuchi et al. 2014). As Jarid1A is associated with HDAC1 and HDAC2 in both complexes, I decided to investigate acetylation levels of H4K16, H3K9 and H3K56 upon Jarid1A depletion, as these are known targets of this class of histone deacetylases (Dovey et al. 2010; Wu et al. 2014). I observed a significant increase of acetylation at H4K16 in Jarid1A knockdown cells, as well as strong hyperaceylation at H3K9 and H3K56, which however did not reach statistical significance. Reduced Jarid1A levels in the cell may perturb the recruitment of the SIN3 and the NuRD complex and thus lead to reduced activity of histone deacetylases at chromatin. It

is, however, also possible that enhanced activity of a histone acetyltransferase is responsible for the observed hyperacetylation at H3K9, H3K56 and H4K16. To gain more insights in the interplay between Jarid1A and histone deacetylation further experiments will be required.

Histone hyperacetylation is generally assumed to result in decondensation of chromatin facilitating accessibility to transcription factors or repair proteins (Görisch et al. 2005). Especially acetylation at H4K16 was reported to interfere with DNA fiber compaction, leading to a rather open chromatin structure by reducing the inter-nucleosome interaction (Zhang et al. 2016). To study chromatin condensation I used the MNase assay, whereby the DNA is cleaved in the linker regions between the nucleosomes by micrococcal nuclease (Telford and Stewart 1989). The sensitivity of the DNA to the MNase is dependent on the grade of decondensation and can be investigated by partial MNase digestion (Liu et al. 2013). In my hands chromatin of control cells and of Jarid1A depleted cells showed a similar sensitivity to the MNase treatment. As the MNase assay is a rather insensitive method requiring broad changes in chromatin compaction, it is possible that the grade of histone hyperacetylation upon Jarid1A depletion is not sufficient to make the decondensation visible (Goodarzi et al. 2011). Other groups also reported that histone hyperacetylation does not translate into altered MNase digestion pattern (Perry and Chalkley 1981; Gilbert et al. 2007). Although reduced formation of compact chromatin fibres by acetylation of H4K16 was clearly demonstrated by certain groups (Shogren-Knaak et al. 2006; Dorigo et al. 2003, Zhang et al. 2016), it may not visibly influence chromatin compaction at all size scales of analyzed structures (Taylor et al. 2013). Even if no distinct alteration in the chromatin structure is visible, the impact of the observed hyperacetylation on cellular processes upon Jarid1A depletion may be wide-ranging.

5.3 Influence on recruitment of DNA damage response factors and efficiency of DSB respair

In general, histone hyperacetylation is associated with higher radiosensitivity and often HDACi are used in combination with irradiation to enhance the effect of radiotherapy in the treatment of cancer (Groselj et al. 2013). The effects of the HDAC inhibitors show a wide mode of action depending on the class of deacetylases they are inhibiting. E.g. inhibition of HDAC1 and HDAC2 or class III HDACs (sirtuines) can interfere with DNA damage signalling, DSB detection or DSB repair pathway choice by preventing successful detection of DSBs (van Meter et al. 2016), by disturbing the effective activation of ATM (Thurn et al. 2013), or by influencing the expression of repair proteins like BRCA1 (Zhang et al. 2007; Kachhap et al. 2010). It was shown that H4K16 acetylation influences DSB repair pathway choice by diminishing 53BP1 binding to the damage site, thus preventing repair by NHEJ and favouring repair by HR (Hsiao

et al. 2013; Tang et al. 2013). Others, however, observed that chromatin decondensation after HDACi treatment had no effect on 53BP1 recruitment (Khurana et al. 2014) or that 53BP1 binding is even enhanced (Murr et al. 2006). Published data on BRCA1 recruitment to damage sites under conditions of HDAC inactivation are e.g. quite inconsistent. Some claim reduced BRCA1 foci formation at DSBs in cells with hyperacetylation (Fukuda et al. 2015), while others report an increased BRCA1 binding to chromatin after HDAC inhibition and associated hyperacetylation (Tang et al. 2013). Fukuda and colleagues could observe diminished binding of both 53BP1 and BRCA1, hinting at a disturbance of both NHEJ and HR repair of DSB in cells with enhanced H4K16 acetylation (Fukuda et al. 2015).

I hypothesized that the significant enhancement of radiosensitivity in Jarid1A-depleted cells observed in this work after irradiation with x-rays could be associated with the hyperacetylation phenotype. I therefore investigated the influence of Jarid1A depletion on the recruitment of DNA damage response and repair proteins to DNA DSB induced by ionizing irradiation. I could not detect diminished recruitment or binding of 53BP1 or BRCA1 in Jarid1A depleted cells after irradiation with carbon ions in the immunfluorescence experiments. Similarly, the recruitment and foci formation of Rad51 at ion-induced DSBs was not affected by the hyperacetylation after Jarid1A knockdown. Analysis of the number of residual IRIF after prolonged repair incubation is a frequently used tool for assessing DSB repair efficiency (Löbrich et al. 2010; Bakr et al. 2015). Residual γH2AX foci at 24 h and 48 h after X-irradiation did not differ between cells transfected with scr siRNA or Jarid1A siRNA, suggesting that the increased radiation sensitivity of Jarid1A-depleted cells observed in our work cannot be explained by altered DSB repair efficiency. Also the number of residual 53BP1 and Rad51 foci did not differ between the samples, arguing against a difference in pathway use. To verify these observations I assessed the performance of NHEJ and HR by a plasmid-based DNA DSB repair assay. Via plasmid-based repair assays it was shown by others that HR or/and NHEJ were affected after treatment with HDACi or depletion of HDACs (Miller et al. 2010; Koprinarova et al. 2011). I could not observe any influence on DSB repair, neither on HR nor NHEJ pathway, upon Jarid1A depletion in my experiments. I conclude that inspite of the hyperacetylation phenotype, recruitment, binding and elimination of the damage response and repair proteins investigated here were not influenced by Jarid1A depletion, nor was DSB repair. That means that histone hyperacetylation as seen after knockdown of Jarid1A may be not sufficient to fully phenocopy the effects of HDAC inactivation.

To explain the observed discrepancies in the recruitment of DSB repair proteins, it has to be mentioned that the action of HDAC inhibitors is to a certain extent unspecific and not only histone acetylation if affected. Therefore, the many effects of HDACi treatment described in the literature cannot be compared directly with the effects of hyperacetylation on H4K16, H3K9

and H3K56 upon Jarid1A depletion. For example, the expression of Rad51 upon treatment with HDACis was shown to be decreased in different tumor cells (Kachhap et al. 2010; Krumm et al. 2016).

A major part of the irradiation experiments performed here were conducted with a charged particle microbeam (SNAKE) that enables irradiation of cells with an exact number of particles where the linear energy transfer (LET) can be adjusted by the choice of the ion species and the ion energy (Hauptner et al. 2004). A microbeam with carbon ions was used for this issue as the linear energy transfer (LET) of these ions is increased compared to irradiation with photons. This results in increased damage density and facilitates specific detection of ionizing radiation-induced foci (IRIF). Along a track with 10 µm length about 30 DSB are formed through the nucleus, leading to clustered DSBs visually detectable as IRIF that form along the ion track with high reproducibility (Hauptner et al. 2006; Reindl et al. 2015). This is in contrast to laser-microirradiation. Depending on the laser system and the conditions of irradiation, laser irradiation induces various types and amounts of DNA damage that cannot be clearly characterized (Bekker-Jensen 2006; Dinant et al. 2007). Even small deviations in the laser irradiation conditions can lead to discrepancies in the protein recruitment at the damage site (Cruz et al. 2016), which makes it difficult to gain reproducible and reliable results. Additionally, damage densities are extremly high. This can lead to detection of proteins at the damage site that in general are not foci-forming and would not be visibly recruited to the damage under physiological conditions (Seiler et al. 2011; Suzuki et al. 2011). Laser irradiation can also lead to unspecific chromatin alterations (Drexler and Ruiz-Gomez 2015).

5.4 Responsible demethylases and damage response proteins for the loss of H3K4me3/me2 and of active RNA Polymerase II in γH2AX-decorated chromatin regions

Enhanced radiosensitivity of Jarid1A-depleted cells could also be related to a function in demethylation of H3K4me3/2 in γH2AX-decorated chromatin regions (Seiler et al. 2011). The loss of H3K4me3/me2 and active RNA polymerase II at γH2AX foci after ion irradiation was not visibly attenuated by depletion of Jarid1A in my intensity correlation analysis experiments. As the mode of action of histone demethylases in the damage response is often dependent on early damage response proteins, like e.g. ATM or PARP1 (Mosammaparast et al. 2013; Khoury-Haddad et al. 2014; Cao et al. 2016), I additionally checked the behaviour of H3K4me3/me2 at γH2AX regions after inhibition of ATM, ATR and PARP1. Inhibition of these key damage response proteins did also not visibly impair the demethylation of H3K4me3/me2 in γH2AX-decorated chromatin regions. It is, however, a major weakness of this work that with

the image analysis programs available I could not perform a quantitative analysis of the degree of anti-correlation between H3K4me3/2 (or active RNA Pol II) and γH2AX. I used the ICA introduced by Li and colleagues that defines positive and negative correlation by comparing the pixels of two different stained cellular structures (Li et al. 2004). Unfortunately this tool is only of limited usefulness in my experimental conditions, where the most of the cell nucleus is not stained and only a few pixels exist (γH2AX-foci), respectively only pixels with relatively low fluorescence intensity exist (H3K4me3). Positive or negative correlation of weak signals is scarcely considered. During the experimental phase of this thesis, no method to perform a quantitative intensity correlation analysis suitable for my purposes was available. Reindl and colleagues developed a modification of intensity correlation analysis (ICA), using a reduced version of the product of the differences from the mean (rPDM) to qualitatively and quantitatively analyze the spatial correlation of proteins that are present only in sub-regions of the cell (Reindl 2015; Reindl et al. 2017). But it is still questionable, if this method leads to reliable quantitative results for the conditions in my test-setup, where a correlation between a rather weak signal with a lot of pixel like the pan-nuclear histone modification H3K4me3 and a strong signal with just a few pixel like repair foci shall be investigated.

Very recently, Gong and colleagues reproduced data from our lab (Seiler et al. 2011) showing visible accumulation of Jarid1A and loss of H3K4me3 at laser-induced damage sites (Gong et al. 2017). These authors also showed by ChIP a loss of H3K4me3 at FokI-induced damage sites which was attenuated (about 25% reduction compared to about 50% reduction) by knock-down of Jarid1A. Loss of H3K4me3 at FokI-sites was also attenuated by treatment with the Jarid1 inhibitor CPI-4557, which inhibits Jarid1A, Jarid1B and Jarid1C in comparable manner (Vinogradova et al. 2016). In their hands, recruitment of Jarid1A and associated loss of H3K4me3 were dependent on PARylation by PARP1. In addition, Gong and colleagues observed reduced Rad51 foci formation at DSB sites and a reduction of HR repair events in DSB reporter constructs of about 50% (Gong et al. 2017).

The discrepancy regarding the role of Jarid1A for loss of H3K4me3 may be explained by different methods used (IF vs ChIP) and it can be argued that a 25% difference may be difficult to detect without quantitative evaluation. On the other hand, the discrepancy regarding recruitment of DSB repair factors and completion of DSB repair events cannot be explained at the moment. In any case, the fact that loss of H3K4me3 is only incompletely attenuated by depletion of Jarid1A suggests the involvement of other Jarid1 demethylases. Indeed, Li and colleagues reported that H3K4me3 levels in the vicinity of enzyme-induced DSBs are largely regulated by the demethylase Jarid1B (Li et al. 2014). Functional overlap of Jarid1A and Jarid1B has been found in certain instances (Islam et al. 2011; Chicas et al. 2012), but the relative importance of these closely related demethylases in the DNA damage response has

not been systematically investigated and it may differ between different cell lines. As I failed to deplete Jarid1B via RNAi or to inhibit Jarid1B via PBIT, I could not verify these effects of Jarid1B depletion in my cells.

5.5 Gene expression changes after Jarid1A depletion

To reveal the reasons for the observed higher radiosensitivity after Jarid1A depletion, I investigated the influence of the knockdown on radiation-induced gene expression alterations. As Jarid1A is involved in transcriptional regulation by removing a histone modification linked to active transcription, it is generally considered to contribute to corepression. On the other hand, the observed hyperacetylation after Jarid1A-depletion may have a rather activating effect on the expression of various genes. 1731 differentially expressed genes after Jarid1A depletion were detected, of which 44.6% show up-regulation and 55.4% down-regulation. This is in accordance to the results of the microarray analysis of Nishibuchi and colleagues, who found a similar proportion of up- and downregulated genes in their experiments after siRNA-mediated knockdown of Jarid1A (Nishibuchi et al. 2014). When comparing the results, there is a prominent difference in the number of deregulated genes after Jarid1A depletion. By comparison with control transfected cells, they found 435 genes, while I found 1731 genes significantly deregulated after knockdown of Jarid1A. A further look at their results shows only a small overlap between the deregulated genes in their experiment compared to our experiment. The performance of the microarray analysis was quite similar, but they used HeLa cells with different origin (Nishibuchi et al. 2014). According to pathway analysis, the most affected genes of the Jarid1A depletion in my hands are involved in cell metabolism and extracellular matrix organization. The effect of the deregulated pathways may probably be rather small as there was no evidence for influenced cell viability or proliferation after Jarid1A depletion in unirradiated cells in my experiments. The most significantly regulated genes Nishibuchi and colleagues found after Jarid1A and CHD4 depletion are associated with developmental processes like anatomical structure and tissue development. Nevertheless, similar to my results, regulation of cell migration was also among the significant deregulated pathways in their gene expression analysis (Nishibuchi et al. 2014).

In addition, I looked at the transcriptional response to irradiation. It has to be mentioned that regulation of damage response and DNA repair is mainly regulated on the protein level rather than on the mRNA level as most DNA repair occurs quickly after damage induction (Lu et al. 2006; Christmann and Kaina 2013). Still, a variety of genes are differentially expressed after treatment of cells with ionizing radiation as reaction to the induced DNA damage. Genes responsive to ionizing radiation are mostly involved in cell cycle regulation, apoptosis, cell

signalling, DNA damage response, metabolism and general stress induction (Tusher et al. 2001; Jen and Cheung 2003). A large part of IR-responsive genes are either regulated by the transcription factor p53 or NF-κB (Rashi-Elkeles et al. 2014). As I performed the microarray analysis with p53-compromised HeLa cells, upregulation of p53-dependent genes like CDKN1A, CCNG1 or MDM2 could not be observed after irradiation of the cells (Tusher et al. 2001; Macaeva et al. 2016). Some NF-κB-dependent genes generally found to be up-regulated after irradiation were induced in our different siRNA transfected HeLa cells. Additionally, many genes involved in the regulation of mitosis and in formation of the mitotic spindle were down-regulated, e.g. Aurora A kinase, Cyclin B1 and some centromere proteins, which is quite typical as reaction of cells shortly after exposure to ionizing radiation (Kao et al. 1997; Mezentsev and Amundson, 2011). Correspondingly, pathway enrichment analysis of the irradiated HeLa cells displayed deregulation of cell cycle and cellular responses to stress, but not to programmed cell death or DNA repair independent from the transfected siRNA. To sum up, gene expression analysis indicates no differences in the pathways responsive to ionizing radiation between the control and the Jarid1A depleted cells.

Various genes are differentially expressed solely in Jarid1A-depleted cells 2 h after irradiation with a fold change of at least 1,5. Pathway enrichment analysis revealed extracellular matrix organization and connected beta integrin signalling as affected pathways attributable to deregulation of many genes encoding collagens, alpha integrines or other proteins that are somehow involved in ECM dynamics. The ECM is a complex, tightly regulated network and it plays an important role in the control of cell growth, survival and migration. Disturbance of its organization can have diverse effects on cells and provoke various diseases like tissue fibrosis and cancer (Lu et al. 2011). Recently it was observed that it can influence the radiation sensitivity of cells. Dickreuter and colleagues observed decreased activity of repair by classical NHEJ in HeLa cells as shown by NHEJ reporter assay and reduced expression of DNA repair proteins of NHEJ like Ku70 and components of the MRN complex upon β1 integrin inhibition (Dickreuter et al. 2016). In our reporter assays I could not see reduced repair via NHEJ upon Jarid1A depletion. This can be attributed to the fact that the expression of alpha and not of beta integrines occurs in cells after Jarid1A knockdown. Possibly, the impact of diminished expression of some alpha integrine subunits is negligible as more different alpha integrines than beta integrines exist (Takada et al. 2007). Anyway, deregulation of alpha integrines regarding radiation sensitivity and DNA repair is not yet investigated. In microarray analysis I also observed altered expression of genes expressing collagens after Jarid1A depletion. As some genes are up- and some genes are down-regulated, it is hardly possible to assess the consequences for the cells.

Pathway enrichment analysis with the genes solely deregulated in knockdown cells after irradiation gave no further hint at changes in damage response or DNA repair pathways. As enrichment analysis reveals only pathways, when a set of functionally-related genes is differentially expressed, I searched for single genes involved in DDR pathways with a significant modified expression after Jarid1A depletion and irradiation and investigated their expression on protein level. I found interesting genes like PARP1, HSP90AA1, NFKBIE, KDM5B, YBX1, INCENP, SMC1A and CENPF differentially expressed without a visible effect on regular cellular pathways. As revealed by Western Blotting all of them showed an ordinary protein expression. The changes on mRNA level are only about 1,6 - 2.0 fold increased or decreased, what might still be too low to have an influence on the protein level. It also has to be mentioned that Western Blot analysis may be a method too insensitive to confirm small potential differences in protein expression. Additionally, it is challenging to choose the appropriate time points to examine mRNA expression and the expression of related proteins. Often, irradiation-induced changes in gene expression can only be seen shortly after radiation-insult, but it is hard to predict the time point of the impact on protein expression.

The reliability of gene expression analysis via microarrays is widely discussed and remains questionable. The capabilities of microarray studies are limited due to fluctuating intracellular conditions, sample contaminations, the amplification process and many other experiment-specific factors as well as statistical data processing (reviewed in Jaksik et al. 2015). Generally, well-planned experimental design and accurate data-analysis can overcome these issues (Draghici et al. 2006; Jaksik et al. 2015). On the subject of the grading of the reliability of our microarray analysis, the following conclusions can be drawn: On the one hand, the results of Nishibuchi and colleagues after Jarid1A depletion mentioned above show some differences to our results, although they used the same cell line and the same microarray platform (Nishibuchi et al. 2014). This may be referable to the heterogeneity of the HeLa cell line and potential differences in cell density, cell morphology or cell cycle phase before RNA isolation. Differences in statistical data processing can also explain deviations of the results. On the other hand, the results of the gene expression changes after irradiation of the HeLa cells correlates very well with data in the literature and with the compromised p53 status of the used HeLa cells indicating that I produced reliable data.

However, many studies provide evidence that often a remarkable discrepancy between mRNA and protein levels in vitro and in vivo exist (in human cells as well as in tissues). Microarray or RNA sequencing methods indicate that only about 40% of protein levels are consistent with the measured mRNA expression (Lundberg et al. 2010; Vogel et al. 2010; Wilhelm et al. 2014). Even significant mRNA increases do not compulsively lead to an increase in protein expression as observed by Taquet and colleagues when studying mRNA and protein expression of

somatostatin and chemokine receptors in Crohn`s disease patients (Taquet et al. 2009). Consequently, mRNA expression does not reliably reflect the protein level in cells and is therefore just partly suitable for a prediction of the proteome.

5.6 Influence of R-2-HG incubation on histone demethylases

2-hydoxyglutarate produced by different tumor cells with IDH1/2 mutations inhibits α-KG-dependent dioxygenases like histone demethylases and the TET family of 5-methlycytosine (5mC) hydroxylases (Figueroa et al. 2010; Xu et al. 2011). To study the effects on histone demethylation, I aimed to mimic the IDH1/2 mutation by adding a cell permeable ester of R-2-HG directly to the cells. At the concentrations and incubations times used in different cell lines no visible inhibition of α-KG-dependent histone demethylases was detectable, as shown by steady levels of H3K4me3 and H3K9me3. By detection of H3K4me3 and H3K9me3 the inhibition of the KDM5/Jarid1 subfamiliy (KDM5A-KDM5D) and of the KDM4 subfamiliy (KDM4A-KDM4E) of demethylases should have been made visible (Cloos et al. 2008; Labbé et al. 2014). Several research groups reported that IDH1 mutations lead to increased histone methylations at H3K9, H3K27, H3K79 or H3K4 (Xu et al. 2011; Lu et al. 2012; Turcan et al. 2012). What concentration of R-2-HG is needed to fully phenocopy the IDH mutation is not clear, since data in the literature are contoversial. Dang and colleagues showed that mutant isocitrate deydrogenase directly converts α-KG in 2-HG, which leads to an increase of 2-HG in the cell to around 5 mM 2-HG, while a cell with wildtype IDH1 only has trace amounts of 2-HG (Dang et al. 2009). Reitmann and colleagues reported that a concentration of 0.1 mM of R-2-HG in the medium results in the same level of intracellular R-2HG as produced in knock-in IDH1 mutant HTC116 cells (Reitmann et al. 2014). Generally, efficient concentration for inhibition of α-KG-dependent dioxygenases is dependent on the sensitivity of the respective enzyme against the oncometabolite and shows a broad variation from 0.1 mM to 10 mM (Reitmann et al. 2014; Lu et al. 2012; Oizel et al. 2015). HIF hydroxylases are not influenced at all by R-2-HG, when using the same concentration at which KDM4 demethylases are inhibited (Chowdhury et al. 2011). Lu and colleagues observed in their experiments a clear increase of the tri-methylation at H3K9 but not at H3K4 leading to the assumption that KDM4 demethylases are more sensitive to R-2-HG than KDM5/Jarid1 demethylases (Lu et al. 2012). I assume that the sensitivity to R-2-HG is also dependent on the used cell line. I cannot exclude that the concentrations I used were too low to induce effective inhibition of the KDM4 and KDM5 histone demethylases in A172, U-87 MG and HTC116 cells. Further, the incubation times described in the literature are quite diverse and vary in the range from 6 h to 6 days (Reitmann et al. 2014; Li et al. 2015; Oizel et al. 2015; Chen et al. 2016). I chose an incubation

time of 6 days, as stability experiments revealed that 2-HG is stable for at least 7 days in solution (Kalinina et al. 2012). Nevertheless, it is possible that R-2-HG is partly degraded in the cell cuture medium at 37°C.

In my hands, growth properties and migration were not influenced after incubation of glioma cells with R-2-HG. Studies investigating cellular growth and migration behaviour of cells with IDH mutations show differing results. When introducing mutated IDH into IDH wild-type glioma cells, Bralten and colleagues observed a decrease in cell proliferation (Bralten et al. 2011), while others saw no differences in cell proliferation or migration between HT1080 cells expressing mutant IDH leading to accumulation of R-2-HG and HT1080 cells expressing an empty vector (Ma et al. 2015). Koivunen and colleagues were able to show enhanced proliferation and increased colony formation in normal cells after introduction of the IDH1 mutation. It has to be mentioned that it took around 14 cell passages after transfection of the vector with the mutated IDH1 to make this observation (Koivunen et al. 2012).

Within the scope of this thesis it was not possible to further analyse the effect of R-2-HG on glioblastoma cells. With short-term addition of R-2-HG to cells in culture it may be not possible to entirely mimic the IDH1 mutations in glioblastoma cells or only by adding a much higher concentration of the oncometabolite. Transfection of cells with a vector carrying the mutated IDH1 followed by a few cell passages might be a better tool to study the IDH1 mutation and the effect on Jarid1 demethyases. I additionally assume that efficacy of R-2-HG against different α-KG dioxygenases is cell line specific and also dependent on other cellular conditions. Generally, unspecific inhibitors like R-2-HG are not suitable to gain universally valid insights in the mechanistic of reprogramming of epigenetics and cellular metabolism.

5.7 Conclusion and Outlook

The present work intended to study the role of JmjC domain-containing family of histone demethylases on chromatin structure, as well as on DNA damage response and DSB repair upon irradiation with ionizing irradiation. Due to the loss of H3K4me3/me2 and a concomitant loss of active RNA polymerase II at γH2AX-decorated DNA damage sites induced by ionizing radiation and due to accumulation of Jarid1A at laser-induced damage sites (Seiler at al. 2011), my main focus was the demethylase Jarid1A. Collectively, the data presented here show increased hyperacetylation and increased radiosensitivity upon depletion of Jarid1A, while recruitment of DNA damage/DSB repair factors and the DSB repair via NHEJ and HR itself remain unaffected. The observed hyperacetylation and increased tri-methylation at H3K4 does neither obviously influence the higher chromatin order nor affect the recruitment of repair factors to sites of DSBs. As regulator of transcription Jarid1A knockdown deregulates gene

expression of various genes, especially genes encoding for transporters and transferases affecting cell metabolism. The consequences in unirradiated cells are marginal and have no influence on cell proliferation, growth properties or viability. Depletion of Jarid1A in irradiated cells induces some disturbance in pathways affecting the extracellular matrix organization. Additionally some changes in the expression of genes involved in damage response or/and in cell cycle and transcriptional regulation could be observed that are, however, not visible on protein level. Investigation of a possible role for Jarid1A in the loss of H3K4me3/me2 in γH2AX-decorated chromatin regions and loss of active RNA polymerase II from these regions showed negative results. This is compatible with observations by Li and colleagues who found that H3K4me3 levels in the vicinity of enzyme-induced DSB are largely regulated by Jarid1B (Li et al. 2014). Controverse results were published very recently by Gong and colleagues, who found Jarid1A recruitment to laser-induced damage and failure of H3K4me3 loss associated with reduced recruitment of Rad51 upon Jarid1A depletion (Gong et al. 2017). I propose a model where Jarid1A and Jarid1B act in concert with other factors in chromatin remodeling and DSB repair after damage induction by ionizing radiation. Knockdown of solely the Jarid1A demethylase influences chromatin modifications and radiosensitivity without visibly affecting recruitment of repair proteins to ion-induced DSBs. Due to the lack of a specific potent Jarid1A inhibitor, the possibility of further effects occurring upon complete depletion of Jarid1A could not been tested here. Thus, the mechanistic basis of the significantly increased radiosensitivity seen upon depletion of Jarid1A remains to be elucidated. To give a final statement, inhibition of solely Jarid1A or Jarid1B should be performed. Unfortunately, development of specific cell permeable inhibitors against Jarid1 demethylases is very challenging. The catalytic site of JmjC domain-containing histone demethylases exhibits a close structural homology among different demethylase families. Consequently, inhibitors often block KDM4, KDM6 and KDM5 demethylases simultaneously (Johansson et al. 2016; Taylor-Papadimitriou and Burchell 2017). A lot of research is going on to find potent and more specific compounds (Gehling et al. 2016; Horton et al. 2016; Labadie et al. 2016; Westaway et al. 2016). Design of specific inhibitors against a particular demethylase of the Jarid1 family is even more complex as the mode of action and the protein domains are nearly identical.

Regarding the deregulation of Jarid1 demethylases in various diseases, especially numerous cancers (Hou et al. 2012; Teng et al. 2013; Yamamoto et al. 2014), a high need for specific inhibitors for research purposes and therapeutic usage persists. As epigenetic processes are reversible, enzyme-mediated processes have emerged as promising targets for cancer therapy. In recent years many studies had a focus on the interplay between epigenetic pathways and the DNA damage response for a better understanding of the mechanisms and to find targets for therapy (reviewed in Smits et al. 2014). Due to the observed radiosensitizing

effect after targeting Jarid1A, small molecule inhibitors in combination with radiotherapy could give rise to an effective therapeutic benefit in designated cancer diseases. Data from ongoing and future studies on the topic of the detailed roles of Jarid1 demethylases in repressive complexes, oncogenic signalling and DNA damage response as well as related epigenetic biomarkers for classification and diagnosis of associated diseases are required to develop new therapeutic approaches.

6 References

Akimoto, C.; Kitagawa, H.; Matsumoto, T.; Kato, S. (2008): Spermatogenesis-specific association of SMCY and MSH5. In: *Genes Cells* 13 (6), p. 623–633. DOI: 10.1111/j.1365-2443.2008.01193.x.

Alam, H.; Gu, B.; Lee, M.G. (2015): Histone methylation modifiers in cellular signaling pathways. In: *Cell Mol Life Sci.* 72, p. 4577–4592. doi: 10.1007/s00018-015-2023-y.

Albert, M.; Schmitz, S.U.; Kooistra, S.M.; Malatesta, M.; Morales T.C.; Rekling, J.C. et al. (2013): The Histone Demethylase Jarid1b Ensures Faithful Mouse Development by Protecting Developmental Genes from Aberrant H3K4me3. In: *PLoS Genet* 9 (4), p. e1003461. DOI: 10.1371/journal.pgen.1003461.

Amary, M.F.; Bacsi, K.; Maggiani, F.; Damato, S.; Halai, D.; Berisha, F. et al. (2011): IDH1 and IDH2 mutations are frequent events in central chondrosarcoma and central and periosteal chondromas but not in other mesenchymal tumours. In: *The Journal of pathology* 224 (3), p. 334–343. DOI: 10.1002/path.2913.

Amendola, P.G.; Zaghet, N.; Ramalho, J.J.; Johansen, J.V.; Boxem, M.; Salcini, A.E. (2017): JMJD-5/KDM8 regulates H3K36me2 and is required for late steps of homologous recombination and genome integrity. In: *PLoS Genet.* 13 (2), p. e1006632. doi: 10.1371/journal.pgen.1006632.

Auer, S.; Hable, V.; Greubel, C.; Drexler, G.A.; Schmid, T.E.; Belka, C. et al. (2011): Survival of tumor cells after proton irradiation with ultra-high dose rates. In: *Radiation oncology (London, England)* 6, p. 139. DOI: 10.1186/1748-717X-6-139.

Aymard, F.; Bugler, B.; Schmidt, C.K.; Guillou, E.; Caron, P; Briois, S. et al. (2014): Transcriptionally active chromatin recruits homologous recombination at DNA double-strand breaks, Nat.Struct. Mol. Biol. 21 (2014) 366−374.

Babushku, T. (2016): Identification and validation of the amounts of certain candidate proteins in untransfected and siRNA transfected HeLa cells after irradiation, and comparison with their amounts after JARID1A knockdown. Reaearch course lab report. Ludwig-Maximilians-University of Munich, Faculty of Biology.

Bakr, A.; Köcher, S.; Volquardsen, J.; Petersen, C.; Borgmann, K.; Dikomey, E. et al. (2016): Impaired 53BP1/RIF1 DSB mediated end-protection stimulates CtIP-dependent end resection and switches the repair to PARP1-dependent end joining in G1. In: *Oncotarget* 7 (36), p. 57679–57693.

Bakr, A.; Oing, C.; Köcher, S.; Borgmann, K.; Dornreiter, I; Petersen, C. et al. (2015): Involvement of ATM in homologous recombination after end resection and RAD51 nucleofilament formation. In: *Nucleic Acids Res.* 43 (6), p. 3154–3166. doi: 10.1093/nar/gkv160.

Banelli, B.; Carra, E.; Barbieri, F.; Würth, R.; Parodi, F.; Pattarozzi, A. et al. (2015): The histone demethylase KDM5A is a key factor for the resistance to temozolomide in glioblastoma. In: *Cell cycle (Georgetown, Tex.)* 14 (21), p. 3418–3429. DOI: 10.1080/15384101.2015.1090063.

Barski, A.; Cuddapah, S.; Cui, K.; Roh, T.; Schones, D.E.; Wang, Z. et al. (2007): High-Resolution Profiling of Histone Methylations in the Human Genome. In: *Cell* 129 (4), p. 823–837. DOI: 10.1016/j.cell.2007.05.009.

Bekker-Jensen, S. (2006): Spatial organization of the mammalian genome surveillance machinery in response to DNA strand breaks. In: *The Journal of Cell Biology* 173 (2), S. 195–206. DOI: 10.1083/jcb.200510130.

Benevolenskaya, E.V.; Murray, H.L.; Branton, P.; Young, R.A.; Kaelin, W.G. (2005): Binding of pRB to the PHD Protein RBP2 Promotes Cellular Differentiation. In: *Molecular Cell* 18 (6), p. 623–635. DOI: 10.1016/j.molcel.2005.05.012.

Benjamini, Y.; Hochberg, Y. (1995): Controlling the false discovery rate - a practical and powerful approach to multiple testing. In: *J. R. Stat. Soc. B* 57, p. 289-300.

Bensimon, A.; Aebersold, R.; Shiloh, Y. (2011): Beyond ATM: The protein kinase landscape of the DNA damage response. In: *FEBS Lett.* 585, p. 1625–1639. doi: 10.1016/j.febslet.2011.05.013.

Beshiri, M. L.; Holmes, K. B.; Richter, W. F.; Hess, S.; Islam, A. B. M. M. K.; Yan, Q. et al. (2012): Coordinated repression of cell cycle genes by KDM5A and E2F4 during differentiation. In: *Proceedings of the National Academy of Sciences* 109 (45), p. 18499–18504. DOI: 10.1073/pnas.1216724109.

Blair, L.P.; Cao, J.; Zou, M.R.; Sayegh, J.; Yan, Q. (2011): Epigenetic regulation by lysine demethylase 5 (KDM5) enzymes in cancer. In: *Cancers* (Basel) 3, p. 1383–1404. DOI: 10.3390/cancers3011383.

Bolderson, E.; Savage, K. I.; Mahen, R.; Pisupati, V.; Graham, M. E.; Richard, D. J. et al. (2012): Kruppel-associated Box (KRAB)-associated co-repressor (KAP-1) Ser-473 phosphorylation regulates heterochromatin protein 1beta (HP1-beta) mobilization and DNA repair in heterochromatin. In: *J. Biol. Chem.* 287, p. 28122–28131. 10.1074/jbc.M112.368381.

Bralten, L.B.C.; Kloosterhof, N.K.; Balvers, R.; Sacchetti, A.; Lapre, L.; Lamfers, M. et al. (2011): IDH1 R132H decreases proliferation of glioma cell lines in vitro and in vivo. In: *Ann Neurol.* 69, p. 455–63. doi: 10.1002/ana.22390.

Braselmann, H. (2014): CFAssay: Statistical analysis for the Colony Formation Assay. R package version 1.2.0. Available: http://www.bioconductor.org/packages/release/bioc/html/CFAssay.html.

Braselmann, H.; Michna, A.; Heß, J.; Unger, K. (2015): CFAssay: statistical analysis of the colony formation assay. In: *Radiation oncology (London, England)* 10, p. 223. DOI: 10.1186/s13014-015-0529-y.

Cairncross, J.G.; Wang, M.; Jenkins, R.B.; Shaw, E.G.; Giannini, C.; Brachman, D.G. et al. (2014): Benefit from procarbazine, lomustine, and vincristine in oligodendroglial tumors is associated with mutation of IDH. In: *Journal of clinical oncology*. 32 (8), p. 783–790.

Campbell, S. J.; Edwards, R. A.; Leung, C. C. Y.; Neculai, D.; Hodge, C. D.; Dhe-Paganon, S.; Glover, J. N. M. (2012): Molecular Insights into the Function of RING Finger (RNF)-containing Proteins hRNF8 and hRNF168 in Ubc13/Mms2-dependent Ubiquitylation. In: *Journal of Biological Chemistry* 287 (28), p. 23900–23910. DOI: 10.1074/jbc.M112.359653.

Cao, L.; Wei, F.; Du, Y.; Song, B.; Wang, D.; Shen, C. et al. (2016): ATM-mediated KDM2A phosphorylation is required for the DNA damage repair. In: *Oncogene. DOI:* 10.1038/onc.2015.81.

Carmena, M.; Earnshaw, W. C. (2006): INCENP at the kinase crossroads. In: *Nat Cell Biol.* 8, p. 110–111.

Chen, J.; Yao, Y.; Xu, H.; Qin, Z. (2016): Isocitrate Dehydrogenase (IDH)1/2 Mutations as Prognostic Markers in Patients With Glioblastomas. In: *Medicine* 95 (9), p. e2583. DOI: 10.1097/MD.0000000000002583.

Chicas, A.; Kapoor, A.; Wang, X.; Aksoy, O.; Evertts, A. G.; Zhang, M. Q. et al. (2012): H3K4 demethylation by Jarid1a and Jarid1b contributes to retinoblastoma-mediated gene silencing during cellular senescence. In: *Proceedings of the National Academy of Sciences* 109 (23), p. 8971–8976. DOI: 10.1073/pnas.1119836109.

Cho, Y.H.; McCullough, L.E.; Gammon, M.D.; Wu, H.C.; Zhang, Y.J.; Wang, Q. et al. (2015). Promoter Hypermethylation in White Blood Cell DNA and Breast Cancer Risk. In: *J Cancer* 6, p. 819–24. doi: 10.7150/jca.12174.

Chou, D. M.; Adamson, B.; Dephoure, N. E.; Tan, X.; Nottke, A. C.; Hurov, K. E. et al. (2010): A chromatin localization screen reveals poly (ADP ribose)-regulated recruitment of the repressive polycomb and NuRD complexes to sites of DNA damage. In: *Proceedings of the National Academy of Sciences* 107 (43), p. 18475–18480. DOI: 10.1073/pnas.1012946107.

Chowdhury, R.; Yeoh, K.K.; Tian, Y.; Hillringhaus, L.; Bagg, E.A.; Rose, N.R. et al. (2011): The oncometabolite 2-hydroxyglutarate inhibits histone lysine demethylases. In: *EMBO Rep* 12 (5), p. 463–469. DOI: 10.1038/embor.2011.43.

Christensen, J.; Agger, K.; Cloos, P.A.C.; Pasini, D.; Rose, S.; Sennels, L. et al. (2007): RBP2 Belongs to a Family of Demethylases, Specific for Tri-and Dimethylated Lysine 4 on Histone 3. In: *Cell* 128 (6), p. 1063–1076. DOI: 10.1016/j.cell.2007.02.003.

Christmann, M.; Kaina, B. (2013): Transcriptional regulation of human DNA repair genes following genotoxic stress: Trigger mechanisms, inducible responses and genotoxic adaptation. In: *Nucleic Acids Res.* 41, p. 8403–8420.

Clapier, C.R.; Cairns, B.R. (2009): The Biology of Chromatin Remodeling Complexes. In: *Annu. Rev. Biochem.* 78 (1), p. 273–304. DOI: 10.1146/annurev.biochem.77.062706.153223.

Cloos, P.A.C.; Christensen, J.; Agger, K.; Helin, K. (2008): Erasing the methyl mark: histone demethylases at the center of cellular differentiation and disease. In: *Genes Dev.* 22 (9), p. 1115–1140. DOI: 10.1101/gad.1652908.

Clouaire, T.; Legube, G. (2015): DNA double strand break repair pathway choice: a chromatin based decision? In: *Nucleus* 6, p. 107–113. doi:10.1080/19491034.2015.1010946.

Cowell, I.G.; Sunter, N.J.; Singh, P.B.; Austin, C.A.; Durkacz, B.W.; Tilby, M.J. et al. (2007): γH2AX Foci Form Preferentially in Euchromatin after Ionising-Radiation. In: *PLoS ONE* 2 (10), p. e1057. DOI: 10.1371/journal.pone.0001057.

Crawford, D. F.; Piwnica-Worms, H. (2001): The G(2) DNA damage checkpoint delays expression of genes encoding mitotic regulators. In: *The Journal of biological chemistry* 276 (40), p. 37166–37177. DOI: 10.1074/jbc.M103414200.

Cremer, M.; Schmid, V.J.; Kraus, F.; Markaki, Y.; Hellmann, I.; Maiser, A. et al. (2017): Initial high - resolution microscopic mapping of active and inactive regulatory sequences proves non-random 3D arrangements in chromatin domain clusters. In: *Epigenetics Chromatin* 10, p. 39.

Dang, L.; White, D.W.; Gross, S.; Bennett, B.D.; Bittinger, M.A.; Driggers, E.M. et al. (2009): Cancer-associated IDH1 mutations produce 2-hydroxyglutarate. In: *Nature* 462 (7274), p. 739–744. DOI: 10.1038/nature08617.

Davis, A.J.; Chen, D.J. (2013): DNA double strand break repair via non-homologous end-joining. In: *Transl. Cancer Res.* 2, p. 130–143.

Decottignies, A. (2013): Alternative end-joining mechanisms: a historical perspective. In: *Front.* Genet. 4. DOI: 10.3389/fgene.2013.00048.

Dileep, V.; Rivera-Mulia, J.C.; Sima, J.; Gilbert, D.M. (2015): Large-scale chromatin structure–function relationships during the cell cycle and development: insights from replication timing. In: *Cold Spring Harb Symp Quant Biol* 80, p. 53-63.

Dimitrova, E.; Turberfield, A. H.; Klose, R. J. (2015): Histone demethylases in chromatin biology and beyond. In: *EMBO Rep.* 16, p. 1620–1639. DOI: 10.15252/embr.201541113.

Dixon, J.R.; Selvaraj, S.; Yue, F.; Kim, A.; Li, Y.; Shen, Y. et al. (2012): Topological domains in mammalian genomes identified by analysis of chromatin interactions. In: *Nature* 485 (7398), p. 376–380.

Doil, C.; Mailand, N.; Bekker-Jensen, S.; Menard, P.; Larsen, D.H.; Pepperkok, R. et al. (2009): RNF168 Binds and Amplifies Ubiquitin Conjugates on Damaged Chromosomes to Allow Accumulation of Repair Proteins. In: *Cell* 136 (3), p. 435–446. DOI: 10.1016/j.cell.2008.12.041.

Draghici, S.; Khatri, P.; Eklund, A.C.; Szallasi, Z. (2006): Reliability and reproducibility issues in DNA microarray measurements. In: *Trends Genet* 22, p. 101–109.

Drexler, G.A.; Siebenwirth, C.; Drexler, S.E.; Girst, S.; Greubel, C.; Dollinger, G. et al. (2015): Live cell imaging at the Munich ion microbeam SNAKE - a status report. In: *Radiat Oncol.* 10, p. 42. doi: 10.1186/s13014-015-0350-7.

Du, G.; Drexler, G.A.; Friedland, W.; Greubel, C.; Hable, V.; Krücken, R. et al. (2011): Spatial Dynamics of DNA Damage Response Protein Foci along the Ion Trajectory of High-LET Particles. In: *Radiation Research* 176 (6), p. 706–715. DOI: 10.1667/RR2592.1.

Esteller, M. (2002): CpG island hypermethylation and tumor suppressor genes: a booming present, a brighter future. In: *Oncogene* 21, p. 5427–5440.

Faraway, J.J. (2006): Extending the Linear Model with R: Generalized Linear, Mixed Effects and Nonparametric Regression Models. Chapman & Hall, Boca Raton, FL.

Figueroa, M.E.; Abdel-Wahab, O.; Lu, C.; Ward, P.S.; Patel, J.; Shih. A. (2010): Leukemic IDH1 and IDH2 mutations result in a hypermethylation phenotype, disrupt TET2 function, and impair hematopoietic differentiation. In: *Cancer Cell* 18, p. 553–567. doi: 10.1016/j.ccr.2010.11.015.

Friedl, A.A.; Mazurek, B.; Seiler, D.M. (2012): Radiation-induced alterations in histone modification patterns and their potential impact on short-term radiation effects. In: *Front Oncol.* 2, p. 117.

Fukuda, T.; Wu, W.; Okada, M.; Maeda, I.; Kojima, Y.; Hayami, R. et al. (2015): Class I histone deacetylase inhibitors inhibit the retention of BRCA1 and 53BP1 at the site of DNA damage. In: *Cancer Sci.*, 106: p. 1050–1056. DOI: 10.1111/cas.12717.

Gale, M.; Sayegh, J.; Cao, J.; Norcia, M.; Gareiss, P.; Hoyer, D. et al. (2016): Screen-identified selective inhibitor of lysine demethylase 5A blocks cancer cell growth and drug resistance. In: *Oncotarget* 7 (26), p. 39931–39944. doi: 10.18632/oncotarget.9539.

Gehling, V.S.; Bellon, S.F.; Harmange, J.-C.; LeBlanc, Y.; Poy, F.; Odate, S. et al. (2016): Identification of potent, selective KDM5 inhibitors. In: *Bioorg. Med. Chem. Lett.* 26, p. 4350–4354.

Gilbert, N.; Thomson, I.; Boyle, S.; Allan, J.; Ramsahoye, B.; Bickmore, W.A. (2007): DNA methylation affects nuclear organization, histone modifications, and linker histone binding but not chromatin compaction. In: *The Journal of Cell Biology* 177 (3), p. 401–411. DOI: 10.1083/jcb.200607133.

Girst, S.; Hable, V.; Drexler, G.A.; Greubel, C.; Siebenwirth, C.; Haum, M. et al. (2013): Subdiffusion supports joining of correct ends during repair of DNA double-strand breaks. In: *Sci Rep.* 3, p. 2511.

Gong, F.; Chiu, L.Y.; Cox, B.; Aymard, F.; Clouaire, T.; Leung, J.W. et al. (2015): Screen identifies bromodomain protein ZMYND8 in chromatin recognition of transcription-associated DNA damage that promotes homologous recombination. In: *Genes Dev* 29, p. 197–211. doi: 10.1101/gad.252189.114.

Gong, F.; Clouaire, T.; Aguirrebengoa, M.; Legube, G.; Miller, K.M. (2017): Histone demethlyase KDM5A regulates the ZMYND8-NuRD chromatin remodeler to promote DNA repair. In: *The Journal of Cell Biology*. doi:10.1083/jcb.201611135.

Goodarzi, A.A.; Kurka, T.; Jeggo, P.A. (2011): KAP-1 phosphorylation regulates CHD3 nucleosome remodeling during the DNA double-strand break response. In: *Nat Struct Mol Biol* 18 (7), p. 831–839. DOI: 10.1038/nsmb.2077.

Grabarz, A.; Barascu, A.; Guirouilh-Barbat, J.; Lopez, B.S. (2012): Initiation of DNA double strand break repair: signaling and single-stranded resection dictate the choice between homologous recombination, non-homologous end-joining and alternative end-joining. In: *Am J Cancer Res* 2, p. 249–268.

Greubel, C.; Hable, V.; Drexler, G.A.; Hauptner, A.; Dietzel, S.; Strickfaden, H. et al. (2008): Competition effect in DNA damage response. In: *Radiat Environ Biophys.* 47, p. 423–429. doi: 10.1007/s00411-008-0182-z.

Groselj, B.; Sharma, N.L.; Hamdy, F.C.; Kerr, M.; Kiltie, A.E. (2013:) Histone deacetylase inhibitors as radiosensitisers: effects on DNA damage signalling and repair. In: *Br J Cancer,* 108: p: 748–54. doi: 10.1038/bjc.2013.21.

Hable, V.; Drexler, G.A.; Brüning, T., Burgdorf, C.; Greubel, C.; Derer, A. et al. (2012): Recruitment kinetics of DNA repair proteins Mdc1 and Rad52 but not 53BP1 depend on damage complexity. In: *PLoS One* 7, e41943. doi: 10.1371/journal.pone.0041943.

Haince, J.; McDonald, D.; Rodrigue, A.; Dery, U.; Masson, J.; Hendzel, M. J. et al. (2008): PARP1-dependent Kinetics of Recruitment of MRE11 and NBS1 Proteins to Multiple DNA Damage Sites. In: *Journal of Biological Chemistry* 283 (2), p. 1197–1208. DOI: 10.1074/jbc.M706734200.

Halacli, S.O.; Canpinar, H.; Cimen, E.; Sunguroglu, A. (2013): Effects of gamma irradiation on cell cycle, apoptosis and telomerase activity in p53 wild-type and deficient HCT116 colon cancer cell lines. In: *Oncology letters* 6 (3), p. 807–810. DOI: 10.3892/ol.2013.1441.

Hanahan, D.; Weinberg, R.A. (2011): Hallmarks of cancer: the next generation. In: *Cell* 144, p. 646–674.

Hauptner, A.; Dietzel, S.; Drexler, G. A.; Reichart, P.; Krücken, R.; Cremer, T. et al. (2004): Microirradiation of cells with energetic heavy ions. In: *Radiation and Environmental Biophysics* 42 (4), p. 237–245. DOI: 10.1007/s00411-003-0222-7.

Hauptner, A.; Friedland, W.; Dietzel, S.; Drexler, G.A.; Greubel, C.; Hable, V. et al. (2006): Spatial distribution of DNA-double-strand breaks from ion tracks. In: *R Acad Sci Lett Copenhagen* 52, p. 59–85.

Hayakawa, T.; Ohtani, Y.; Hayakawa, N.; Shinmyozu, K.; Saito, M.; Ishikawa, F. et al. (2007): RBP2 is an MRG15 complex component and down-regulates intragenic histone H3 lysine 4 methylation. In: *Genes Cells* 12 (6), p. 811–26.

Horton, J.R.; Liu, X.; Gale, M.; Wu, L.; Shanks, J.R.; Zhang, X. et al. (2016): Structural basis for KDM5A histone lysine demethylase inhibition by diverse compounds. In: *Cell Chem. Biol.* 23, p. 769–781.

Hou, J.; Wu, J.; Dombkowski, A.; Zhang, K.; Holowatyj, A.; Boerner, J.L. et al. (2012): Genomic amplification and a role in drug-resistance for the KDM5A histone demethylase in breast cancer. In: *Am J Transl Res.* 4, p. 247–256.

Hsiao, K.; Mizzen, C.A. (2013): Histone H4 deacetylation facilitates 53BP1 DNA damage signaling and double-strand break repair. In: *Journal of molecular cell biology* 5 (3), p. 157–165. DOI: 10.1093/jmcb/mjs066.

Huang, P.; Chen, C.; Chou, C.; Sargeant, A.M.; Kulp, S.K.; Teng, C. et al. (2010): Histone Deacetylase Inhibitors Stimulate Histone H3 Lysine 4 Methylation in Part Via Transcriptional Repression of Histone H3 Lysine 4 Demethylases. In: *Molecular Pharmacology* 79 (1), p. 197–206. DOI: 10.1124/mol.110.067702.

Hynes, R. O. (2002): Integrins: bidirectional, allosteric signaling machines. In: *Cell* 110, p. 673–687. doi: 10.1016/S0092-8674(02)00971-6.

Ikura, M.; Furuya, K.; Matsuda, S.; Matsuda, R.; Shima, H.; Adachi, J. et al. (2015): Acetylation of histone H2AX at Lys 5 by the TIP60 histone acetyltransferase complex is essential for the dynamic binding of NBS1 to damaged chromatin. In: *Molecular and Cellular Biology. DOI:* 10.1128/MCB.00757-15.

Imai, R.; Nozaki, T.; Tani, T.; Kaizu, K.; Hibino, K.; Ide, S. et al. (2017): Density imaging of heterochromatin in live cells using orientation-independent-DIC microscopy. In: *Mol Biol Cell* , 28 (23), p. 3349-3359. doi: 10.1091/mbc.E17-06-0359.

Islam, A.B.; Richter, W.F.; Lopez-Bigas, N.; Benevolenskaya, E.V. (2014): Selective targeting of histone methylation. In: *Cell Cycle* 10 (3), p. 413–424. DOI: 10.4161/cc.10.3.14705.

Itoh, Y.; Sawada, H.; Suzuki, M.; Tojo, T.; Sasaki, R.; Hasegawa, M. et al. (2015): Identification of Jumonji AT-Rich Interactive Domain 1A Inhibitors and Their Effect on Cancer Cells. In: *ACS medicinal chemistry letters* 6 (6), p. 665–670. DOI: 10.1021/acsmedchemlett.5b00083.

Iwase, S.; Lan, F.; Bayliss, P.; de la Torre-Ubieta, L.; Huarte, M.; Qi, H.H. et al. (2007): The X-Linked Mental Retardation Gene SMCX/JARID1C Defines a Family of Histone H3 Lysine 4 Demethylases. In: *Cell* 128 (6), p. 1077–1088. DOI: 10.1016/j.cell.2007.02.017.

Izzo, A.; Schneider, R. (2016): The role of linker histone H1 modifications in the regulation of gene expression and chromatin dynamics. In: *Biochim Biophys Acta.* (3), p. 486–495. doi: 10.1016/j.bbagrm.2015.09.003.

Jakob, B.; Splinter, J.; Conrad, S.; Voss, K.-O.; Zink, D.; Durante, M. et al. (2011): DNA double-strand breaks in heterochromatin elicit fast repair protein recruitment, histone H2AX phosphorylation and relocation to euchromatin. In: *Nucleic Acids Research* 39 (15), p. 6489–6499. DOI: 10.1093/nar/gkr230.

Jaksik, R.; Iwanaszko, M.; Rzeszowska-Wolny, J.; Kimmel, M. (2015): Microarray experiments and factors which affect their reliability. In: *Biol Direct*.10, p. 46. doi: 10.1186/s13062-015-0077-2.

Jeggo, P.A.; Löbrich, M. (2006): Contribution of DNA repair and cell cycle checkpoint arrest to the maintenance of genomic stability. In: *DNA Repair* 5 (9-10), p. 1192–1198. DOI: 10.1016/j.dnarep.2006.05.011.

Jen, K.Y.; Cheung, V.G. (2003): Transcriptional response of lymphoblastoid cells to ionizing radiation. In: *Genome Res.* 13, p. 2092–100.

Ji, X.; Jin, S.; Qu, X.; Li, K.; Wang, H.; He, H. et al. (2015): Lysine-specific demethylase 5C promotes hepatocellular carcinoma cell invasion through inhibition BMP7 expression. In: *BMC cancer* 15 (1), p. 801. DOI: 10.1186/s12885-015-1798-4.

Jones, P.A.; Baylin, S.B. (2007): The epigenomics of cancer. In: *Cell* 128, p. 683–92.

Kachhap, S.K.; Rosmus, N.; Collis, S.J.; Kortenhorst, M.S.; Wissing, M.D.; Hedayati,M. et al. (2010): Downregulation of homologous recombination DNA repair genes by HDAC inhibition in prostate cancer is mediated through the E2F1 transcription factor. In: *PLoS One* 5, e11208.

Kalinina, J.; Carroll, A.; Wang, L.; Yu, Q.; Mancheno, D.E.; Wu. S. et al. (2012): Detection of "oncometabolite" 2-hydroxyglutarate by magnetic resonance analysis as a biomarker of IDH1/2 mutations in glioma. In: *J Mol Med.* 90 (10), p. 1161–71.

Kao, G.D.; McKenna, W.G.; Maity, A.; Blank, K.; Muschel, R.J. (1997): Cyclin B1 availability is a rate-limiting component of the radiation-induced G2 delay in HeLa cells. In: *Cancer Res.* 57, p. 753–758.

Karagiannis, T.C.; Harikrishnan, K.N.; El-Osta, A. (2007): Disparity of histone deacetylase inhibition on repair of radiation-induced DNA damage on euchromatin and constitutive heterochromatin compartments. In: *Oncogene,* 26, p. 3963-71. DOI: 10.1038/sj.onc.1210174.

Kernytsky, A.; Wang, F.; Hansen, E.; Schalm, S.; Straley, K.; Gliser, C. et al. (2015): IDH2 mutation-induced histone and DNA hypermethylation is progressively reversed by small-molecule inhibition. In: *Blood* 125, p. 296–303.

Khoury-Haddad, H.; Guttmann-Raviv, N.; Ipenberg, I.; Huggins, D.; Jeyasekharan, A. D.; Ayoub, N. (2014): PARP1-dependent recruitment of KDM4D histone demethylase to DNA damage sites promotes double-strand break repair. In: *Proceedings of the National Academy of Sciences* 111 (7), p. E728–E737. DOI: 10.1073/pnas.1317585111.

Khurana, S.; Kruhlak, M.J.; Kim, J.; Tran, A.D.; Liu, J.; Nyswaner, K. et al (2014): A macrohistone variant links dynamic chromatin compaction to BRCA1-dependent genome maintenance. In: *Cell Rep*. 2014; 8: p. 1049–1062. doi:10.1016/j.celrep.2014.07.024.

Kim, I.A.; Kim, I.H.; Kim, H.J.; Chie, E.K.; Kim, J.S. (2010): HDAC inhibitor-mediated radiosensitization in human carcinoma cells: a general phenomenon? In: *J Radiat Res.* 51, p. 257–263. DOI: 10.1269/jrr.09115.

Kim, J.G.; Park, M.T.; Heo, K.; Yang, K.M.; Yi, J.M. (2013): Epigenetics meets radiation biology as a new approach in cancer treatment. In: *Int J Mol Sci* 14 (7), p. 15059–15073.

Kim, T.Y.; Zhong, S.; Fields, C.R.; Kim, J.H.; Robertson, K.D. (2006): Epigenomic profiling reveals novel and frequent targets of aberrant DNA methylation-mediated silencing in malignant glioma. In: *Cancer Res.* 66, p. 7490–7501.

Klose, R.J.; Kallin, E.M.; Zhang, Y. (2006): JmjC-domain-containing proteins and histone demethylation. In: *Nat Rev Genet* 7 (9), p. 715–727. DOI: 10.1038/nrg1945.

Klose, R.J.; Yan, Q.; Tothova, Z.; Yamane, K.; Erdjument-Bromage, H.; Tempst, P. et al. (2007): The Retinoblastoma Binding Protein RBP2 Is an H3K4 Demethylase. In: *Cell* 128 (5), p. 889–900. DOI: 10.1016/j.cell.2007.02.013.

Koivunen, P.; Lee, S.; Duncan, C.G.; Lopez, G.; Lu, G.; Ramkissoon, S. et al. (2012): Transformation by the (R)-enantiomer of 2-hydroxyglutarate linked to EGLN activation. In: *Nature* 483, p. 484–8. doi: 10.1038/nature10898.

Koprinarova, M.; Botev, P.; Russev, G. (2011): Histone deacetylase inhibitor sodium butyrate enhances cellular radiosensitivity by inhibiting both DNA nonhomologous end joining and homologous recombination. In: *DNA Repair (Amst)* 10, p. 970–977.

Kornberg, R.D. (1977): Structure of chromatin. In: *Annual review of biochemistry* 46(1), p. 931–54.

Kouzarides, T. (2007): Chromatin Modifications and Their Function. In: *Cell* 128 (4), p. 693–705.

Krumm, A.; Barckhausen, C.; Kucuk, P.; Tomaszowski, K.H.; Loquai, C., Fahrer, J. et al. (2016): Enhanced histone deacetylase activity in malignant melanoma provokes RAD51 and FANCD2-triggered drug resistance. In: *Cancer Res.* 76, p. 3067–3077.

Labadie, S.S.; Dragovich, P.S.; Cummings, R.T.; Deshmukh. G.; Gustafson, A.; Han, N. et al. (2016): Design and evaluation of 1,7-naphthyridones as novel KDM5 inhibitors. In: *Bioorg Med Chem Lett* 26 (18), p. 4492-6. doi: 10.1016/j.bmcl.2016.07.070.

Labbé, R.M.; Holowatyj, A.; Yang, Z.Q. (2013): Histone lysine demethylase (KDM) subfamily 4: structures, functions and therapeutic potential. In: *Am J Transl Res* 6, p. 1–15.

Landsverk, K.S.; Patzke, S.; Rein, I.D.; Stokke, C.; Lyng, H.; de Angelis, P.M. et al. (2011): Three independent mechanisms for arrest in G2 after ionizing radiation. In: *Cell cycle (Georgetown, Tex.)* 10 (5), p. 819–829. DOI: 10.4161/cc.10.5.14968.

Lee, M.G.; Wynder, C.; Bochar, D.A.; Hakimi, M.; Cooch, N.; Shiekhattar, R. (2006): Functional interplay between histone demethylase and deacetylase enzymes. In: *Mol. Cell. Biol.* 26 (17), p. 6395–6402. DOI: 10.1128/MCB.00723-06.

Li, F.; He, X.; Ye, D.; Lin, Y.; Yu, H.; Yao, C. et al. (2015): NADP(+)-IDH Mutations promote hypersuccinylation that impairs mitochondria respiration and induces apoptosis resistance. In: *Mol Cell.* 60, p. 661–75. doi: 10.1016/j.molcel.2015.10.017.

Li, Q. (2004): A Syntaxin 1, G o, and N-Type Calcium Channel Complex at a Presynaptic Nerve Terminal: Analysis by Quantitative Immunocolocalization. In: *Journal of Neuroscience* 24 (16), p. 4070–4081. DOI: 10.1523/JNEUROSCI.0346-04.2004.

Li, S.; Chou, A.P.; Chen, W.; Chen, R.; Deng, Y.; Phillips, H.S. et al. (2013): Overexpression of isocitrate dehydrogenase mutant proteins renders glioma cells more sensitive to radiation. In: *Neuro-oncology* 15 (1), p. 57–68. DOI: 10.1093/neuonc/nos261.

Li, S.; Li, C.; Ryu, H.; Lim, S.; Jang, W.; Jung, S. (2016): Bacitracin Inhibits the Migration of U87-MG Glioma Cells via Interferences of the Integrin Outside-in Signaling Pathway. In: *J Korean Neurosurg Soc*. 59 (2), p. 106–116.

Li, X.; Liu, L.; Yang, S.; Song, N.; Zhou, X.; Gao, J. et al. (2014): Histone demethylase KDM5B is a key regulator of genome stability. In: *Proceedings of the National Academy of Sciences* 111 (19), p. 7096–7101. DOI: 10.1073/pnas.1324036111.

Li, X.; Corsa, Callie A.S.; Pan, P.W.; Wu, L.; Ferguson, D.; Yu, X. et al. (2010): MOF and H4 K16 acetylation play important roles in DNA damage repair by modulating recruitment of DNA damage repair protein Mdc1. In: *Molecular and Cellular Biology* 30 (22), p. 5335–5347. DOI: 10.1128/MCB.00350-10.

Li, X.; Heyer, W. D. (2008): Homologous recombination in DNA repair and DNA damage tolerance. In: *Cell Res.* 18, p. 99–113.

Liang, G.; Lin, J.C.; Wie, V.; Yoo, C.; Cheng, J.C.; Nguyen, C.T. et al. (2004): Distinct localization of histone H3 acetylation and H3-K4 methylation to the transcription start sites in the human genome. In: *Proc Natl Acad Sci USA* 101, p. 7357–7362.

Liang, X.; Zeng, J.; Wang, L.; Fang, M.; Wang, Q.; Zhao, M. et al. (2013): Histone demethylase retinoblastoma binding protein 2 is overexpressed in hepatocellular carcinoma and negatively regulated by hsa-miR-212. In: *PLoS One* 8, e69784 doi: 10.1371/journal.pone.0069784.

Liu, B.; Wang, Z.; Ghosh, S.; Zhou, Z. (2013): Defective ATM-Kap-1-mediated chromatin remodeling impairs DNA repair and accelerates senescence in progeria mouse model. In: *Aging cell* 12 (2), p. 316–318. DOI: 10.1111/acel.12035.

Löbrich, M.; Shibata, A.; Beucher, A.; Fisher, A.; Ensminger, M.; Goodarzi, A.A. et al. (2010): gammaH2AX foci analysis for monitoring DNA double-strand break repair: strengths, limitations and optimization. In: *Cell Cycle* 9, p. 662–669.

Lu, C.; Ward, P.S.; Kapoor, G.S.; Rohle, D.; Turcan, S.; Abdel-Wahab, O. et al. (2012): IDH mutation impairs histone demethylation and results in a block to cell differentiation. In: *Nature* 483 (7390), p. 474–478. DOI: 10.1038/nature10860.

Lu, P.; Takai, K.; Weaver, V.M.; Werb, Z. (2011): Extracellular matrix degradation and remodeling in development and disease. In: *Cold Spring Harb Perspect Biol.* 3 (12).

Lu, X.; de la Pena, L.; Barker, C.; Camphausen, K.; Tofilon, P.J. (2006): Radiation-induced changes in gene expression involve recruitment of existing messenger RNAs to and away from polysomes. In: *Cancer Res.* 66, p. 1052–1061.

Luger, K.; Mäder, A.W.; Richmond, R.K.; Sargent, D.F.; Richmond, T.J. (1997): Crystal structure of the nucleosome core particle at 2.8 Å resolution. In: *Nature* 389, p. 251–260. doi: 10.1038/38444.

Lundberg, E.; Fagerberg, L.; Klevebring, D.; Matic, I.; Geiger, T.; Cox, J. et al. (2010). Defining the transcriptome and proteome in three functionally different human cell lines. In. *Mol. Syst. Biol.* 6, p. 450.

Ma, S.; Jiang, B.; Deng, W.; Gu, Z.K.; Wu, F.Z.; Li, T. et al. (2015): D-2-hydroxyglutarate is essential for maintaining oncogenic property of mutant IDH-containing cancer cells but dispensable for cell growth. In: *Oncotarget* 6, p. 8606–20. doi: 10.18632/oncotarget.3330.

Macaeva, E.; Saeys, Y.; Tabury, K.; Janssen, A.; Michaux, A.; Benotmane, M.A. et al. (2016): Radiation-induced alternative transcription and splicing events and their applicability to practical biodosimetry. In: *Scientific Reports* 6, p. 19251.

Mansour, W.Y.; Dahm-Daphi, J. (2010): The alternative end-joining pathway for repair of DNA double-strand breaks requires PARP1 but is not dependent upon microhomologies. In: *Nucleic Acids Res*. 38, p. 6065–6077.

Mansour, W. Y.; Schumacher, S.; Rosskopf, R.; Rhein, T.; Schmidt-Petersen, F.; Gatzemeier, F. et al. (2008): Hierarchy of nonhomologous end-joining, single-strand annealing and gene conversion at site-directed DNA double-strand breaks. In: *Nucleic Acids Research* 36 (12), p. 4088–4098. DOI: 10.1093/nar/gkn347.

Mao, Z.; Bozzella, M.; Seluanov, A.; Gorbunova, V. (2008): DNA repair by nonhomologous end joining and homologous recombination during cell cycle in human cells. In: *Cell cycle* 7, p. 2902–2906.

Mardis, E.R.; Ding, L.; Dooling, D.J.; Larson, D.E.; McLellan, M.D.; Chen, K. et al. (2009): Recurring mutations found by sequencing an acute myeloid leukemia genome. In: *The New England journal of medicine* 361 (11), p. 1058–1066. DOI: 10.1056/NEJMoa0903840.

Maroschik, B.; Gurtler, A.; Kramer, A.; Rossler, U.; Gomolka, M.; Hornhardt, S. et al. (2014): Radiation-induced alterations of histone post-translational modification levels in lymphoblastoid cell lines. In: *Radiat Oncol.* 9, p. 15.

Matthews, L.; Gopinath, G.; Gillespie, M.; Caudy, M.; Croft, D.; de Bono, B. et al. (2009): Reactome knowledgebase of human biological pathways and processes. In: *Nucleic acids research* 37, p. 619–622.

McGrath, J.; Trojer, P. (2015): Targeting histone lysine methylation in cancer. In: *Pharmacology & therapeutics* 150, p. 1–22. DOI: 10.1016/j.pharmthera.2015.01.002.

Megova, M.; Drabek, J.; Koudelakova, V.; Trojanec, R.; Kalita, O.; Hajduch, M. (2014): Isocitrate dehydrogenase 1 and 2 mutations in gliomas. In: *Journal of neuroscience research* 92 (12), p. 1611–1620.

Mersfelder, E. L.; Parthun, M. R. (2006): The tale beyond the tail: histone core domain modifications and the regulation of chromatin structure. In: *Nucleic Acids Research* 34 (9), p. 2653–2662. DOI: 10.1093/nar/gkl338.

Mezentsev, A.;, Amundson, S.A. 2011: Global gene expression responses to low- or high-dose radiation in a human three-dimensional tissue model. In: *Radiat Res* 175, p. 677–688.

Miller, K.M.; Tjeertes, J.V.; Coates, J.; Legube, G.; Polo, S.E.; Britton, S. et al. (2010): Human HDAC1 and HDAC2 function in the DNA-damage response to promote DNA nonhomologous end-joining. In: *Nature structural & molecular biology* 17 (9), p. 1144–1151. DOI: 10.1038/nsmb.1899.

Mirzoeva, O.K.; Petrini, J.H. (2003): DNA replication-dependent nuclear dynamics of the mre11 complex. In: *Mol. Cancer Res.*1, p. 207–218.

Misteli, T.; Soutoglou, E. (2009): The emerging role of nuclear architecture in DNA repair and genome maintenance. In: *Nat Rev Mol Cell Biol.*10, p. 243–54. doi: 10.1038/nrm2651.

Mitra, D.; Das, P.M.; Huynh, F.C.; Jones, F.E. (2011): Jumonji/ARID1 B (JARID1B) protein promotes breast tumor cell cycle progression through epigenetic repression of microRNA let-7e. In: *J. Biol. Chem.* 286 (47), p. 40531–40535. DOI: 10.1074/jbc.M111.304865.

Mosammaparast, N.; Kim, H.; Laurent, B.; Zhao, Y.; Lim, H. J.; Majid, M. C. et al. (2013): The histone demethylase LSD1/KDM1A promotes the DNA damage response. In: *The Journal of Cell Biology* 203 (3), p. 457–470. DOI: 10.1083/jcb.201302092.

Mottamal, M.; Zheng, S.; Huang, T.L.; Wang, G. (2015): Histone deacetylase inhibitors in clinical studies as templates for new anticancer agents. In: *Molecules (Basel, Switzerland)* 20 (3), p. 3898–3941. DOI: 10.3390/molecules20033898.

Muramatsu, D.; Kimura, H.; Kotoshiba, K.; Tachibana, M.; Shinkai, Y. (2016): Pericentric H3K9me3 formation by HP1 Interaction-defective Histone Methyltransferase Suv39h1. In: *Cell Structure and Function* 41, p. 145–152. doi: 10.1247/csf.16013.

Murr, R.; Loizou, J.I.; Yang, Y.; Cuenin, C.; Li, H.; Wang, Z.; Herceg, Z. (2006): Histone acetylation by Trrap–Tip60 modulates loading of repair proteins and repair of DNA double-strand breaks. In: *Nat Cell Biol* 8 (1), p. 91–99. DOI: 10.1038/ncb1343.

Naumann, U.; Harter, P.N.; Rubel, J.; Ilina, E.; Blank, A.; Esteban, H.B. et al. (2013): Glioma cell migration and invasion as potential target for novel treatment strategies. In: *Translat.Neurosci.* 4, p. 314. doi:10.2478/s13380-013-0126-1.

NCBI Gene. Bethesda (MD): National Library of Medicine (US), National Center for Biotechnology Information; 2004 – 2018 Jan 21. Available from: https://www.ncbi.nlm.nih.gov/gene/

Neumayer, G.; Nguyen, M.D. (2014): TPX2 impacts acetylation of histone H4 at lysine 16: implications for DNA damage response. In: *PLoS ONE* 9 (11), p. e110994. DOI: 10.1371/journal.pone.0110994.

Nishibuchi, G.; Shibata, Y.; Hayakawa, T.; Hayakawa, N.; Ohtani, Y.; Sinmyozu, K. et al. (2014): Physical and Functional Interactions between the Histone H3K4 Demethylase KDM5A and the Nucleosome Remodeling and Deacetylase (NuRD) Complex. In: *Journal of Biological Chemistry* 289 (42), p. 28956–28970. DOI: 10.1074/jbc.M114.573725.

Ohtani, K.; Dimmeler, S. (2011): Epigenetic regulation of cardiovascular differentiation. In: *Cardiovascular Research* 90 (3), p. 404–412. DOI: 10.1093/cvr/cvr019.

Oizel, K.; Gratas, C.; Nadaradjane, A.; Oliver, L.; Vallette, F.M.; Pecqueur, C. (2015): D-2-Hydroxyglutarate does not mimic all the IDH mutation effects, in particular the reduced etoposide-triggered apoptosis mediated by an alteration in mitochondrial NADH. In: *Cell death & disease* 6, e1704.

Outchkourov, N.S.; Muiño, J.M.; Kaufmann, K.; van IJcken, W.F.J.; Koerkamp, M.J.G.; van Leenen, D. et al. (2013): Balancing of Histone H3K4 Methylation States by the Kdm5c/SMCX Histone Demethylase Modulates Promoter and Enhancer Function. In: *Cell Reports* 3 (4), p. 1071–1079. DOI: 10.1016/j.celrep.2013.02.030.

Pandita, T.K.; Richardson, C. (2009): Chromatin remodeling finds its place in the DNA double-strand break response. In: *Nucleic Acids Res.* 37, p. 1363–1377.

Pasini, D.; Hansen, K.H.; Christensen, J.; Agger, K.; Cloos, P.A.C.; Helin, K. (2008): Coordinated regulation of transcriptional repression by the RBP2 H3K4 demethylase and Polycomb-Repressive Complex 2. In: *Genes & Development* 22 (10), p. 1345–1355. DOI: 10.1101/gad.470008.

Paull, T.T. (2015): Mechanisms of ATM activation. In: *Annu. Rev. Biochem.* 84, p. 711–738.

Penterling, C. (2013): Auswirkungen eines *Knockdowns* der Demethylase Jarid1A auf die zelluläre Strahlenantwort. Master thesis. Ludwig-Maximilians-University of Munich, Faculty of Biology.

Perry, M.; Chalkley, R. (1981): The effect of histone hyperacetylation on the nuclease sensitivity and the solubility of chromatin. In: *J. Biol. Chem.* 256, p. 3313–3318.

Pfaffl, M.W. (2001): A new mathematical model for relative quantification in real-time RT-PCR. In: *Nucleic Acids Research* 29 (9), p. 45e-45. DOI: 10.1093/nar/29.9.e45.

Probst, A.V.; Dunleavy, E.; Almouzni, G. (2009): Epigenetic inheritance during the cell cycle. In: *Nat. Rev. Mol. Cell Biol.* 10 (3), p. 192–206. DOI: 10.1038/nrm2640.

Qi, L.; Zhu, F.; Li, S.H.; Si, L.B.; Hu, L.K.; Tian, H. (2014): Retinoblastoma binding protein 2 (RBP2) promotes HIF-1α-VEGF-induced angiogenesis of non-small cell lung cancer via the Akt pathway. In: *PLoS One* 9 (8):e106032. doi: 10.1371/journal.pone.0106032.

Qiao, N.; Wang, S.; Hu, L. (2015): Retinoblastoma-binding protein 2 induces epithelial-mesenchymal transition in esophageal squamous cancer cells. In: *Biotechnol Lett.* 37 (12), p. 2365-70.

Rashi-Elkeles, S.; Warnatz, H.J.; Elkon, R.; Kupershtein, A.; Chobod, Y.; Paz, A. et al. (2014): Parallel Profiling of the Transcriptome, Cistrome, and Epigenome in the Cellular Response to Ionizing Radiation. In: *Science Signaling* 7, p. 325:11. doi:10.1126/scisignal.2005032.

Reactome Database: https://reactome.org/

Reindl, J.; Drexler, G.A.; Girst, S.; Greubel, C.; Siebenwirth, C.; Drexler S.E. et al. (2015): Nanoscopic exclusion between Rad51 and 53BP1 after ion irradiation in human HeLa cells. In: *Phys Biol.* 12, p. 066005. doi: 10.1088/1478-3975/12/6/066005.

Reindl, J.; Girst, S.; Walsh, D.W.; Greubel, C.; Schwarz, B.; Siebenwirth, C. et al. (2017): Chromatin organization revealed by nanostructure of irradiation induced gammaH2AX, 53BP1 and Rad51 foci. In: *Sci Rep*. 7, p. 40616.

Reitman, Z.J.; Duncan, C.G.; Poteet, E.; Winters, A.; Yan, L.; Gooden, D.M. et al. (2014): Cancer-associated Isocitrate Dehydrogenase 1 (IDH1) R132H Mutation and D-2-Hydroxyglutarate Stimulate Glutamine Metabolism under Hypoxia. In: *Journal of Biological Chemistry* 289 (34), p. 23318–23328. DOI: 10.1074/jbc.M114.575183.

Reitman, Z.J.; Yan, H. (2010): Isocitrate dehydrogenase 1 and 2 mutations in cancer: alterations at a crossroads of cellular metabolism. In: *Journal of the National Cancer Institute* 102 (13), p. 932–941. DOI: 10.1093/jnci/djq187.

Reynolds, P.; Botchway, S.W.; Parker, A.W.; O'Neill, P. (2013): Spatiotemporal dynamics of DNA repair proteins following laser microbeam induced DNA damage - when is a DSB not a DSB? In: *Mutation research* 756 (1-2), p. 14–20. DOI: 10.1016/j.mrgentox.2013.05.006.

Rolon-Reyes, K.; Kucheryavykh, Y.V.; Cubano, L.A.; Inyushin, M.; Skatchkov, S.N.; Eaton, M.J. et al. (2015): Microglia activate migration of glioma cells through a Pyk2 intracellular pathway. In: *Plos One* 10, e0131059.

Rouet, P.; Smih, F.; Jasin, M. (1994): Expression of a site-specific endonuclease stimulates homologous recombination in mammalian cells. In: *Proc. Natl. Acad. Sci. U. S. A.* 91, p. 6064–6068.

Rujirabanjerd, S.; Nelson, J.; Tarpey, P.S.; Hackett, A.; Edkins, S.; Raymond, F.L. et al. (2010): Identification and characterization of two novel JARID1C mutations: suggestion of an emerging genotype-phenotype correlation. In: *Eur. J. Hum. Genet.* 18 (3), p. 330–335. DOI: 10.1038/ejhg.2009.175.

Saksouk, N.; Simboeck, E.; Dffejardin, J. (2015): Constitutive heterochromatin formation and transcription in mammals. In: *Epigenetics Chromatin* 8 (3), p. 3. doi: 10.1186/1756-8935-8-3.

Sayegh, J.; Cao, J.; Zou, M. R.; Morales, A.; Blair, L. P.; Norcia, M. et al. (2013): Identification of Small Molecule Inhibitors of Jumonji AT-rich Interactive Domain 1B (JARID1B) Histone Demethylase by a Sensitive High Throughput Screen. In: *Journal of Biological Chemistry* 288 (13), p. 9408–9417. DOI: 10.1074/jbc.M112.419861.

Scheffner, M.; Werness, B.A.; Huibregtse, J.M.; Levine, A.J.; Howley, P.M. (1990): The E6 oncoprotein encoded by human papillomavirus types 16 and 18 promotes the degradation of p53. In: *Cell* 63, p. 1129–1136.

Schipler, A.; Iliakis, G. (2013): DNA double-strand-break complexity levels and their possible contributions to the probability for error-prone processing and repair pathway choice. In: *Nucleic Acids Res*. 41 (16), p. 7589–7605.

Schreiber, V.; Dantzer, F.; Ame, J.; de Murcia, G. (2006): Poly(ADP-ribose): novel functions for an old molecule. In: *Nat Rev Mol Cell Biol* 7 (7), p. 517–528. DOI: 10.1038/nrm1963.

Scibetta, A.G.; Santangelo, S.; Coleman, J.; Hall, D.; Chaplin, T.; Copier, J. et al. (2007): Functional Analysis of the Transcription Repressor PLU-1/JARID1B. In: *Molecular and Cellular Biology* 27 (20), p. 7220–7235. DOI: 10.1128/MCB.00274-07.

Seiler, D.M.; Rouquette, J.; Schmid, V.J.; Strickfaden, H.; Ottmann, C.; Drexler, G.A. et al. (2011): Double-strand break-induced transcriptional silencing is associated with loss of tri-methylation at H3K4. In: *Chromosome Res* 19 (7), p. 883–899. DOI: 10.1007/s10577-011-9244-1.

Sharma, S.V.; Lee, D.Y.; Li, B.; Quinlan, M.P.; Takahashi, F.; Maheswaran, S. et al. (2010): A chromatin-mediated reversible drug-tolerant state in cancer cell subpopulations. In: *Cell* 141 (1), p. 69–80. DOI: 10.1016/j.cell.2010.02.027.

Shen, X.; Zhuang, Z.; Zhang, Y.; Chen, Z.; Shen, L.; Pu, W. et al. (2015): JARID1B modulates lung cancer cell proliferation and invasion by regulating p53 expression. In: *Tumor Biol.* 36 (9), p. 7133-42. DOI: 10.1007/s13277-015-3418-y.

Shi, L.; Oberdoerffer, P. (2012): Chromatin dynamics in DNA double-strand break repair. In: *Biochimica et biophysica acta* 1819 (7), p. 811–819. DOI: 10.1016/j.bbagrm.2012.01.002.

Shi, Y.; Lan, F.; Matson, C.; Mulligan, P.; Whetstine, J.R.; Cole, P.A. et al. (2004): Histone demethylation mediated by the nuclear amine oxidase homolog LSD1. In: *Cell* 119 (7), p. 941–953. DOI: 10.1016/j.cell.2004.12.012.

Shibata, A. (2017): Regulation of repair pathway choice at two-ended DNA double-strand breaks. In: *Mutat Res Fund Mol Mech Mutagen* 803–805, p. 51–55.

Shmakova, A.; Batie, M.; Druker, J.; Rocha, S. (2014): Chromatin and oxygen sensing in the context of JmjC histone demethylases. In: *Biochem J*. 462, p. 385–395.

Shogren-Knaak, M.; Ishii, H.; Sun, J.M.; Pazin, M.J.; Davie, J.R.; Peterson, C.L. (2006): Histone H4-K16 acetylation controls chromatin structure and protein interactions. In: *Science* 311, p. 844–847. doi: 10.1126/science.1124000.

Simandlova, J.; Zagelbaum, J.; Payne, M.J.; Chu, W.K.; Shevelev, I.; Hanada, K. (2013): FBH1 helicase disrupts RAD51 filaments in vitro and modulates homologous recombination in mammalian cells. In: *J. Biol. Chem.* 288, p. 34168–34180. doi: 10.1074/jbc.M113.484493.

Smits, K.M.; Melotte, V.; Niessen, H.E.; Dubois, L.; Oberije, C.; Troost, E.G. et al. (2014): Epigenetics in radiotherapy: where are we heading? In: *Radiother Oncol.* 111, p. 168–177.

Soares, L.M.; He, P.C.; Chun, Y.; Suh, H.; Kim, T.; Buratowski, S. (2017): Determinants of histone H3K4 methylation patterns. In: *Mol Cell* 68(4), p. 773-785. doi: 10.1016/j.molcel.2017.10.013.

Solovei, I.; Thanisch, K.; Feodorova, Y. (2016): How to rule the nucleus: divide et impera. In: *Curr. Opin. Cell Biol* 40, p. 47–59.

Soria, G.; Polo, Sophie E.; Almouzni, G. (2012): Prime, Repair, Restore: The Active Role of Chromatin in the DNA Damage Response. In: *Molecular Cell* 46 (6), p. 722–734. DOI: 10.1016/j.molcel.2012.06.002.

Srivastava, N.; Raman, M.J. (2007): Homologous recombination-mediated double-strand break repair in mouse testicular extracts and comparison with different germ cell stages. In: *Cell Biochem Funct.* 25, p. 75–86. doi: 10.1002/cbf.1375.

Strahl, B.D.; Allis, D. (2000): The language of covalent histone modifications. In: *Nature* 403, p. 41–45.

Sun, Y.; Jiang, X.; Xu, Y.; Ayrapetov, M.K.; Moreau, L.A.; Whetstine, J.R. et al. (2009): Histone H3 methylation links DNA damage detection to activation of the tumour suppressor Tip60. In: *Nat Cell Biol* 11 (11), p. 1376–1382. DOI: 10.1038/ncb1982.

Swygert, S.G. & Peterson, C.L. (2014): Chromatin dynamics: interplay between remodeling enzymes and histone modifications. In: *Biochim. Biophys. Acta* 1839, p. 728–736.

Takada, Y.; Ye, X. and Simon, S. (2007): The integrins. In: *Genome Biol.* 8, p. 215.

Takata, H.; Hanafusa, T.; Mori, T.; Shimura, M.; Iida, Y.; Ishikawa, K. et al. (2013): Chromatin compaction protects genomic DNA from radiation damage. In: *PLoS One* 8, e75622. doi: 10.1371/journal.pone.0075622.

Tang, J.; Cho, N.W.; Cui, G.; Manion, E.M.; Shanbhag, N.M.; Botuyan, M.V. et al. (2013): Acetylation limits 53BP1 association with damaged chromatin to promote homologous recombination. In: *Nature structural & molecular biology* 20 (3), p. 317–325. DOI: 10.1038/nsmb.2499.

Taquet, N.; Dumont, S.; Vonesch, J.L.; Hentsch, D.; Reimund, J.M.; Muller, C.D. (2009): Differential between protein and mRNA expression of CCR7 and SSTR5 receptors in Crohn's disease patients. In: *Mediators Inflamm.* 2009, p. 285812. doi: 10.1155/2009/285812.

Taylor-Papadimitriou, J.; Burchell, J. (2017): Jarid1/KDM5 demethylases as cancer targets? In: *Expert Opin Ther Targets* 21 (1), p. 5-7. DOI:10.1080/14728222.2017.1263616.

Telford, D.J.; Stewart, B.W. (1989): Micrococcal nuclease: Its specificity and use for chromatin analysis. In: *Int. J. Biochem* 21, p. 127–138.

Teng, Y.; Lee, C.; Li, Y.; Chen, Y.; Hsiao, P.; Chan, M. et al. (2013): Histone Demethylase RBP2 Promotes Lung Tumorigenesis and Cancer Metastasis. In: *Cancer Research* 73 (15), p. 4711–4721. DOI: 10.1158/0008-5472.CAN-12-3165.

Tepel, M.; Roerig, P.; Wolter, M.; Gutmann, D.H.; Perry, A.; Reifenberger, G. et al. (2008): Frequent promoter hypermethylation and transcriptional downregulation of the NDRG2 gene at 14q11.2 in primary glioblastoma. In: *Int J Cancer* 123, p. 2080–2086.

Thurn, K.T.; Thomas, S.; Raha, P.; Qureshi, I; Munster, P.N. (2013): Histone deacetylase regulation of ATM-mediated DNA damage signaling. *Mol. Cancer Ther.* 12, p. 2078–2087.

Toyota, M.; Ahuja, N.; Ohe-Toyota, M.; Herman, J.G.; Baylin, S.B.; Issa, J.P. (1999): CpG island methylator phenotype in colorectal cancer. In: *Proc Natl Acad Sci U S A* 96, p. 8681–8686. doi: 10.1073/pnas.96.15.8681.

Trojer, P.; Reinberg, D. (2007): Facultative Heterochromatin: Is There a Distinctive Molecular Signature? In: *Molecular Cell* 28 (1), p. 1–13. DOI: 10.1016/j.molcel.2007.09.011.

Tse, C.; Sera, T.; Wolffe, A.P.; Hansen, J.C. (1998): Disruption of higher-order folding by core histone acetylation dramatically enhances transcription of nucleosomal arrays by RNA polymerase III. In: *Mol. Cell. Biol.* 18, p. 4629–4638.

Tsukada, Y.; Fang, J.; Erdjument-Bromage, H.; Warren, M.E.; Borchers, C.H.; Tempst, P.; Zhang, Y. (2006): Histone demethylation by a family of JmjC domain-containing proteins. In: *Nature* 439 (7078), p. 811–816. DOI: 10.1038/nature04433.

Turcan, S.; Rohle, D.; Goenka, A.; Walsh, L.A.; Fang, F.; Yilmaz, E. et al (2012): IDH1 mutation is sufficient to establish the glioma hypermethylator phenotype. In: Nature 483, p. 479–483.

Tusher, V.G.; Tibshirani, R.; Chu, G. 2001: Significance analysis of microarrays applied to the ionizing radiation response. In: *Proc. Natl. Acad. Sci.* 98, p. 5116–5121.

van Attikum, H.; Fritsch, O.; Gasser, S.M. (2007): Distinct roles for SWR1 and INO80 chromatin remodeling complexes at chromosomal double-strand breaks. In: *The EMBO journal* 26 (18), p. 4113–25.

van Gent, D.C.; Hoeijmakers, J.H.; Kanaar, R. (2001): Chromosomal stability and the DNA double-stranded break connection. In: *Nat Rev Genet* 2, p. 196–206.

van Meter, M.; Simon, M.; Tombline, G.; May, A.; Morello, T.D.; Hubbard, B.P. et al. (2016): JNK Phosphorylates SIRT6 to Stimulate DNA Double-Strand Break Repair in Response to Oxidative Stress byRecruiting PARP1 to DNA Breaks. *Cell Rep* 16, p. 2641–2650.

Vashishtha, M.; Ng, C.W.; Yildirim, F.; Gipson, T.A.; Kratter, I.H.; Bodai, L. et al. (2013): Targeting H3K4 trimethylation in Huntington disease. In: *Proc. Natl. Acad. Sci. U.S.A.* 110 (32), p. E3027-36. DOI: 10.1073/pnas.1311323110.

Vinogradova, M.; Gehling, V.S.; Gustafson, A.; Arora, S.; Tindell, C.A.; Wilson, C. et al. 2016: An inhibitor of KDM5 demethylases reduces survival of drug-tolerant cancer cells. In: *Nat Chem Biol.* 12 (7), p. 531–538. doi: 10.1038/nchembio.2085.

Vogel, C.; de Sousa Abreu, R.; Ko, D.; Le, S.Y.; Shapiro, B.A.; Burns, S.C. et al. (2010): Sequence signatures and mRNA concentration can explain two-thirds of protein abundance variation in a human cell line. In: *Molecular systems biology* 6 (1), p. 400.

Wang, L.; Mao, Y.; Du, G.; He, C.; Han, S. (2015): Overexpression of JARID1B is associated with poor prognosis and chemotherapy resistance in epithelial ovarian cancer. In: *Tumor Biol.* 36 (4), p. 2465–2472. DOI: 10.1007/s13277-014-2859-z.

Wang, Q.; Wei, J.; Su, P.; Gao, P. (2015): Histone demethylase JARID1C promotes breast cancer metastasis cells via down regulating BRMS1 expression. In: *Biochemical and biophysical research communications* 464 (2), p. 659–666. DOI: 10.1016/j.bbrc.2015.07.049.

Wang, S.; Wang, Y.; Wu, H.; Hu, L. (2013): RBP2 induces epithelial-mesenchymal transition in non-small cell lung cancer. In: *PLoS One* 8, e84735.

Wang, X.W.; Ciccarino, P.; Rossetto, M.; Boisselier, B.; Marie, Y.; Desestret, V. et al. (2014): IDH mutations: genotype-phenotype correlation and prognostic impact. In: *BioMed research international,* 540236.

Westaway, S.M.; Preston, A.G.; Barker, M.D.; Brown, F.; Brown, J.A.; Campbell, M. et al. (2016): Cell Penetrant inhibitors of the KDM4 and KDM5 families of histone lysine demethylases. 2. Pyrido[3,4-d]pyrimidin-4(3H)-one derivatives. In: *J. Med. Chem.* 59, p. 1370–1387.

Wilhelm, M.J.; Schlegl, H.; Hahne, A.; Moghaddas Gholami, M.; Lieberenz, M.M.; Savitski, E. et al. (2014): Mass-spectrometry-based draft of the human proteome. In: *Nature* 509 (7502), p. 582-7.

Woodcock, C.L.; Ghosh, R.P. (2010): Chromatin Higher-order Structure and Dynamics. In: *Cold Spring Harbor Perspectives in Biology* 2 (5), p. a000596. DOI: 10.1101/cshperspect.a000596.

Xu, W.; Yang, H.; Liu, Y.; Yang, Y.; Wang, P.; Kim, S. et al. (2011): Oncometabolite 2-Hydroxyglutarate Is a Competitive Inhibitor of α-Ketoglutarate-Dependent Dioxygenases. In: *Cancer Cell* 19 (1), p. 17–30. DOI: 10.1016/j.ccr.2010.12.014.

Yamamoto, S.; Wu, Z.; Russnes, H.G.; Takagi, S.; Peluffo, G.; Vaske, C. et al. (2014): JARID1B Is a Luminal Lineage-Driving Oncogene in Breast Cancer. In: *Cancer Cell* 25 (6), p. 762–777. DOI: 10.1016/j.ccr.2014.04.024.

Yan, H.; Parsons, D.W.; Jin, G.; McLendon, R.; Rasheed, B.A.; Yuan, W. et al. (2009): IDH1 and IDH2 mutations in gliomas. In: *N Engl J Med.* 360 (8), p. 765–73. doi: 10.1056/NEJMoa0808710.

Yang, H.; Ye, D.; Guan, K.L.; Xiong, Y. (2012): IDH1 and IDH2 mutations in tumorigenesis: mechanistic insights and clinical perspectives. In: *Clin Cancer Res.*18, p. 5562–5571.

Yen, C.; Huang, H.; Shu, C.; Hou, M.; Yuan, S.; Wang, H. et al. (2016): DNA methylation, histone acetylation and methylation of epigenetic modifications as a therapeutic approach for cancers. In: *Cancer Letters* 373, p. 185–192.

Young, L.C.; McDonald, D.W.; Hendzel, M.J. (2013): Kdm4b Histone Demethylase Is a DNA Damage Response Protein and Confers a Survival Advantage following Irradiation. In: *Journal of Biological Chemistry* 288 (29), p. 21376–21388. DOI: 10.1074/jbc.M113.491514.

Zahnow, C.A.; Topper, M.; Stone, M.; Murray-Stewart, T.; Li, H.; Baylin, S.B. et al. (2016): Inhibitors of DNA Methylation, Hostone Deacetylation, and Histone Demethylation: A Perfect Combination for Cancer Therapy. In: *Adv Cancer Res.* 130, p. 55-111.

Zeng, J.; Ge, Z.; Wang, L.; Li, Q.; Wang, N.; Björkholm, M. et al. (2010): The Histone Demethylase RBP2 Is Overexpressed in Gastric Cancer and Its Inhibition Triggers Senescence of Cancer Cells. In: *Gastroenterology* 138, p. 981-92.

Zhang, P.; Torres, K.; Liu, X.; Liu, C.G.; Pollock, R.E. (2016): An Overview of Chromatin-Regulating Proteins in Cells. In: *Curr Protein Pept Sci* 17(5), p. 401-10.

Zhang, R.; Erler, J.; Langowski, J. (2016): Histone Acetylation Regulates Chromatin Accessibility: Role of H4K16 in Inter-nucleosome Interaction. In: *Biophys J.* 112 (3), p. 450-459. doi: 10.1016/j.bpj.2016.11.015.

Zhang, T.; Cooper, S.; Brockdorff, N. (2015): The interplay of histone modifications—Writers that read. In: *EMBO Rep* 16, p. 1467–1481. doi: 10.15252/embr.201540945.

Zhang, Y.; Carr, T.; Dimtchev, A.; Zaer, N.; Dritschilo, A.; Jung, M. (2007): Attenuated DNA damage repair by trichostatin A through BRCA1 suppression. In: *Radiat. Res.* 168, p. 115–124.

7 Abbreviations

2-HG	2-hydroxyglutarate
3D	three-dimensional
53BP1	p53-binding protein 1
A488	Alexa fluorochrome 488
α-KG	α-ketoglutarate
ATM	Ataxia telangiectasia mutated
ATP	Adenosine triphosphate
ATR	Ataxia telangiectasia and Rad3 related
bp	Base pairs
BRCA1	breast cancer type 1 susceptibility protein
BSA	bovine serum albumine
Cdk1	Cyclin-dependent kinase 1
Cy3	Cyanin 3
DAPI	4’,6-diamidino-2-phenylindole
DDR	DNA damage response
DEPC	diethylpyrocarbonate
DMEM	Dulbecco`s modified eagle medium
DNA	Deoxyribo-nucleic acid
DSB	Double-strand break
ECL	Electrochemiluminescence
ECM	Extracellular matrix organization
EDTA	Ethylenediaminetetraacetic acid
EtOH	Ethanol
FBS	Fetal bovine serum
γH2AX	phosphorylated H2AX
Gy	Gray
h	Hour
HAT	Histone acetyltransferase
HDAC	Histone deacetylase
HP1	Heterochromatin protein 1
HR	Homologous recombination
HRP	Horseraddish peroxidase
ICA	Intensity correlation analysis
IDH1/2	isocitrate dehydrogenase 1/2

IF	immunofluorescence
IRIF	Ionizing radiation-induced foci
Jarid1A	Jumonji-ARID protein 1a (synonyms: RBP2, KDM5A)
Jarid1B	Jumonji-ARID protein 1b (synonyms: PLU1, KDM5B)
Jarid1C	Jumonji-ARID protein 1c (synonyms: SMCX, KDM5C)
Jarid1D	Jumonji-ARID protein 1d (synonyms: SMCY, KDM5D)
JmjC/JmjN	Jumonji C/N domain-containing
kDa	Kilodalton
KDM	Lysine (K) demethylase
mA	Milliampere
Mb	Megabase
MDC1	Mediator of DNA damage checkpoint 1
MeV	Megaelectronvolts
min	Minute
MRN	Mre11-Rad50-Nbs1 complex
mRNA	messenger RNA
µm	Micrometer
NADP	Nicotinamide adenine dinucleotide phosphate
NHEJ	Non-homologous end joining
nm	Nanometer
NuRD	Nucleosome remodeling complex
p.A.	Pro analysi
PARP1	Poly [ADP-ribose] polymerase 1
pATM	phosphorylated ATM
PBS	Phosphate buffered saline
PCA	Peptide competition assay
pChk2	phosphorylated Chk2
PCR	Polymerase chain reaction
PDM	Product of the differences from the mean
PFA	Paraformaldehyde
PHD	Plant homeo domain
PTM	post-translational modifications
qRT-PCR	Quantitative Real-Time-PCR
RBP2	Retinoblastoma-binding protein 2
RNA	Ribonucleic acid

rpm	Rounds per minute
RPMI	Roswell park memorial institute cell culture medium
RT	Room temperature
SD	standard deviation
shRNA	Short/small hairpin RNA
siRNA	Small interfering RNA
SNAKE	Superconducting Nanoscope for Applied Nuclear Experiments
TA	Tris-Acetate
TAD	Topologically associating domain
TGS	Tris-Glycine-SDS
V	Volt

8 List of figures and tables

8.1 Figures

8.2 Tables

9 Appendix

9.1 Appendix A

Sequences of used plasmids

LOCUS pEJ 4845 bp DNA linear

1 tagttattaa tagtaatcaa ttacggggtc attagttcat agcccatata tggagttccg
61 cgttacataa cttacggtaa atggcccgcc tggctgaccg cccaacgacc cccgcccatt
121 gacgtcaata atgacgtatg ttcccatagt aacgccaata gggactttcc attgacgtca
181 atgggtggag tatttacggt aaactgccca cttggcagta catcaagtgt atcatatgcc
241 aagtacgccc cctattgacg tcaatgacgg taaatggccc gcctggcatt atgcccagta
301 catgacctta tgggactttc ctacttggca gtacatctac gtattagtca tcgctattac
361 catggtgatg cggttttggc agtacatcaa tgggcgtgga tagcggtttg actcacgggg
421 atttccaagt ctccacccca ttgacgtcaa tgggagtttg ttttggcacc aaaatcaacg
481 ggactttcca aaatgtcgta acaactccgc cccattgacg caaatgggcg gtaggcgtgt
541 acggtgggag gtctatataa gcagagctgg tttagtgaac cgtcagatcc gctagcgcta
601 ccggactcag atctcgagtc caccgagaca tctacttgat caatcgaaca ctgcggaatt
661 ctagggataa cagggtaatt aagcttctgc agaccatgga gattaccctg ttatccctac
721 cccggggata ctgacggtac ctcaataatc cgatcgaagt ctactgatcg aggatccacc
781 ggtcgccacc atggtgagca agggcgagga gctgttcacc ggggtggtgc ccatcctggt
841 cgagctggac ggcgacgtaa acggccacaa gttcagcgtg tccggcgagg gcgagggcga
901 tgccacctac ggcaagctga ccctgaagtt catctgcacc accggcaagc tgcccgtgcc
961 ctggcccacc ctcgtgacca ccctgaccta cggcgtgcag tgcttcagcc gctaccccga
1021 ccacatgaag cagcacgact tcttcaagtc cgccatgccc gaaggctacg tccaggagcg
1081 caccatcttc ttcaaggacg acggcaacta caagacccgc gccgaggtga agttcgaggg
1141 cgacaccctg gtgaaccgca tcgagctgaa gggcatcgac ttcaaggagg acggcaacat
1201 cctggggcac aagctggagt acaactacaa cagccacaac gtctatatca tggccgacaa
1261 gcagaagaac ggcatcaagg tgaacttcaa gatccgccac aacatcgagg acggcagcgt
1321 gcagctcgcc gaccactacc agcagaacac ccccatcggc gacggccccg tgctgctgcc
1381 cgacaaccac tacctgagca cccagtccgc cctgagcaaa gaccccaacg agaagcgcga
1441 tcacatggtc ctgctggagt tcgtgaccgc cgccgggatc actctcggca tggacgagct
1501 gtacaagtaa agcggccgcg actctagatc ataatcagcc ataccacatt tgtagaggtt
1561 ttacttgctt taaaaaacct cccacacctc cccctgaacc tgaaacataa aatgaatgca
1621 attgttgttg ttaacttgtt tattgcagct tataatggtt acaaataaag caatagcatc
1681 acaaatttca caaataaagc attttttca ctgcattcta gttgtggttt gtccaaactc
1741 atcaatgtat cttaaggcgt aaattgtaag cgttaatatt ttgttaaaat tcgcgttaaa
1801 tttttgttaa atcagctcat tttttaacca ataggccgaa atcggcaaaa tcccttataa
1861 atcaaaagaa tagaccgaga tagggttgag tgttgttcca gtttggaaca agagtccact
1921 attaaagaac gtggactcca acgtcaaagg gcgaaaaacc gtctatcagg gcgatggccc
1981 actacgtgaa ccatcaccct aatcaagttt tttggggtcg aggtgccgta aagcactaaa
2041 tcggaaccct aaagggagcc cccgatttag agcttgacgg ggaaagccgg cgaacgtggc
2101 gagaaaggaa gggaagaaag cgaaaggagc gggcgctagg gcgctggcaa gtgtagcggt
2161 cacgctgcgc gtaaccacca cacccgccgc gcttaatgcg ccgctacagg gcgcgtcagg
2221 tggcactttt cggggaaatg tgcgcggaac ccctatttgt ttatttttct aaatacattc
2281 aaatatgtat ccgctcatga gacaataacc ctgataaatg cttcaataat attgaaaaag
2341 gaagagtcct gaggcggaaa gaaccagctg tggaatgtgt gtcagttagg gtgtggaaag
2401 tccccaggct ccccagcagg cagaagtatg caaagcatgc atctcaatta gtcagcaacc
2461 aggtgtggaa agtccccagg ctccccagca ggcagaagta tgcaaagcat gcatctcaat
2521 tagtcagcaa ccatagtccc gcccctaact ccgcccatcc cgcccctaac tccgcccagt
2581 tccgcccatt ctccgcccca tggctgacta atttttttta tttatgcaga ggccgaggcc
2641 gcctcggcct ctgagctatt ccagaagtag tgaggaggct tttttggagg cctaggcttt
2701 tgcaaagatc gatcaagaga caggatgagg atcgtttcgc atgattgaac aagatggatt
2761 gcacgcaggt tctccggccg cttgggtgga gaggctattc ggctatgact gggcacaaca
2821 gacaatcggc tgctctgatg ccgccgtgtt ccggctgtca gcgcaggggc gcccggttct
2881 ttttgtcaag accgacctgt ccggtgccct gaatgaactg caagacgagg cagcgcggct
2941 atcgtggctg gccacgacgg gcgttccttg cgcagctgtg ctcgacgttg tcactgaagc
3001 gggaagggac tggctgctat tgggcgaagt gccggggcag gatctcctgt catctcacct

3061 tgctcctgcc gagaaagtat ccatcatggc tgatgcaatg cggcggctgc atacgcttga
3121 tccggctacc tgcccattcg accaccaagc gaaacatcgc atcgagcgag cacgtactcg
3181 gatggaagcc ggtcttgtcg atcaggatga tctggacgaa gagcatcagg ggctcgcgcc
3241 agccgaactg ttcgccaggc tcaaggcgag catgcccgac ggcgaggatc tcgtcgtgac
3301 ccatggcgat gcctgcttgc cgaatatcat ggtggaaaat ggccgctttt ctggattcat
3361 cgactgtggc cggctgggtg tggcggaccg ctatcaggac atagcgttgg ctacccgtga
3421 tattgctgaa gagcttggcg gcgaatgggc tgaccgcttc ctcgtgcttt acggtatcgc
3481 cgctcccgat tcgcagcgca tcgccttcta tcgccttctt gacgagttct tctgagcggg
3541 actctggggt tcgaaatgac cgaccaagcg acgcccaacc tgccatcacg agatttcgat
3601 tccaccgccg ccttctatga aaggttgggc ttcggaatcg ttttccggga cgccggctgg
3661 atgatcctcc agcgcgggga tctcatgctg gagttcttcg cccaccctag ggggaggcta
3721 actgaaacac ggaaggagac aataccggaa ggaacccgcg ctatgacggc aataaaaaga
3781 cagaataaaa cgcacggtgt tgggtcgttt gttcataaac gcggggttcg gtcccagggc
3841 tggcactctg tcgatacccc accgagaccc cattggggcc aatacgcccg cgtttcttcc
3901 ttttccccac cccacccccc aagttcgggt gaaggcccag ggctcgcagc caacgtcggg
3961 gcggcaggcc ctgccatagc ctcaggttac tcatatatac tttagattga tttaaaactt
4021 catttttaat ttaaaaggat ctaggtgaag atccttttg ataatctcat gaccaaaatc
4081 ccttaacgtg agttttcgtt ccactgagcg tcagaccccg tagaaaagat caaaggatct
4141 tcttgagatc ctttttttct gcgcgtaatc tgctgcttgc aaacaaaaaa accaccgcta
4201 ccagcggtgg tttgtttgcc ggatcaagag ctaccaactc tttttccgaa ggtaactggc
4261 ttcagcagag cgcagatacc aaatactgtc cttctagtgt agccgtagtt aggccaccac
4321 ttcaagaact ctgtagcacc gcctacatac ctcgctctgc taatcctgtt accagtggct
4381 gctgccagtg gcgataagtc gtgtcttacc gggttggact caagacgata gttaccggat
4441 aaggcgcagc ggtcgggctg aacgggggggt tcgtgcacac agcccagctt ggagcgaacg
4501 acctacaccg aactgagata cctacagcgt gagctatgag aaagcgccac gcttcccgaa
4561 gggagaaagg cggacaggta tccggtaagc ggcagggtcg gaacaggaga gcgcacgagg
4621 gagcttccag ggggaaacgc ctggtatctt tatagtcctg tcgggtttcg ccacctctga
4681 cttgagcgtc gatttttgtg atgctcgtca ggggggcgga gcctatggaa aaacgccagc
4741 aacgcggcct ttttacggtt cctggccttt tgctggcctt ttgctcacat gttctttcct
4801 gcgttatccc ctgattctgt ggataaccgt attaccgcca tgcat
//

LOCUS pMCC-EGFP-P_(572) 6314 bp DNA linear

1 tcgataatga aagaccccac ctgtaggttt ggcaagctag cttaagtaac gccattttgc
61 aaggcatggg aaaaatacat aactgagaat agagaagttc agatcaaggt caggaacaga
121 gaaacaggag aatatgggcc aaacaggata tctgtggtaa gcagttcctg ccccgctcag
181 ggccaagaac agttggaaca ggagaattgg gccaaacagg atatctgtgg taagcagttc
241 ctgccccgct cagggccaag aacagatggt ccccagatgc ggtcccgccc tcagcagttt
301 ctagacataa cttacggtaa atggcccgcc tggctgaccg cccaacgacc cccgcccatt
361 gacgtcaata atgacgtatg ttcccatagt aacgccaata gggactttcc attgacgtca
421 atgggtggag tatttacggt aaactgccca cttggcagta catcaagtgt atcatatgcc
481 aagtacgccc cctattgacg tcaatgacgg taaatggccc gcctggcatt atgcccagta
541 catgacctta tgggactttc ctacttggca gtacatctac gtattagtca tcgctattac
601 catggtgatg cggttttggc agtacatcaa tgggcgtgga tagcggtttg actcacgggg
661 atttccaagt ctccacccca ttgacgtcaa tgggagtttg ttttggcacc aaaatcaacg
721 ggactttcca aaatgtcgta acaactccgc cccattgacg caaatgggcg gtaggcgtgt
781 acggtgggag gtctatataa gcagagctcg tttagtgaac cgtcagatcg cctggagacg
841 ccatccacgc tgttttgacc tccatagaag acaccgggac cgatccagcc tcgaggaact
901 ggaaaaccag aaagttaact ggtaagttta gtcttttgt cttttatttc aggtcccgga
961 tcgaattgcg gccgcgaatt aagcttgcac gcgtcctaag gactagttcg cgagggccca
1021 tggtgagcaa gggcgaggag ctgttcaccg gggtggtgcc catcctggtc gagctggacg
1081 gcgacgtaaa cggccacaag ttcagcgtgt ccggcgaggg cgagggcgat gccacctacg
1141 gcaagctgac cctgaagttc atctgcacca ccggcaagct gcccgtgccc tggcccaccc
1201 tcgtgaccac cctgacctac ggcgtgcagt gcttcagccg ctaccccgac cacatgaagc
1261 agcacgactt cttcaagtcc gccatgcccg aaggctacgt ccaggagcgc accatcttct
1321 tcaaggacga cggcaactac aagacccgcg ccgaggtgaa gttcgagggc gacaccctgg
1381 tgaaccgcat cgagctgaag ggcatcgact tcaaggagga cggcaacatc ctggggcaca
1441 agctggagta caactacaac agccacaacg tctatatcat ggccgacaag cagaagaacg
1501 gcatcaaggt gaacttcaag atccgccaca acatcgagga cggcagcgtg cagctcgccg

1561 accactacca gcagaacacc cccatcggcg acggccccgt gctgctgccc gacaaccact
1621 acctgagcac ccagtccgcc ctgagcaaag accccaacga gaagcgcgat cacatggtcc
1681 tgctggagtt cgtgaccgcc gccgggatca ctctcggcat ggacgagctg tacaagtaag
1741 aattcagctt ttaaaacagc tctggggttg tacccacccc agaggcccac gtggcggcta
1801 gtactccggt attgcggtac ccttgtacgc ctgttttata ctcccttccc gtaacttaga
1861 cgcacaaaac caagttcaat agaaggggt acaaaccagt accaccacga acaagcactt
1921 ctgtttcccc ggtgatgtcg tatagactgc ttgcgtggtt gaaagcgacg gatccgttat
1981 ccgcttatgt acttcgagaa gcccagtacc acctcggaat cttcgatgcg ttgcgctcag
2041 cactcaaccc cagagtgtag cttaggctga tgagtctgga catccctcac cggtgacggt
2101 ggtccaggct gcgttggcgg cctacctatg gctaacgcca tgggacgcta gttgtgaaca
2161 aggtgtgaag agcctattga gctacataag aatcctccgg cccctgaatg cggctaatcc
2221 caacctcgga gcaggtggtc acaaaccagt gattggcctg tcgtaacgcg caagtccgtg
2281 gcggaaccga ctactttggg tgtccgtgtt tccttttatt ttattgtggc tgcttatggt
2341 gacaatcaca gattgttatc ataaagcgaa ttggattgcg gccggccgcc acgaccggtg
2401 ccgccaccat cccctgaccc acgcccctga cccctcacaa ggagacgacc ttccatgacc
2461 gagtacaagc ccacggtgcg cctcgccacc cgcgacgacg tcccccgggc cgtacgcacc
2521 ctcgccgccg cgttcgccga ctaccccgcc acgcgccaca ccgtcgaccc ggaccgccac
2581 atcgagcggg tcaccgagct gcaagaactc ttcctcacgc gcgtcgggct cgacatcggc
2641 aaggtgtggg tcgcggacga cggcgccgcg gtggcggtct ggaccacgcc ggagagcgtc
2701 gaagcggggg cggtgttcgc cgagatcggc ccgcgcatgg ccgagttgag cggttcccgg
2761 ctggccgcgc agcaacagat ggaaggcctc ctggcgccgc accggcccaa ggagcccgcg
2821 tggttcctgg ccaccgtcgg cgtctcgccc gaccaccagg gcaagggtct gggcagcgcc
2881 gtcgtgctcc ccggagtgga ggcggccgag cgcgccgggg tgcccgcctt cctggagacc
2941 tccgcgcccc gcaacctccc cttctacgag cggctcggct tcaccgtcac cgccgacgtc
3001 gagtgcccga aggaccgcgc gacctggtgc atgacccgca agcccggtgc ctgacgcccg
3061 ccccacgacc cgcagcgccc gaccgaaagg agcgcacgac cccatgagct tcgatccaga
3121 catgataaga tacattgatg agtttggaca aaccacaact agaatgcagt gaaaaaaatg
3181 ctttatttgt gaaatttgtg atgctattgc tttatttgta accattataa gctgcaataa
3241 acaagttaac aacaacaatt gcattcattt tatgtttcag gttcaggggg aggtgtggga
3301 ggtttttaa agcaagtaaa acctctacaa atgtggtatg gctgattatg atcctgcctc
3361 gcgcgtttcg gtgatgacgg tgaaaacctc tgacacatgc agctcccgga gacggtcaca
3421 gcttgtctgt aagcggatgc cgggagcaga caagcccgtc agggcgcgtc agcgggtgtt
3481 ggcgggtgtc ggggcgcagc catgacccag tcacgtagcg atagcggagt gtagatcccc
3541 aacttgtcaa cctcatttca aaatgtatat agaaagccca aagacaataa caaaaatatt
3601 cttgtagaac aaaatgggaa agaatgttcc actaaatatc aagatttaga gcaaagcatg
3661 agatgtgtgg ggatagacag tgaggctgat aaaatagagt agagctcaga aacagaccca
3721 ttgatatatg taagtgacct atgaaaaaaa tatggcattt tacaatggga aaatgatgat
3781 ctttttcttt tttagaaaaa cagggaaata tatttatatg taaaaaataa aagggaaccc
3841 atatgtcata ccatacacac aaaaaaattc cagtgaatta taagtctaaa tggagaaggc
3901 aaaactttaa atcttttaga aaataatata gaagcatgcc atcatgactt cagtgtagag
3961 aaaaatttct tatgactcaa agtcctaacc acaaagaaaa gattgttaat tagattgcat
4021 gaatattaag acttattttt aaaattaaaa aaccattaag aaaagtcagg ccatagaatg
4081 acagaaaata tttgcaacac cccagtaaag agaattgtaa tatgcagatt ataaaaagaa
4141 gtcttacaaa tcagtaaaaa ataaaactag acaaaaattt gaacagatga aagagaaact
4201 ctaaataatc attacacatg agaaactcaa tctcagaaat cagagaacta tcattgcata
4261 tacactaaat tagagaaata ttaaaaggct aagtaacatc tgtggcaata ttgatggtat
4321 ataaccttga tatgatgtga tgagaacagt gacctgcagg catgcaagct agcttactgg
4381 cttaactatg cggcatcaga gcagattgta ctgagagtgc accatatgtc gggccgcgtt
4441 gctggcgttt ttccataggc tccgcccccc tgacgagcat cacaaaaatc gacgctcaag
4501 tcagaggtgg cgaaacccga caggactata aagataccag gcgtttcccc ctggaagctc
4561 cctcgtgcgc tctcctgttc cgaccctgcc gcttaccgga tacctgtccg cctttctccc
4621 ttcgggaagc gtggcgcttt ctcatagctc acgctgtagg tatctcagtt cggtgtaggt
4681 cgttcgctcc aagctgggct gtgtgcacga acccccgtt cagcccgacc gctgcgcctt
4741 atccggtaac tatcgtcttg agtccaaccc ggtaagacac gacttatcgc cactggcagc
4801 agccactggt aacaggatta gcagagcgag gtatgtaggc ggtgctacag agttcttgaa
4861 gtggtggcct aactacggct acactagaag gacagtattt ggtatctgcg ctctgctgaa
4921 gccagttacc ttcggaaaaa gagttggtag ctcttgatcc ggcaaacaaa ccaccgctgg
4981 tagcggtggt ttttttgttt gcaagcagca gattacgcgc agaaaaaaag gatctcaaga
5041 agatcctttg atcttttcta cggggtctga cgctcagtgg aacgaaaact cacgttaagg
5101 gattttggtc atgagattat caaaaaggat cttcacctag atccttttaa attaaaaatg
5161 aagttttaaa tcaatctaaa gtatatatga gtaaacttgg tctgacagtt accaatgctt

5221 aatcagtgag gcacctatct cagcgatctg tctatttcgt tcatccatag ttgcctgact
5281 ccccgtcgtg tagataacta cgatacggga gggcttacca tctggcccca gtgctgcaat
5341 gataccgcga gacccacgct caccggctcc agatttatca gcaataaacc agccagccgg
5401 aagggccgag cgcagaagtg gtcctgcaac tttatccgcc tccatccagt ctattaattg
5461 ttgccgggaa gctagagtaa gtagttcgcc agttaatagt gcgcaacgtt gttgccattg
5521 ctacaggcat cgtggtgtca cgctcgtcgt ttggtatggc ttcattcagc tccggttccc
5581 aacgatcaag gcgagttaca tgatccccca tgttgtgcaa aaaagcggtt agctccttcg
5641 gtcctccgat cgttgtcaga agtaagttgg ccgcagtgtt atcactcatg gttatggcag
5701 cactgcataa ttctcttact gtcatgccat ccgtaagatg cttttctgtg actggtgagt
5761 actcaaccaa gtcattctga gaatagtgta tgcggcgacc gagttgctct tgcccggcgt
5821 caacacggga taataccgcg ccacatagca gaactttaaa agtgctcatc attggaaaac
5881 gttcttcggg gcgaaaactc tcaaggatct taccgctgtt gagatccagt tcgatgtaac
5941 ccactcgtgc acccaactga tcttcagcat cttttacttt caccagcgtt tctgggtgag
6001 caaaaacagg aaggcaaaat gccgcaaaaa agggaataag ggcgacacgg aaatgttgaa
6061 tactcatact cttccttttt caatattatt gaagcattta tcagggttat tgtctcatga
6121 gcggatacat atttgaatgt atttagaaaa ataaacaaat aggggttccg cgcacatttc
6181 cccgaaaagt gccacctgac gtctaagaaa ccattattat catgacatta acctataaaa
6241 ataggcgtat cacgaggccc tttcgtcttc aagaattggt cgatcgacca attctcatgt
6301 ttgacagctt atca
//

LOCUS pCMV-I-SceI 5492 bp DNA linear

1 cccattcgcc attcaggctg cgcaactgtt gggaagggcg atcggtgcgg gcctcttcgc
61 tattacgcca gctggcgaaa gggggatgtg ctgcaaggcg attaagttgg gtaacgccag
121 ggttttccca gtcacgacgt tgtaaaacga cggccagtgc caagctgatc tatacattga
181 atcaatattg gcaattagcc atattagtca ttggttatat agcataaatc aatattggct
241 attggccatt gcatacgttg tatctatatc ataatatgta catttatatt ggctcatgtc
301 caatatgacc gccatgttga cattgattat tgactagtta ttaatagtaa tcaattacgg
361 ggtcattagt tcatagccca tatatggagt tccgcgttac ataacttacg gtaaatggcc
421 cgcctggctg accgcccaac gacccccgcc cattgacgtc aataatgacg tatgttccca
481 tagtaacgcc aatagggact ttccattgac gtcaatgggt ggagtattta cggtaaactg
541 cccacttggc agtacatcaa gtgtatcata tgccaagtcc gccccctatt gacgtcaatg
601 acggtaaatg gcccgcctgg cattatgccc agtacatgac cttacgggac tttcctactt
661 ggcagtacat ctacgtatta gtcatcgcta ttaccatggt gatgcggttt tggcagtaca
721 ccaatgggcg tggatagcgg tttgactcac ggggatttcc aagtctccac cccattgacg
781 tcaatgggag tttgttttgg caccaaaatc aacgggactt tccaaaatgt cgtaataacc
841 ccgccccgtt gacgcaaatg ggcggtaggc gtgtacggtg ggaggtctat ataagcagag
901 ctcgtttagt gaaccgtcag aattcagatc tggtaccacg cgtatcgata agcttgcatg
961 cctgcaggtc gacttatttc aggaaagttt cggaggagat agtgttcggc agtttgtaca
1021 tcatctgcgg gatcaggtac ggtttgatca ggttgtagaa gatcaggtaa gacatagaat
1081 cgatgtagat gatcggtttg tttttgttga tttttacgta acagttcagt tggaatttgt
1141 tacgcagacc cttaaccagg tattctactt cttcgaaagt gaaagactgg gtgttcagta
1201 cgatcgattt gttggtagag tttttgttgt aatcccattt accaccatca tccatgaacc
1261 agtatgccag agacatcggg gtcaggtagt tttcaaccag gttgttcggg atggtttttt
1321 tgttgttaac gatgaacagg ttagccagtt tgttgaaagc ttggtgtttg aaagtctggg
1381 cgccccaggt gattaccagg ttacccaggt ggttaacacg ttctttttttg tgcggcgggg
1441 acagtaccca ctgatcgtac agcagacata cgtggtccat gtatgctttg tttttccact
1501 cgaactgcat acagtaggtt ttaccttcat cacgagaacg gatgtaagca tcacccagga
1561 tcagaccgat acctgcttcg aactgttcga tgttcagttc gatcagctgg gatttgtatt
1621 ctttcagcag tttagagttc ggaccgaggt tcattacctg gttttttttg atgtttttcc
1681 cgcatagtca ggaacatcgt atgggtacat aaatcgtggg tcttctactt ttcgtttttt
1741 ttttggtggt gctgcgtgtt gtgcgtctgc tgttgcttcg tcgtctgatg atgatcccat
1801 agtggcggcg gatccgatcc cgggtggcat ccctgtgacc cctccccagt gcctctcctg
1861 gccctggaag ttgccactcc agtgcccacc agccttgtcc taataaaatt aagttgcatc
1921 attttgtctg actaggtgtc cttctataat attatggggt ggaggggggt ggtatggagc
1981 aaggggcaag ttgggaagac aacctgtagg gcctgcgggg tctattggga accaagctgg
2041 agtgcagtgg cacaatcttg gctcactgca atctccgcct cctgggttca agcgattctc
2101 ctgcctcagc ctcccgagtt gttgggattc caggcatgca tgaccaggct cagctaattt
2161 ttgtttttt ggtagagacg gggtttcacc atattggcca ggctggtctc caactcctaa

2221 tctcaggtga tctacccacc ttggcctccc aaattgctgg gattacaggc gtgaaccact
2281 gctcccttcc ctgtccttct gattttaaaa taactatacc agcaggagga cgtccagaca
2341 cagcataggc tacctgccat ggcccaaccg gtgggacatt tgagttgctt gcttggcact
2401 gtcctctcat gcgttgggtc cactcagtag atgcctgttg aattgggtac gcggccagct
2461 tctgtggaat gtgtgtcagt tagggtgtgg aaagtcccca ggctccccag caggcagaag
2521 tatgcaaagc atgcatctca attagtcagc aaccaggtgt ggaaaagtcc ccaggctccc
2581 cagcaggcag aagtatgcaa agcatgcatc tcaattagtc agcaaccata gtcccgcccc
2641 taactccgcc catcccgccc ctaactccgc ccagttccgc ccattctccg ccccatggct
2701 gactaatttt ttttatttat gcagaggccg aggccgcctc ggcctctgag ctattccaga
2761 agtagtgagg aggcttttt ggaggcctag gcttttgcaa aaagctcctc gaggaactga
2821 aaaaccagaa agttaattcc ctatagtgag tcgtattaaa ttcgtaatca tggtcatagc
2881 tgtttcctgt gtgaaattgt tatccgctca caattccaca caacatacga gccggaagca
2941 taaagtgtaa agcctggggt gcctaatgag tgagctaact cacattaatt gcgttgcgct
3001 cactgcccgc tttccagtcg ggaaacctgt cgtgccagct gcattaatga atcggccaac
3061 gcgcggggag aggcggtttg cgtattgggc gctcttccgc ttcctcgctc actgactcgc
3121 tgcgctcggt cgttcggctg cggcgagcgg tatcagctca ctcaaaggcg gtaatacggt
3181 tatccacaga atcaggggat aacgcaggaa agaacatgtg agcaaaaggc cagcaaaagg
3241 ccaggaaccg taaaaggccg cgttgctggc gtttttccat aggctccgcc cccctgacga
3301 gcatcacaaa aatcgacgct caagtcagag gtggcgaaac ccgacaggac tataaagata
3361 ccaggcgttt ccccctggaa gctccctcgt gcgctctcct gttccgaccc tgccgcttac
3421 cggatacctg tccgcctttc tcccttcggg aagcgtggcg ctttctcaat gctcacgctg
3481 taggtatctc agttcggtgt aggtcgttcg ctccaagctg ggctgtgtgc acgaaccccc
3541 cgttcagccc gaccgctgcg ccttatccgg taactatcgt cttgagtcca acccggtaag
3601 acacgactta tcgccactgg cagcagccac tggtaacagg attagcagag cgaggtatgt
3661 aggcggtgct acagagttct tgaagtggtg gcctaactac ggctacacta gaaggacagt
3721 atttggtatc tgcgctctgc tgaagccagt taccttcgga aaaagagttg gtagctcttg
3781 atccggcaaa caaaccaccg ctggtagcgg tggttttttt gtttgcaagc agcagattac
3841 gcgcagaaaa aaaggatctc aagaagatcc tttgatcttt tctacggggt ctgacgctca
3901 gtggaacgaa aactcacgtt aagggatttt ggtcatgaga ttatcaaaaa ggatcttcac
3961 ctagatcctt ttaaattaaa aatgaagttt taaatcaatc taaagtatat atgagtaaac
4021 ttggtctgac agttaccaat gcttaatcag tgaggcacct atctcagcga tctgtctatt
4081 tcgttcatcc atagttgcct gactccccgt cgtgtagata actacgatac gggagggctt
4141 accatctggc cccagtgctg caatgatacc gcgagaccca cgctcaccgg ctccagattt
4201 atcagcaata aaccagccag ccggaagggc cgagcgcaga agtggtcctg caactttatc
4261 cgcctccatc cagtctatta attgttgccg ggaagctaga gtaagtagtt cgccagttaa
4321 tagtttgcgc aacgttgttg ccattgctac aggcatcgtg gtgtcacgct cgtcgtttgg
4381 tatggcttca ttcagctccg gttcccaacg atcaaggcga gttacatgat cccccatgtt
4441 gtgcaaaaaa gcggttagct ccttcggtcc tccgatcgtt gtcagaagta agttggccgc
4501 agtgttatca ctcatggtta tggcagcact gcataattct cttactgtca tgccatccgt
4561 aagatgcttt tctgtgactg gtgagtactc aaccaagtca ttctgagaat agtgtatgcg
4621 gcgaccgagt tgctcttgcc cggcgtcaat acgggataat accgcgccac atagcagaac
4681 tttaaaagtg ctcatcattg gaaaacgttc ttcggggcga aaactctcaa ggatcttacc
4741 gctgttgaga tccagttcga tgtaacccac tcgtgcaccc aactgatctt cagcatcttt
4801 tactttcacc agcgtttctg ggtgagcaaa aacaggaagg caaaatgccg caaaaaaggg
4861 aataagggcg acacggaaat gttgaatact catactcttc ctttttcaat attattgaag
4921 catttatcag ggttattgtc tcatgagcgg atacatattt gaatgtattt agaaaaataa
4981 acaaataggg gttccgcgca catttccccg aaaagtgcca cctgacgcgc cctgtagcgg
5041 cgcattaagc gcggcgggtg tggtggttac gcgcagcgtg accgctacac ttgccagcgc
5101 cctagcgccc gctcctttcg ctttcttccc ttcctttctc gccacgttcg ccggctttcc
5161 ccgtcaagct ctaaatcggg gcatcccttt agggttccga tttagtgctt tacggcacct
5221 cgaccccaaa aaacttgatt agggtgatgg ttcacgtagt gggccatcgc cctgatagac
5281 ggtttttcgc cctttgacgt tggagtccac gttctttaat agtggactct tgttccaaac
5341 tggaacaaca ctcaacccta tctcggtcta ttcttttgat ttataaggga ttttgccgat
5401 ttcggcctat tggttaaaaa atgagctgat ttaacaaaaa tttaacgcga attttaacaa
5461 aatattaaca aaatattaac gtttacaatt tc
//

9.2 Appendix B

Comparable levels of Jarid1A in HeLa, U2OS and MCF-7 cells

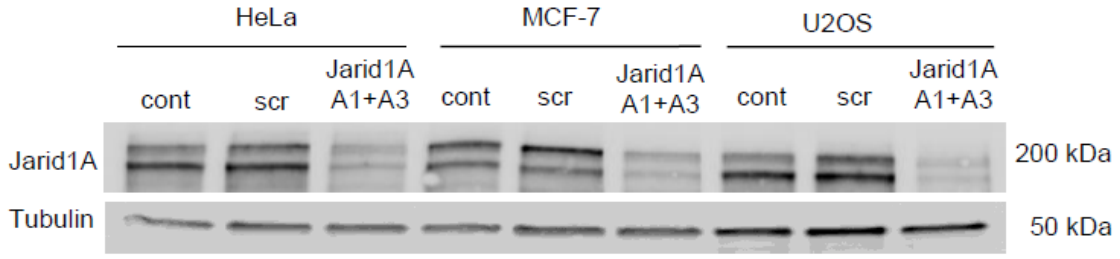

Figure B. 1: Decreased levels of Jarid1A in whole cell protein extracts of HeLa, MCF-7 and U2OS cells after siRNA transfection. Western blot images show levels of Jarid1A in untransfected cells (cont), in cells transfected with scrambled siRNA (scr) and in cells transfected with Jarid1A A1+A3 siRNA. The controls and scr siRNA transfected cells of all three cell lines show comparable levels of Jarid1A.

Peptide competition assay of the antibody r-α-H3K4me3 (Abcam 8580) via Immunofluorescence

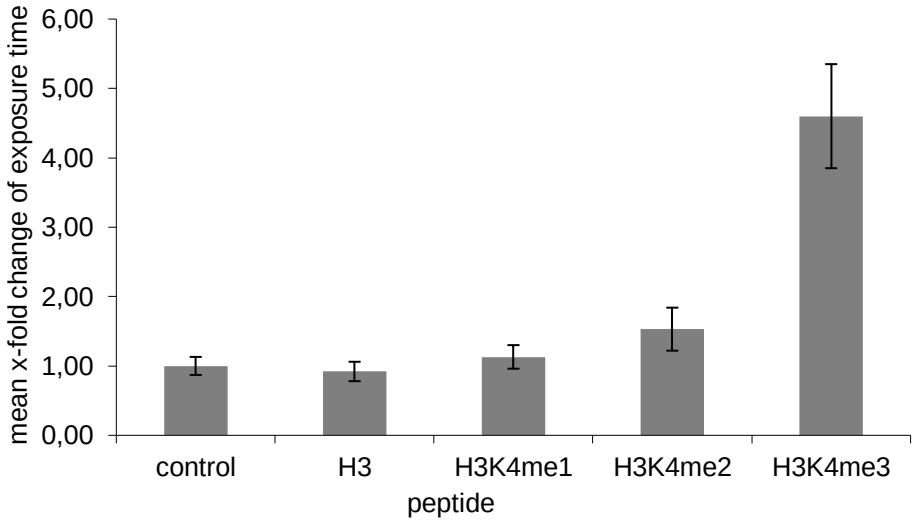

Figure B. 2: X-fold change of mean exposure time with standard deviation in images, where primary antibody was incubated with different peptides. Primary H3K4me3 antibody was incubated with a 100-fold molar excess of one of the above indicated peptides. Exposure time was measured in seven images of each condition and was normalized to exposure time of the control (no peptide). Only after incubation of the primary antibody with its specific peptide H3K4me3, exposure time is significantly increased.

Peptide competition assay of the antibody r-α-H3K4me3 (Abcam 8580) via Western Blotting

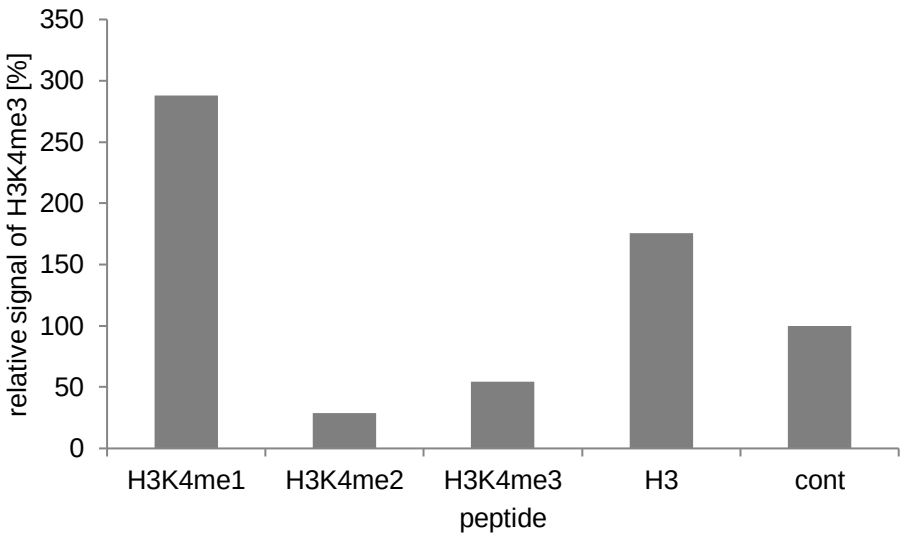

Figure B. 3: Relative signals of H3K4me3 after incubation of the antibody with the different peptides are represented in the graph. Primary H3K4me3 antibody was incubated with a 100-fold molar excess of one of the above indicated peptides. Sample incubated with H3K4me3 antibody without peptide was used as control. The antibody is efficiently blocked by the peptides H3K4me2 and H3K4me3.

9.3 Appendix C

Depletion of Jarid1A enhances radiosensitivity

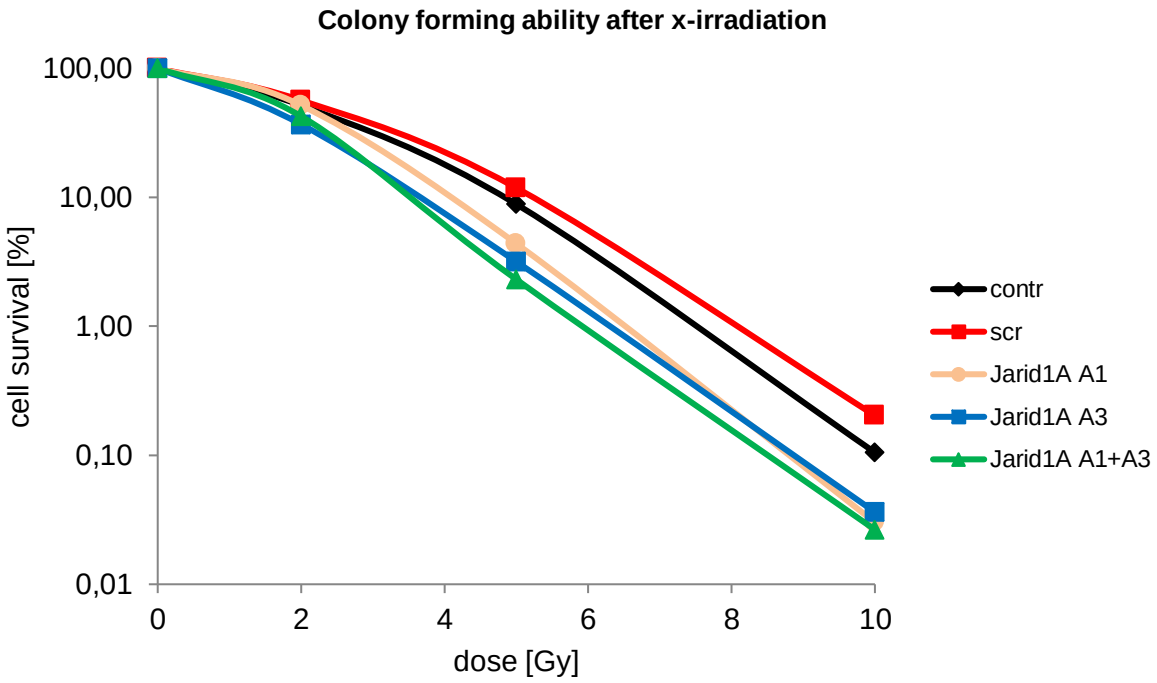

Figure C: Survival fraction of the differently treated HeLa cells irradiated at 72 h after siRNA transfection. Cells were irradiated with 0 Gy, 2 Gy 5 Gy or 10 Gy x-rays and incubated for 10 days before fixation and methylene blue staining of colonies.

9.4 Appendix D

Early formation of γH2AX foci is not affected by depletion of Jarid1A.

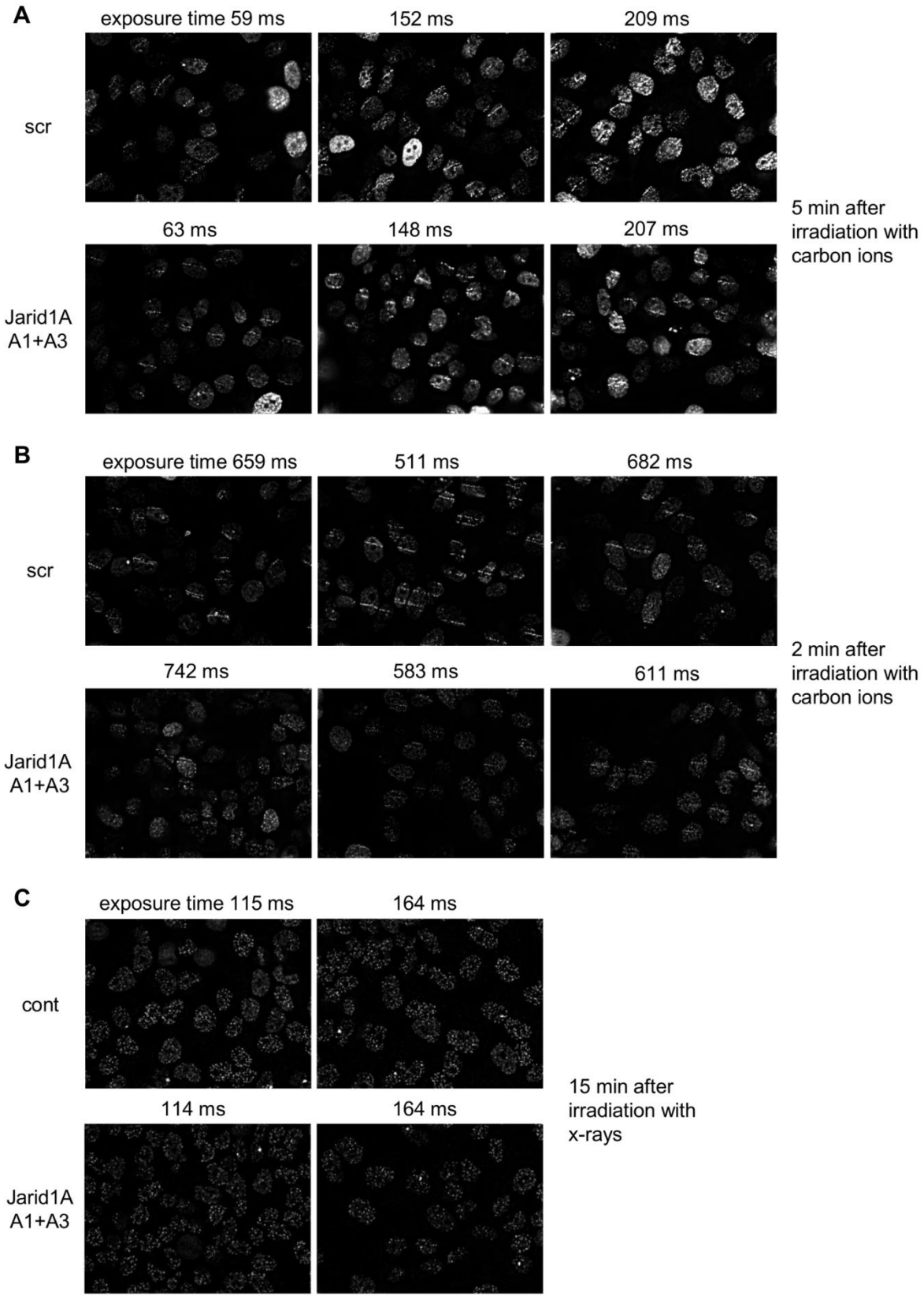

Figure D: 72 h after transfection with scr or Jarid1A A1+A3 siRNA, HeLa cells were irradiated in a small angle configuration with 55 MeV carbon ions and fixed after 5 min (A) and 2 min (B), or irradiated with 5 Gy X-rays and fixed after 15 min (C). Indirect immunofluorescence was performed to detect the foci formation of γH2AX. Numbers indicate microscopic exposure times, thus enabling direct comparison of signal intensities.

9.5 Appendix E

No inhibition of Jarid1B after treatment of cells with different concentrations of PBIT as shown by steady H3K4me3 levels in Western Blotting experiments

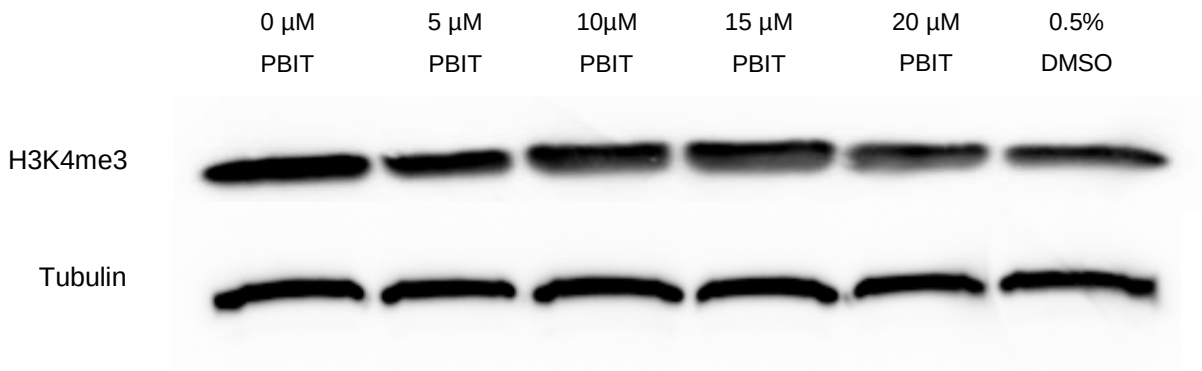

Figure E.1: Relative signals of H3K4me3 after 72 h incubation of HeLa cells with different concentrations of PBIT. DMSO was used as control.

Treatment of cells with PBIT does not disturb H3K4me3 demethylation at γH2AX decorated damage sites

DMSO

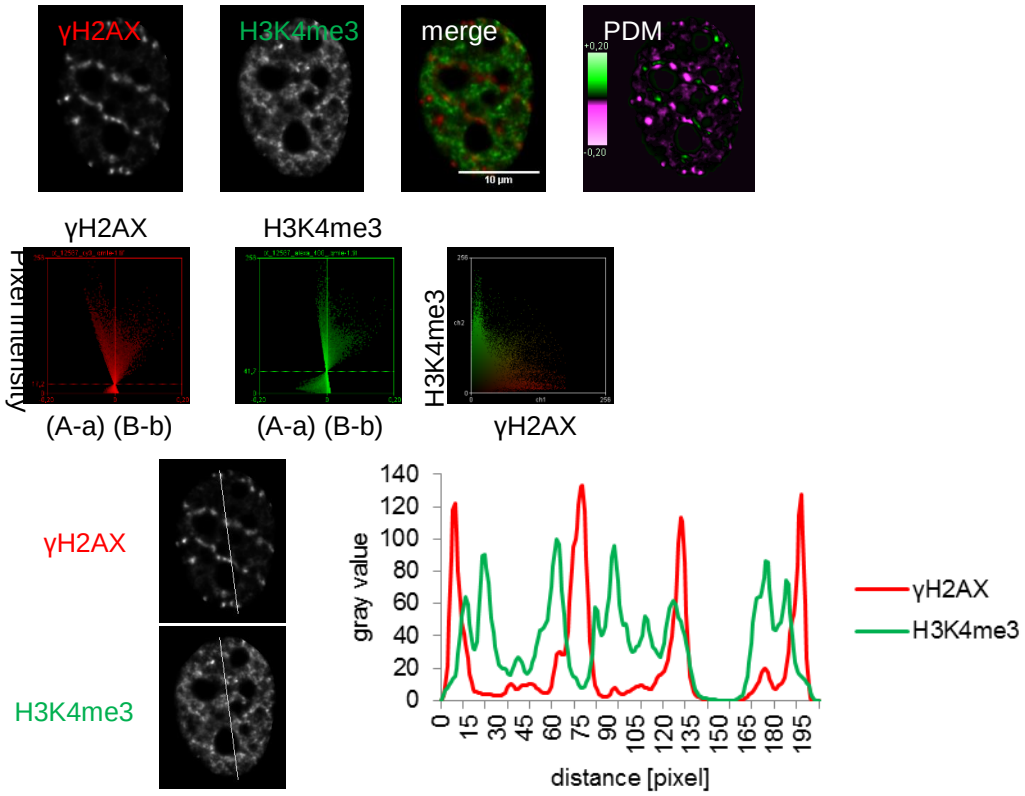

PBIT

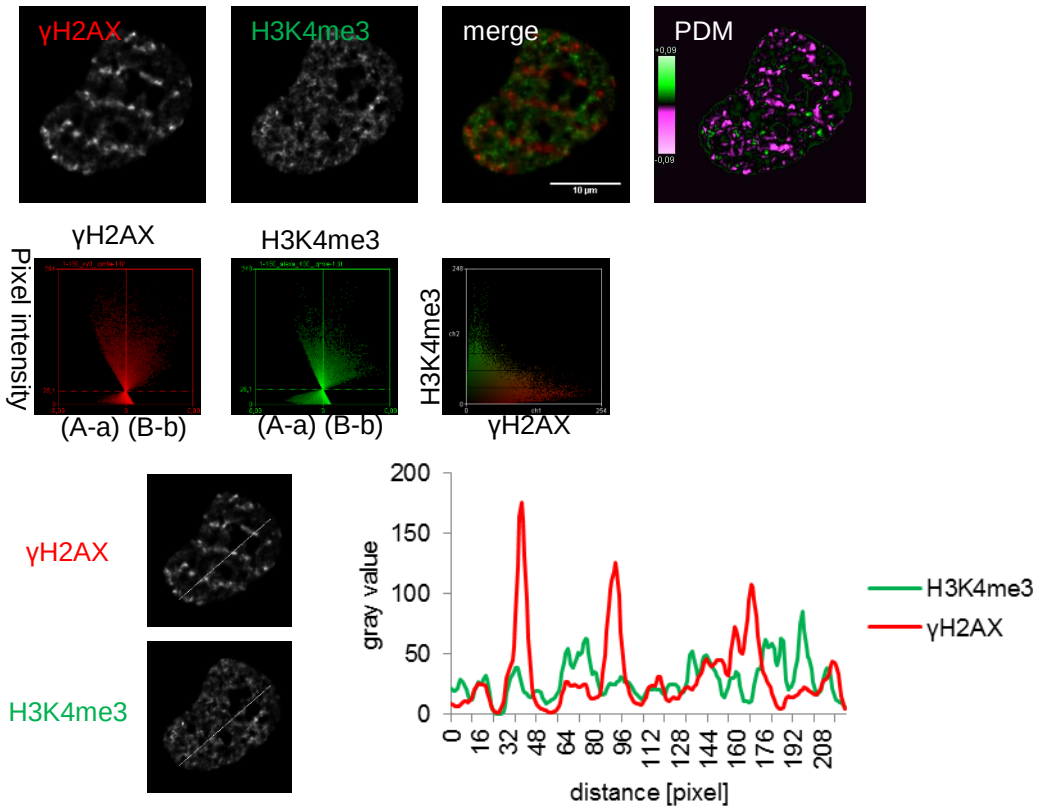

Figure E.2: HeLa cells were treated with 15 µM of the Jarid1B inhibitor PBIT 72 h prior to irradiation. DMSO was used as control. Cells were exposed to ion microirradiation with single carbon ions applied in a 1 x 5 µm linear pattern. Cells were incubated for 1 h before fixation and indirect immunofluorescence detection of γH2AX and H3K4me3. Correlation analysis was done as described in chapter 3.3.1. In all panels the top rows show single slices of 3D microscopic images (red channel, green channel and merge). In addition, to determine positive or negative correlation between signal intensities in both channels for each pixel, the product of the mean (PDM) map is shown. In the PDM maps, negative correlation at positions of γH2AX foci is visualized by pink signals; positive correlation is shown by green signals, whereas black indicates random distribution of both signals. In the second row of each panel, plots of signal intensity vs. PDM in the respective channels and the corresponding intensity scatter plots are shown. PDM plots skewed to negative values demonstrate anti-correlation. In the third row, profiles of the signal intensities along the indicated lines also demonstrate underrepresentation of H3K4me3 at damage sites.

Inhibition of ATR by VE-821 does not disturb H3K4me3 demethylation γH2AX decorated damage sites

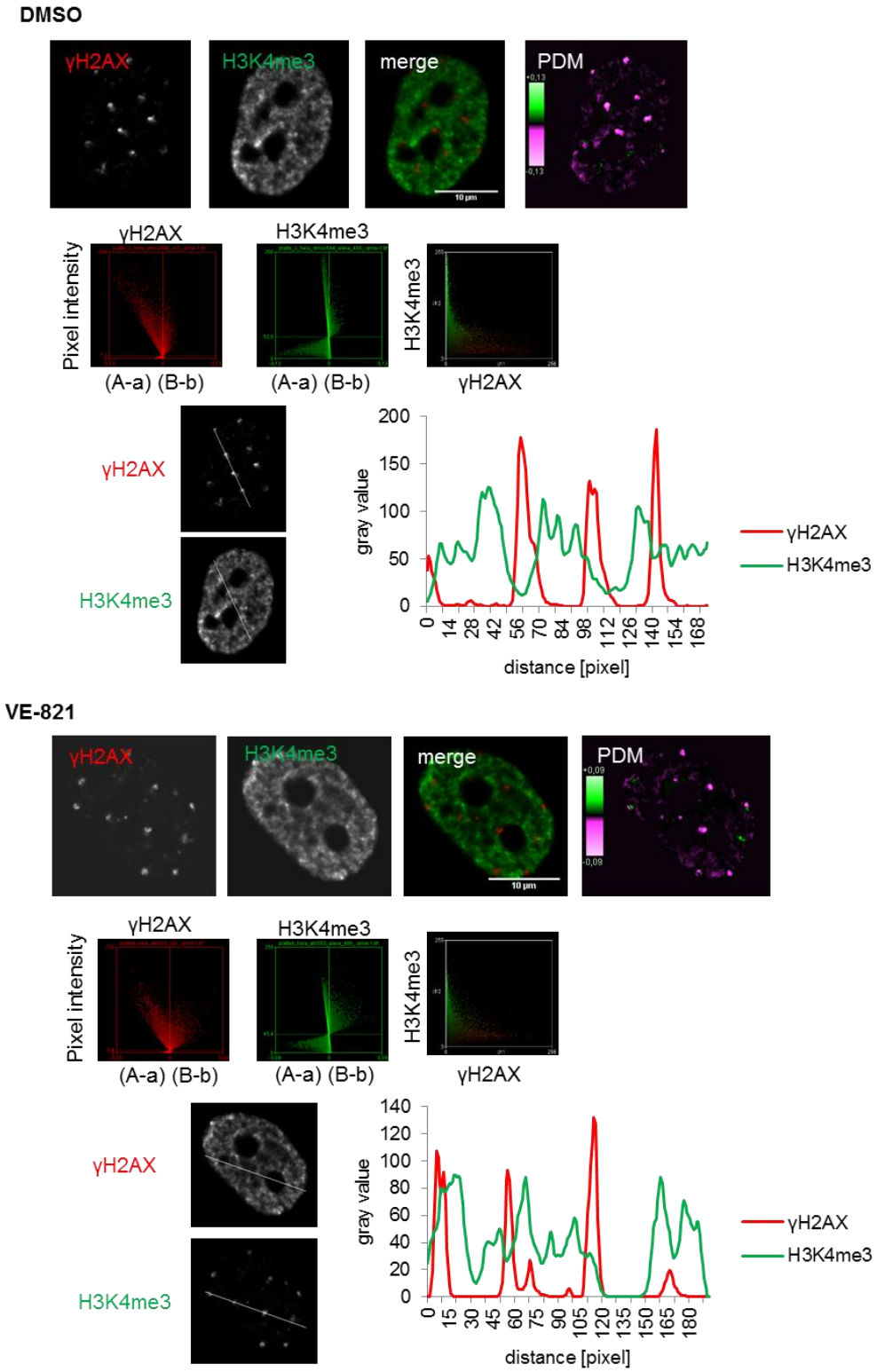

Figure E.3: HeLa cells were treated with 10 µM VE-821 for ATR inhibition 1 h prior to irradiation. DMSO was used as control. Cells were exposed to ion microirradiation with single carbon ions applied in a 5 µm x 5 µm matrix pattern. Cells were incubated for 1 h before fixation and indirect

immunofluorescence detection of γH2AX and H3K4me3. Correlation analysis was done as described in chapter 3.3.1. In all panels the top rows show single slices of 3D microscopic images (red channel, green channel and merge). In addition, to determine positive or negative correlation between signal intensities in both channels for each pixel, the product of the mean (PDM) map is shown. In the PDM maps, negative correlation at positions of γH2AX foci is visualized by pink signals; positive correlation is shown by green signals, whereas black indicates random distribution of both signals. In the second row of each panel, plots of signal intensity vs. PDM in the respective channels and the corresponding intensity scatter plots are shown. PDM plots skewed to negative values demonstrate anti-correlation. In the third row, profiles of the signal intensities along the indicated lines also demonstrate underrepresentation of H3K4me3 at damage sites.

9.6 Appendix F

Table F.1: Significantly deregulated pathways revealed by Reactome pathway enrichment analysis after Jarid1A depletion (compared to untransfected cells) in unirradiated cells (p < 0.05; FDR < 0.05). *Bold face: level 1, normal font: level 2, slanted font: level 3 and higher; pink: Extracellular matrix organization, orange: Immune system, grey: Signal transduction*

Gene Set	Deregulated genes in Gene Set [%]	Genes
Regulation of Complement cascade	30.43	C3, C4A, C4B, C4BPB, CD55, CFH, CFHR3
Assembly of collagen fibrils and other multimeric structures	16.67	COL18A1, COL7A1, COL8A1, CTSL, CTSV, ITGB4, LAMB3, LOXL1, LOXL4
Signaling by FGFR in disease	9.94	ADCY9, AGO1, CASP9, CDKN1A, CUX1, FGF2, FGFR3, GSK3A, ITPR1, LRRFIP1, MAPK1, NRG1, PDE1C, PIK3R2, PRKCA, RPS6KB2, STAT5B
Collagen formation	12.79	COL16A1, COL18A1, COL25A1, COL7A1, COL8A1, CTSL, CTSV, ITGB4, LAMB3, LOXL1, LOXL4
VEGFR2 mediated cell proliferation	24	ITPR1, MAPK1, PRKCA, PRKCB, SPHK1, VEGFA
Downstream signal transduction	9.68	ADCY9, AGO1, CASP9, CDKN1A, FGF2, FGFR3, GSK3A, ITPR1, MAPK1, NRG1, PDE1C, PIK3R2, PRKCA, RPS6KB2, STAT5B
Extracellular matrix organization	7.98	COL16A1, COL18A1, COL25A1, COL7A1, COL8A1, CTSL, CTSV, F11R, FGF2, ITGA11, ITGB4, LAMB3, LAMC1, LOXL1, LOXL4, MMP19, MMP24, NID1, PRKCA, SDC4, TNXB
DAP12 signaling	9.49	ADCY9, AGO1, CASP9, CDKN1A, FGF2, FGFR3, GSK3A, ITPR1, MAPK1, NRG1, PDE1C, PIK3R2, PRKCA, RPS6KB2, VAV3
Downstream signaling of activated FGFR	9.79	ADCY9, AGO1, CASP9, CDKN1A, FGF2, FGFR3, GSK3A, ITPR1, MAPK1, NRG1, PDE1C, PIK3R2, PRKCA, RPS6KB2
Signaling by PDGF	8.99	ADCY9, AGO1, CASP9, CDKN1A, FGF2, FGFR3, GSK3A, ITPR1, MAPK1, NRG1, PDE1C, PDGFC, PIK3R2, PRKCA, RPS6KB2, STAT5B

Table F.2: Significantly deregulated pathways revealed by Reactome pathway enrichment analysis in scr transfected cells after irradiation (p < 0.05; FDR < 0.05). *Bold face: level 1, normal font: level 2, slanted font: level 3 and higher; green: Cell Cycle, red: Cellular responses to stress, blue: Programmed cell death, orange: Signal transduction*

Gene Set	Ratio of Protein in Gene Set	Genes
Formation of Senescence-Associated Heterochromatin Foci (SAHF)	23.53	HIST1H1A, HIST1H1D, HIST1H1E, HMGA2
DNA Damage/Telomere Stress Induced Senescence	8.62	CDKN1B, HIST1H1A, HIST1H1D, HIST1H1E, HMGA2
Activation of DNA fragmentation factor	23.08	HIST1H1A, HIST1H1D, HIST1H1E
Apoptosis induced DNA fragmentation	23.08	HIST1H1A, HIST1H1D, HIST1H1E
Cellular Senescence	3.8	CDKN1B, HIST1H1A, HIST1H1D, HIST1H1E, HMGA2, IL6
Resolution of Sister Chromatid Cohesion	5	CCNB1, CDCA8, CENPA, KIF18A, SGOL1
Chemokine receptors bind chemokines	7.27	CCL2, CXCL1, CXCL2, CXCL3
Mitotic Prometaphase	4.63	CCNB1, CDCA8, CENPA, KIF18A, SGOL1
Cell Cycle, Mitotic	2.03	AURKA, BORA, CCNB1, CDCA8, CDKN1B, CENPA, KIF18A, NEK2, SGOL1
Peptide ligand-binding receptors	3.16	CCL2, CXCL1, CXCL2, CXCL3, GALR3, UTS2R

Depletion of Jarid1A plus irradiation has no influence on expression of CENPF, PARP1 and NFKBIE on the protein level.

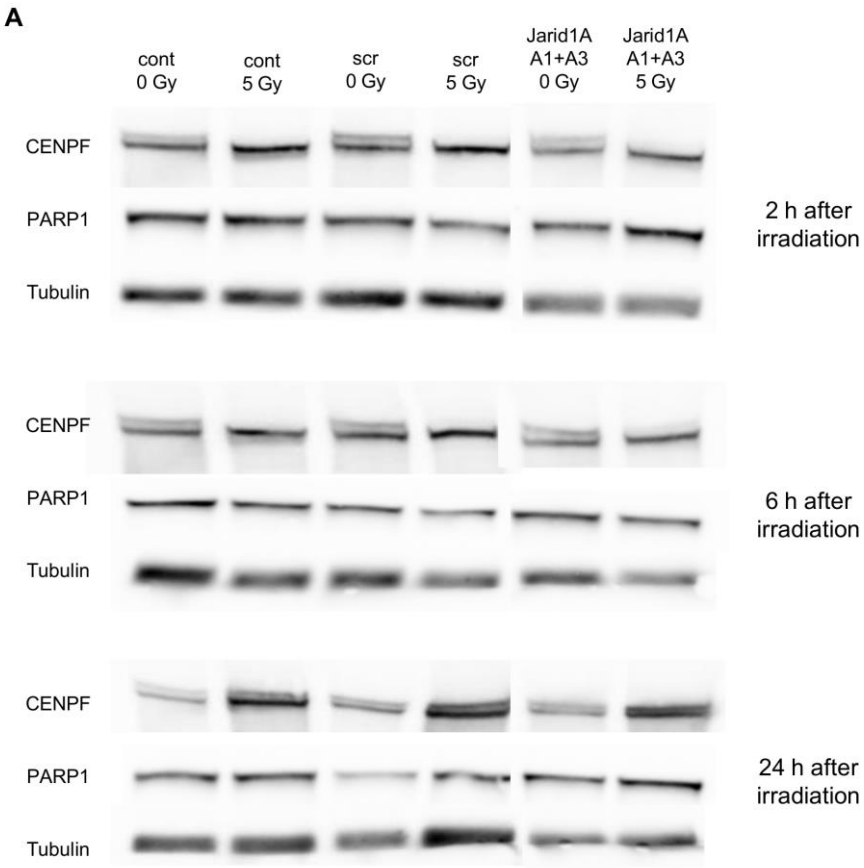

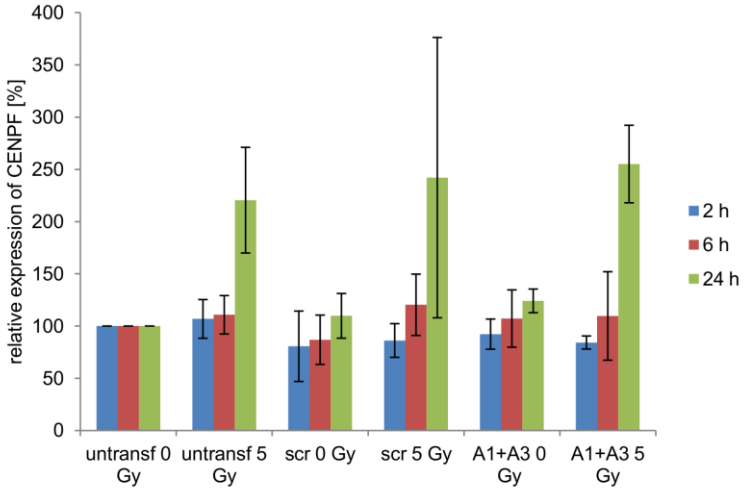
relative expression of CENPF [%]
400
350
300
250
200
150
100
50
0
untransf 0 Gy
untransf 5 Gy
scr 0 Gy
scr 5 Gy
A1+A3 0 Gy
A1+A3 5 Gy
2 h
6 h
24 h

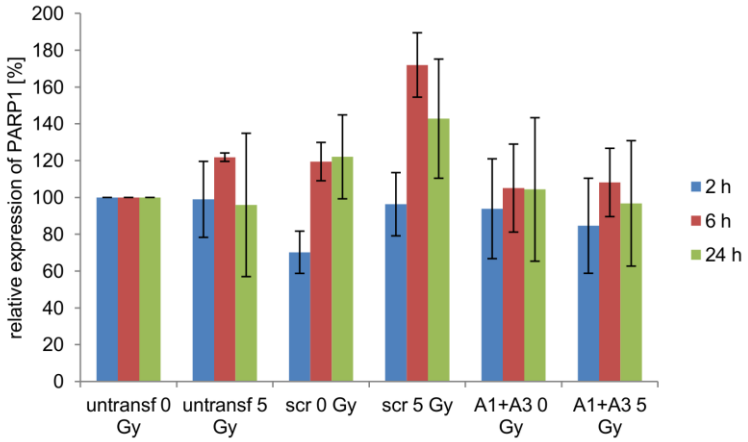
relative expression of PARP1 [%]
200
180
160
140
120
100
80
60
40
20
0
untransf 0 Gy
untransf 5 Gy
scr 0 Gy
scr 5 Gy
A1+A3 0 Gy
A1+A3 5 Gy
2 h
6 h
24 h

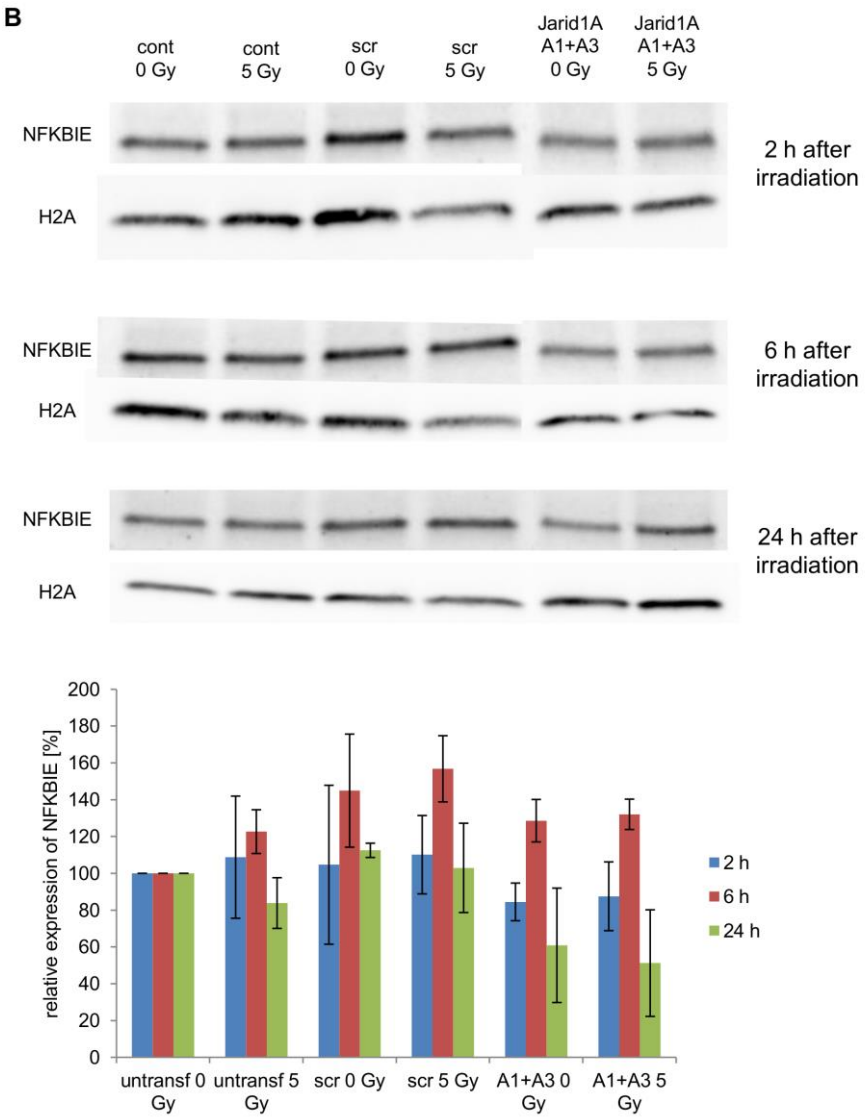

Figure F: Western Blot images of (A) CENPF, PARP1 and (B) NFKBIE in HeLa untransfected cells, control transfected cells and Jarid1A depleted cells 2 h, 6 h and 24 h after irradiation with 5 Gy. Graphs display the normalized average amount (+/- SD) of (A) CENPF, PARP1 and (B) NFKBIE determined by quantitative analysis of Western blots of protein extracts obtained in (A) three or (B) four independent experiments.

9.7 Appendix G

H3K4me3 and H3K9me3 levels in HTC116 after incubation with different concentrations of R-2-HG remains unchanged.

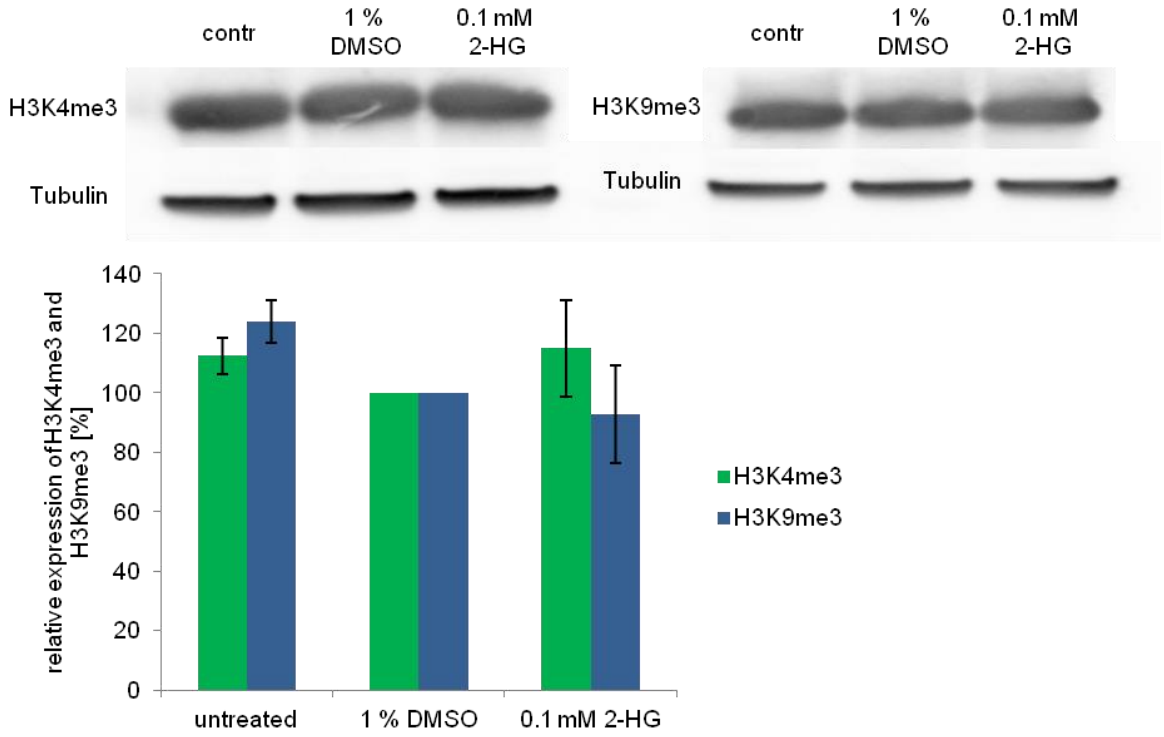

Figure G: Steady levels of H3K4me3 and H3K9me3 in HCT116 cells after incubation with 0.1 mM of R-2-HG. Western blot images show levels of H3K4me3 and H3K9me3 in HCT116 cells treated with R-2-HG for 6 days. 1% DMSO was used as control. Graph displays the normalized average amount (+/- SD) of H3K4me3 and H3K9me3 protein determined by quantitative analysis of Western blots of protein extracts obtained in three independent experiments.

Acknowledgments

I would like to thank my supervisor PD Dr. Anna A. Friedl for having given me the opportunity to perform my Ph.D. in her lab. Thank you for your great support and your confidence in me during all these years. You always encouraged and motivated me.

Next, I would like to thank Prof. Dr. Heinrich Leonhardt for his second opinion on my thesis.

I would like to thank Dr. Guido Drexler for his countless advices. I appreciate your huge practical expertise and supportive ideas.

A special thank goes to Claudia Böhland for her great support in the lab with Western Blotting, FACS analysis and during beamtimes. Thank you also for the entertaining lunch and coffee breaks. You often saved my day in the lab.

Further, I want to thank Iris Bauer for technical assistance and help with different experiments and Ramona Stamp and Belinda Maroschik for being such great office colleagues.

Next, I would like to thank Dr. Kristian Unger for having given me the opportunity to perform qRT-PCR and microarray analysis in the Helmholtz Zentrum, his great support with microarray analysis and for having performed the whole statistical evaluation of the microarray results. Big thank goes also to Aaron Selmaier, Laura Daika and Christina Wilke in his team for their technical help with microarray analysis and qRT-PCR.

I would like to thank the whole team of Prof. Dr. Günther Dollinger for having performed the ion-radiation at SNAKE. Stefanie Girst, Judith Reindl, Christoph Greubel, Christian Siebenwirth and Günther Dollingter thank you for your great support during beamtimes.

Thanks to Dr. Randolph Caldwell for the help with the FACS analysis and to Herbert Braselmann for statistical evaluation of the colony formation assays

I would like to thank Dr. Wael Mansour and Dr. Kerstin Borgmann for having sent me the plasmids for the repair assays.

A thank goes to all master students under my surveillance for supporting me in the lab.

Thank you Evi for the coffee breaks and your delicious cupcakes. It is great that we still keep the tradition of our after work meetings.

Last but not least I want to thank my family and friends for always believing in me. Thanks to my parents and grandparents for the emotional and financial support during my whole studies. A special thank goes to my mum, who was always there for me with her ongoing support and her honest encouragement.